

Final Report

Drilled Shaft Resistance Based on Diameter, Torque and Crowd (Drilling Resistance vs. Rock Strength) Phase II

FDOT Contract No. BDV31-977-20
UF Contract No. 00114038

Submitted by:

Michael McVay, Ph.D.
Michael Rodgers, M.E.

Department of Civil and Coastal Engineering
University of Florida
Gainesville, Florida 32611

Developed for the



David Horhota, Ph.D., P.E., Project Manager

June 2016

DISCLAIMER

The opinions, findings, and conclusions expressed in this publication are those of the authors and not necessarily those of the Florida Department of Transportation.

SI (MODERN METRIC) CONVERSION FACTORS (FROM FHWA) APPROXIMATE CONVERSIONS TO SI UNITS

SYMBOL	WHEN YOU KNOW	MULTIPLY BY	TO FIND	SYMBOL
LENGTH				
in	inches	25.4	millimeters	mm
ft	feet	0.305	meters	m
yd	yards	0.914	meters	m
mi	miles	1.61	kilometers	km
SYMBOL	WHEN YOU KNOW	MULTIPLY BY	TO FIND	SYMBOL
AREA				
in ²	square inches	645.2	square millimeters	mm ²
ft ²	square feet	0.093	square meters	m ²
yd ²	square yard	0.836	square meters	m ²
ac	acres	0.405	hectares	ha
mi ²	square miles	2.59	square kilometers	km ²
SYMBOL	WHEN YOU KNOW	MULTIPLY BY	TO FIND	SYMBOL
VOLUME				
fl oz	fluid ounces	29.57	milliliters	mL
gal	gallons	3.785	liters	L
ft ³	cubic feet	0.028	cubic meters	m ³
yd ³	cubic yards	0.765	cubic meters	m ³
NOTE: volumes greater than 1000 L shall be shown in m ³				
SYMBOL	WHEN YOU KNOW	MULTIPLY BY	TO FIND	SYMBOL
MASS				
oz	ounces	28.35	grams	g
lb	pounds	0.454	kilograms	kg
T	short tons (2000 lb)	0.907	megagrams (or "metric ton")	Mg (or "t")
SYMBOL	WHEN YOU KNOW	MULTIPLY BY	TO FIND	SYMBOL
TEMPERATURE (exact degrees)				
°F	Fahrenheit	5 (F-32)/9 or (F-32)/1.8	Celsius	°C
SYMBOL	WHEN YOU KNOW	MULTIPLY BY	TO FIND	SYMBOL
ILLUMINATION				
fc	foot-candles	10.76	lux	lx
fl	foot-Lamberts	3.426	candela/m ²	cd/m ²
SYMBOL	WHEN YOU KNOW	MULTIPLY BY	TO FIND	SYMBOL
FORCE and PRESSURE or STRESS				
lbf	pound force	4.45	newtons	N
lbf/in ²	pound force per square inch	6.89	kilopascals	kPa

APPROXIMATE CONVERSIONS TO ENGLISH UNITS

SYMBOL	WHEN YOU KNOW	MULTIPLY BY	TO FIND	SYMBOL
LENGTH				
mm	millimeters	0.039	inches	in
m	meters	3.28	feet	ft
m	meters	1.09	yards	yd
km	kilometers	0.621	miles	mi
SYMBOL	WHEN YOU KNOW	MULTIPLY BY	TO FIND	SYMBOL
AREA				
mm ²	square millimeters	0.0016	square inches	in ²
m ²	square meters	10.764	square feet	ft ²
m ²	square meters	1.195	square yards	yd ²
ha	hectares	2.47	acres	ac
km ²	square kilometers	0.386	square miles	mi ²
SYMBOL	WHEN YOU KNOW	MULTIPLY BY	TO FIND	SYMBOL
VOLUME				
mL	milliliters	0.034	fluid ounces	fl oz
L	liters	0.264	gallons	gal
m ³	cubic meters	35.314	cubic feet	ft ³
m ³	cubic meters	1.307	cubic yards	yd ³
SYMBOL	WHEN YOU KNOW	MULTIPLY BY	TO FIND	SYMBOL
MASS				
g	grams	0.035	ounces	oz
kg	kilograms	2.202	pounds	lb
Mg (or "t")	megagrams (or "metric ton")	1.103	short tons (2000 lb)	T
SYMBOL	WHEN YOU KNOW	MULTIPLY BY	TO FIND	SYMBOL
TEMPERATURE (exact degrees)				
°C	Celsius	1.8C+32	Fahrenheit	°F
SYMBOL	WHEN YOU KNOW	MULTIPLY BY	TO FIND	SYMBOL
ILLUMINATION				
lx	lux	0.0929	foot-candles	fc
cd/m ²	candela/m ²	0.2919	foot-Lamberts	fl
SYMBOL	WHEN YOU KNOW	MULTIPLY BY	TO FIND	SYMBOL
FORCE and PRESSURE or STRESS				
N	newtons	0.225	pound force	lbf
kPa	kilopascals	0.145	pound force per square inch	lbf/in ²

*SI is the symbol for the International System of Units. Appropriate rounding should be made to comply with Section 4 of ASTM E380. (Revised March 2003)

TECHNICAL REPORT DOCUMENTATION PAGE

1. Report No.	2. Government Accession No.	3. Recipient's Catalog No.	
4. Title and Subtitle Drilled Shaft Resistance Based on Diameter, Torque and Crowd (Drilling Resistance vs. Rock Strength) Phase II		5. Report Date June 2016	
		6. Performing Organization University of Florida	
7. Author(s) Michael McVay and Michael Rodgers		8. Performing Organization Report No.	
9. Performing Organization Name and Address University of Florida – Dept. of Civil and Coastal Engineering; Engineering School of Sustainable Infrastructure and Environment 365 Weil Hall – P.O. Box 116580 Gainesville, FL 32511-6580		10. Work Unit No. (TRAIS)	
		11. Contract or Grant No. BDV31-977-20	
12. Sponsoring Agency Name and Address Florida Department of Transportation 605 Suwannee Street, MS 30 Tallahassee, FL 32399		13. Type of Report and Period Covered Final Report 03/25/2014 – 6/30/2016	
		14. Sponsoring Agency Code	
15. Supplementary Notes			
<p style="text-align: center;">16. Abstract:</p> <p>The research focused on evaluation of Florida limestone's unconfined compressive strength, q_u, through drilling parameters – crowd, torque, penetration rate, rotational speed, and bit diameter – in both the laboratory and field for assessing a shaft's side shear. Synthetic homogeneous limestone blocks of various strengths were cast in the laboratory and allowed to cure for 14 days; The blocks were then drilled with rock augers of two different diameters at multiple penetration rates and drilling rotational speeds. Both crowd and torque were measured in real time. Estimation of rock strength, q_u from drilling relationships developed by Karasawa (2002a) and Teale (1965) were evaluated. It was found that Teale's specific energy approach could estimate rock strength, q_u using the multiple diameter drill bits expected in field drilled shaft construction.</p> <p>In the field, shaft installation was monitored (crowd, torque, penetration rate, etc.) at three sites (Little River, Overland, and Kanapaha) from which rock strength, q_u was estimated along with shaft side shear. For side shear, FDOT's design equation in limestone was used with split tension strength initially estimated from q_t/q_u ratio established by field cores; subsequently, Johnston's q_u vs. q_t/q_u relationship was used. The estimated unit skin friction in multiple rock formations and segments was compared by instrumented segment during Osterberg, Statnamic, and top-down static load testing. The mean bias (measured/predicted) unit side shear in limestone was 1.00, and the coefficient of variation, CV, was 0.07. The results suggest that estimating rock strength and shaft side shear using drilling parameters is viable, especially considering the currently available rig monitoring equipment (Jean Lutz, Bauer, etc.).</p>			
17. Key Word Drilling, monitoring, rock strength, shaft side shear		18. Distribution Statement No restrictions.	
19. Security Classif. (of this report): Unclassified	20. Security Classif. (of this page): Unclassified	21. No. of Pages 248	22. Price

EXECUTIVE SUMMARY

Over the past 20 years, there has been an increase in the use of drilled shafts. This can be attributed to limited available sizes of driven piles and noise and vibration issues during driven pile installation. Unfortunately, the development of construction monitoring in assessing shaft capacity in drilled shafts has lagged that of driven piles. For instance, driven pile capacities can be assessed during the installation process by evaluating dynamic forces and/or blows per foot during driving. Whereas drilled shafts currently employ no means to assess shaft capacity except for inspection of the soil/rock removed during the installation process. All drilled shaft capacity assessments are performed on completed shafts, meaning there is no change in shaft length due to monitoring the construction process. Often times, the determination of rock strength requires destructive testing which is expensive, takes a significant amount of time, and requires the availability of sound core samples. Of great interest is the assessment of rock quality, strength, and total socket length during the drilling process in real time which could lead to the appropriate selection of shaft lengths and reduced uncertainties. For instance, it could be expected that monitoring the drilling process could ensure the minimum mean rock strength is found or lengths of nominal rock strength in a shaft were observed during installation.

This project focused on developing and evaluating the relationship between five rock drilling parameters (crowd, torque, penetration rate, rotational speed, and drill bit diameter) and rock strength (e.g., unconfined compression, q_u). This required both a laboratory and field investigation.

In the laboratory, synthetic limestone (Gatorock) was developed at four different design strengths – 10, 20, 40, and 120 tons per square foot, tsf – that were representative of Florida's numerous limestone formations. The Gatorock was cast into large blocks (22.5" x 22.5" x 40") that were subsequently drilled using various combinations of the five drilling parameters. The results were wirelessly transmitted in real time to an external computer and recorded for analysis. During the analysis multiple developed drilling equations were investigated. From the investigation, a unique relationship was developed using Teale's specific energy equation for rotary non-percussive drilling in rock. The developed relationship provided the strongest correlation between the five drilling parameters and compressive strength. From this, a new equation was developed that can be used to measure rock strength in real time during field drilling.

In the field, the five drilling parameters were measured on the drill rig using Jean Lutz monitoring equipment, which records and transmits the data wirelessly to an external computer in real time away from the drilling. The Jean Lutz equipment included pressure transducers used to tap into the hydraulic lines providing torque and crowd to the drill bit, a proximity sensor to monitor rotational speed at the rotary table, a rotary encoder mounted on the rim of the main cable winch to monitor penetration rate, a junction box to receive the signals from each sensor, and a data acquisition module to record, display, and transmit the data wirelessly in real time, via Bluetooth, to an external computer.

Throughout the course of the research project, field monitoring took place at three separate locations where load testing occurred. The locations were in Quincy, FL (Little River Bridge), Jacksonville, FL (Overland Bridge), and Gainesville, FL (Kanapaha). The test shafts at each location were monitored during installation. Monitoring in these locations provided direct comparison of the estimated shaft capacity obtained during monitored drilling to the actual capacity of installed shafts measured using conventional methods. Additionally, each location used a different type of load test, O-cell testing at Little River, Statnamic testing at Overland and a traditional top-down static load test at Kanapaha.

For side shear comparisons, FDOT's recommended design equation, for limestone socketed shafts, was used with compressive strength, q_u , measured through monitoring and split tension strength, q_t , estimated from the q_t/q_u ratio developed for Florida geomaterials using Johnston's criterion. The estimated unit skin friction, in multiple rock formations, was compared with load test results from instrumented segments that reached failure within the same rock sockets. The mean bias (measured/predicted) for unit side shear in limestone was 1.00, and the coefficient of variation, CV, was 0.07. The results suggest that estimating rock strength and shaft side shear using drilling parameters is viable, especially considering the currently available rig monitoring equipment (Jean Lutz, Bauer, etc.). Further testing is suggested due to the size of the data set.

Table of Contents

<u>Chapter</u>	<u>Page</u>
Disclaimer	ii
SI (Modern Metric) Conversion Factors (from FHWA) Approximate Conversions to SI Units	iii
Approximate Conversions to English Units	iv
Technical Report Documentation Page	v
Executive Summary	vi
List of Tables	x
List of Figures	xv
Chapter 1 Introduction	1
1.1 Background	2
1.2 Scope	3
Chapter 2 Laboratory Measurements of Drilling Parameters on Synthetic Limestone	6
2.1 Development of Synthetic Limestone, Gatorock.....	6
2.2 Development of a Laboratory Drilling Environment.....	8
2.2.1 Coupler System to Monitor Laboratory Drilling	8
2.2.2 Laboratory Coupler Calibration	11
2.2.3 Laboratory Drilling Procedure.....	16
2.3 Lab Data Analyses.....	26
2.3.1 q_u vs. q_t	26
2.3.2 Effects of Bit Diameter.....	27
2.3.3 Increasing Force and Torque Relationship.....	39
2.3.4 Torque and Force vs. Penetration Rate per Rotational Speed Ratio (u/N).....	41
2.3.5 Torque and Crowd vs. Compressive and Tensile Strengths	44
2.3.6 Developed D_s vs. q_u and D_s vs. q_t Curves.....	47
2.3.7 Development of e vs. q_u Curve using Teale's Equations, 1965.....	49
2.3.8 Comparing Teale and Karasawa.....	52
Chapter 3 Preliminary Monitoring of Field Drilling (Pilot Projects)	60
3.1 Development of Equipment for Shaft Installation Monitoring in Real Time	60
3.1.1 Surveying Florida Contractors and District Geotechnical Engineers	60
3.1.2 Monitoring Equipment	61
3.2 Pilot Project Overview.....	63

3.3 Little River.....	64
3.3.1 Converting the Raw Data	66
3.3.2 Preliminary Field Monitoring Analysis.....	80
3.4 Overland Test Shaft Preliminary Analysis.....	117
3.4.1 Developing Drill Rig Equations for Crowd and Torque Conversion	117
3.5 Johnston's Criteria	124
Chapter 4 Full-Scale Drilled Shaft Installation with Capacity Estimated real time from Drilling Parameters followed by Static Load Testing	142
4.1 Kanapaha Overview.....	142
4.2 Kanapaha Site Investigation	142
4.3 Core Data Analysis	147
4.4 Drill Rig Investigation	164
4.5 Monitoring Equipment Installation	166
4.5.1 Rotational Speed Sensor	166
4.5.2 Penetration Rate Sensor	167
4.5.3 Torque and Crowd Sensors	168
4.6 Rebar Cage Instrumentation	170
4.7 Shaft Installations.....	174
4.7.1 East Shaft.....	175
4.7.2 Test Shaft.....	180
4.7.3 West Shaft.....	184
4.8 Top-Down Static Load Test	189
4.8.1 Load Frame Construction.....	190
4.8.2 Load Test Instrumentation.....	194
4.8.3 Load Test Procedure.....	194
Chapter 5 Kanapaha Drilled Shaft Monitoring and Load Test Analysis	196
5.1 Drilling Data.....	196
5.2 Individual Shaft Analysis.....	197
5.2.1 Test Shaft Analysis.....	206
5.2.2 East Shaft Analysis	213
5.2.3 West Shaft Analysis	215
5.3 Load Test Data	218
5.3.1 Strain Gauge Load Distribution	218
5.3.2 T-Z Curves at Kanapaha Test Site	220
5.4 Comparative Analysis	222
Chapter 6 Conclusions and Recommendations.....	226
6.1 Conclusions.....	226
6.2 Recommendations.....	230
List of References	232

LIST OF TABLES

<u>Table</u>	<u>Page</u>
Table 1 - Compressive strength results for Gatorock cores and cast cylinders.....	8
Table 2 - Instron calibration results	13
Table 3 - Equation comparison and results.....	14
Table 4 - Torque calibration results showing offsetting axial force values (Ch 2 and 4)	15
Table 5 - 287 psi original drilling results	19
Table 6 - 287 psi updated drilling results.....	19
Table 7 - 375 psi original drilling results	19
Table 8 - 375 psi updated drilling results.....	19
Table 9 - 673 psi original drilling results	19
Table 10 - 673 psi updated drilling results.....	20
Table 11 - Projected strengths (20 RPM).....	22
Table 12 - Actual strengths (20 RPM)	22
Table 13 - Projected strengths (40 RPM).....	22
Table 14 - Actual strengths (40 RPM).....	23
Table 15 - Recorded drillings (4.5" bit)	24
Table 16 - Recorded drillings (6").....	25
Table 17 - Karasawa's effect of bit diameter on I_s , S_e , and D_s (2002b report).....	48
Table 18 - Summary of the drilled shaft survey results	61
Table 19 - Field monitoring system comparison.....	62
Table 20 - Rotational speeds for transitioning between gears	67
Table 21 - Karasawa preliminary analysis of O-cell test shaft.....	74
Table 22 - O-cell test shaft analysis raw data results	88
Table 23 - O-cell test shaft analysis geometric mean results	89

Table 24 - O-cell test shaft analysis limiting method results.....	89
Table 25 - O-cell test shaft analysis FDOT method results.....	89
Table 26 - O-cell test shaft analysis FDOT* method results.....	90
Table 27 - O-cell test shaft LN transformed method results	90
Table 28 - O-cell test shaft analysis raw data results.....	99
Table 29 - O-cell test shaft analysis geometric mean results.....	100
Table 30 - O-cell test shaft analysis limiting method results.....	100
Table 31 - O-cell test shaft analysis FDOT method results.....	100
Table 32 - O-cell test shaft analysis FDOT* method results.....	101
Table 33 - O-cell test shaft LN transformed method results	101
Table 34 - O-cell test shaft analysis raw data results.....	104
Table 35 - O-cell test shaft analysis geometric mean results	104
Table 36 - O-cell test shaft analysis limiting method results.....	104
Table 37 - O-cell test shaft analysis FDOT method results.....	105
Table 38 - O-cell test shaft analysis FDOT* method results.....	105
Table 39 - O-cell test shaft LN transformed method results	105
Table 40 - O-cell test shaft analysis raw data results.....	107
Table 41 - O-cell test shaft analysis geometric mean results.....	107
Table 42 - O-cell test shaft analysis limiting method results.....	107
Table 43 - O-cell test shaft analysis FDOT method results.....	108
Table 44 - O-cell test shaft analysis FDOT* method results.....	108
Table 45 - O-cell test shaft LN transformed method results	108
Table 46 - O-cell test shaft analysis raw data results.....	109
Table 47 - O-cell test shaft analysis geometric mean results.....	109
Table 48 - O-cell test shaft analysis limiting method results.....	109

Table 49 - O-cell test shaft analysis FDOT method results	110
Table 50 - O-cell test shaft analysis FDOT* method results.....	110
Table 51 - O-cell test shaft LN transformed method results	110
Table 52 - O-cell test shaft analysis raw data results	111
Table 53 - O-cell test shaft analysis geometric mean results	111
Table 54 - O-cell test shaft analysis limiting method results.....	111
Table 55 - O-cell test shaft analysis FDOT method results.....	112
Table 56 - O-cell test shaft analysis FDOT* method results.....	112
Table 57 - O-cell test shaft LN transformed method results	112
Table 58 - O-cell test shaft analysis raw data results	113
Table 59 - O-cell test shaft analysis geometric mean results	113
Table 60 - O-cell test shaft analysis limiting method results.....	113
Table 61 - O-cell test shaft analysis FDOT method results	114
Table 62 - O-cell test shaft analysis FDOT* method results.....	114
Table 63 - O-cell test shaft LN transformed method results	114
Table 64 - O-cell test shaft analysis raw data results	115
Table 65 - O-cell test shaft analysis geometric mean results	115
Table 66 - O-cell test shaft analysis limiting method results.....	115
Table 67 - O-cell test shaft analysis FDOT method results	116
Table 68 - O-cell test shaft analysis FDOT* method results.....	116
Table 69 - O-cell test shaft LN transformed method results	116
Table 70 - Load transfer summary for Overland test shaft 2	120
Table 71 - Test shaft 2 preliminary analysis results	124
Table 72 - Core data from Little River indicating dissimilar materials.....	125
Table 73 - Pilot projects reanalyzed using the limestone equation	136

Table 74 - Pilot projects reanalyzed using the limestone equation with correction factor	136
Table 75 - Pilot projects reanalyzed using the Florida geomaterials equation	136
Table 76 - Little River monitoring results using the FL geomateris equation to predict q_t	137
Table 77 - Overland monitoring results using the FL geomaterials equation to predict q_t	137
Table 78 - Little River monitoring results using q_t slope adjustments with pairing criteria	138
Table 79 - Overland monitoring results using q_t slope adjustments with paring criteria	138
Table 80 - Updated monitoring results including strain gauge zone 8.....	140
Table 81 - Estimated skin friction for depths 40 to 45 feet	152
Table 82 - Estimated skin friction for depths 45 to 50 feet	152
Table 83 - Limestone properties used in MultiPier simulations for the east shaft.....	153
Table 84 - Limestone properties used in MultiPier simulations for the test shaft.....	153
Table 85 - Limestone properties used in MultiPier simulations for the west shaft.....	153
Table 86 - Load test loading log sheet	195
Table 87 - Design method rankings	205
Table 88- Monitored readings indicating rig malfunction.....	210
Table 89 - Monitored readings indicating a void was encountered	211
Table 90 - Test shaft load test results (Predicted).....	222
Table 91 - East shaft load test results (Predicted)	222
Table 92 - West shaft load test results (Predicted)	222
Table 93 - East shaft load test results (Predicted – reduced for tension loading)	223
Table 94 - West shaft load test results (Predicted – reduced for tension loading)	223
Table 95 - Test shaft load test results (rig malfunction section, 45 to 48ft, removed) .	224
Table 96 - Test shaft load test results (zero specific energy data removed)	224
Table 97 - Test shaft results (zero specific energy data points and rig malfunction section removed).....	224

Table 98 – Comparative analysis summary for the entire research project..... 229

LIST OF FIGURES

<u>Figure</u>	<u>Page</u>
Figure 1 - Spatial profile of boring rock strength at 17 th Street Bridge, Fort Lauderdale .	2
Figure 2 - Relationship between uniaxial compressive strength of rock, S_c , and drillability strength of rock, D_s (Karasawa et al., 2002).....	3
Figure 3 - Instrumented drill rod	9
Figure 4 - Laboratory coupler system (Left) and laboratory drilling set-up (Right).	10
Figure 5 - Coupler system drilling into a large Gatorock block	11
Figure 6 - Instron calibration setup.....	12
Figure 7 - Applied loads vs. measured loads (zero intercept equation).....	13
Figure 8 - Applied loads vs. measured loads (intercept equation)	14
Figure 9 - Torque calibration	15
Figure 10 - Water circulation system to represent wet-hole shaft installation.....	17
Figure 11 - New drilling method (left) and old drilling method (right).....	18
Figure 12 – Real-time readings showing sinusoidal wave pattern	20
Figure 13 - Torque and crowd vs. depth for a single laboratory drilling.....	21
Figure 14 - q_u vs. q_t plot with linear and 2 nd order polynomial curve fitting	26
Figure 15 - Torque vs. compressive strength (N = 20 rpm, u = 0.16 in/min)	27
Figure 16 - Force vs. compressive strength (N = 20 rpm, u = 0.16 in/min)	28
Figure 17 - Torque vs. tensile strength (N = 20 rpm, u = 0.16 in/min).....	28
Figure 18 - Force vs. tensile strength (N = 20 rpm, u = 0.16 in/min)	29
Figure 19 - Torque vs. compressive strength (N = 20 rpm, u = 0.28 in/min)	29
Figure 20 - Force vs. compressive strength (N = 20 rpm, u = 0.28 in/min)	30
Figure 21 - Torque vs. tensile strength (N = 20 rpm, u = 0.28 in/min).....	30
Figure 22 - Force vs. tensile strength (N = 20 rpm, u = 0.28 in/min)	31
Figure 23 - Torque vs. compressive strength (N = 20 rpm, u = 0.40 in/min)	31

Figure 24 - Force vs. compressive strength (N = 20 rpm, u = 0.40 in/min)	32
Figure 25 - Torque vs. tensile strength (N = 20 rpm, u = 0.40 in/min)	32
Figure 26 - Force vs. tensile strength (N = 20 rpm, u = 0.40 in/min)	33
Figure 27 - Torque vs. compressive strength (N = 40 rpm, u = 0.32 in/min)	33
Figure 28 - Force vs. compressive strength (N = 40 rpm, u = 0.32 in/min)	34
Figure 29 - Torque vs. tensile strength (N = 40 rpm, u = 0.32 in/min)	34
Figure 30 - Force vs. tensile strength (N = 40 rpm, u = 0.32 in/min)	35
Figure 31 - Torque vs. compressive strength (N = 40 rpm, u = 0.56 in/min)	35
Figure 32 - Force vs. compressive strength (N = 40 rpm, u = 0.56 in/min)	36
Figure 33 - Torque vs. tensile strength (N = 40 rpm, u = 0.56 in/min)	36
Figure 34 - Force vs. tensile strength (N = 40 rpm, u = 0.56 in/min)	37
Figure 35 - Torque vs. compressive strength (N = 40 rpm, u = 0.80 in/min)	37
Figure 36 - Force vs. compressive strength (N = 40 rpm, u = 0.80 in/min)	38
Figure 37 - Torque vs. tensile strength (N = 40 rpm, u = 0.80 in/min)	38
Figure 38 - Force vs. tensile strength (N = 40 rpm, u = 0.80 in/min)	39
Figure 39 - Crowd vs. Torque (4.5" bit) with linear and 2 nd order polynomial curve fitting	40
Figure 40 - Crowd vs. Torque (6" bit) with linear and 2 nd order polynomial curve fitting	40
Figure 41 - Torque vs u/N (4.5" bit)	42
Figure 42 - Crowd vs u/N (4.5" bit)	42
Figure 43 - Torque vs u/N (6" bit)	43
Figure 44 - Force vs u/N (6" bit)	43
Figure 45 - Torque vs compressive strength with linear and 2 nd order polynomial curve fitting	44
Figure 46 - Crowd vs compressive strength with linear and 2 nd order polynomial curve fitting	45
Figure 47 - Torque vs tensile strength with linear and 2 nd order polynomial curve fitting	45

Figure 48 - Crowd vs tensile strength with linear and 2 nd order polynomial curve fitting	46
Figure 49 - D_s vs q_u plot	47
Figure 50 - D_s vs q_t plot.....	48
Figure 51 - Specific energy vs compressive strength.....	51
Figure 52 - Specific energy vs tensile strength	51
Figure 53 - D_s vs q_u (grouped by rotational speeds).....	52
Figure 54 - e vs q_u (grouped by rotational speeds)	53
Figure 55 - D_s vs q_t (grouped by rotational speeds)	53
Figure 56 - e vs q_t (grouped by rotational speeds)	54
Figure 57 - D_s vs q_u (grouped by penetration rates for 20 RPM drillings).....	55
Figure 58 - e vs q_u (grouped by penetration rates for 20 RPM drillings).....	55
Figure 59 - D_s vs q_u (grouped by penetration rates for 40 RPM drillings).....	56
Figure 60 - e vs q_u (grouped by penetration rates for 40 RPM drillings).....	56
Figure 61 - D_s vs q_t (grouped by penetration rates for 20 RPM drillings)	57
Figure 62 - e vs q_t (grouped by penetration rates for 20 RPM drillings)	57
Figure 63 - D_s vs q_t (grouped by penetration rates for 40 RPM drillings)	58
Figure 64 - e vs q_t (grouped by penetration rates for 40 RPM drillings)	58
Figure 65 - Jean Lutz monitoring system.	63
Figure 66 - O-cell strain gauge load distribution from Little River.....	64
Figure 67 - Little River boring in the footprint of the O-cell test shaft	65
Figure 68 - RPM frequency distribution.....	66
Figure 69 - Raw data torque frequency distribution	68
Figure 70 - Converted torque frequency distribution	68
Figure 71 - Raw data torque frequency distribution with rotational speed breakdown ..	69
Figure 72 - Converted torque frequency distribution with rotational speed breakdown .	69

Figure 73 - Raw data penetration rate frequency distribution.....	70
Figure 74 - Converted penetration rate frequency distribution	70
Figure 75 - Raw data crowd frequency distribution	71
Figure 76 - Converted crowd frequency distribution.....	71
Figure 77 - Rotational speed vs. elevation plot	72
Figure 78 - Penetration Rate vs. elevation plot	72
Figure 79 - Crowd vs. elevation plot.....	73
Figure 80 - Torque vs. elevation plot.....	73
Figure 81 - Raw data compressive strength vs. elevation plot.....	74
Figure 82 - Raw data compressive strength frequency distribution.....	75
Figure 83 - Raw data skin friction frequency distribution.....	75
Figure 84 - Raw data compressive strength probability plot for Normal Distribution	76
Figure 85 - Compressive strength natural log probability plot	77
Figure 86 - Raw data skin friction probability plot for Normal Distribution	77
Figure 87 - Skin friction natural log probability plot	78
Figure 88 - Compressive strength natural log frequency distribution	79
Figure 89 - Skin friction natural log frequency distribution.....	79
Figure 90 - Compressive strength probability density function.....	81
Figure 91 - Skin friction probability density function	81
Figure 92 - Compressive strength frequency distribution, SG 7 to SG6.....	82
Figure 93 - Skin friction frequency distribution, SG 7 to SG6	83
Figure 94 - Compressive strength frequency distribution, SG 6 to O-cell.....	83
Figure 95 - Skin friction frequency distribution, SG 6 to O-cell.....	84
Figure 96 - Compressive strength frequency distribution, O-cell to SG 5.....	84
Figure 97 - Skin friction frequency distribution, O-cell to SG 5.....	85

Figure 98 - Compressive strength frequency distribution, SG 5 to SG 4.....	85
Figure 99 - Skin friction frequency distribution, SG 5 to SG 4	86
Figure 100 - Compressive strength frequency distribution, SG 4 to SG 3.....	86
Figure 101 - Skin friction frequency distribution, SG 4 to SG 3	87
Figure 102 - Compressive strength frequency distribution, SG 3 to SG 2.....	87
Figure 103 - Skin friction frequency distribution, SG 3 to SG 2	88
Figure 104 - Lab drilling q_u vs q_t plot to show q_t/q_u slope	91
Figure 105 – Strength vs. specific energy	92
Figure 106 - Little River q_u vs. q_t plot to show q_t/q_u slope.....	92
Figure 107 - Little River boring and shaft locations	94
Figure 108 - Little River boring D3 q_t/q_u analysis using all elevations	94
Figure 109 - Little River boring B4 q_t/q_u analysis using all elevations	95
Figure 110 - Little River boring B5 q_t/q_u analysis using all elevations	95
Figure 111 - Little River boring B6 q_t/q_u analysis using all elevations	96
Figure 112 - Little River boring B7 q_t/q_u analysis using all elevations	96
Figure 113 - Little River boring B8 q_t/q_u analysis using all elevations	97
Figure 114 - Little River boring B9 q_t/q_u analysis using all elevations	97
Figure 115 - Little River boring q_t/q_u analysis using all elevations and boring locations	98
Figure 116 - Little River q_t/q_u analysis using all depths and boring locations, outliers removed	99
Figure 117 - Little River q_u stratification, indicating zones.....	102
Figure 118 - Little River q_t/q_u analysis using data from elevations +45' to +30' at all locations	103
Figure 119 - Little River q_t/q_u analysis, elevations +30' to 0' at all locations, outliers removed	103
Figure 120 - Little River q_t/q_u analysis using data from elevations +45' to +30' from boring B8.....	106

Figure 121 - Little River q_t/q_u analysis using data from elevations +30' to 0' from boring B8	106
Figure 122 - Bauer BG 30 crowd specs from serial plate, max crowd and operating pressure	118
Figure 123 - Bauer BG 30 specs from serial plate, showing model type and operating pressure	118
Figure 124 - Bauer BG 30 spec sheet, showing torque operating pressure and maximum crowd	119
Figure 125 - Bauer BG 30 specs, showing model type and maximum torque.....	119
Figure 126 - Overland test shaft 2 T-Z curves.....	121
Figure 127 - Overland test shaft 2 compressive strength frequency distribution for segment 2	122
Figure 128 - Overland test shaft 2 skin friction frequency distribution for segment 2 ..	122
Figure 129 - Overland test shaft 2 compressive strength frequency distribution for segment 3	123
Figure 130 - Overland test shaft 2 skin friction frequency distribution for segment 3 ..	123
Figure 131 - q_t/q_u vs q_u for concrete (Anoglu et al., 2006).....	126
Figure 132 – q_t/q_u vs. q_u for clay and limestone using Johnston's criteria	128
Figure 133 – q_t/q_u vs. q_u developed using only Little River q_u data.....	129
Figure 134 – Comparison of q_t/q_u vs. q_u curves	129
Figure 135 - Comparison of q_t/q_u vs. q_u curves with the new Florida geomaterials curve	131
Figure 136 – Florida geomaterials q_t equation	132
Figure 137 - split tension strength vs. water content with predicted q_t values for 23 Florida sites.....	133
Figure 138 - Dry unit weight vs. split tension strength with predicted and measured q_t values from 23 Florida sites	134
Figure 139 - Dry unit weight vs. split tension strength with average predicted and measured q_t values from 23 Florida sites	135
Figure 140 - Little River O-cell shaft profile, indicating strain gauge zone 8.....	139

Figure 141 - Unit side shear for each monitored strain gauge zone.....	140
Figure 142 - Kanapaha site investigation locations.....	142
Figure 143 - Seismic line EW 3 results for P-wave and S-wave and Poisson ratio.....	143
Figure 144 - Limestone recovered at a depth of 30 feet (grey clay at the top of the spoon)	144
Figure 145 - Highly weathered limestone at a depth of 30 feet.....	145
Figure 146 - Kanapaha boring locations.....	146
Figure 147 - Displays the first competent rock cores recovered at the site.....	147
Figure 148 - q_u frequency distribution for depths 40 to 45 feet.....	148
Figure 149 - q_t frequency distribution for depths 40 to 45 feet.....	148
Figure 150 - q_u frequency distribution for depths 45 to 50 feet.....	149
Figure 151 - q_t frequency distribution for depths 45 to 50 feet.....	149
Figure 152 - Failure modes in compression tests: (a) Axial splitting, (b) shearing.....	150
Figure 153 - Skin friction frequency distribution for depths 40 to 45 feet.....	151
Figure 154 - Skin friction frequency distribution for depths 45 to 50 feet.....	151
Figure 155 - MultiPier result showing (a) the induced moment by offsetting the rebar cage and (b) the demand to capacity ratio, D/C, which is used to determine the factor of safety.....	155
Figure 156 - East reaction shaft profile.....	157
Figure 157 - East reaction shaft steel cross-section – layout 1.....	158
Figure 158 - East reaction shaft steel cross-section – layout 2.....	159
Figure 159 - Test shaft profile.....	160
Figure 160 - Test shaft steel cross-section.....	161
Figure 161 - West reaction shaft profile.....	162
Figure 162 - West reaction shaft steel cross-section – layout 1.....	163
Figure 163 - West reaction shaft steel cross-section – layout 2.....	164
Figure 164 - SoilMec SR30 drill rig.....	165

Figure 165 - Rotational speed sensor	167
Figure 166 - Penetration rate sensor	168
Figure 167 - Compartment where torque and crowd sensors and the junction box was placed	169
Figure 168 - SoilMec SR30 operator's manual displaying torque and crowd sensor ports	170
Figure 169 - Geokon 4200 vibrating wire strain gauge attached to rebar cage.....	171
Figure 170 - East shaft rebar cage displaying instrumentation	172
Figure 171 - Test shaft displaying instrumentation.....	173
Figure 172 - Rebar cages displaying instrumentation	174
Figure 173 - East reaction shaft real-time drill monitoring.....	176
Figure 174 - Rebar cage being lifted by two cranes to reduce bending	177
Figure 175 - Rebar cage being placed over the hole	178
Figure 176 - Rebar cage hung using chains and shaft being concreted	179
Figure 177 - East shaft completed	180
Figure 178 - Test shaft real-time drill monitoring.....	181
Figure 179 - Rebar cage being placed into the hole	182
Figure 180 - Rebar cage hung by chains before concreting.....	183
Figure 181 - Test shaft with beauty ring placed before final leveling.....	184
Figure 182 - West shaft real-time monitoring	185
Figure 183 - West shaft displaying slurry loss.....	186
Figure 184 - West shaft cave-in and slurry loss	187
Figure 185 - West shaft cave-in and slurry loss down to the water table	188
Figure 186 - West shaft before final leveling and elevation adjustment	189
Figure 187 - Reaction shaft adapter secured to the shaft	190
Figure 188 - Girders being placed on the reaction shaft adapters and leveled	191

Figure 189 - Cross beam being secured in place on top of the girders	192
Figure 190 - Completed load frame setup.....	193
Figure 191 - Steel plates being secured between the load cell and loading pyramid..	193
Figure 192 – q_u frequency distribution – 40 to 45 feet.....	196
Figure 193 – q_u frequency distribution – 45 to 50 feet.....	197
Figure 194 – q_u frequency distribution of individual shafts – 40 to 45 feet	198
Figure 195 - q_u frequency distribution of individual shafts – 45 to 50 feet	198
Figure 196 – East Shaft q_u Frequency Distribution, 40 ft to 45 ft.	200
Figure 197 - Test Shaft q_u Frequency Distribution, 40 ft to 45 ft.	201
Figure 198 - West shaft q_u frequency distribution, 40 ft to 45 ft.....	202
Figure 199 - East shaft q_u frequency distribution, 45 ft to 50 ft.....	203
Figure 200 - Test shaft q_u frequency distribution, 45 ft to 50 ft.....	204
Figure 201 - East shaft q_u frequency distribution, 45 ft to 50 ft.....	205
Figure 202 - Test shaft q_u frequency distribution.....	206
Figure 203 - Test Shaft f_s frequency distribution	207
Figure 204 - Test shaft depth vs. q_u	207
Figure 205 - Test shaft depth versus skin friction.....	208
Figure 206 - Test shaft depth vs. specific energy.....	208
Figure 207 - Test shaft q_u frequency distribution with zero specific energy data points removed	212
Figure 208 - Test shaft: f_s frequency distribution with zero specific energy data points removed	213
Figure 209 - East shaft q_u frequency distributions.....	213
Figure 210 - East shaft f_s frequency distribution.....	213
Figure 211 - East shaft depth vs. compressive strength	214
Figure 212 - East shaft depth vs. skin friction	214

Figure 213 - East shaft depth vs. specific energy	215
Figure 214 - West shaft q_u frequency distribution.....	215
Figure 215 - West shaft f_s frequency distribution.....	216
Figure 216 - West shaft depth vs. compressive strength	216
Figure 217 - West shaft depth vs. skin friction	217
Figure 218 - West shaft depth vs. specific energy	217
Figure 219 - Test shaft strain gauge load distribution	218
Figure 220 - East shaft strain gauge load distribution	219
Figure 221 - West shaft strain gauge load distribution	219
Figure 222 - Test Shaft T-Z curves	221
Figure 223 - East and West Shaft T-Z curves	221
Figure 224 - Unit side shear comparison from all monitoring sites.....	227
Figure 225 - Unit side shear bias analysis	228
Figure 226 - Unit side shear bias analysis (rig malfunction section removed).....	229

CHAPTER 1 INTRODUCTION

Foundation design is an engineering practice moving from experience to science and math-based principles. Foundation engineers must consider multiple layers of soil and rock with limited a priori information and high levels of variability. However, new codes based on reliability, such as Load and Resistance Factor Design, LRFD, allow designers to increase resistances if they are capable of reducing the uncertainty of in situ soil and rock conditions.

In Florida, over 90% of the Florida Department of Transportation “FDOT” structures are founded on deep foundations, including driven piles and drilled shafts. However, due to the limited availability of sizes as well as noise and vibration issues encountered during driven pile construction, drilled shafts have seen an increased use over the past 20 years. Unfortunately, the development of drilled shaft construction monitoring to assess shaft capacity has lagged that of driven piles. This leads to a high degree of uncertainty and results in lower resistance factors in LRFD design.

Of great interest is the assessment of soil/rock strength properties during the shaft construction process (i.e., drilling) to account for subsurface variability. For instance, shown in Figure 1 is the mean and standard deviation of the rock’s strength by boring at 17th Street Bridge in Fort Lauderdale, Florida. Based on obtained core data, the shaft located at coordinates ($x = 9$, $y = 24$) would have nearly half the axial capacity of the shaft located at ($x = 18$, $y = 10$), approximately 16.5 feet away. In the case of redundant shafts, coring used for design may only be taken in a few areas and not necessarily within the footprint of each shaft. This could lead to a large overestimation of a shaft’s capacity and result in catastrophic failure. For the case of non-redundant shafts, the FDOT requires coring within the footprint of each shaft for visual inspection (i.e., presence of rock or not), but testing the cores to assess rock strength is not performed as this delays construction. Consequently, if the strength of the soil/rock could be assessed in real time by monitoring the drilling process, the degree of uncertainty in the shaft’s true capacity would be greatly reduced. This would provide quality assurance to the foundation engineer and the drilling contractor. In addition, construction costs could be reduced by eliminating the need to greatly overdesign to account for the uncertainty and variability of in situ soil/rock conditions.

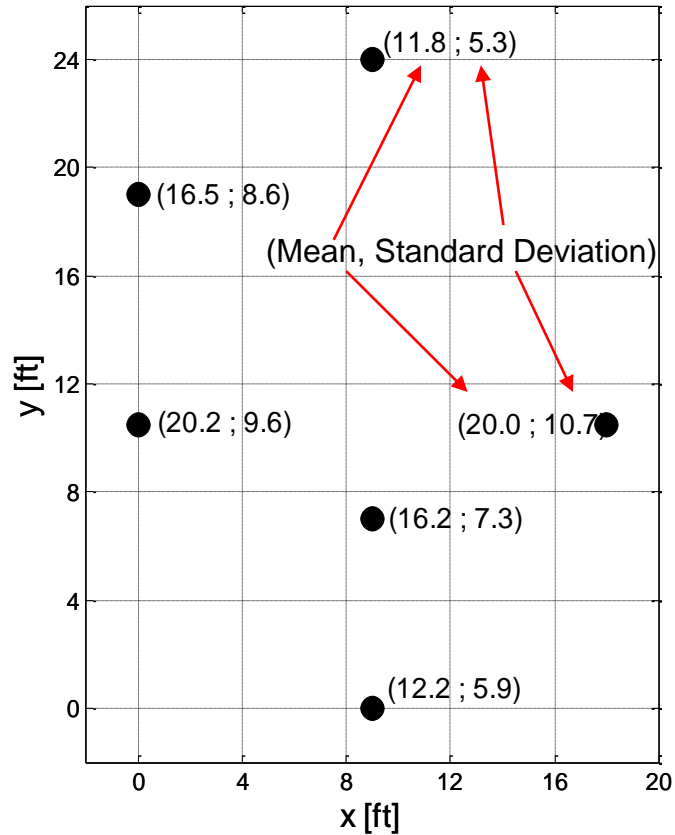


Figure 1 - Spatial profile of boring rock strength at 17th Street Bridge, Fort Lauderdale

1.1 Background

Assessment of rock strength during drilling is an active research area in the “Energy Resource” fields, such as oil and gas recovery (Hoerock and Bratcher, 1996; Karasawa et al., 2002a). Within these fields the focus is on controlling the drilling process to limit damage and improve drilling efficiency, which is controlled by in-situ rock strength. Karasawa et al. (2002a, 2002b) showed that in-situ rock strength is correlated to the following five drilling parameters:

1. Crowd or downward axial force, F
2. Vertical penetration rate, u
3. Torque applied to the drilling bit, T
4. Drilling tool diameter, d
5. Rotational speed of drilling tool, N

He noted that $8T/d^2$ at a given Fu/N , tends to increase with increasing rock strength, and the effect of tooth wear on the relationship for each rock is small. Karasawa goes

on to describe the slope of u/N vs. F/d as a_F and u/N vs. $8T/d^2$ as a_T and develops the “drillability strength of rock”, D_s , expressed as a_F/a_T^2 . He then found that D_s was directly correlated to the unconfined compressive strength of rock, S_c or q_u , as shown in Figure 2 for different types of rock.

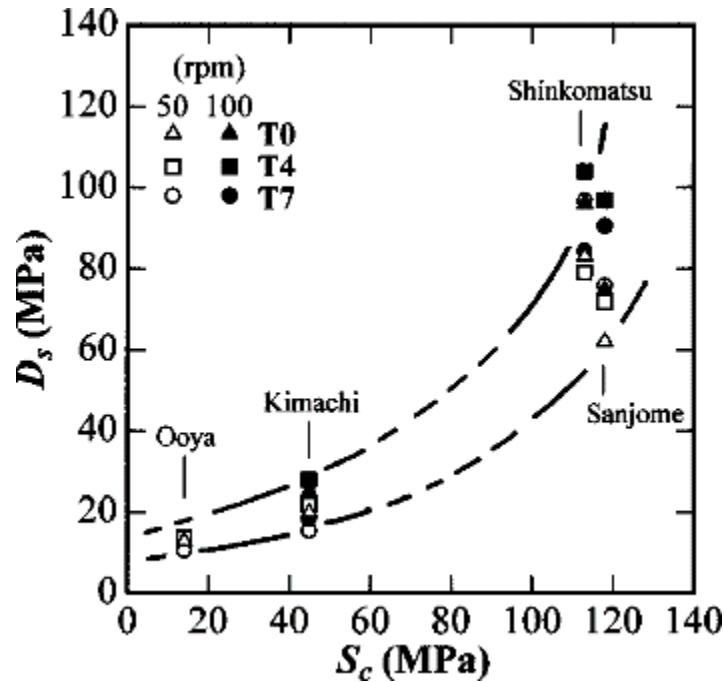


Figure 2 - Relationship between uniaxial compressive strength of rock, S_c , and drillability strength of rock, D_s (Karasawa et al., 2002)

Evident from Figure 2 is the existence of correlation between “drillability strength” and unconfined compressive strength (rock strength). Also of interest is the existence of correlation between drilling parameters and the splitting tensile strength, q_t , of rock, and if the same correlation would hold for different Florida limestone formations (e.g., Ocala, Suwannee, Avon Park, etc.). Once the strength of rock is assessed, the unit skin friction or side shear capacity of the drilled shaft may be determined using various methods, providing a means to assess shaft capacity in real time.

1.2 Scope

The goal of this research was to provide a viable method for monitoring drilled shaft installations in real time during the drilling process, reducing spatial uncertainty concerns and providing a means to measure the capacity of drilled shafts socketed into Florida limestone. Currently, there are no methods to quantify production shaft capacities during installation similar to driven piles. This generally results in a few costly load tests to be performed on a site. Unfortunately the limited load tests do not address the spatial variability concerns, i.e., Figure 1. Therefore, the current goal is to validate the monitoring process and capacity estimates by comparing the results obtained during

monitoring with conventional methods (i.e., load tests and core data). In order to accomplish this goal, the research included the following four tasks:

1. Completing laboratory drillings using planned design strengths and recording drilling parameters F , u , T , N , d . (Task 1).
2. Developing relationships for soil/rock strength from the laboratory monitored drilling parameters. (Task 2)
3. Monitoring “pilot project” field drillings using drilling parameters recorded from the drill rig, validating the drilling parameter-rock strength relationship developed in the lab and developing final drilling equations. (Task 3)
4. Validating the finalized drilling equations by comparing monitored drilling measurements of rock strength to lab tested core strengths and results from a final top down static load test. (Tasks 4 and 5)

During the drilling process, monitoring will provide real time compressive strength estimates, which can be used to ensure the material being drilled meets the expectations of the shaft design. It is important to identify monitoring resistance in terms of compressive strength as this is the conventional strength property used for estimating drilled shaft capacities. This approach also provides the option to use numerous drilled shaft design methods to estimate shaft capacity during the installation process. This is important because engineers may use different methods (FDOT, Kulhawy, Gupta, etc.) to estimate shaft capacity and nearly all of the methods rely on compressive strength data. For this research, shaft capacity estimates based on compressive strength will only focus on one method. This will be the current FDOT recommended method for estimating shaft capacity using laboratory strength data.

To monitor the operational drilling parameters (F , T , N , u , and d) on known in-situ rock strengths, a series of laboratory tests had to first be performed. A synthetic limestone (Gatorock) was cast with a range of rock strengths representative of Florida limestone (soft-weathered, medium and strong). The specimens were constructed from ground up limestone (screenings), cement and water and constructed to be homogenous throughout. Specimens were drilled using two different rock auger bit diameters, two rotational speeds and three penetration rate settings. Torque and crowd were continuously monitored and recorded in real time throughout each drilling test. Next, relationships such as Karasawa et al. (2002a, 2002b) and Teale (1965) were investigated for estimating rock strength. The investigation was the basis for the development of strength parameters, q_u and q_t , to assess the skin friction (side shear), f_s , of drilled shafts using monitored drilling parameters.

To measure T , F , N , and u on the drill rig for field monitoring, hydraulic pressure lines controlling crowd and torque had to be tapped with individual pressure transducers. The recorded pressures were then converted to physical measures (i.e., lbf for crowd and in-lbs for torque) for compatibility with laboratory drilling equations. Measuring rotational speed of the drilling tool, N , required a proximity sensor to be attached near

the rotating collar of the rotary table with no conversion necessary for compatibility. Vertical movement of the drilling tool, u , was monitored from line movement of the cabling attached to the Kelly bar and main winch using a rotary encoder. Penetration rate was determined as a function of movement per unit time with no conversion necessary for compatibility. All drilling parameters and estimated strengths were recorded and displayed as a function of depth as the drilling tool was advanced.

For comparison purposes, drilled shafts with planned load testing (i.e., axial load tests) were monitored. The load test results were compared to the estimated side shear from monitored drilling parameters and estimated strengths, q_u and q_t . Rock samples recovered from cores adjacent to the test shafts were also used in the comparative analysis. The rock specimens recovered in the field were tested in the lab (State Materials Office, SMO) for both unconfined compression, q_u , and split tension, q_t . Of great interest, is the q_t/q_u relationship of the recovered rock specimens and how this relationship changes with various limestone formations throughout the state of Florida. It was expected to accurately assess a shaft's capacity, adjustments for site specific limestone formations, q_t/q_u , may be required.

Finally, the research was validated with the full scale monitoring of three drilled shaft installations in combination with a top down static load test; where the reaction shafts were also instrumented and measured for uplift. Prior to the shaft installations, core samples were recovered and tested at the SMO. A static prediction of each shaft's capacity was performed using FDOT methods. For the measured results, the steel reinforced cage for both the test and reaction shafts were instrumented at a number of locations to assess T-Z curves from the static load test. During shaft construction, drilling parameters, F , T , N , u , and d , were monitored and recorded. The in-situ rock strength was assessed and used to provide an estimate of side shear over multiple rock layers. Comparisons of the monitored drilling, laboratory core testing and measured skin friction (load test) were then performed for each instrumented layer of the shaft; as well as a comparison of total side resistance.

CHAPTER 2 LABORATORY MEASUREMENTS OF DRILLING PARAMETERS ON SYNTHETIC LIMESTONE

2.1 Development of Synthetic Limestone, Gatorock

To develop relationships for drilling parameters and compressive strengths of limestone, a series of laboratory drillings needed to be conducted on a wide range of limestone compressive strengths. Obtaining large limestone rocks to drill into, similar to Karasawa et al. (2002a, 2002b), was not practical. As well, uniformity issues were a concern since Florida limestone can be quite variable from sample to sample and may produce poor results. Therefore, a homogenous drilling medium needed to be developed that was representative of Florida limestone.

In past UF research, synthetic limestone, known as “Gatorock”, was developed and used in a number of laboratory experiments including: Bullock (2004), McVay et al. (2004), and Sheppard et al. (2006). Gatorock provides a simplistic method to model natural Florida limestone with the ability to control the desired compressive strength. Also, by using a synthetic limestone, it enables the creation of a homogenous formation with a wide range of design strengths typical of limestone found throughout Florida. For this research the Gatorock needed to be created in a simplistic manner and easily repeatable for various compressive strengths. It also needed to be developed at 14-day strength to provide a quick turnaround for laboratory drillings as well as maintain moisture within the synthetic rock, which is typical of in-situ limestone.

Gatorock mixtures generally consist of limestone screenings (crushed limestone), cement and water. Limestone screenings, are a fine aggregate with 100% passing a #4 sieve, and are ideal for use in Gatorock production as the smaller well graded aggregate sizes (<4.75 mm) provide a homogenous mixture. This eliminates the risk that a single larger sized piece of aggregate will greatly influence the overall material properties of the synthetic rock mass. Florida Portland cement combined with water was used as the bonding agent within the synthetic rock matrix, drastically speeding up the natural limestone bonding process which typically occurs over thousands to millions of years. Florida Portland cement is an ideal substitute to natural bonding agents as the main ingredient of Portland cement, calcium oxide (CaO), is derived from limestone. In the natural limestone formation process, calcite (CaCO₃) precipitate accumulates to form a carbonate matrix, which holds together larger carbonic sedimentary rocks to form a limestone rock mass. As the calcite precipitate accumulates, inclusions of sand, clay and organic matter are deposited within the matrix. This produces a carbonate matrix, which often includes impurities such as iron, silica, magnesium and in some cases aluminum. These impurities are the additional chemical ingredients found in Florida Portland cement, reinforcing the concept of Portland cement being an ideal replacement to natural bonding agents.

The development of Gatorock for this research began using guidelines of a Controlled Low-Strength Material, CLSM, reported by ACI Committee 229. CLSM guidelines were used because compressive strengths of a CLSM are relatively low, 1,200 psi or less, and initial Gatorock design strengths were to be 70, 140 and 280 psi (later changed to 140, 280, 556, 1,667 psi). Conventional CLSM mixtures consist of water, Portland cement, fine or coarse aggregate or both and fly ash or similar products. However, the use of standardized materials is not necessary. ACI 229 (1999) states, the selection of materials should be based on availability, cost, specific application and the necessary characteristics of the mixture, including flowability (slump), strength (compressive strength), excavatability (drillability) and density (unit weight). As screenings are generally considered a waste material, ACI 229 provided a standard method of using non-standard materials to develop a homogenous drilling medium that is representative of Florida limestone.

The total unit weight of a CLSM typically ranges from 115-145 pounds per cubic foot, pcf, which is within the typical range of Florida limestone, 95 -165 pcf, recovered in core samples throughout the state. The Gatorock developed using CLSM guidelines produced unit weights, γ , ranging from approximately 105 pcf to 125 pcf which is in agreement with typical Florida limestone. Additionally, the properties of CLSMs cross boundaries between soils and concrete according to ACI 229 and "in service" CLSMs (compressive strength of 50 -100 psi) exhibit characteristic properties of soils and equate to an allowable bearing capacity of a well-compacted soil (ACI 229, 1999). This is beneficial as field drilling will pass through several layers of varying material (sand, clay, limestone and intermediate geo-material, IGM) and laboratory drillings will only focus on drilling into material representative of limestone. However, it is possible that lower strength Gatorock could be representative of some higher compacted in-situ soils encountered in field drillings.

Once all of the Gatorock mix designs were complete, a method for casting large scale Gatorock blocks (22.5" x 22.5" x 40") used for laboratory drilling was developed. However, the target strength of the large scale blocks had to be verified to ensure reported compressive strengths for each block matched those of test cylinders cast from the same mix. For verification, five blocks were cored using a four inch core barrel, each providing a core sample approximately eight inches long by four inches in diameter, matching the cast cylinder dimensions, and providing a 2:1 ratio which is compliant with ASTM (2002) standards for compression testing of field cores. The cores and test cylinders from each Gatorock block were then subjected to unconfined compression testing and compared based on their compressive strengths. The following results were obtained:

Table 1 - Compressive strength results for Gatorock cores and cast cylinders

Cylinder 1	Cylinder 2	Cylinder 3	Avg qu (psi)	Core qu (psi)	% diff
348	334.2	341	341.1	381.4	10.57%
462.4	461.8	502.2	475.5	528	9.94%
520.6	490.9	445.9	485.8	489.7	0.80%
278.4	293.3	266.7	279.4	315.3	11.39%
360.2	355.3	360.4	358.7	347.9	-3.10%

From the core results, Table 1, it is evident that the majority of cores produced compressive strengths slightly higher than the cast cylinders. This was considered acceptable as the differences in strength were relatively low, generally 10% or less, and inherently created a conservative approach for estimating rock strength. This completed the Gatorock development and provided an accurate homogenous synthetic representation of Florida limestone used in all laboratory drilling and subsequent analyses.

2.2 Development of a Laboratory Drilling Environment

In order to conduct measured small scale drillings, instrumentation and monitoring equipment had to be developed. This consisted of modifying an existing drill press to meet field drilling standards, developing a coupler system to monitor drilling parameters in real time using a wireless data transmitter, locating small scale drill bits that best represent the cutting action of field drill bits, calibrating all the equipment and developing a reliable drilling method to best represent field drilling. Additionally, methods for analyzing the data had to be developed.

2.2.1 Coupler System to Monitor Laboratory Drilling

The majority of the work developing the laboratory drilling environment was creating the coupler system to monitor drilling parameters in real time. The rotational speed and penetration rate were set parameters controlled by a variable frequency drive installed on the drill press to provide rotational speeds typical of field drilled shaft installations based on survey results. However, torque and crowd were a byproduct of these set of drilling parameters and needed to be continuously monitored and recorded in real time. To achieve this, strain gauges and torque rosettes were placed on an Aluminum drill rod, connecting the drill bit to the drill press, and transmitted wirelessly to an external computer using a wireless data transmitter. A wireless data transmitter was used because constant rotation during drilling prevented the use of wires running to an external computer. The strain gauges and torque rosettes were setup in a full bridge system to compensate for temperature effects. Each gauge type (torque and crowd), was oriented 180 degrees apart to compensate for bending. The alternating gauge types were oriented 90 degrees apart from each other as seen in Figure 3.

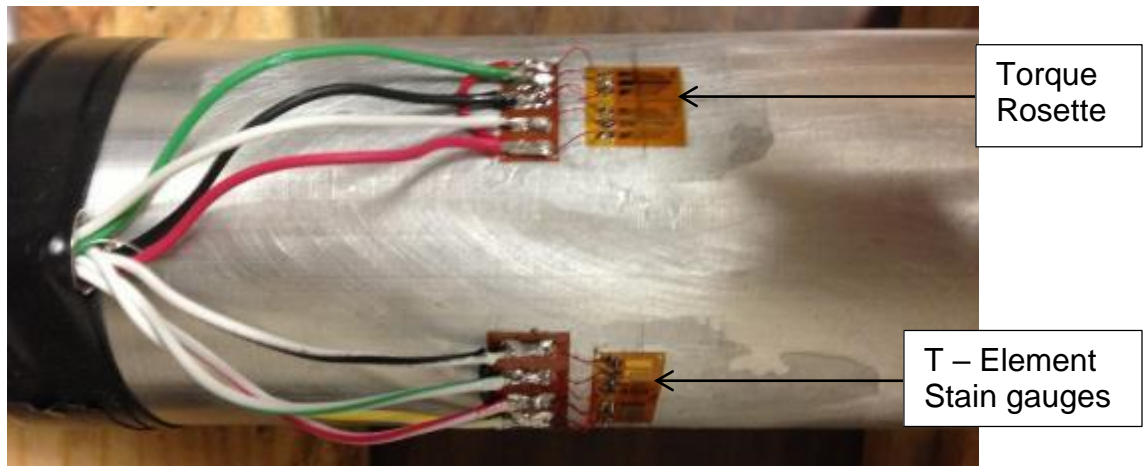


Figure 3 - Instrumented drill rod

The wall thickness of the aluminum rod, Figure 3, was designed to withstand the applied drilling forces while providing a large enough strain range to reduce noise within the system and ensure accurate readings. The length of the drill rod was designed to provide an undisturbed portion of the shaft two and a half times the rod diameter from each end to the gauges. This eliminated edge effects (Saint-Venant's principle) and also ensured accurate readings. Finally, the full length of the coupler system was designed to fit the available clearance between the chuck of the drill press and the Gatorock blocks which rested on the floor. **Error! Reference source not found.** shows the developed laboratory coupler system and drilling setup.

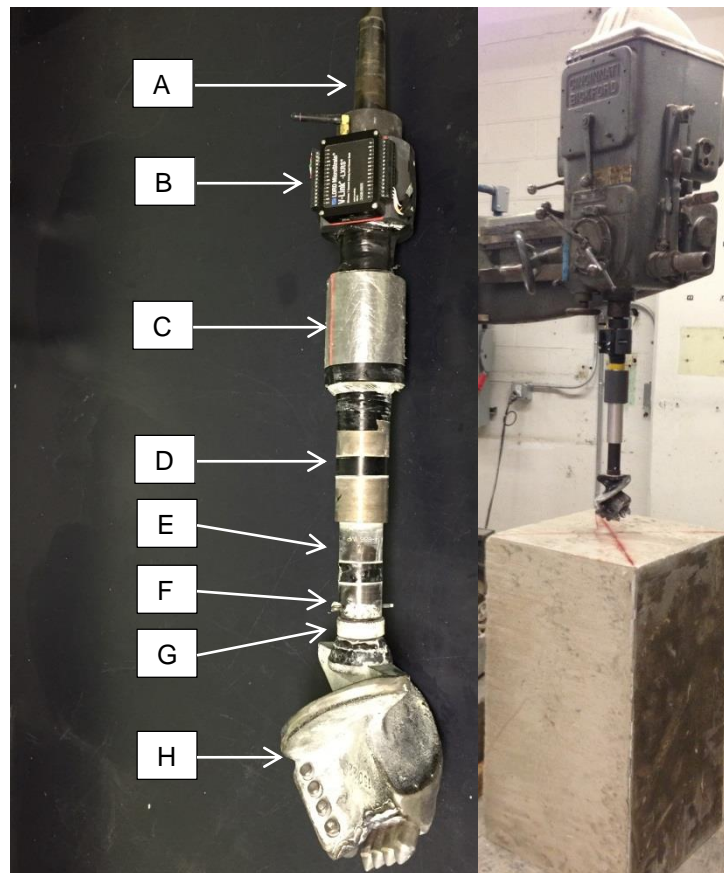


Figure 4 - Laboratory coupler system (Left) and laboratory drilling set-up (Right). A) Chuck connecting the coupler to the drill press. B) Wireless data transmitter mounted on PVC sleeve with rubber padding to reduce vibrations. C) PVC shield protecting strain gauges and torque rosettes. D) Aluminum drill rod where torque and crowd are monitored. E) Connection collar between the drill rod and the drill bit. F) Pin lock similar to drilled shaft Kelly bar drill bit connections. G) Spacer to reduce wobbling at the drill bit connection. H) Small scale rock auger bit with rotating conical carbide teeth.

The coupler's main shaft is a hollow cylinder with a one inch inner diameter and two inch outer diameter constructed from an aluminum rod, fourteen inches in length. The base of the main shaft has male threading which attaches the connection collar. The connection collar connects the drill bit using a pin lock system similar to a drilled shaft rig Kelly bar connection. Between the collar and the drill bit is a steel washer that helps reduce wobbling of the bit at the pin lock connection. At the top of the main shaft a sch. 80 PVC sleeve was mounted that allows the data transmitter to be attached. Rubber compression padding was used between the main shaft and the PVC sleeve to reduce vibrations felt by the data transmitter which may disturb readings. The top four inches of the main shaft have female inner threading that allows the drill bit chuck to be threaded to the main shaft. The drill bit chuck connects the coupler to the drill press. The remaining ten inches are where monitoring takes place. This provides an

undisturbed portion of the drill rod five inches in both directions meeting the two and a half diameter spacing required to eliminate end effects. A separate Sch. 80 PVC shield protects the gauges from being damaged while drilling. Figure 5 shows the coupler in action, drilling 20 inches into a large Gatorock block.



Figure 5 - Coupler system drilling into a large Gatorock block

After the coupler system was constructed, equations for measuring torque and crowd in real time were developed for the data transmitter software. This required deriving a transfer function for the aluminum shaft that directly converted the strain gage readings, wirelessly transmitted in bits, to measures of torque and crowd. After the transfer function equations were developed for both torque and crowd, a thorough calibration process took place ensuring the readings obtained were highly accurate.

2.2.2 Laboratory Coupler Calibration

At the start of phase II drilling, the researchers investigated the accuracy of the axial forces being recorded during laboratory drillings. The initial investigation that took place in Phase I of the project used axial loads below 55 lb for the calibration. Throughout numerous drillings (i.e., in phases I and II) the recorded axial forces were found to exceed 55 lbs. Therefore the researchers performed another axial calibration using loads of 50, 100, 250, 500, 1,000 and 1,500 lb. To complete the calibration, the Instron device, located on UF's campus, was used to monitor the loading. The setup is shown in Figure 6.



Figure 6 - Instron calibration setup

Before loading was applied, researchers leveled the drill rod with a vertical level. However, much like the laboratory drilling process, eccentric loading was expected. As a result, one side of the rod could experience tension while the other side exhibited compression. During laboratory drilling, this behavior was generally a result of the layout of the drill bit, i.e., line of carbide teeth at different orientations. However, by orienting strain gauges 180 degrees apart, the effects of eccentric loading are eliminated through averaging.

For the calibration using the Instron, a program was created to initiate constant loading for two minutes at each load step. Before and after each load step, a two minute resting period was initiated where no load was applied. Measurements were continuously recorded during the resting period to ensure readings returned to the initial baseline. Averages of the before and after readings were then subtracted from the readings taken during the two minute loading period which provided the actual load measured. In the two minute loading period, 960 readings (recording at 8 Hz for 120 seconds) were captured with 800 of the readings used to create the average for each load step. Table 2 shows the results from the Instron axial calibration.

Table 2 - Instron calibration results

Loading Phase	CH 2	CH 2 Bal	CH 4	CH 4 Bal	Final AVG (lbf)
Baseline 1	24.62		-0.83		
250 lbs	-175.92	-200.78	-328.32	-325.53	263.15
Baseline 2	25.10		-4.76		
500 lbs	-408.84	-434.73	-613.43	-603.09	518.91
Baseline 3	26.69		-15.93		
1000 lbs	-790.00	-816.82	-1253.09	-1237.90	1027.36
Baseline 4	26.95		-14.45		
1500 lbs	-1075.70	-1105.89	-2005.15	-1987.24	1546.56
Baseline 5	33.43		-21.37		
100 lbs	-21.16	-54.56	-171.72	-150.57	102.56
Baseline 6	33.36		-20.93		
50 lbs	4.78	-29.30	-88.52	-68.31	48.80
Baseline 7	34.80		-19.49		

From the collected data two equations were developed, one fitting all the data with a non-zero intercept and the other with a zero intercept. Figures 7 and 8 display the plotted data as measured load vs. applied load for the two scenarios and provides the calibration equations.

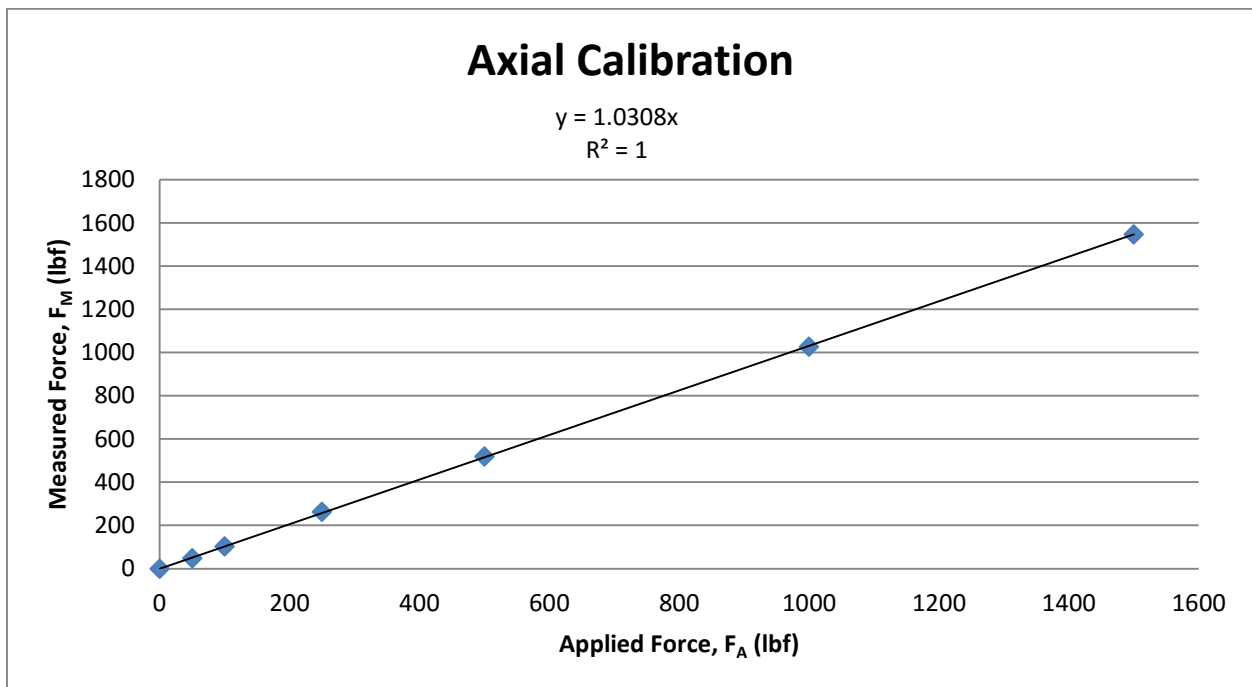


Figure 7 - Applied loads vs. measured loads (zero intercept equation)

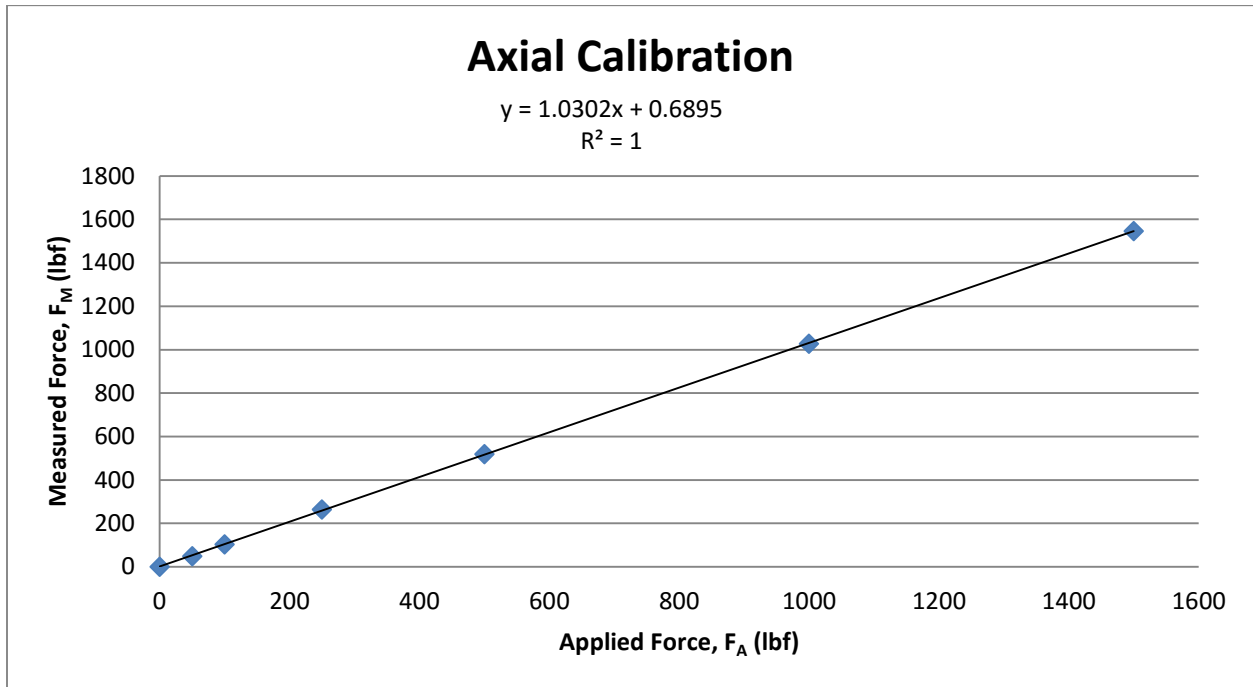


Figure 8 - Applied loads vs. measured loads (intercept equation)

As seen in the two plots, both show an $R^2 = 1$ confirming a linear fit using either equation. Researchers then compared both equations using the tabular data to determine which provided the best fit. Seen here is the tabular comparison using both equations:

Table 3 - Equation comparison and results

Applied Force (lbf)	Measured Force (lbf)	% diff	$y = 1.0302x + 0.6895$		$y = 1.0308x$	
			Adjusted Force (lbf)	% diff	Adjusted Force (lbf)	% diff
0	0	0	0	0	0	0
50	48.80	2.40%	46.70	6.60%	47.34	5.31%
100	102.56	-2.56%	98.89	1.11%	99.50	0.50%
250	263.15	-5.26%	254.77	1.91%	255.29	2.12%
500	518.91	-3.78%	503.03	0.61%	503.41	0.68%
1000	1027.36	-2.74%	996.57	0.34%	996.66	0.33%
1500	1546.56	-3.10%	1500.56	0.04%	1500.35	0.02%
Sum		-15.05%	Sum	10.60%	Sum	8.97%
Avg		-2.51%	Avg	1.77%	Avg	1.49%

From the tabular comparison, the equation with a zero intercept provided the least amount of error and was therefore the equation chosen to make the final adjustments.

Also investigated was the effect a torque load had on the axial force measurements. When applying an axial force, the torque rosettes are designed to experience no loading and this was noticed during axial calibration. However, when a torque load is applied to the system the axial strain gauges do react and this needed to be investigated to ensure results were being reported accurately. Seen below is the torque calibration setup and data recorded from the calibration, where the moment arm was 16 inches:



Figure 9 - Torque calibration

Table 4 - Torque calibration results showing offsetting axial force values (Ch 2 and 4)

M (in-lbs)	W (lbs)	Ch-1	Ch-2	Ch-3	Ch-4	%Diff 1-3	%Diff 2-4
140.8	8.8	-141.34	-55.20	-143.87	54.59	1.79%	1.10%
281.6	17.6	-283.02	-101.77	-283.22	99.32	0.07%	2.41%
422.4	26.4	-423.09	-145.16	-422.82	139.65	-0.06%	3.80%
563.2	35.2	-561.30	-186.70	-560.20	183.56	-0.20%	1.68%

Comparing channels 2 and 4 (axial force gauges) showed that the percent difference between them was very small, i.e., negligible. Channel 2 is negative (compression) and channel 4 is positive (tension). Since the values were nearly equal for every torque loading, but opposite in sign, this suggests that even though the torque loading does provide axial loading, they negated each other out on summing. The average error recorded for applied forces versus measured forces (coupler) were 1.49% for crowd (Table 3) and 0.60% for torque (Table 4, Channels 1 and 3). This confirmed the derived transfer functions for both torque and crowd were accurate, and the system was functioning properly.

2.2.3 Laboratory Drilling Procedure

Once the calibration was complete, a standard laboratory drilling procedure was developed from a thorough investigation of how to drill in the laboratory. The investigation included comparing wet and dry drilling, investigating the number of drillings that could be obtained per block without disturbance, and the lengths of drill runs to prevent “bit bite” which result in spikes in torque and crowd readings.

From the investigation, it was determined that two holes could be drilled into each block without disturbance, drill runs could only be four inches in depth before bit bite set in causing large spikes in readings, and a wet-hole drilling method was required as dry-hole drilling produced a 70% increase in torque on average. In the field, wet-hole construction is almost always used and laboratory drillings needed to be representative of field conditions. Dry-hole drilling was investigated to see if the laboratory drilling process could be simplified. However, the drastic increases in torque from dry drilling compared to wet drilling proved that using a wet-hole drilling method in the lab was unavoidable. Therefore, a water circulation system was developed to best represent field drilling conditions.

In the field as the drill bit is advanced, material is collected on the drill bit and brought back to surface where the bit is removed from the hole and the debris is spun off the bit, cleaning the bit for the next advancement. This process is constantly repeated throughout drilling as this is the only way to remove drilled debris from the hole. Unfortunately, this was not practical in the lab as this process takes nearly ten minutes every time the bit is removed for cleaning and added a significant amount of time to the already lengthy laboratory drilling process. Laboratory drilling times ranged from one to four hours depending on the penetration rate used. Therefore a water circulation system was designed that constantly removed water with drilling debris in suspension from the hole while injecting clean water. The rotation of the bit kept drilling debris in suspension for easy removal. This in combination with shorter drill runs greatly reduced bit bite and provided consistent readings. Figure 10 shows the water circulation system developed to represent the wet-hole construction method most often used in real shaft installations.

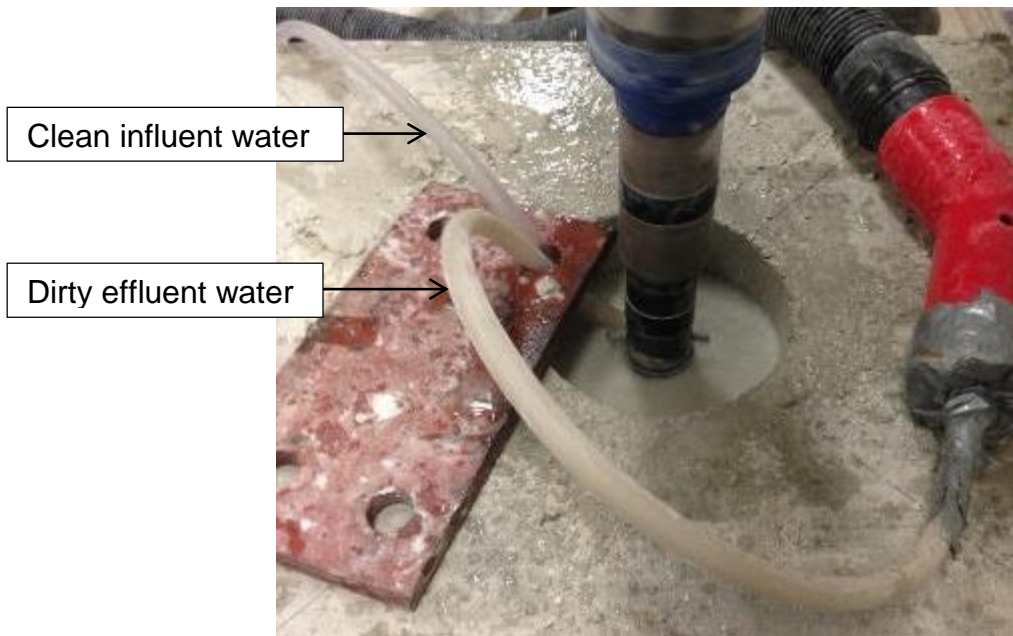


Figure 10 - Water circulation system to represent wet-hole shaft installation

For Phase II of the project, a dedicated laboratory driller was assigned to the project. The dedicated driller began training using leftover blocks from Phase I. During the training sessions, lead researchers were free to observe the drilling process and develop a standard drilling procedure. In previous drillings in Phase I, the drilling procedure was as follows:

- 1 Drill to a depth of 8 inches using the dry drilling method
- 2 Realign the drill head to advance the bit further down the hole
- 3 Add water to the hole via pouring it in with a cup
- 4 Resume drilling, advancing the bit approximately 9 inches continuously removing water via a wet vac and adding water with the cup.
- 5 Remove the bit from the hole
- 6 Remove debris from the bit and the hole (debris removed from hole via shop vac)
- 7 Reattach the cleaned bit
- 8 Lower the drill head and drill the remaining 3 inches

Now that researchers were able to continuously observe the live streamed data, it was noticed that towards the end of the first drill run, there was an increase in torque and force. Researchers decided to shorten the length of each drill run. Instead of advancing the bit 9 inches, the bit would be advanced in 6 inch increments once the initial 8 inches of dry drilling was completed. However, while observing the new method, an increase in both torque and force was observed again. However, the increase was less drastic and when the bit was removed from the hole there was less debris caked on the bit. It was then decided to use 4 inch increments after the initial 8

inches of dry drilling were complete. Along with the new incremental drilling length, a continuous injection of clean water was added to the system via a controlled nozzle attached to a garden hose. This provided a continuous circulation of clean water to the hole as the wet vac removed the water with suspended solids in it. With shortened drill runs and the new water circulation system, the data became far more uniform throughout drilling and eliminated the increase in torque and force observed at the end of each drill run. Moreover, it was observed that, the bit was far less caked with debris when removed from the hole. Images can be seen here:



Figure 11 - New drilling method (left) and old drilling method (right)

The new method for laboratory drilling is as follows:

- 1 Drill to a depth of 8 inches using the dry drilling method
- 2 Remove the bit from the hole
- 3 Remove debris from the bit and the hole (removed from hole via shop vac)
- 4 Reattach the cleaned bit
- 5 Lower the drill head and drill 4 inches using the wet method with constant water circulation
- 6 Repeat steps 2-5 until desired drilling depth is reached (20 inches)

The new drilling method was used for the remainder of laboratory drillings. After researchers discovered the four inch incremental drilling method produced the least amount of variability, it was decided to go back and review previous drillings using the original method. Researchers believed that reanalyzing these drillings using only the first 4 inches of each drill run would result in lower variation throughout the drillings and provide a better representation of each drilled block. Seen here are results from 3 old drillings and the results after reanalyzing the data:

Table 5 - 287 psi original drilling results

Final Results - 287psi - Wet		
Description	T (in-lbs)	F (lbf)
Average	121.2	49.9
Maximum	212.5	70.1
Minimum	58.1	27.2
Std. Deviation	33.3	7.8
CV	0.275	0.157

Table 6 - 287 psi updated drilling results

Final Results - 287psi - Wet		
Description	T (in-lbs)	F (lbf)
Average	96.9	87.7
Maximum	130.1	116.2
Minimum	63.4	65.6
Std. Deviation	13.1	11.5
CV	0.136	0.131

Table 7 - 375 psi original drilling results

Final Results -375psi - Wet		
Description	T (in-lbs)	F (lbf)
Average	230.6	28.8
Maximum	420.4	100.3
Minimum	118.5	6.3
Std. Deviation	67.2	17.1
CV	0.291	0.595

Table 8 - 375 psi updated drilling results

Final Results -375psi - Wet		
Description	T (in-lbs)	F (lbf)
Average	189.2	83.8
Maximum	368.3	127.1
Minimum	114.2	23.4
Std. Deviation	54.6	27.3
CV	0.289	0.326

Table 9 - 673 psi original drilling results

Final Results - 673psi - Wet		
Description	T (in-lbs)	F (lbf)
Average	521.5	124.8
Maximum	849.2	245.9
Minimum	211.6	36.4
Std. Deviation	131.3	52.4
CV	0.252	0.420

Table 10 - 673 psi updated drilling results

Final Results - 673psi - Wet		
Description	T (in-lbs)	F (lbf)
Average	421.0	109.4
Maximum	587.2	230.1
Minimum	209.0	45.7
Std. Deviation	73.5	38.4
CV	0.175	0.351

As evident from all 3 reanalyzed drillings, the variation was reduced for both torque and crowd. Note, the crowd variation was decreased the most by reanalyzing the data.

During the drilling process, 12 readings per revolution were recorded and used to provide an average torque and crowd value for each depth increment which was determined by the penetration rate setting. Averages were taken for each revolution to compensate for bending effects. As stated earlier, gauges of each type were only placed in two locations, 180 degrees apart. This led to bending that was not compensated for in every possible direction. Therefore, readings created a sinusoidal wave pattern as the bit rotated seen in Figure 12.

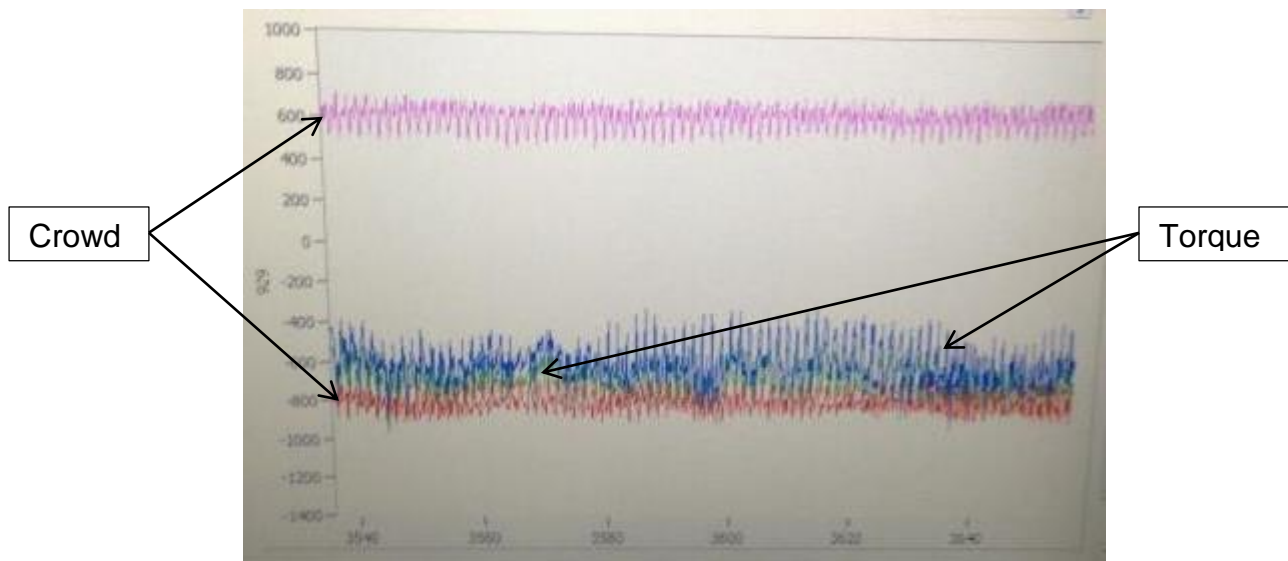


Figure 12 – Real-time readings showing sinusoidal wave pattern

By taking the average of a full rotation, peaks and valleys of the sine waves offset one another and provided an average that accounted for a variable degree of bending during a full revolution. The pink and red lines are for strain gauges that record the crowd. It was noticed during drilling that the bit typically put one side of the rod in constant tension and the other in constant compression and that torque affected both axial force gauges. However, it was confirmed in the calibration process that torque effects are equally applied to both gauges and offset one another. Additionally, axial

force calibration confirmed that when averaging the tension side and the compression side, the opposite forces offset one another, and the average value obtained is highly accurate. Note, because the compressive forces are negative and tensile forces are positive, their average produces the actual compressive force applied to the drill bit. For example, the red crowd line is showing approximately -800 lb and the pink crowd line is showing approximately 600 lb. When averaged, the applied force is -100 lb indicating the drill rod is being compressed by 100 lb of force. The torque rosettes were designed to compensate for applied axial forces and only report the actual torque being applied. Therefore, both torque lines, blue and green, nearly plot on top of one another and are only separated by bending effects, which are compensated for when an average is taken using both lines.

After each drilling was complete, all of the averages obtained at each depth increment were then combined to produce a final average that represents both torque and crowd for the entire length of drilling. This results in hundreds to thousands of data points obtained from averaging each rotation, making up the final average which will be used in equation development. Figure 13 displays the average readings for torque and crowd taken per revolution and plotted versus depth for a single drilling.

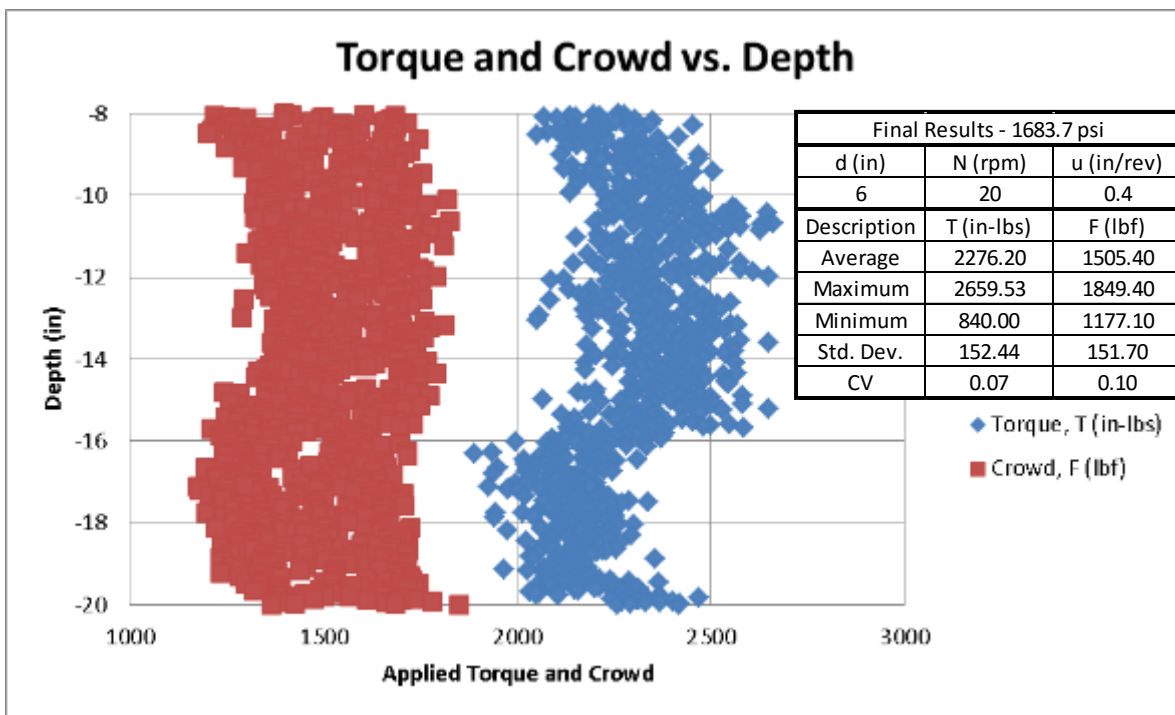


Figure 13 - Torque and crowd vs. depth for a single laboratory drilling

From this drilling, the average torque and crowd displayed in the statistics box are used with the other drilling parameters, also displayed, to report a single data point versus compressive strength, q_c . For instance, the compressive strength, 1,683.7 psi, was

obtained from unconfined compression testing on three to six cylinders casted from the same mix as the large Gatorock block that was drilled (three cylinders are also tested in split tension). This was the method used for all drillings to develop a new drilling equation using a rock auger bit type in a drilling medium representative of Florida limestone.

The following tables illustrate all drillings that were planned to meet the requirements of the scope; followed by the actual strengths that were recorded for each designated drilling:

Table 11 - Projected strengths (20 RPM)

20 RPM								
Penetration Rate (in/rev)	4.5" bit				6" bit			
	Strength (psi)				Strength (psi)			
0.008	140	280	556	1,667	140	280	556	1,667
0.014	140	280	556	1,667	140	280	556	1,667
0.02	140	280	556	1,667	140	280	556	1,667

Table 12 - Actual strengths (20 RPM)

20 RPM								
Penetration Rate (in/rev)	4.5" bit				6" bit			
	Strength (psi)				Strength (psi)			
0.008	135.4	281.5	498.7	1,548.9	135.4	273.9	498.7	1,548.9
0.014	135.4	296.4	650.6	1,601.2	135.4	282.1	622.6	1,601.2
0.02	135.4	279.4	601.9	1,683.7	135.4	279.4	601.9	1,683.7

Table 13 - Projected strengths (40 RPM)

40 RPM								
Penetration Rate (in/rev)	4.5" bit				6" bit			
	Strength (psi)				Strength (psi)			
0.008	140	280	556	1,667	140	280	556	1,667
0.014	140	280	556	1,667	140	280	556	1,667
0.02	140	280	556	1,667	140	280	556	1,667

Table 14 - Actual strengths (40 RPM)

40 RPM								
Penetration Rate (in/rev)	4.5" bit				6" bit			
	Strength (psi)				Strength (psi)			
0.008	135.0	273.9	486.6	1,637.7	135.0	295.1	545.2	1,637.7
0.014	135.0	284.7	545.2	1,514.2	135.0	284.7	486.6	1,514.2
0.02	135.0	317.9	626.5	1,601.0	135.0	281.5	622.6	1,601.0

In addition to the 48 planned drillings to meet the project scope, 33 extra drillings at various strengths and drilling parameters (rate, torque, etc.) were also performed. This provided a total of 81 recorded drilling data points used to develop the field prediction equation.

It was also discovered that as Gatorock block production was coming to an end, the researchers would be two blocks short to provide all the required data points to meet the project scope. It was then decided that for the lower end projected strength of 140 psi, these blocks would be drilled using an incremental method. For a specified design strength (i.e., 135.4 psi), one side of the block would be drilled using the 4.5" bit, 40 RPM and use a different penetration rate for each 4 inch increment of drilling. Previously researchers determined that each drill run should be approximately four inches for the most undisturbed result. Typically, the penetration rate is held constant throughout drilling and the three increments of the drilled block are averaged. However, due to the shortage of blocks, not all proposed drillings were possible using this method. Therefore the final four blocks were drilled using the following method: the first four inches used the slowest penetration rate, the second four inch drill run used the middle penetration rate and the final four inch drill run used the fastest penetration rate. The block was then flipped and the same procedure took place using the 6" bit. The second available block was then drilled using the same procedure but with the 20 RPM setting. By doing this, all needed data points for the designated strengths were collected using only two blocks instead of six blocks. With the remaining two blocks the same procedure was performed, reversing the order of penetration rates (i.e., penetration rates in the following order: Fastest, middle, and slowest). Not only did this method provide all the needed drillings but it also provided a means to compare drilling parameters at the same exact strength. As seen in Table 11 through Table 14, the strengths are not identical. The increase or decrease in various block strength affected the recorded parameters, torque and crowd, used in the comparison. Using multiple drilling parameters for the same block provided direct comparison of the recorded drilling parameters, torque and crowd, at the same specified strength. This provided comparisons similar to Karasawa's methods in 2002. The incremental method is recommended if future drillings are to take place. A far larger number of design strengths could be drilled using the same amount of material used in this project. Typically averages from each four inch drill run were very similar.

The following two tables display all recorded drillings with all parameters, controlled and measured, grouped by bit diameter:

Table 15 - Recorded drillings (4.5" bit)

qu (psi)	qt(psi)	T (in-lbs)	F (lbf)	N (rpm)	u (in/min)	d (in)
135.0	19.3	38.08	32.52	40	0.32	4.5
135.0	19.3	49.5	62.71	40	0.56	4.5
135.0	19.3	58.28	53.07	40	0.80	4.5
135.4	19.3	61.31	89.06	20	0.16	4.5
135.4	19.3	96.39	102.63	20	0.28	4.5
135.4	19.3	108.88	126.55	20	0.40	4.5
145.9	20.1	87.46	145.60	20	0.16	4.5
145.9	20.1	96.39	72.49	20	0.28	4.5
145.9	20.1	130.14	79.16	20	0.40	4.5
155.4	21.2	59.31	60.29	40	0.32	4.5
155.4	21.2	81.66	80.49	40	0.56	4.5
155.4	21.2	81.88	70.63	40	0.80	4.5
250.4	N/A	202.60	101.05	40	0.80	4.5
258.2	N/A	215.65	108.91	40	0.56	4.5
273.9	52.9	159.66	84.00	40	0.32	4.5
279.4	85	204.19	85.82	20	0.40	4.5
281.5	93.4	133.40	73.89	20	0.16	4.5
284.7	74.95	134.88	75.46	40	0.56	4.5
287.0	N/A	96.90	87.70	40	0.56	4.5
287.3	N/A	215.70	98.92	40	0.80	4.5
287.5	N/A	299.78	225.49	40	0.80	4.5
296.4	N/A	175.51	77.99	20	0.28	4.5
296.4	N/A	216.72	78.68	20	0.40	4.5
297.8	N/A	118.99	106.11	40	0.80	4.5
306.2	81.5	96.59	68.37	40	0.32	4.5
310.9	N/A	117.77	86.36	40	0.32	4.5
317.9	86.6	253.26	60.00	40	0.80	4.5
375.0	N/A	189.00	83.80	40	0.56	4.5
398.6	N/A	239.10	121.97	40	0.80	4.5
486.6	96.4	229.42	71.76	40	0.32	4.5
498.7	117.5	259.36	62.11	20	0.16	4.5
545.2	110.7	338.71	62.52	40	0.56	4.5
601.9	111.1	424.50	51.42	20	0.40	4.5
626.5	117	475.10	75.20	40	0.80	4.5
650.6	N/A	416.04	58.29	20	0.28	4.5
673.0	N/A	421.00	109.40	40	0.56	4.5
695.9	N/A	460.08	115.10	40	0.80	4.5
1514.2	323.7	1481.86	602.61	40	0.56	4.5
1548.9	306.3	1280.44	502.05	20	0.16	4.5
1601.0	334.4	1608.18	726.58	40	0.80	4.5
1601.2	306.6	1362.35	477.49	20	0.28	4.5
1637.7	324.9	1242.50	468.74	40	0.32	4.5
1683.7	288.6	2109.51	907.64	20	0.40	4.5

Table 16 - Recorded drillings (6")

qu (psi)	qt(psi)	T (in-lbs)	F (lbf)	N (rpm)	u (in/min)	d (in)
135.0	19.3	72.2	45.02	40	0.32	6.0
135.0	19.3	104.38	38.96	40	0.56	6.0
135.0	19.3	118.86	50.21	40	0.80	6.0
135.4	19.3	130.59	31.53	20	0.16	6.0
135.4	19.3	174.79	37.14	20	0.28	6.0
135.4	19.3	212.03	50.59	20	0.40	6.0
145.9	20.1	136.52	79.10	20	0.16	6.0
145.9	20.1	185.89	110.50	20	0.28	6.0
145.9	20.1	192.37	117.18	20	0.40	6.0
155.4	21.2	89.49	56.12	40	0.32	6.0
155.4	21.2	122.43	87.10	40	0.56	6.0
155.4	21.2	163.63	103.83	40	0.80	6.0
273.9	52.9	264.09	143.94	20	0.16	6.0
277.4	N/A	183.62	93.61	40	0.80	6.0
279.4	85	335.56	181.36	20	0.40	6.0
281.5	93.4	331.97	178.66	40	0.80	6.0
282.1	63.5	312.92	168.05	20	0.28	6.0
284.7	74.95	218.59	118.36	40	0.56	6.0
295.1	N/A	186.32	92.93	40	0.32	6.0
306.2	81.5	205.06	117.08	20	0.16	6.0
306.9	87.3	337.24	167.36	40	0.56	6.0
317.9	86.6	370.66	200.31	20	0.40	6.0
341.1	N/A	302.32	100.20	40	0.80	6.0
398.6	N/A	327.21	81.80	40	0.80	6.0
431.2	130.8	602.15	328.76	40	0.80	6.0
485.8	118	469.84	143.12	40	0.80	6.0
486.6	96.4	431.32	279.93	40	0.56	6.0
498.7	117.5	467.11	265.93	20	0.16	6.0
545.2	110.7	384.46	251.09	40	0.32	6.0
601.9	111.1	633.66	336.82	20	0.40	6.0
622.6	127.2	701.96	410.18	20	0.28	6.0
622.6	127.2	763.82	452.34	40	0.80	6.0
1514.2	323.7	1877.34	1270.55	40	0.56	6.0
1548.9	306.3	1540.39	1108.69	20	0.16	6.0
1601.0	334.4	2216.50	1356.75	40	0.80	6.0
1601.2	306.6	1643.32	643.36	20	0.28	6.0
1637.7	324.9	1475.19	1062.80	40	0.32	6.0
1683.7	288.6	2277.91	1505.40	20	0.40	6.0

As previously stated there were a total of 81 recorded drillings completed. From the 81 drillings, there were 81 compressive strength, q_u , values and 64 tensile strength, q_t , values available for analyses. Of the 81 q_u values, 43 were drilled using the 4.5" bit and 38 were drilled using the 6" bit. Of the 64 q_t values, 29 were drilled using the 4.5" bit and 35 were drilled using the 6" bit. The fewer amount of q_t values was a result of not enough cylinders available for split tension testing due to changes in drilling dates in the early stages of laboratory drillings (i.e., split tension cylinders had to be used for

compression testing the day of drilling as the planned drilling date was pushed back from 14-day drilling to a later date).

2.3 Lab Data Analyses

Once all of the laboratory drillings were complete, an analysis of each drilling parameter took place. The analysis included investigating the effects of bit diameter on applied crowd and torque forces, the crowd and torque relationship, the effects of rotational speed and penetration rate on torque and crowd, and the relationship of torque and crowd with compressive and tensile strengths.

2.3.1 q_u vs. q_t

The first step to the analyses was to compare recorded q_u values vs. recorded q_t values to look for trending of the material tested. The following plot provides this comparison using a linear fit equation and 2nd order polynomial fit equation to describe the trending (Both had their intercepts set to zero):

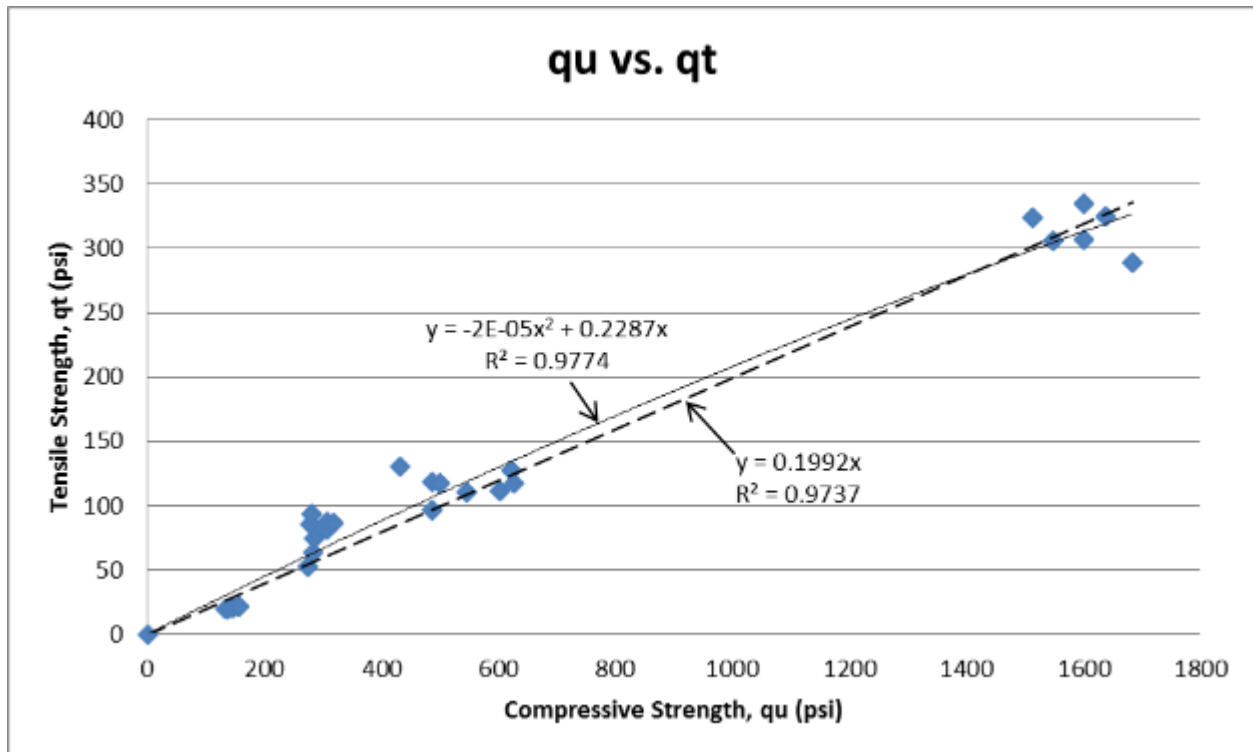


Figure 14 - q_u vs. q_t plot with linear and 2nd order polynomial curve fitting

As seen from the plot, the trending is quite linear. However the second order polynomial does a better job of describing the variability as it has the higher R^2 value ($0.9774 > 0.9737$). From the results it was confirmed that Gatorock mixing and material formation was quite consistent throughout all the laboratory tests.

2.3.2 Effects of Bit Diameter

The next step in the analyses was to compare how changes in bit diameter affected torque and crowd. For this analyses; recorded torque and crowd measurements were compared using variable strengths, compressive and tensile, of Gatorock blocks drilled using the same rotational speeds, N, and penetration rates, u. By comparing in this manner, researchers removed the influence of variable penetration rates and rotational speeds. This provided direct analyses of the influence bit diameter had on recorded torque and crowd measurements compared to their compressive and tensile strengths. The influence of bit diameter was a major concern for transitioning to monitoring in the field where bit diameters are greatly up-scaled (i.e., 4.5" – 6" compared to 36" – 60"). The following plots provide the basis of the analyses (The small dashed trend lines are for the 4.5" bit, the larger dashed lines are for the 6" bit and the solid line is for both bits showing the overall curve fit.):

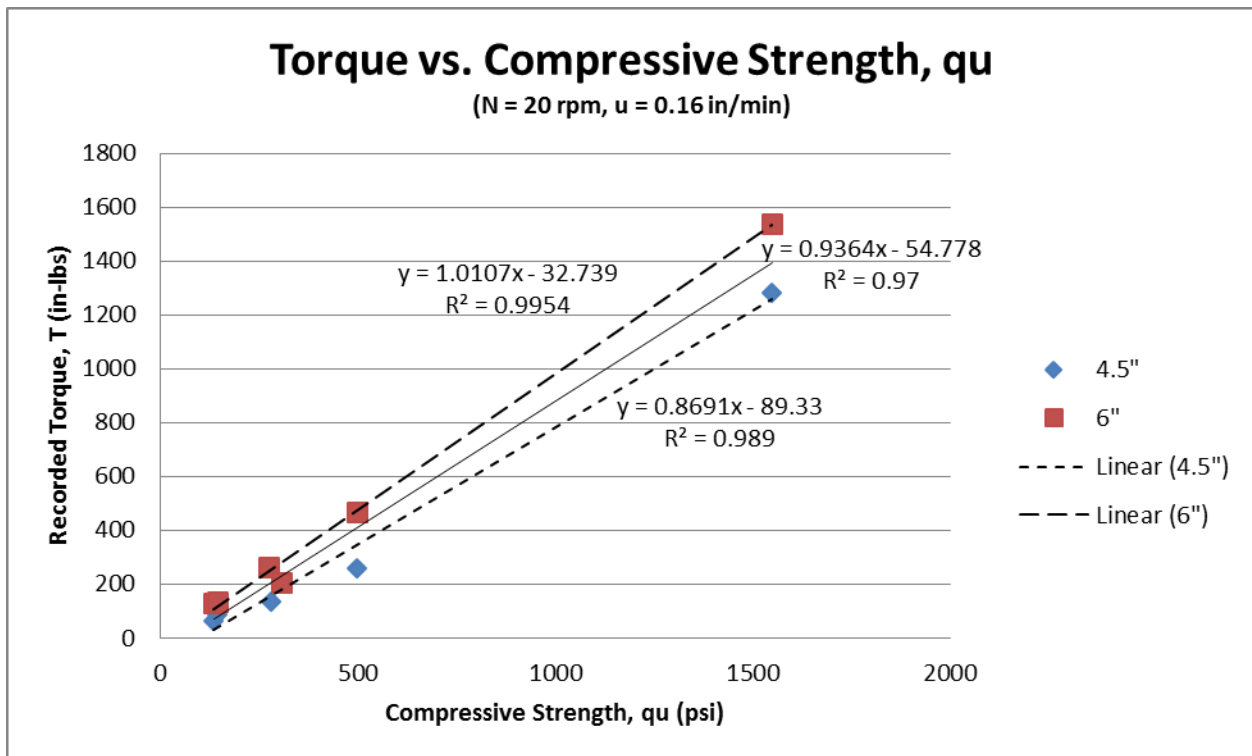


Figure 15 - Torque vs. compressive strength (N = 20 rpm, u = 0.16 in/min)

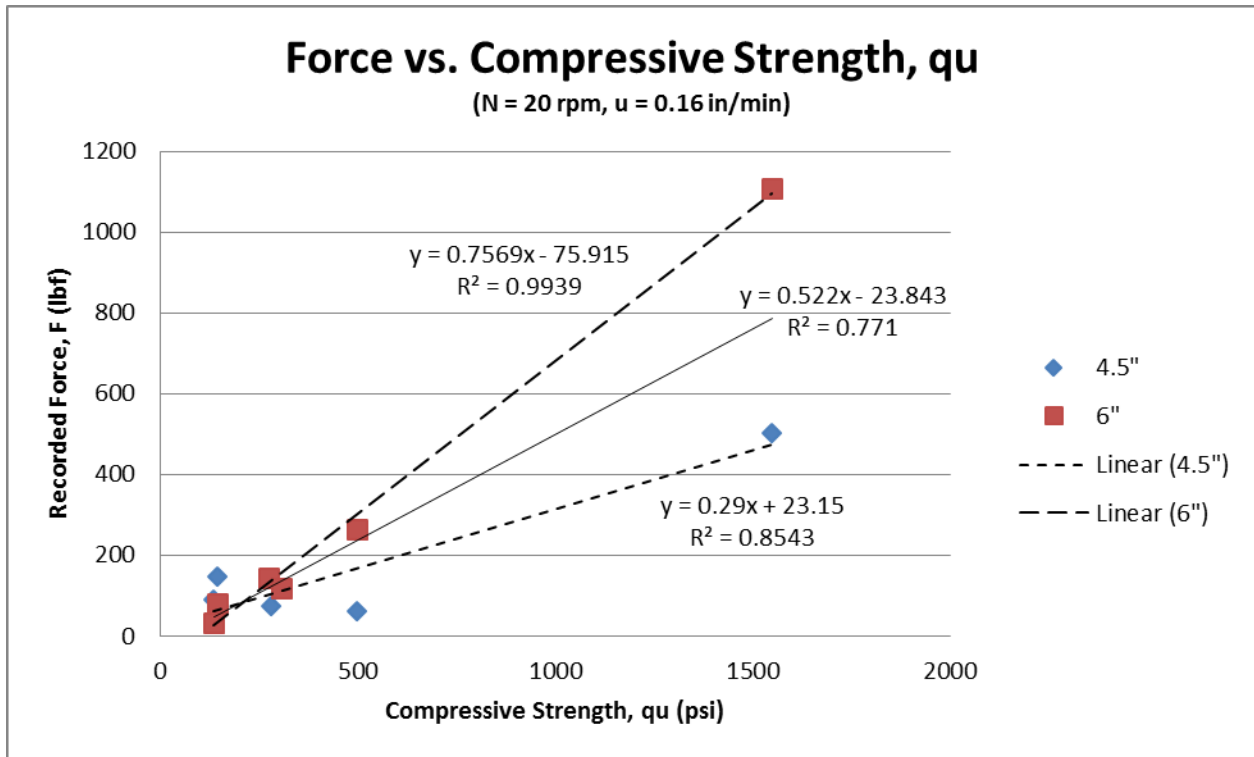


Figure 16 - Force vs. compressive strength (N = 20 rpm, u = 0.16 in/min)

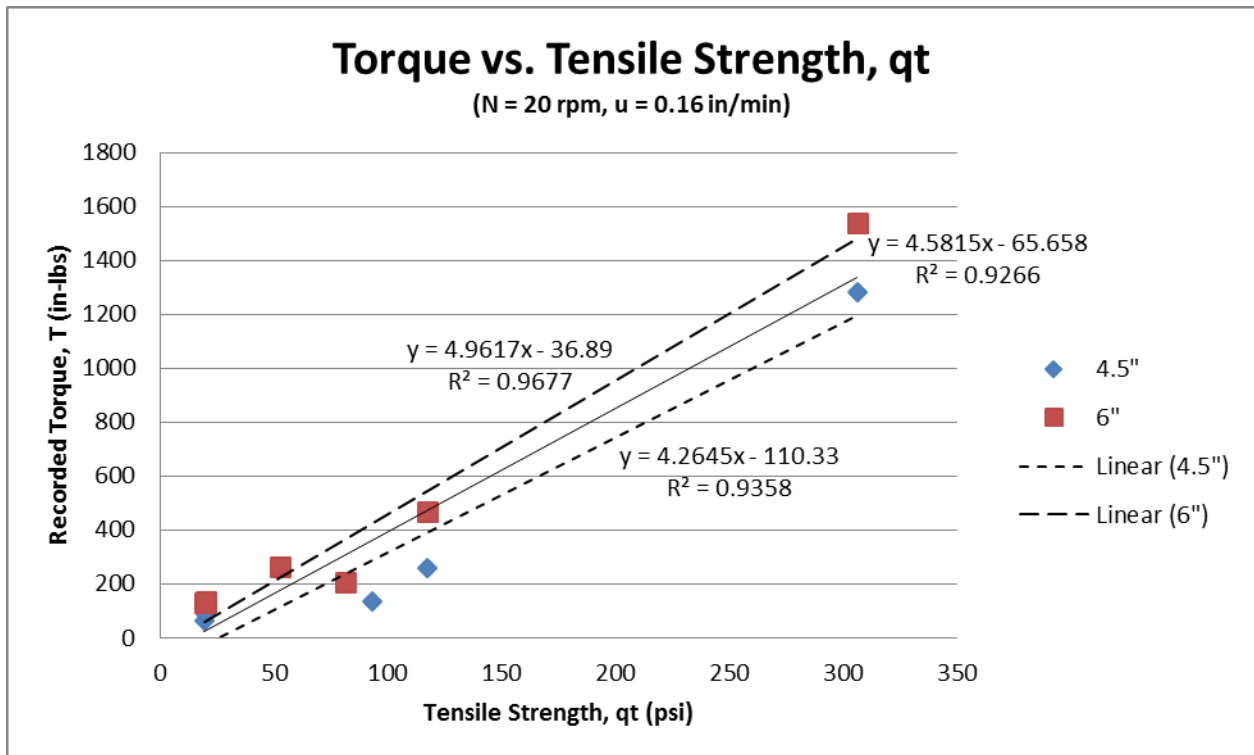


Figure 17 - Torque vs. tensile strength (N = 20 rpm, u = 0.16 in/min)

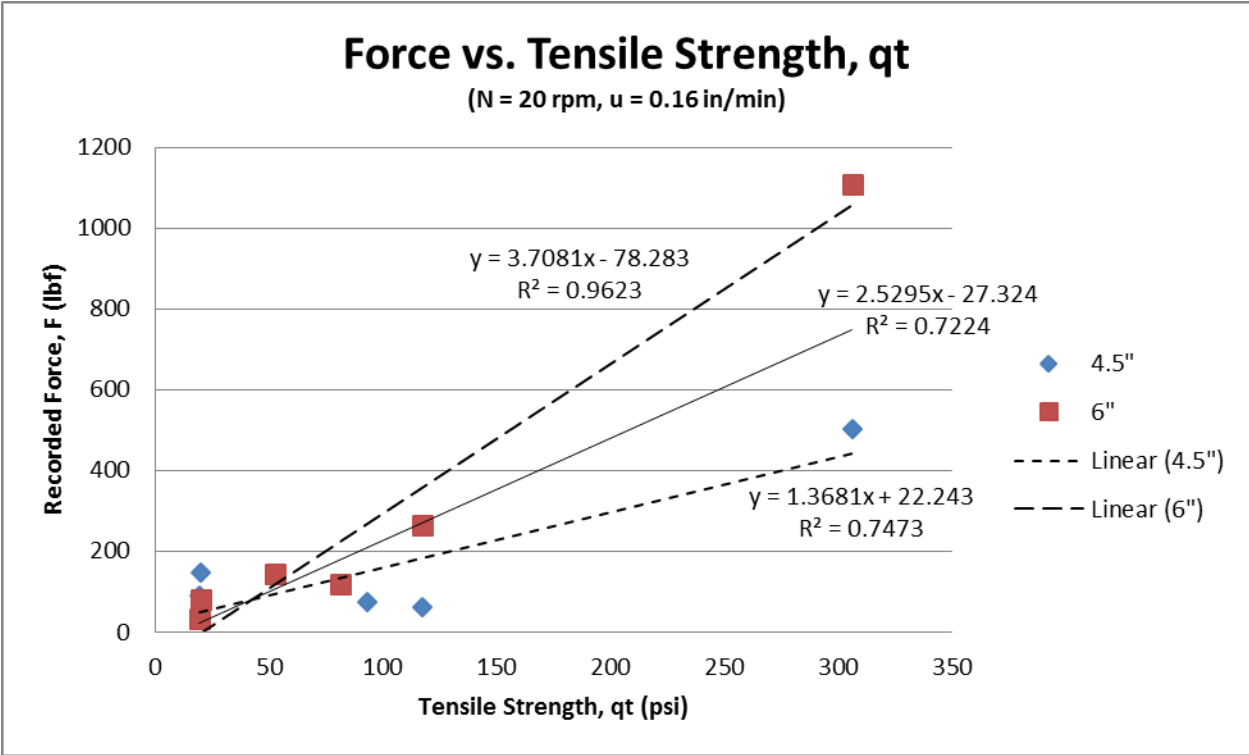


Figure 18 - Force vs. tensile strength (N = 20 rpm, u = 0.16 in/min)

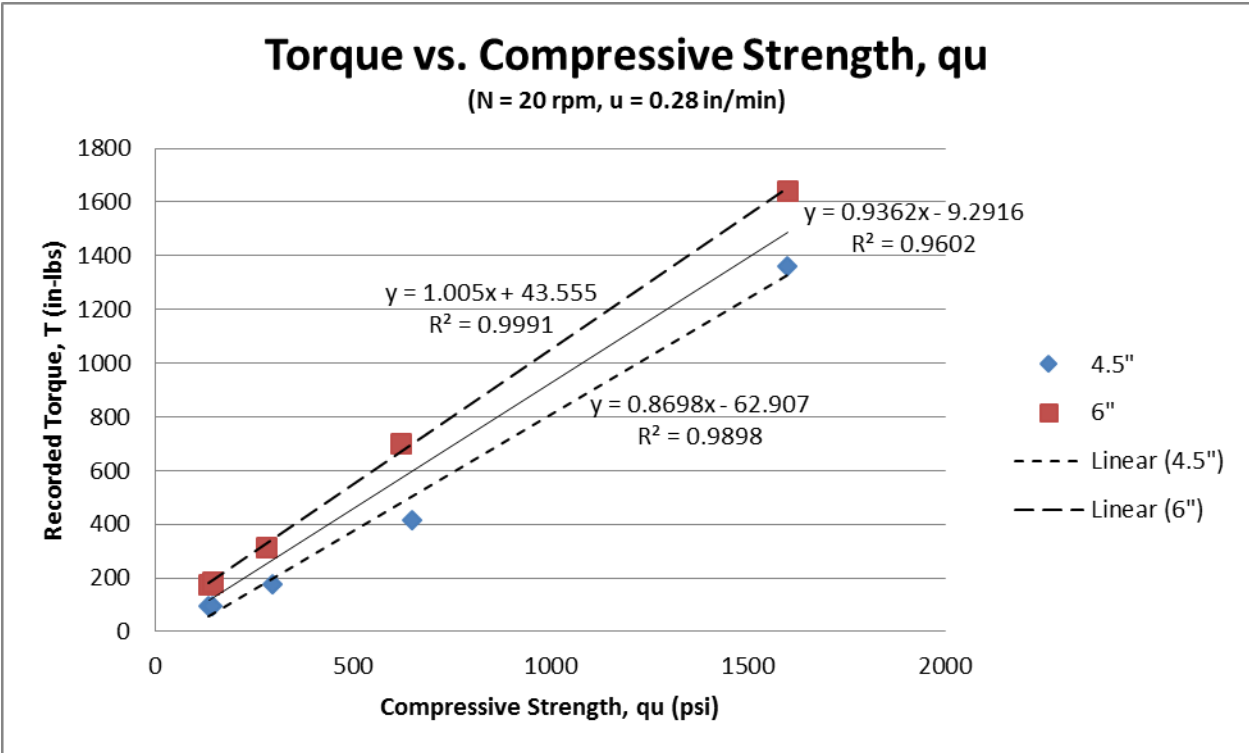


Figure 19 - Torque vs. compressive strength (N = 20 rpm, u = 0.28 in/min)

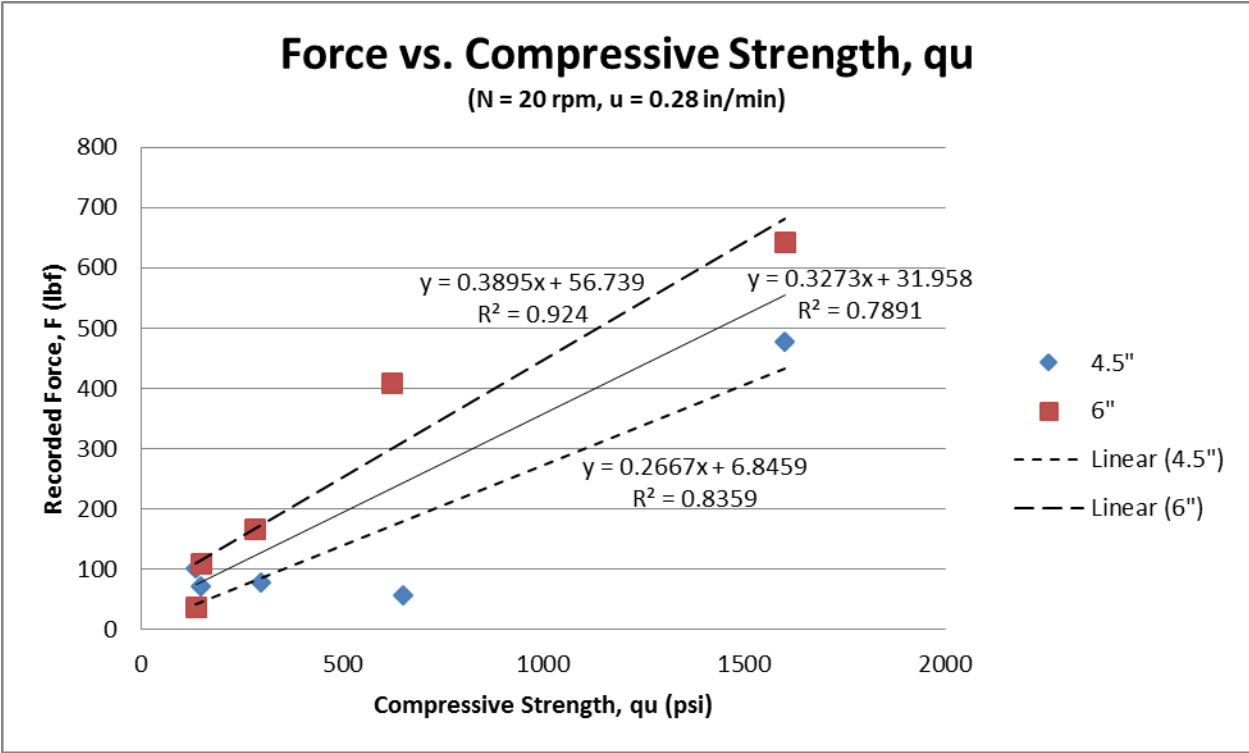


Figure 20 - Force vs. compressive strength (N = 20 rpm, u = 0.28 in/min)

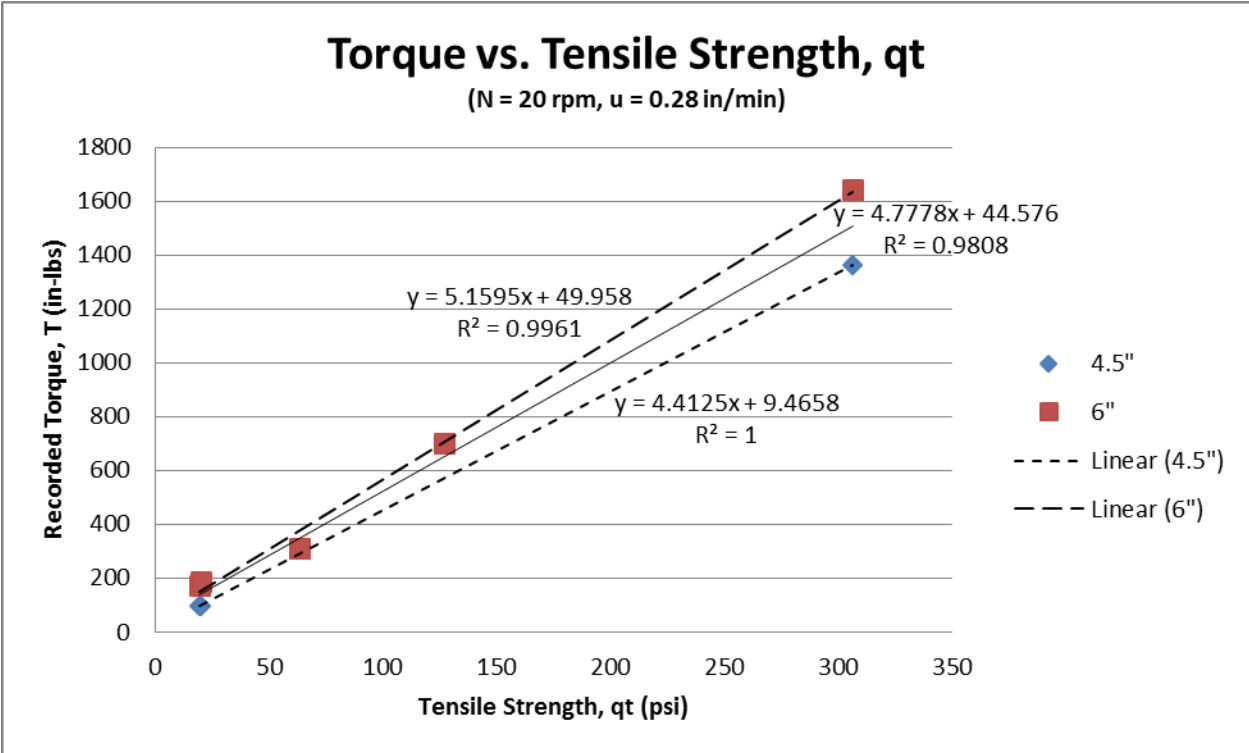


Figure 21 - Torque vs. tensile strength (N = 20 rpm, u = 0.28 in/min)

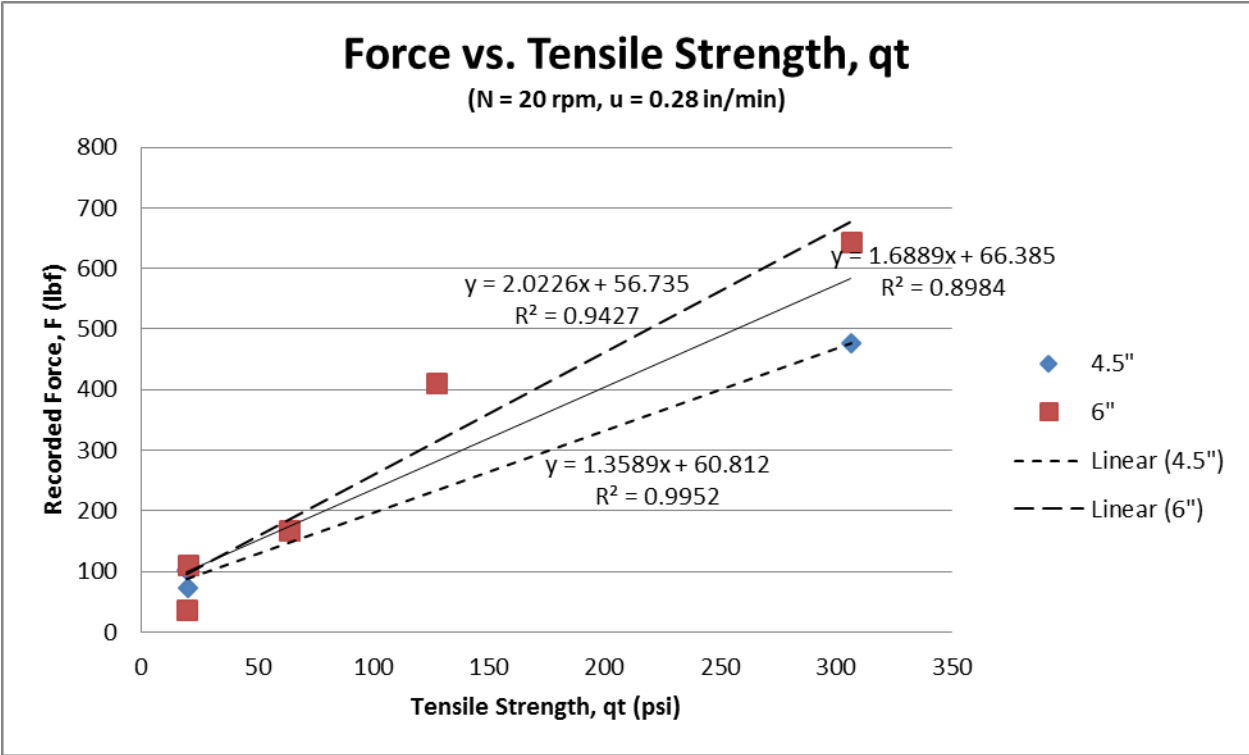


Figure 22 - Force vs. tensile strength (N = 20 rpm, u = 0.28 in/min)

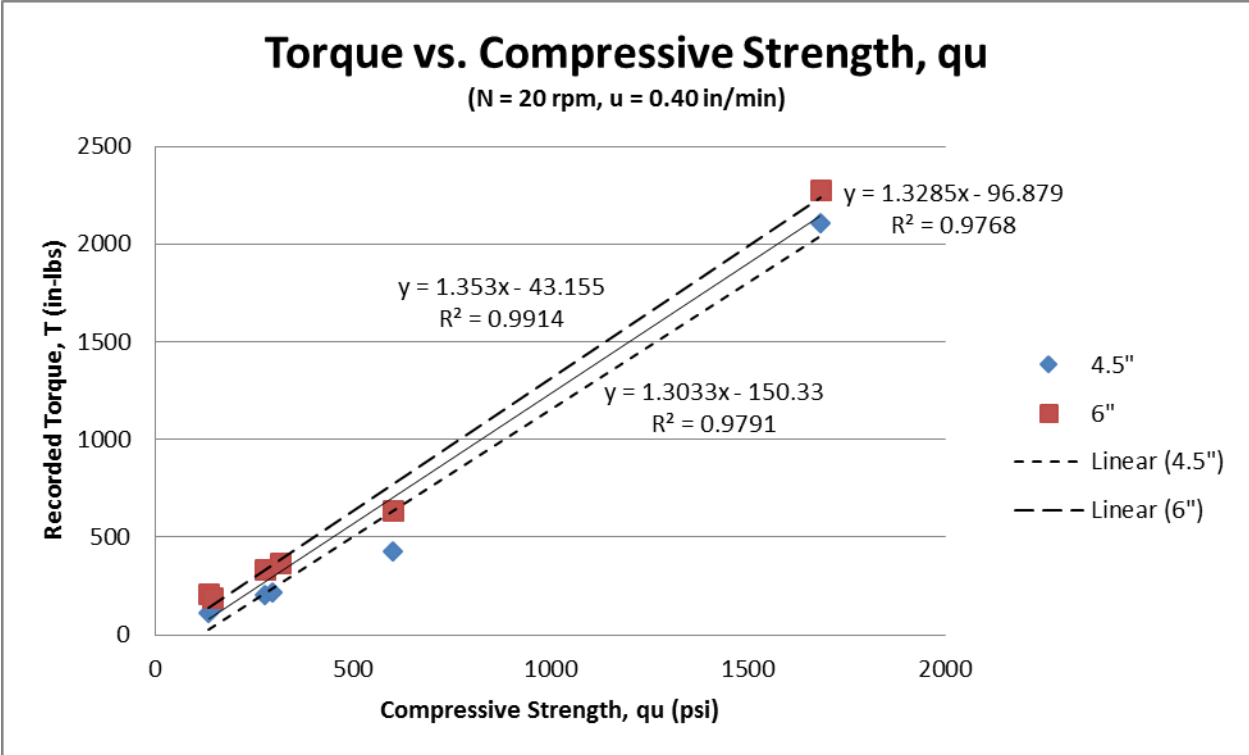


Figure 23 - Torque vs. compressive strength (N = 20 rpm, u = 0.40 in/min)

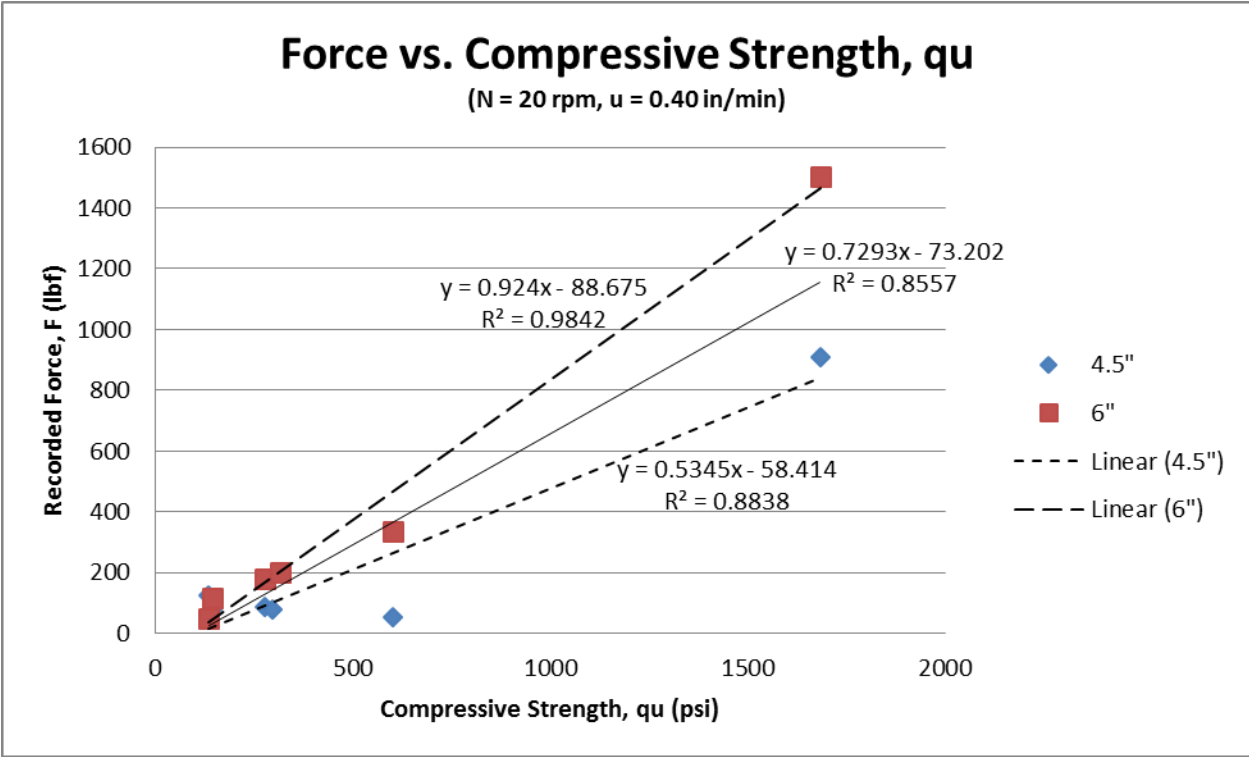


Figure 24 - Force vs. compressive strength (N = 20 rpm, u = 0.40 in/min)

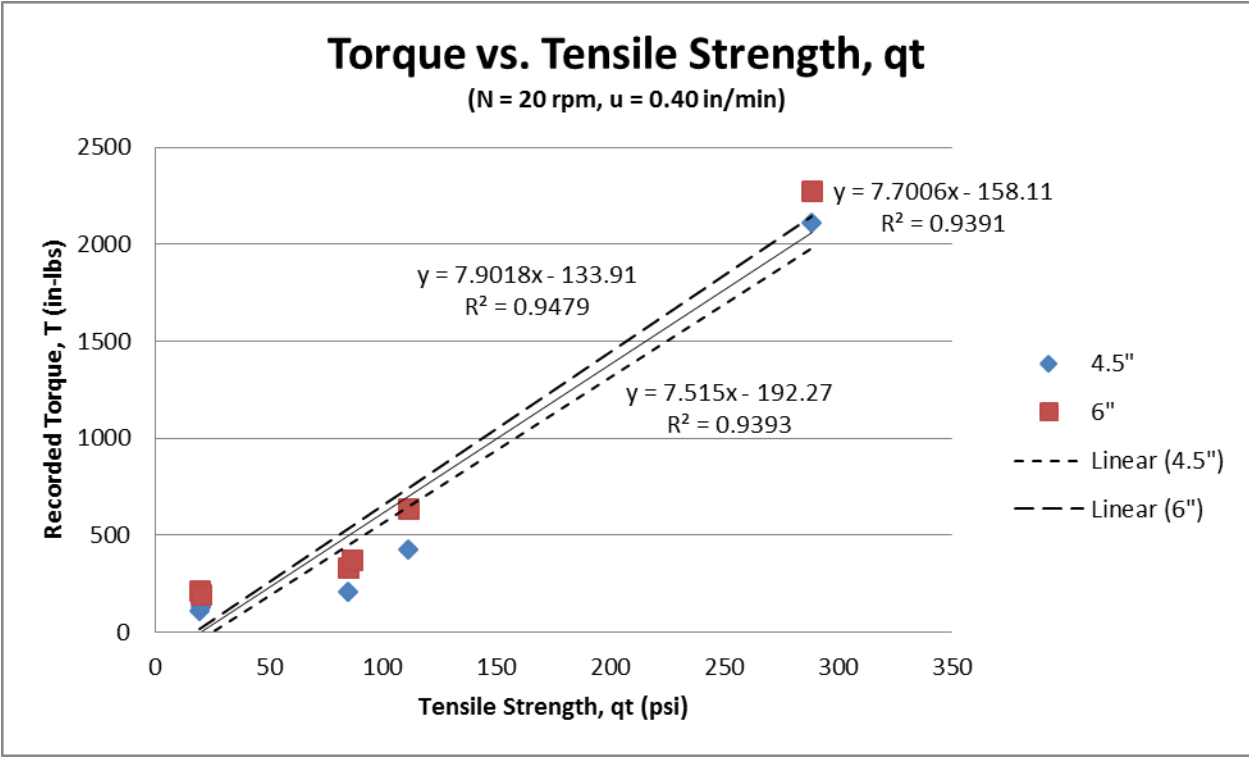


Figure 25 - Torque vs. tensile strength (N = 20 rpm, u = 0.40 in/min)

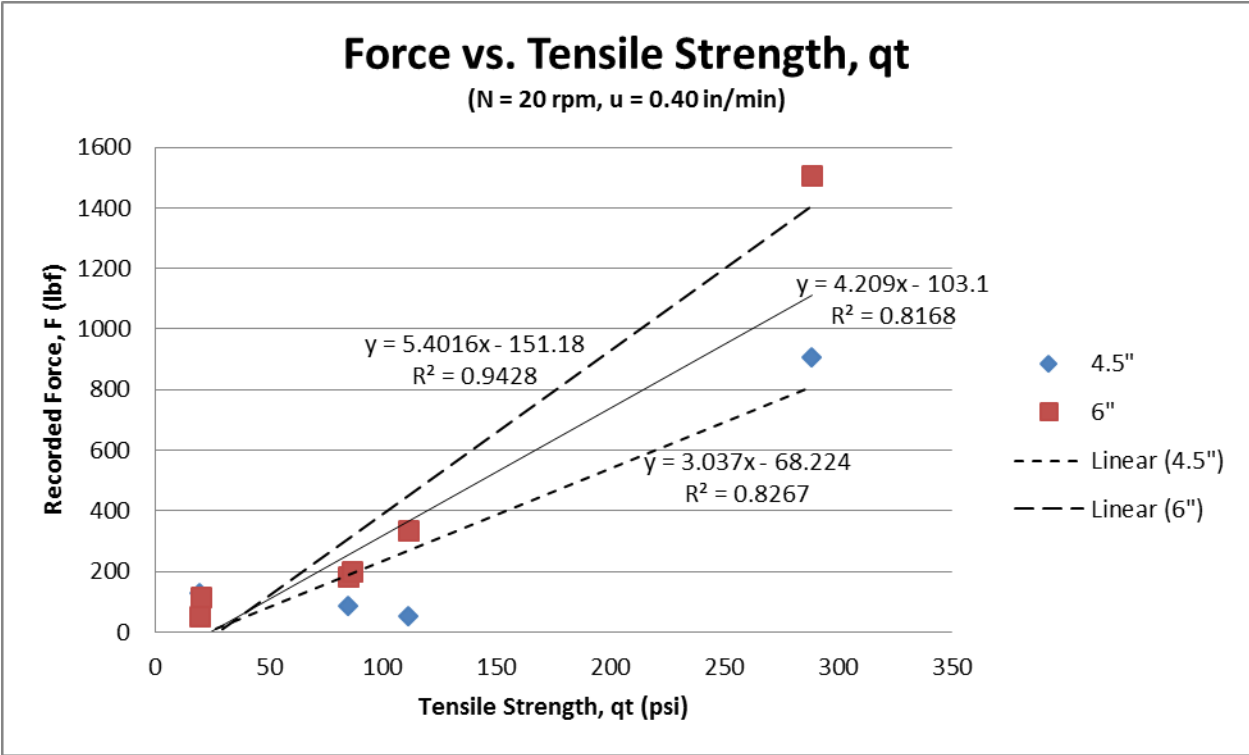


Figure 26 - Force vs. tensile strength (N = 20 rpm, u = 0.40 in/min)

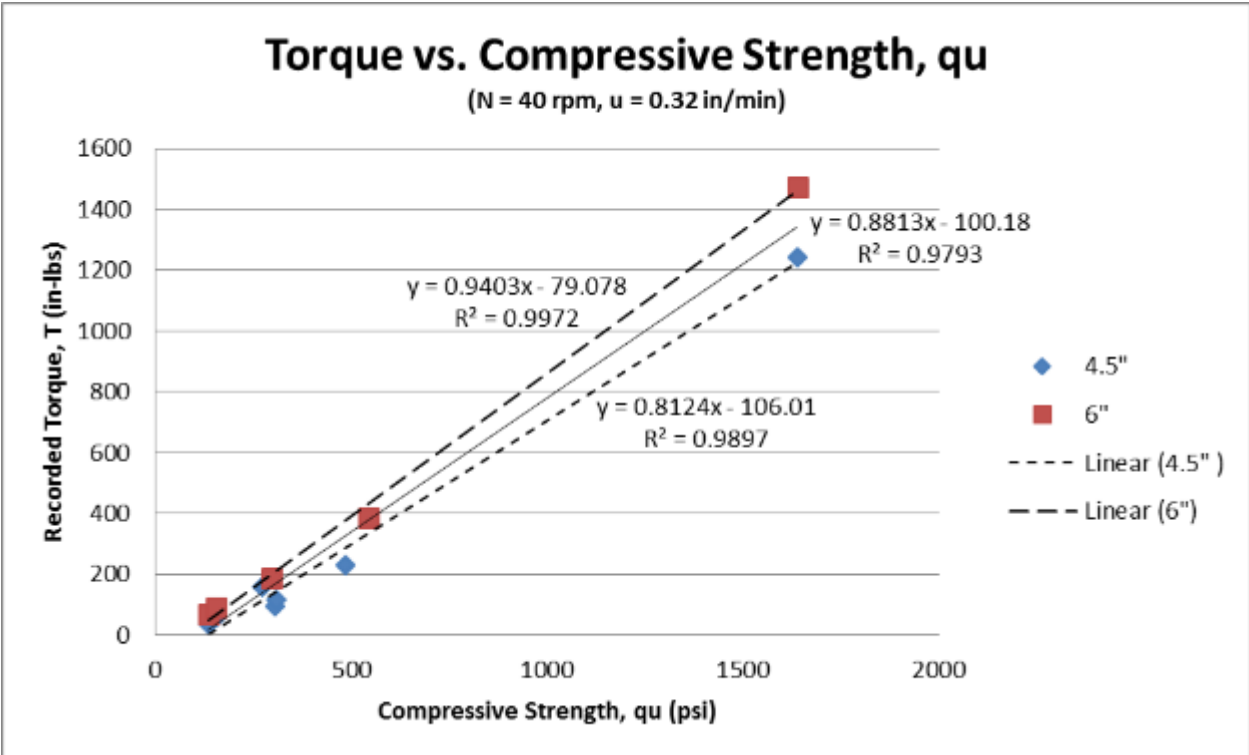


Figure 27 - Torque vs. compressive strength (N = 40 rpm, u = 0.32 in/min)

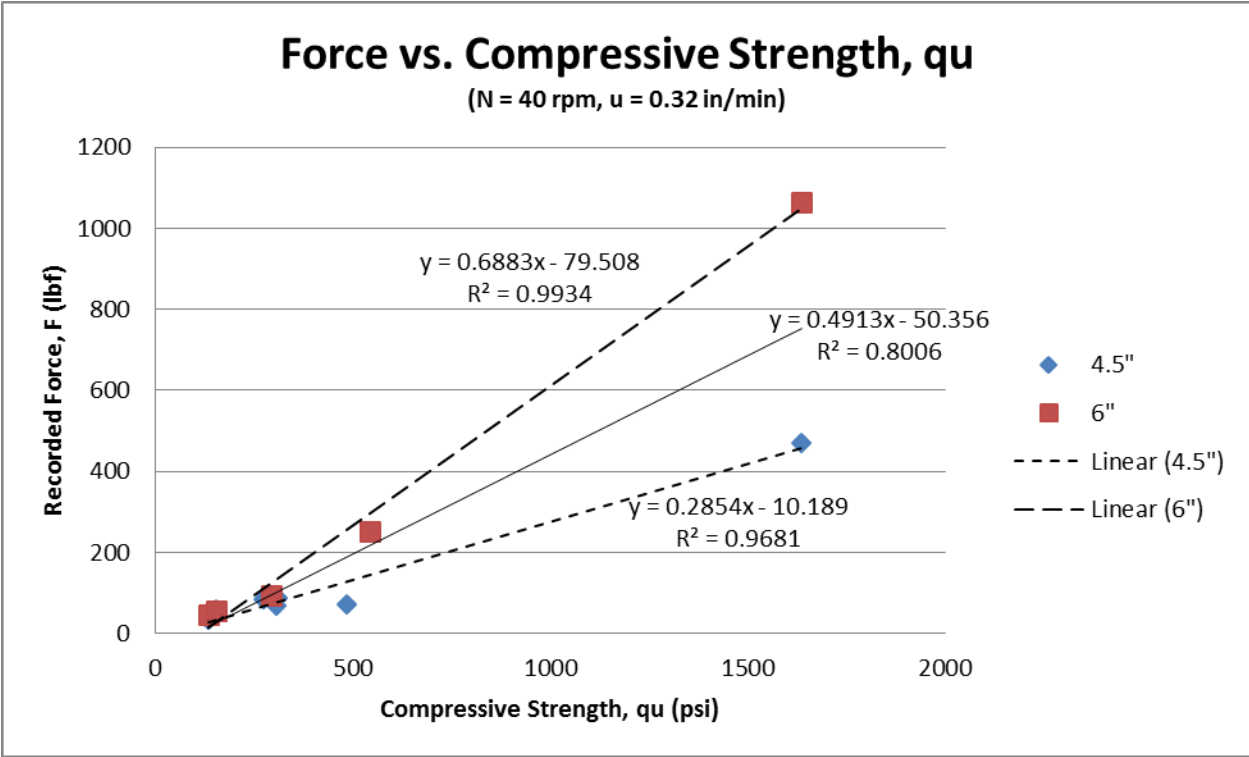


Figure 28 - Force vs. compressive strength (N = 40 rpm, u = 0.32 in/min)

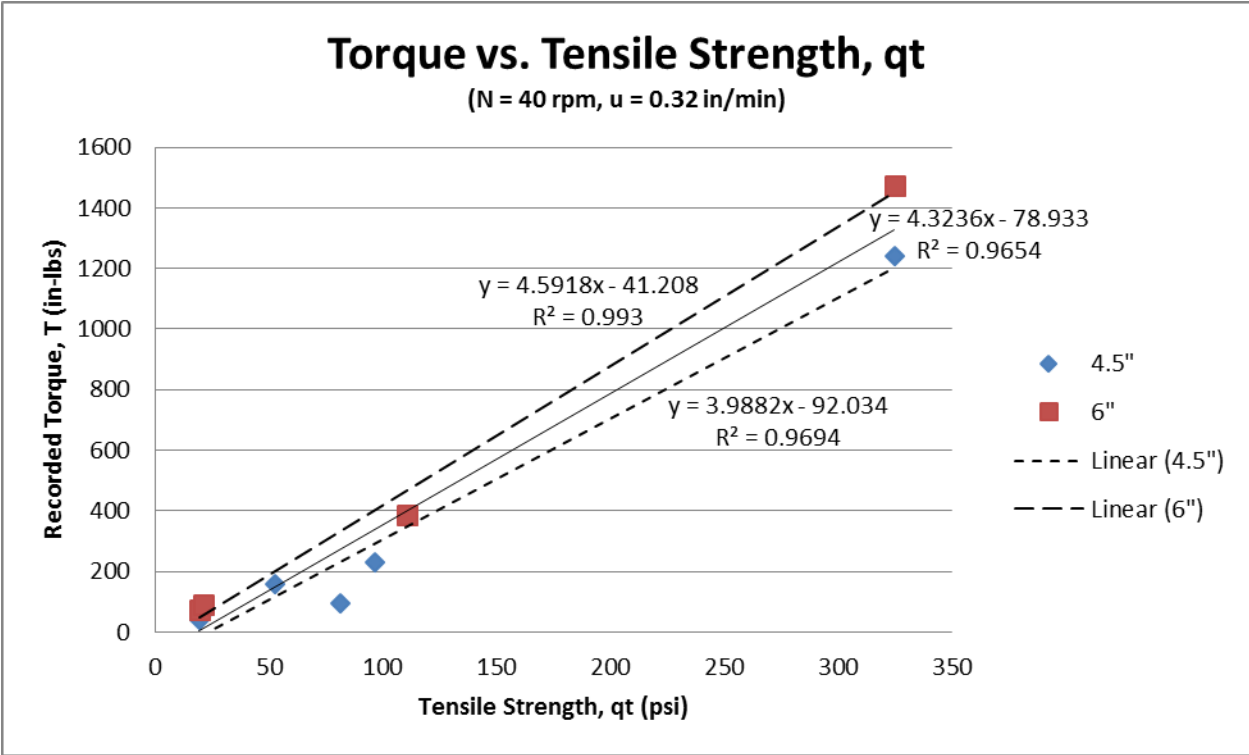


Figure 29 - Torque vs. tensile strength (N = 40 rpm, u = 0.32 in/min)

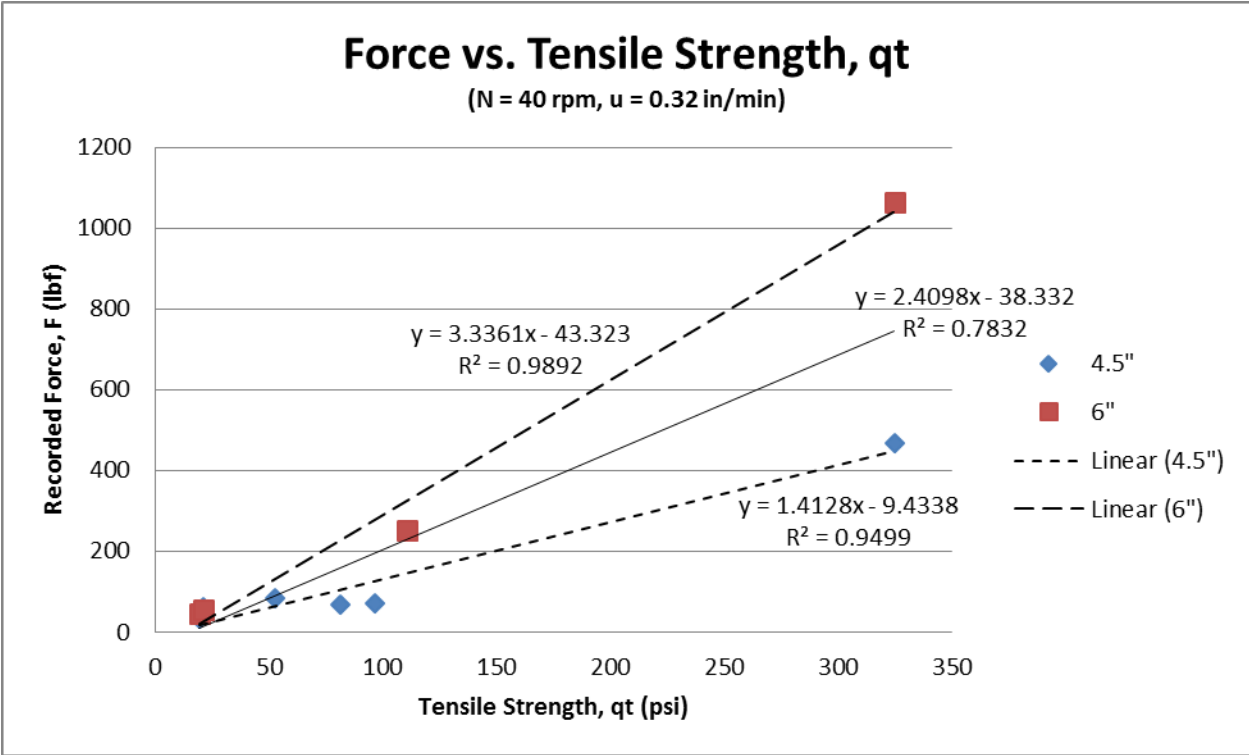


Figure 30 - Force vs. tensile strength (N = 40 rpm, u = 0.32 in/min)

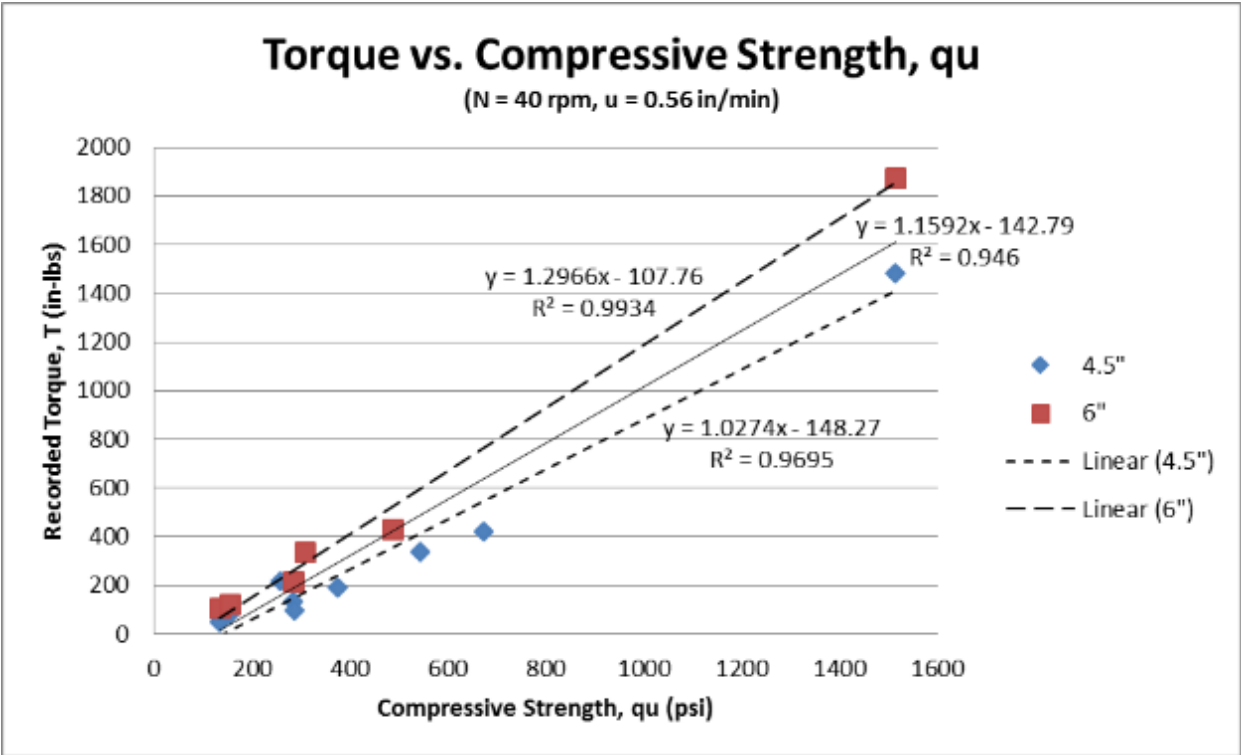


Figure 31 - Torque vs. compressive strength (N = 40 rpm, u = 0.56 in/min)

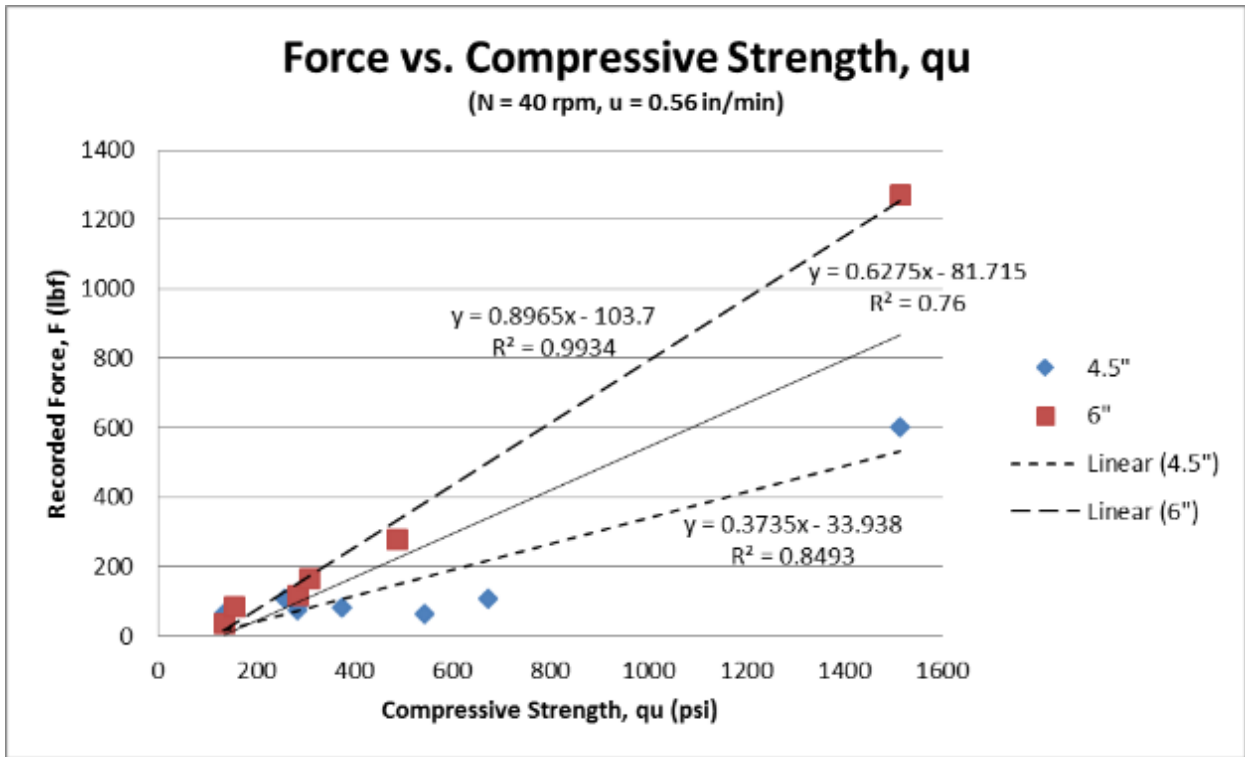


Figure 32 - Force vs. compressive strength (N = 40 rpm, u = 0.56 in/min)

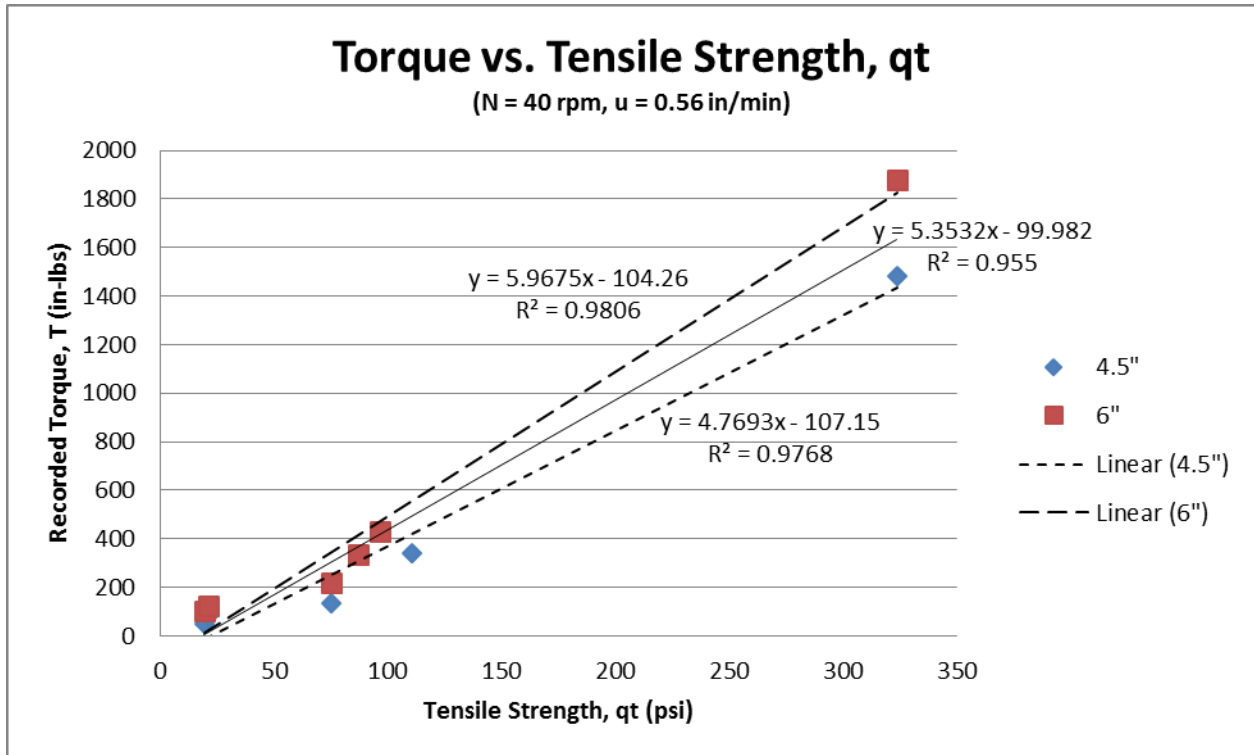


Figure 33 - Torque vs. tensile strength (N = 40 rpm, u = 0.56 in/min)

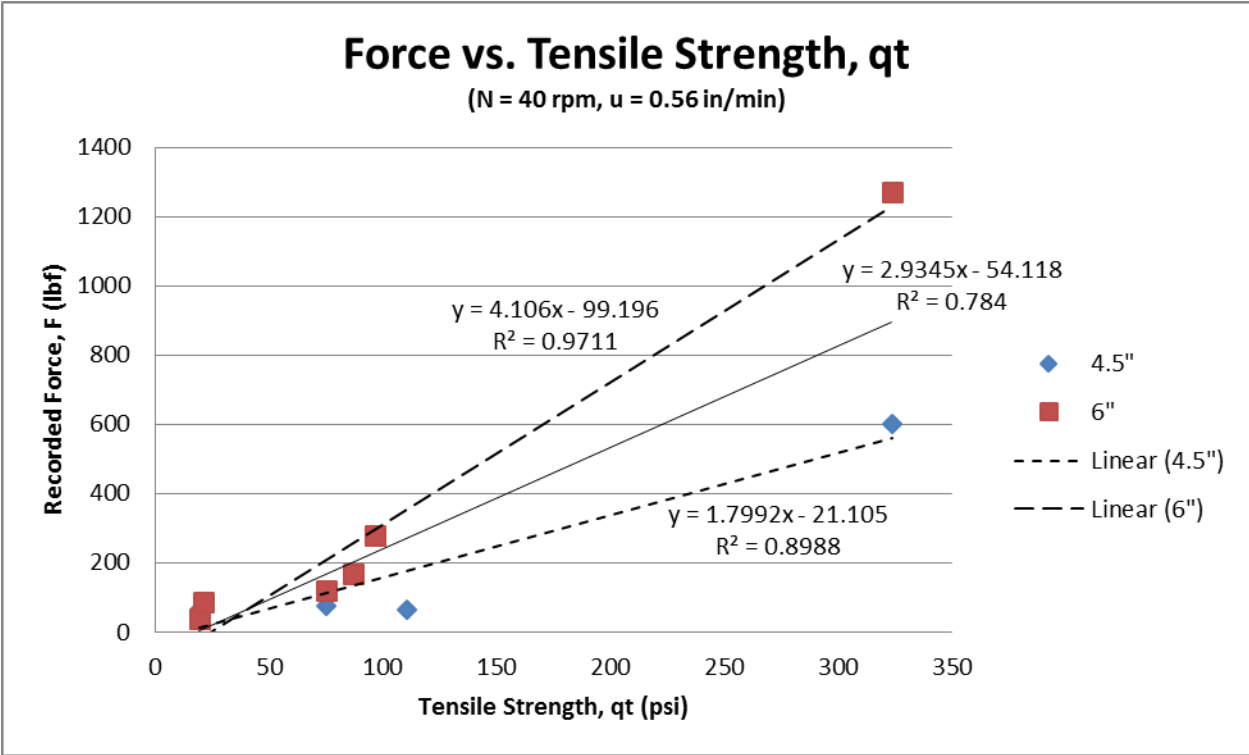


Figure 34 - Force vs. tensile strength (N = 40 rpm, u = 0.56 in/min)

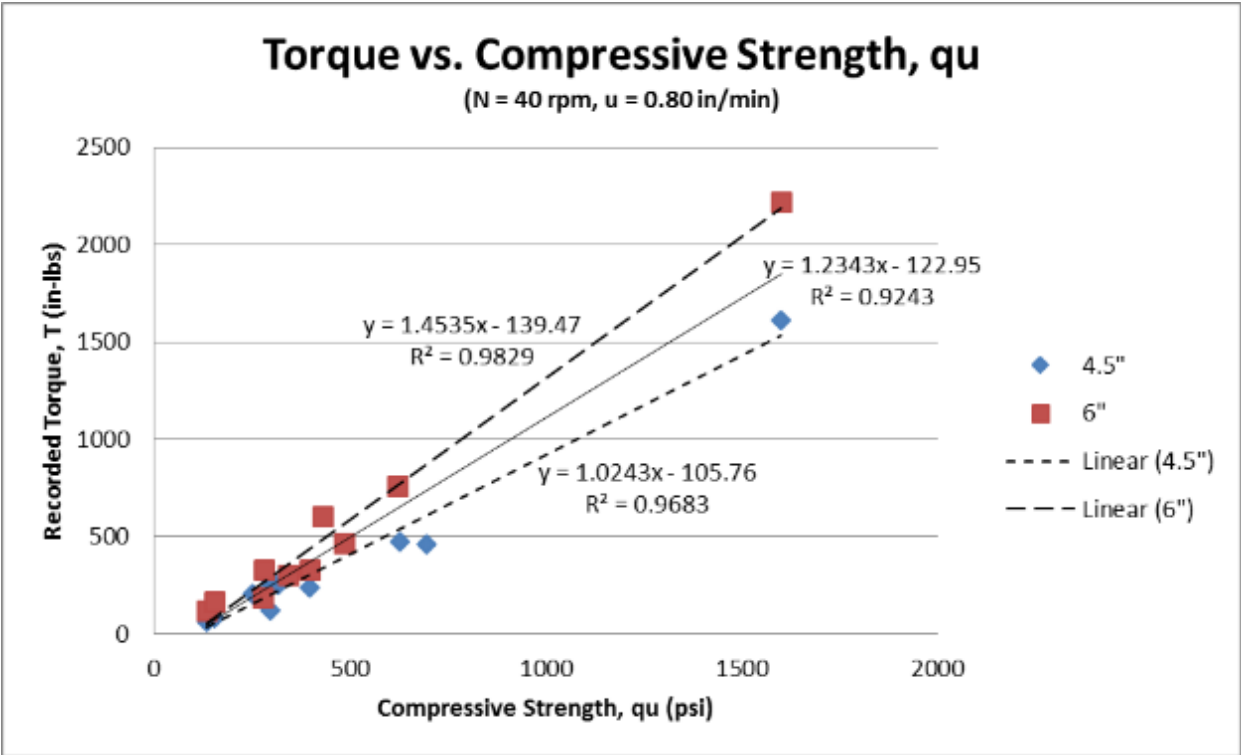


Figure 35 - Torque vs. compressive strength (N = 40 rpm, u = 0.80 in/min)

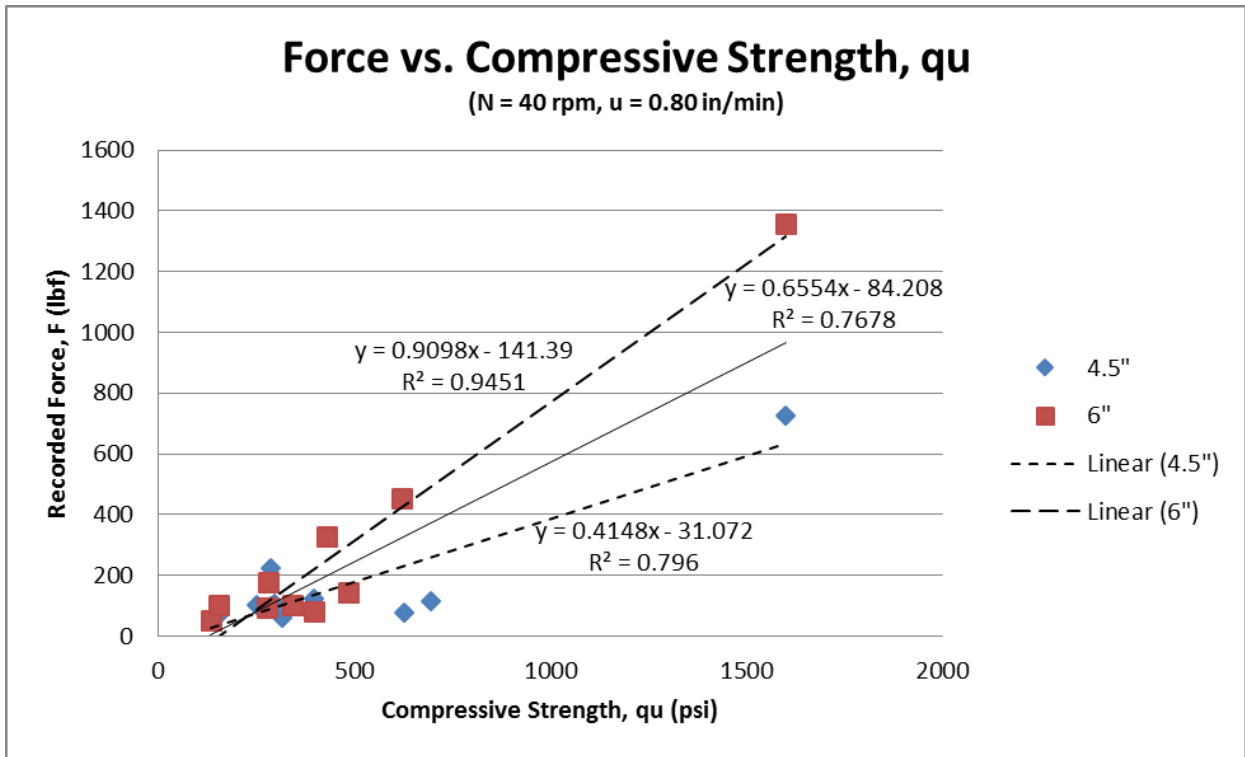


Figure 36 - Force vs. compressive strength (N = 40 rpm, u = 0.80 in/min)

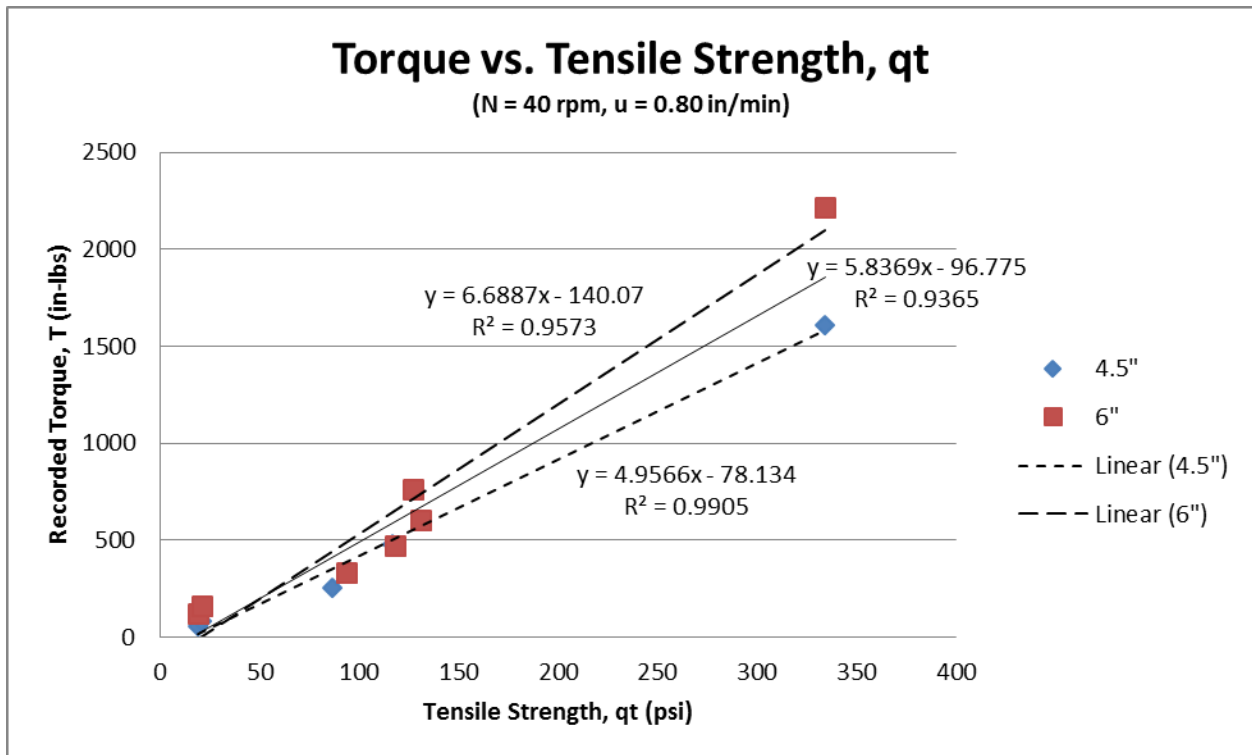


Figure 37 - Torque vs. tensile strength (N = 40 rpm, u = 0.80 in/min)

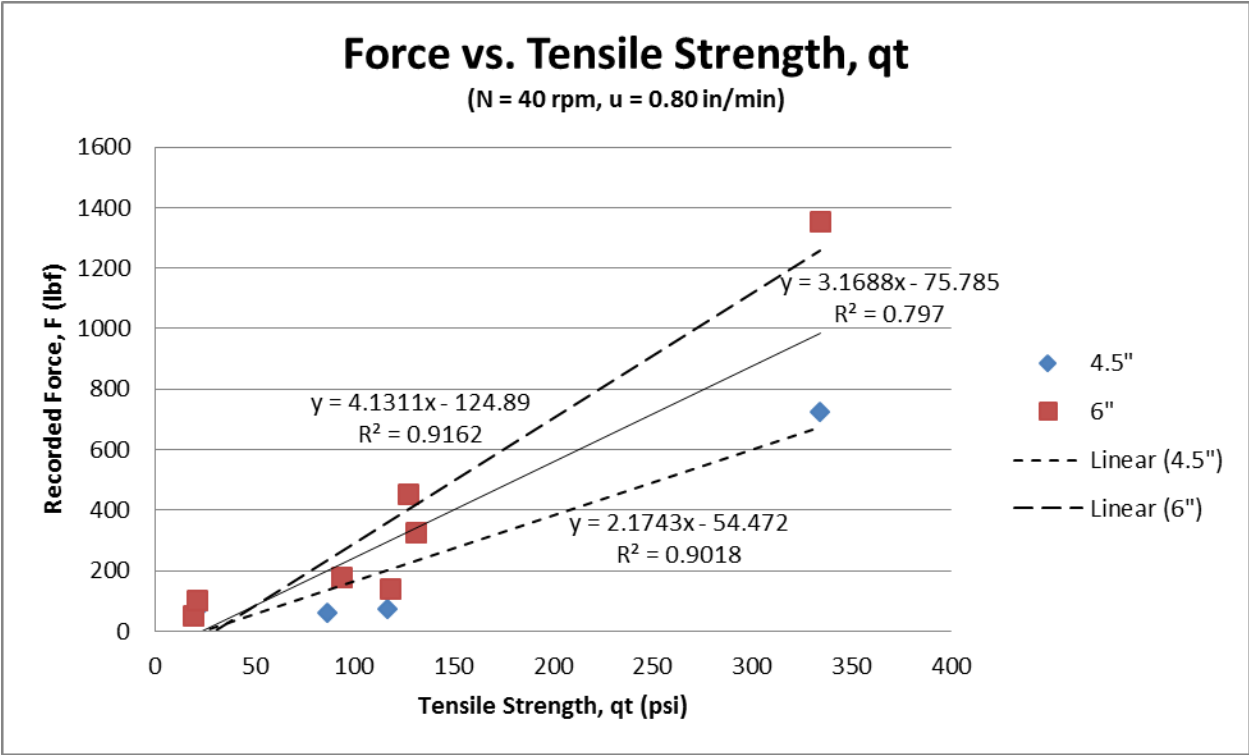


Figure 38 - Force vs. tensile strength (N = 40 rpm, u = 0.80 in/min)

As displayed in the provided plots, it is clear that bit diameter does affect torque and crowd as was expected. The plots also illustrate that crowd is more affected by bit diameter than torque. When comparing the data independently of bit diameter (a single equation for both bit diameters) the average $R^2 = 0.960$ for torque vs. q_u , $R^2 = 0.791$ for crowd vs. q_u , $R^2 = 0.951$ for torque vs. q_t , and $R^2 = 0.800$ for crowd vs. q_t . This validates that the variability of torque is more accurately described by a single equation than the variability of crowd as bit diameters changes.

2.3.3 Increasing Force and Torque Relationship

Investigated next, was how crowd increased with torque independent of the strength of material. This was done by plotting recorded crowd measurements vs. their respective recorded torque measurement. Two plots were created, one for the 4.5" bit and one for the 6" bit. This was done to see if crowd increases with torque at a different rate when using different bit sizes. The two plots are provided here:

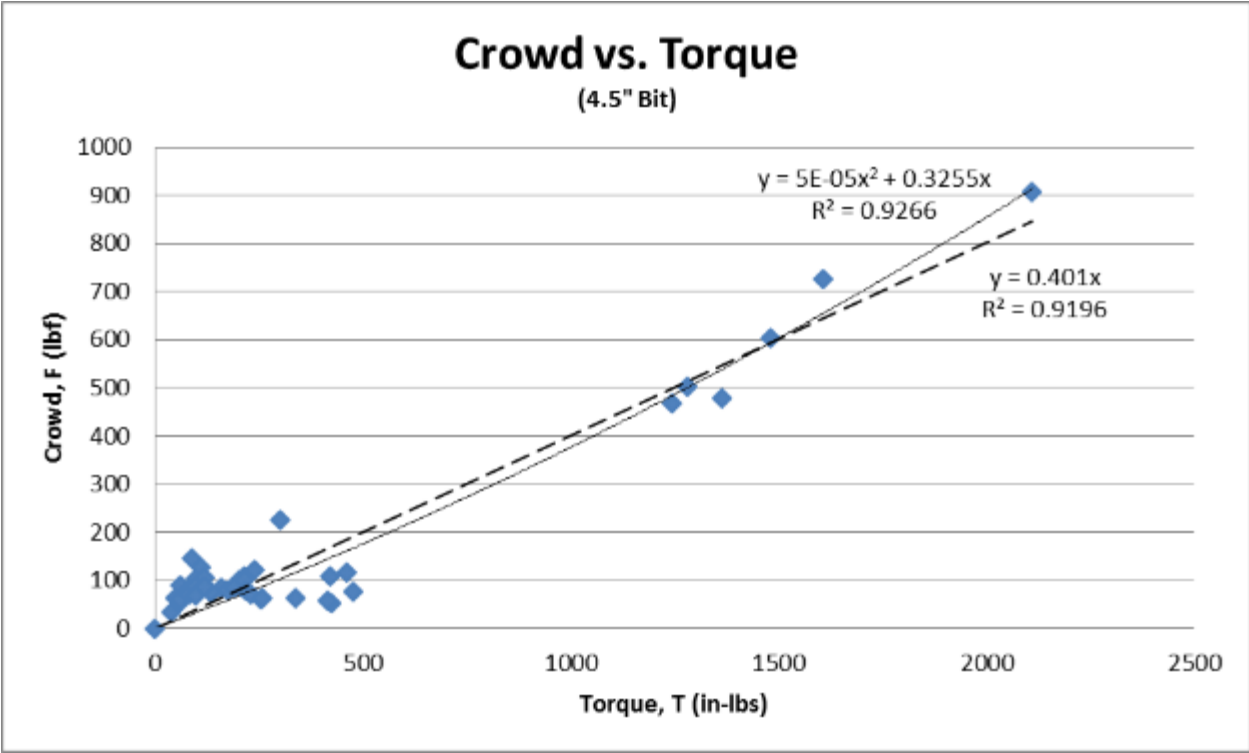


Figure 39 - Crowd vs. torque (4.5" bit) with linear and 2nd order polynomial curve fitting

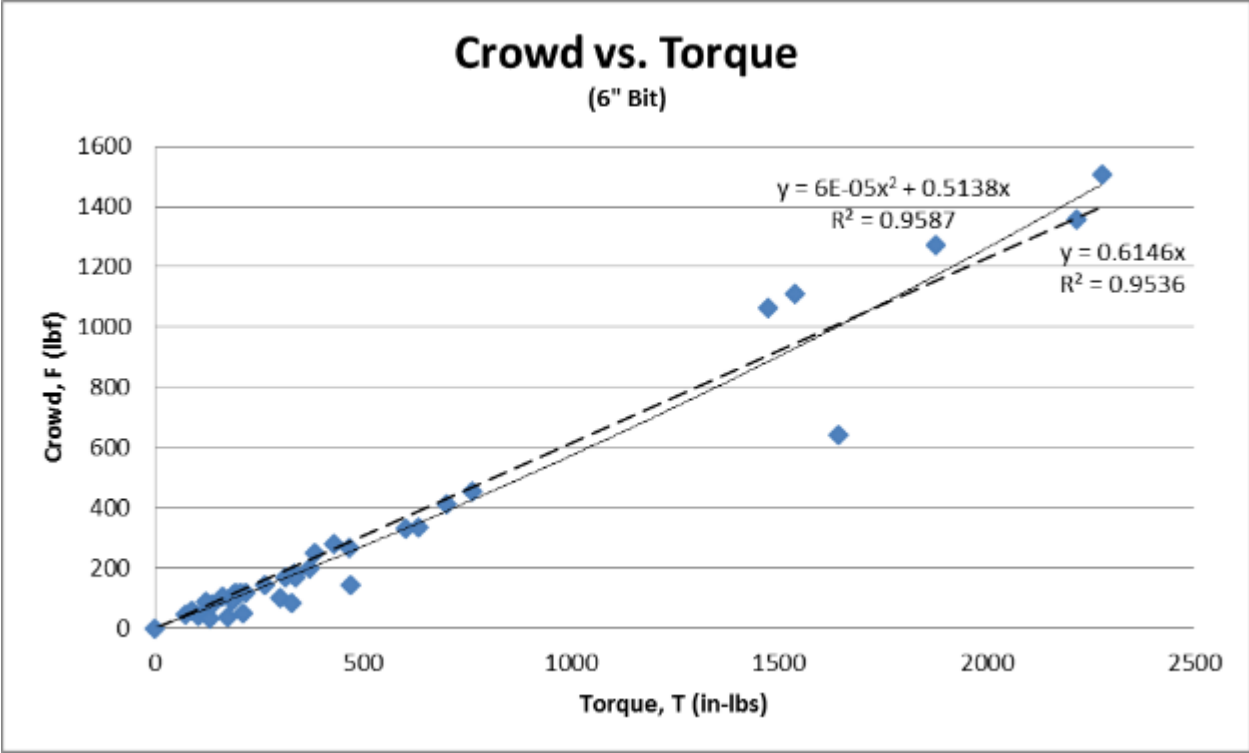


Figure 40 - Crowd vs. Torque (6" bit) with linear and 2nd order polynomial curve fitting

It can be seen that crowd does increase at a higher rate as torque increases using a larger bit diameter. Also of interest is the linear trending of crowd increase with respect to torque. As bit diameter increased, the trend became more linear. This was confirmed by the larger R^2 value for the 6" bit ($R^2 = 0.9536 > R^2 = 0.9196$). These factors were considered for the development of the final equation for field prediction.

2.3.4 Torque and Force vs. Penetration Rate per Rotational Speed Ratio (u/N)

After comparing crowd versus torque, researchers then investigated penetration rate per rotational speed, u/N , plotted vs torque and crowd. This was similar to comparisons made by Karasawa in 2002. However, researchers did not use the normalization that Karasawa used (u/N vs. T was used instead of Karasawa's u/N vs. $8T/d^2$ comparison). This was done to eliminate a bias toward a specific equation moving forward in the development of a final field prediction equation. The research needed to consider all options and not just Karasawa's equation; therefore torque and crowd were compared to the u/N ratios directly without normalization.

When comparisons began it was noticed that strength increases/decreases between groupings used provided a poor result (i.e., using 270 psi, 290 psi and 310 psi with the same u/N ratio provides a poor result because of the changes in compressive strength). Therefore, the low end 140 psi drillings were used for these comparisons. The 140 psi range blocks were drilled using three different penetration rates per block side. This provided a means to investigate the trends of u/N vs. torque and crowd without changes in compressive strength affecting the results. These comparisons can be seen in Figure 41 through Figure 44:

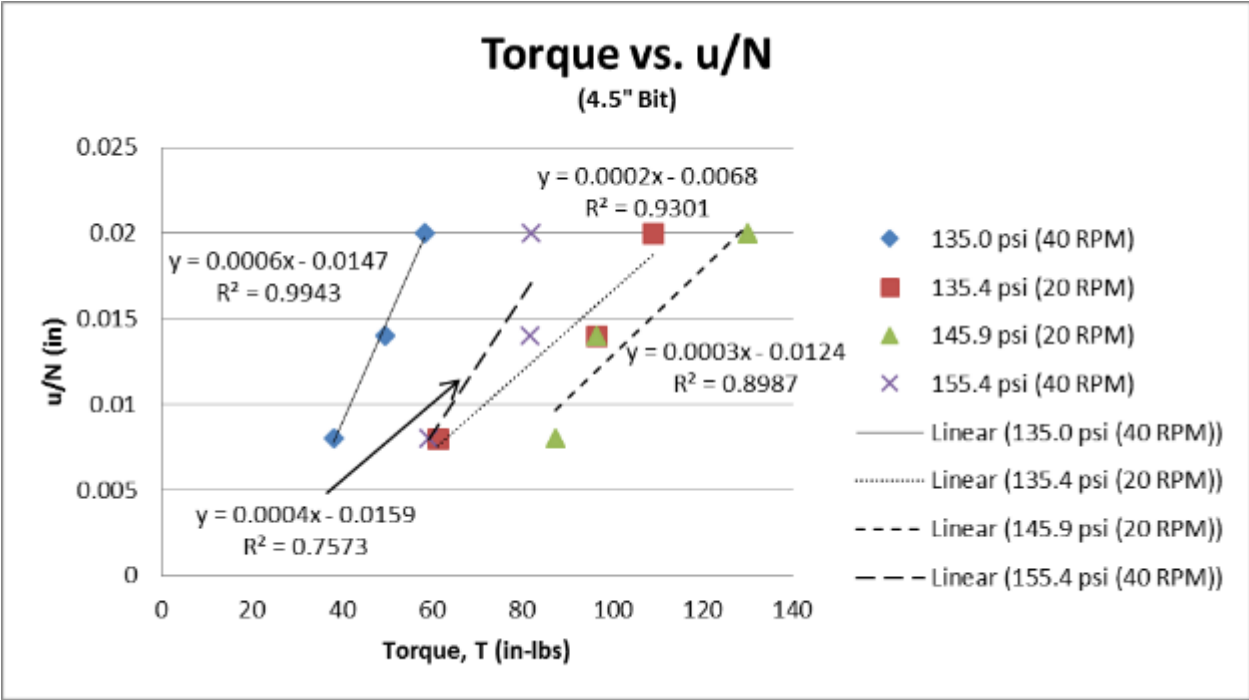


Figure 41 - Torque vs u/N (4.5" bit)

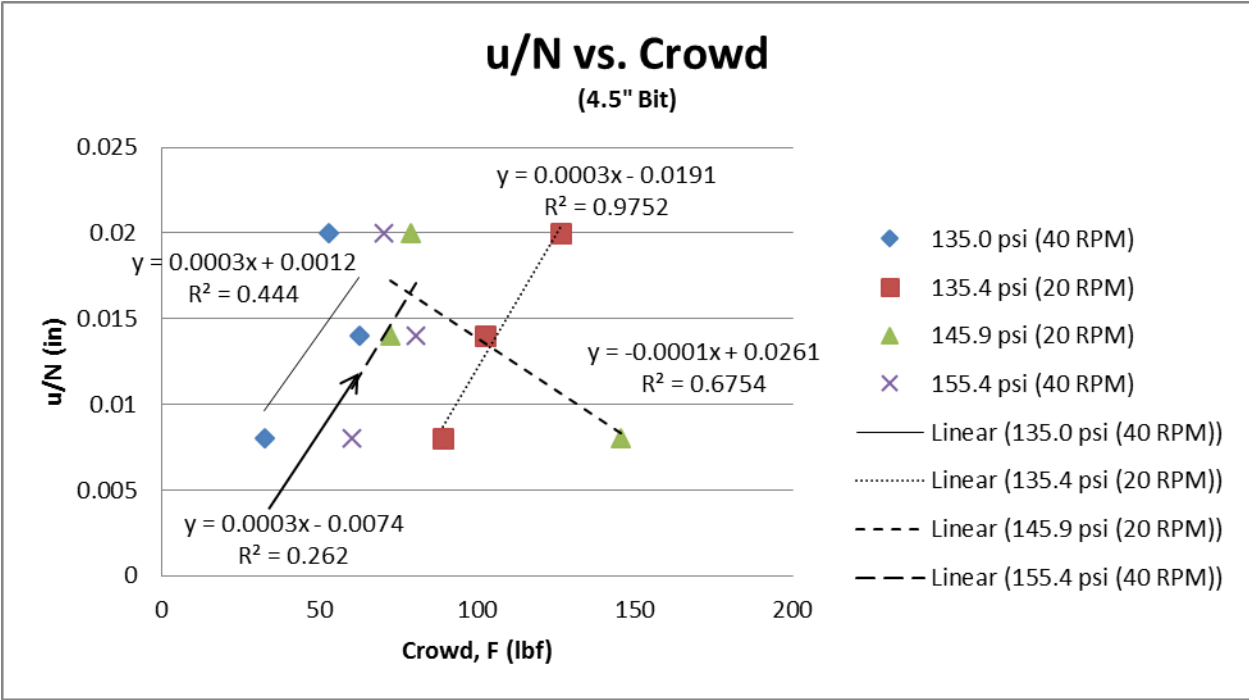


Figure 42 - Crowd vs u/N (4.5" bit)

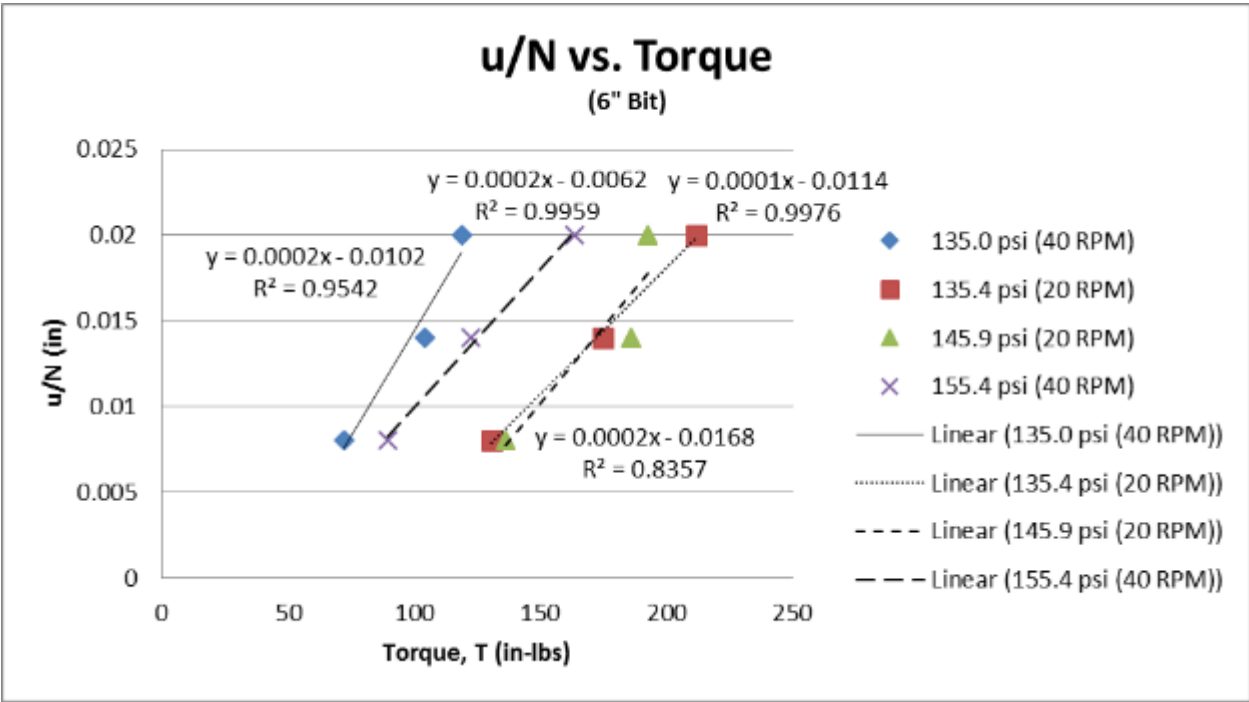


Figure 43 - Torque vs u/N (6" bit)

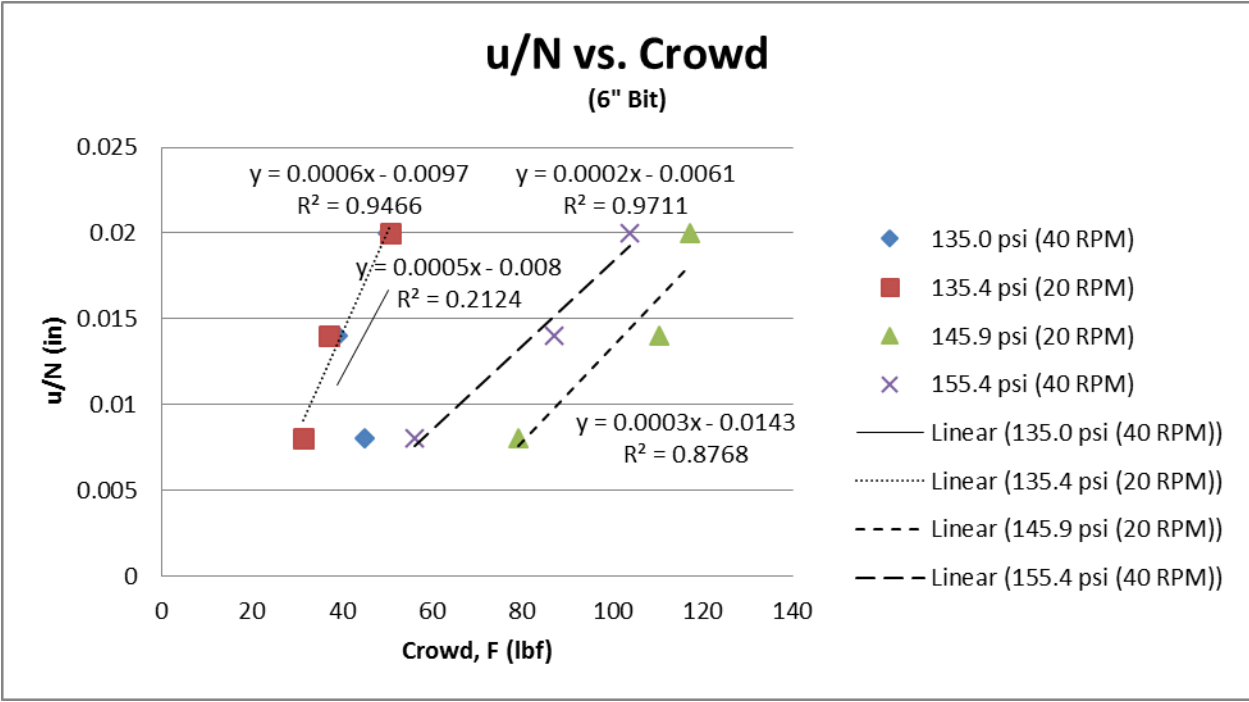


Figure 44 - Force vs u/N (6" bit)

From the provided plots a few trends were noticed:

- Torque and Crowd both show increasing values as the u/N ratio increases
- Lower rotational speeds provide larger torques. This was noticed for both bit diameters where the 40 RPM drillings produced the lowest torques. The highest strength block, 155.5 psi, drilled at 40 RPMs produced a lower torque average than the 135.4 psi block drilled at 20 RPMs. This trend was seen in both the 4.5" and 6" bit diameter plots.
- Trends of torque increasing as rock strength increases are seen in both plots as was expected
- Crowd increases show greater variability with respect to increases in rock strength.

2.3.5 Torque and Crowd vs. Compressive and Tensile Strengths

After investigating the results of u/N vs. torque and crowd plots, researchers then looked for trends when comparing all torque and crowd measurements vs. the respective compressive and tensile strengths of the drilled blocks. If trending of the previous analyses is correct, crowd should show more variability than torque when compared to compressive and tensile strengths. These comparisons can be seen here (Note: linear fit – dashed line, 2nd order polynomial fit – solid line):

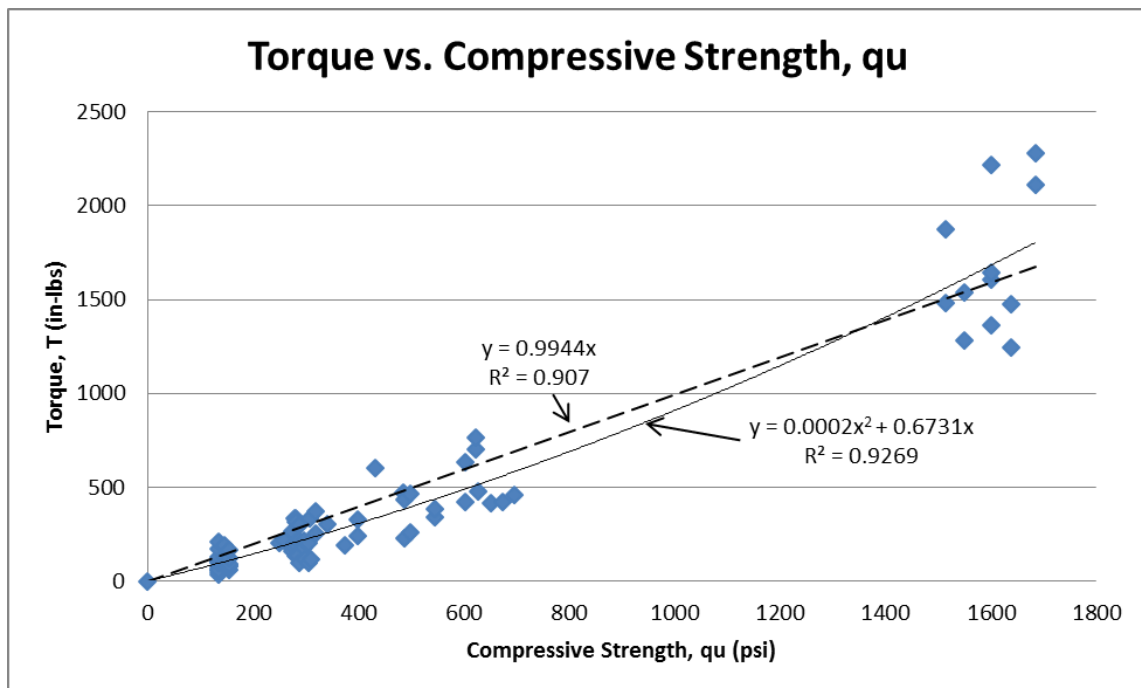


Figure 45 - Torque vs compressive strength with linear and 2nd order polynomial curve fitting

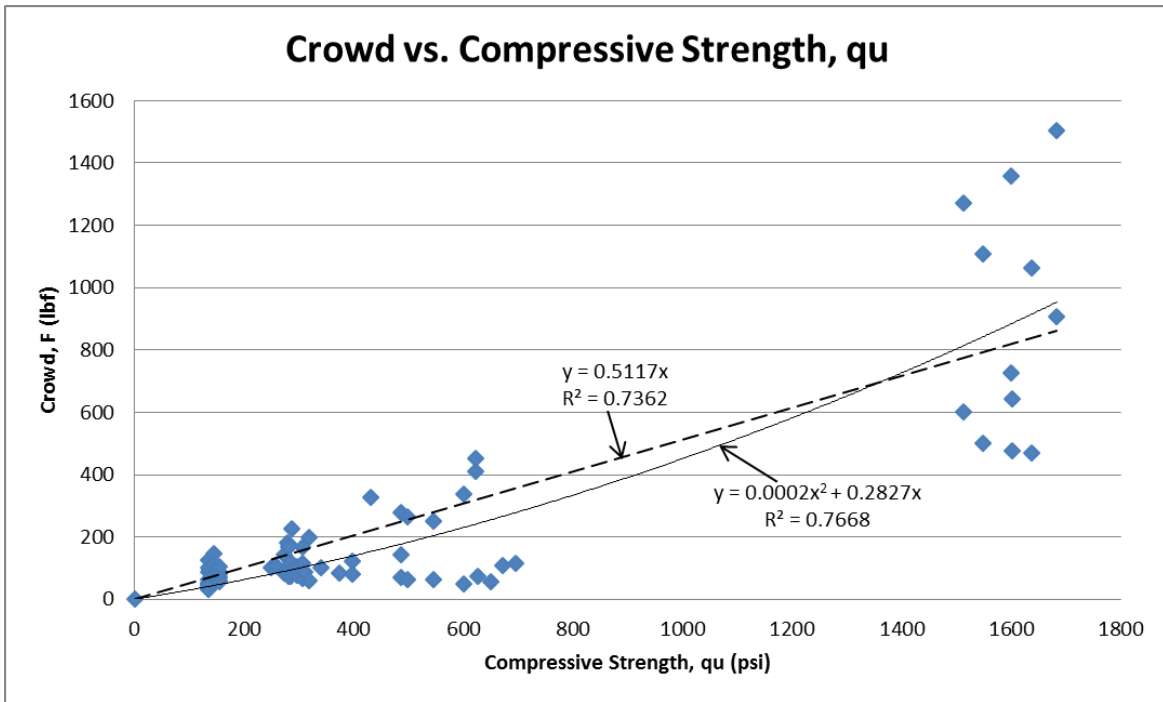


Figure 46 - Crowd vs compressive strength with linear and 2nd order polynomial curve fitting

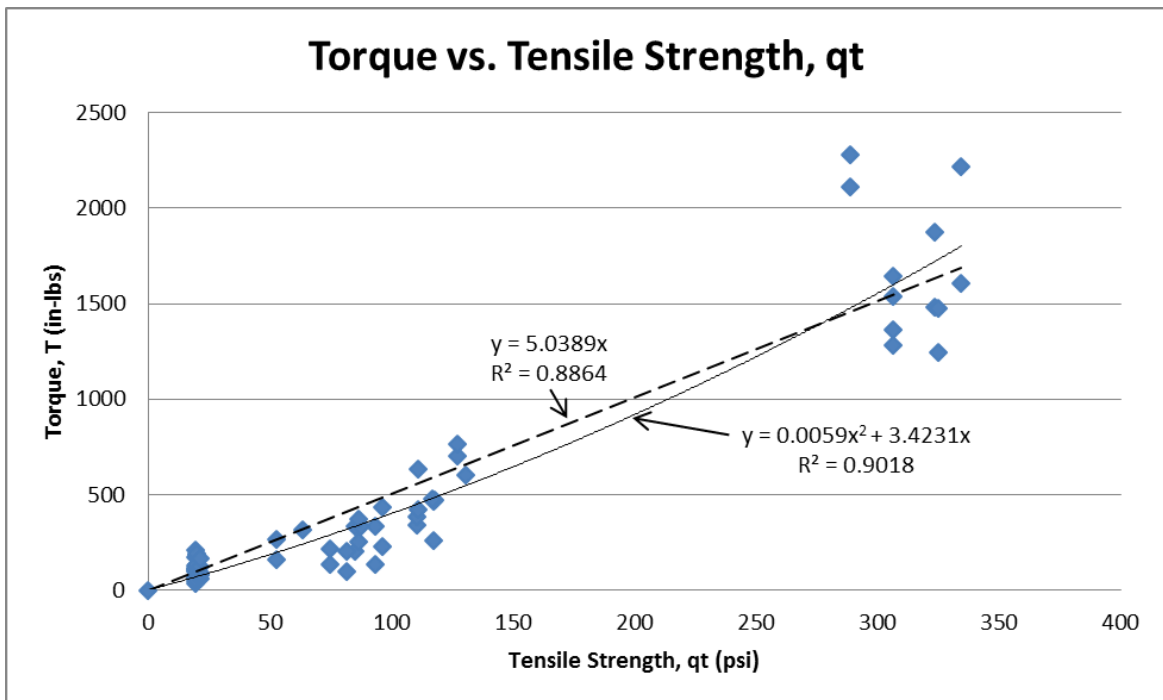


Figure 47 - Torque vs tensile strength with linear and 2nd order polynomial curve fitting

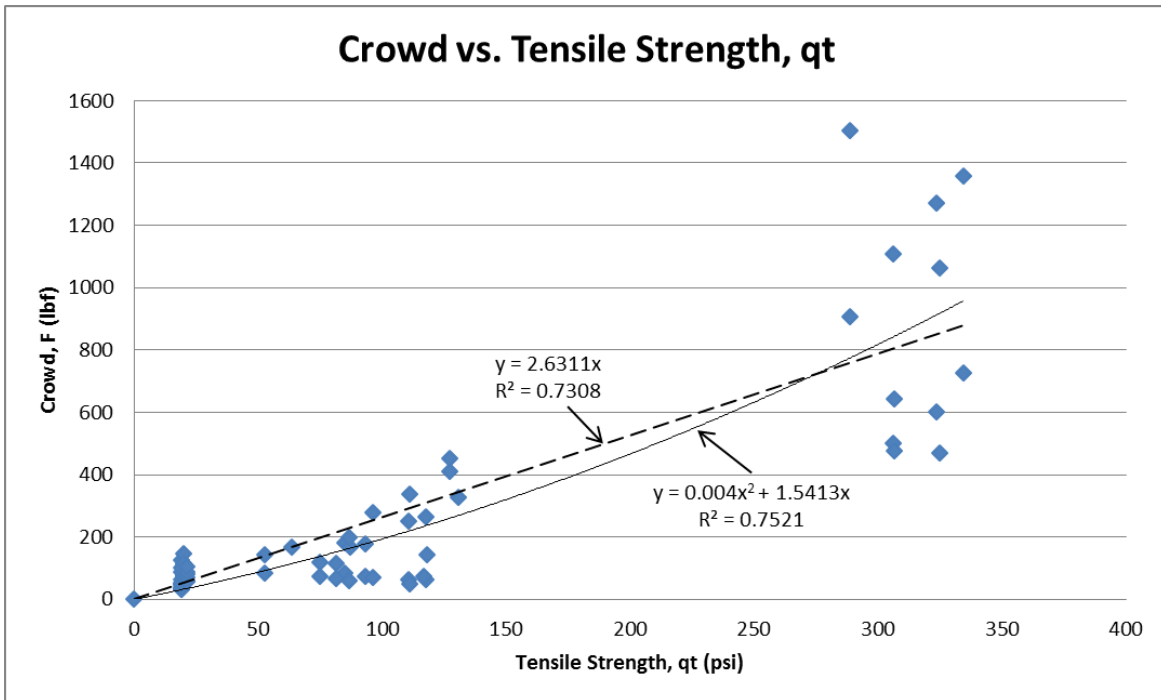


Figure 48 - Crowd vs tensile strength with linear and 2nd order polynomial curve fitting

As expected, crowd displayed far more variability than torque when compared to compressive and tensile strength independent of rotational speed, penetration rate and bit diameter.

From all the previous analyses, conclusions were drawn for torque and crowd:

Torque:

- Shows less dependency on bit diameter
- Shows a strong trend with rotational speed
- Shows a good trend with penetration rate
- Shows good trending when compared to compressive and tensile strength independent of all other drilling parameters

Crowd:

- Shows more dependency on bit diameter
- Shows a poor trend with rotational speed
- Shows a decent trend with penetration rate
- Shows decent trend compared to compressive and tensile strengths independent of all other drilling parameters

From these conclusions it can be stated that torque is a far more reliable drilling parameter than crowd when it comes to predictability. As field equations were developed, this was considered for reliability of prediction. It was identified that any developed field equations will need to be free of bit size dependency as upscaling bit diameters will play a major role. As was noticed, crowd is far more dependent on bit size and provides less reliability compared to all drilling parameters. Therefore, a desirable field equation will place less emphasis on crowd and bit diameter and focus more on torque, rotational speed and penetration rate. The following section provides the finalized D_s vs q_u and D_s vs q_t curves based on Karasawa's drilling equations developed in 2002.

2.3.6 Developed D_s vs. q_u and D_s vs. q_t Curves

Once all lab drillings were completed and the data reduced, the finalized D_s vs. q_u and D_s vs. q_t curves were created. The drillability strength D_s was derived from Karasawa's equation developed in 2002, displayed here:

$$D_s = \frac{64NT^2}{F_{ud}^3} \dots\dots\dots \text{Eq 1}$$

Both curves are presented here with bit sizes analyzed independently and dependently (i.e., an equation and curve fit developed for each bit size and as a whole):

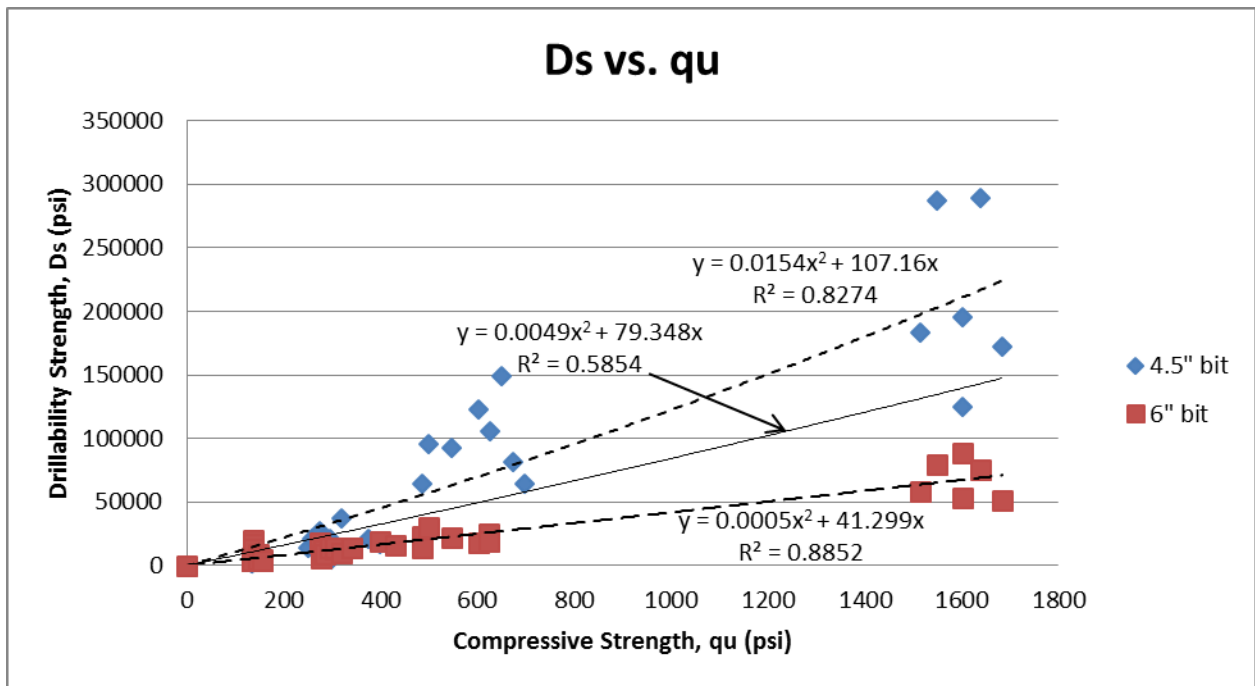


Figure 49 - D_s vs q_u plot

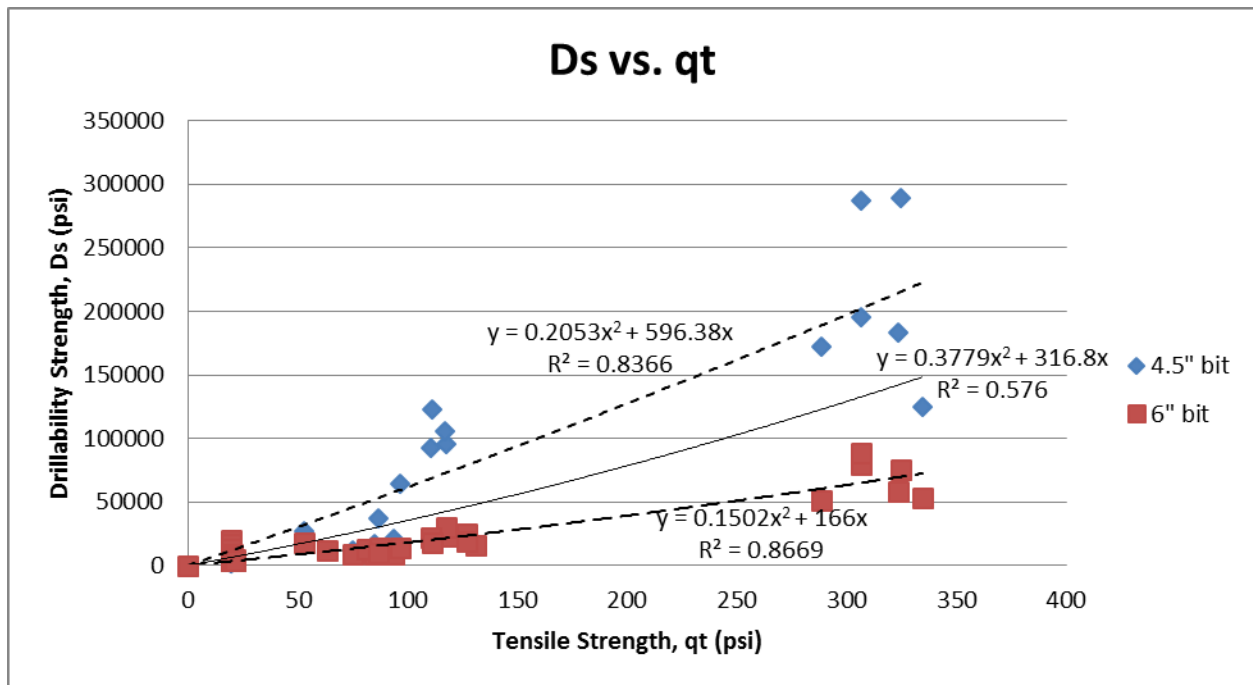


Figure 50 - D_s vs q_t plot

From the developed curves it can be seen that Karasawa's equations are highly dependent on the diameter of the bit. Curve fitting shows good trending for each bit diameter independently from one another but poor trending using a single equation to define all of the drillings. This can also be seen in his report from 2002:

Table 17 - Karasawa's effect of bit diameter on I_s , S_e , and D_s (2002b report)

Bit Dia.	I_s (MPa)	S_e (MPa)	D_s (MPa)
101.6 mm(4")	218	154	108
127.0 mm(5")	229	137	82.0
142.88mm(5-5/8")	231	127	69.6

Rock: Sori Granite (B), Rotary Speed: 50 rpm

From Karasawa's report it was stated, "The drilling tests, using new insert bits with different diameters, were not intended to clarify the complete effect of bit diameter on the rock drillability systematically. Rather the objective of these tests was to

demonstrate one example of how bit diameter affects I_s , S_e , and D_s ". This is likely due to Karasawa's experiments using bit diameters that were representative of field drilling conditions where no up-scaling would be required. As for the purposes of this research application, Karasawa's equations would not be an ideal option moving forward in developing field predictability equations. As stated in the scope, researchers also investigated other various methods for analysis. The most promising of these equations came from Teale's work completed in 1965.

2.3.7 Development of e vs. q_u Curve using Teale's Equations, 1965

In Teale's report, *The Concept of Specific Energy in Rock Drilling*, he states that in rotary non-percussive drilling, work is done by the thrust, F , and the torque, T . If the rotational speed is N , the area of the hole or excavation is A , and the penetration rate is u (all using the standard units researchers have been using), the total work done in one minute is:

$$W = Fu + 2\pi NT \dots \dots \dots \text{Eq 2}$$

The volume of rock excavated in one minute is Au where A is cross-sectional area and u is change in penetration depth.

Putting e as the specific energy, dividing work by volume, gives

$$e = \frac{F}{A} + \left(\frac{2\pi}{A}\right) \left(\frac{NT}{u}\right) \dots \dots \dots \text{Eq 3}$$

Using subscripts t and r to denote the "thrust" and "rotary" components of e ,

$$e_t = \left(\frac{F}{A}\right) \dots \dots \dots \text{Eq 4}$$

and,

$$e_r = \left(\frac{2\pi}{A}\right) \left(\frac{NT}{u}\right) \dots \dots \dots \text{Eq 5}$$

Note that Teale states that the thrust component, (F/A) , is equivalent to the mean "pressure" exerted by the thrust over a cross-sectional area of the hole. Specific energy is, in fact, dimensionally identical with pressure or stress. (Physically this arises from the fact that if a force F acting on and normal to a surface of area A moves through a distance ds , the increment of work done, dW , is equal to Fds . The volume change

effected by the movement, dV , is Ads . If e is the specific energy at any point, then $e = dW/dV = F/A = P$, the pressure at that point.). For a given size of excavation, A is constant so that e_t is directly proportional to F . It is always small in comparison with e_r , i.e., sometimes negligible.

Teale's note where he states the thrust component is always small in comparison with the torque component makes sense when applying it to field drilling. From conversations with multiple rig operators, all of them stated that one should always let the torque to do the work. This was also noticed and recorded during pilot project field monitoring as well. In the field, penetration rates are rarely consistent. However, rotational speeds are almost always held at a consistent rate (not an exact rate). This is because the rig operators will "work" the rock first before advancing the bit. This allows the torque to provide the cutting action and prevents overcrowding of the bit and possible stall or snapping of the Kelly bar. Teale's equation fundamentally makes sense placing more emphasis on the parameters that are providing the majority of the work. Also of interest, it has been witnessed in the field that sometimes rig operators will fracture a rock layer without using rotation or torque. They simply pound the rock layer using crowd until it is fractured. Researchers believe this is not a recommended method, but Teale's equation would compensate for a zero rotary component by placing all the work done on the thrust component (an index value would still be obtained without a torque or rotation component; this would not be possible with Karasawa's equations). Teale's equation also provides less bit diameter dependency than Karasawa's equation. The bit diameter is squared for Teale's equation and cubed for Karasawa's equation. This is because Teale only uses bit diameter to define the area of the excavation whereas Karasawa places additional emphasis on bit diameter. The following are the developed specific energy vs compressive strength plot, e vs. q_u and the specific energy vs. split tension strength plot, e vs. q_t :

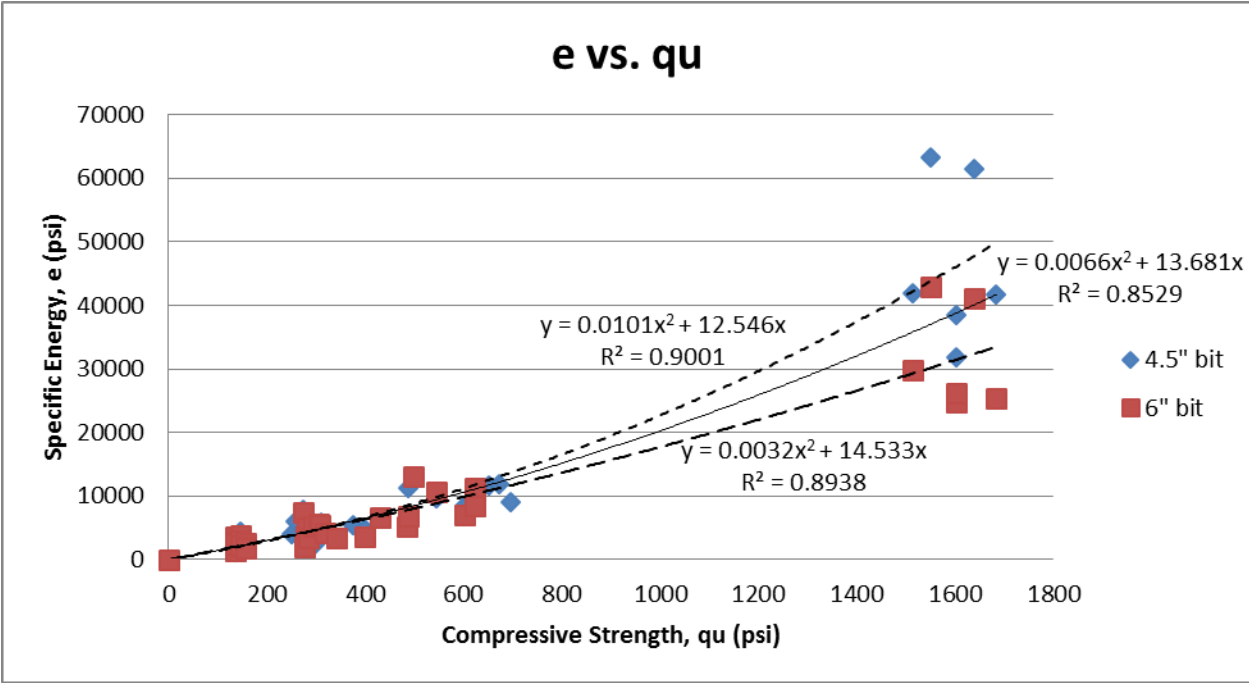


Figure 51 - Specific energy vs compressive strength

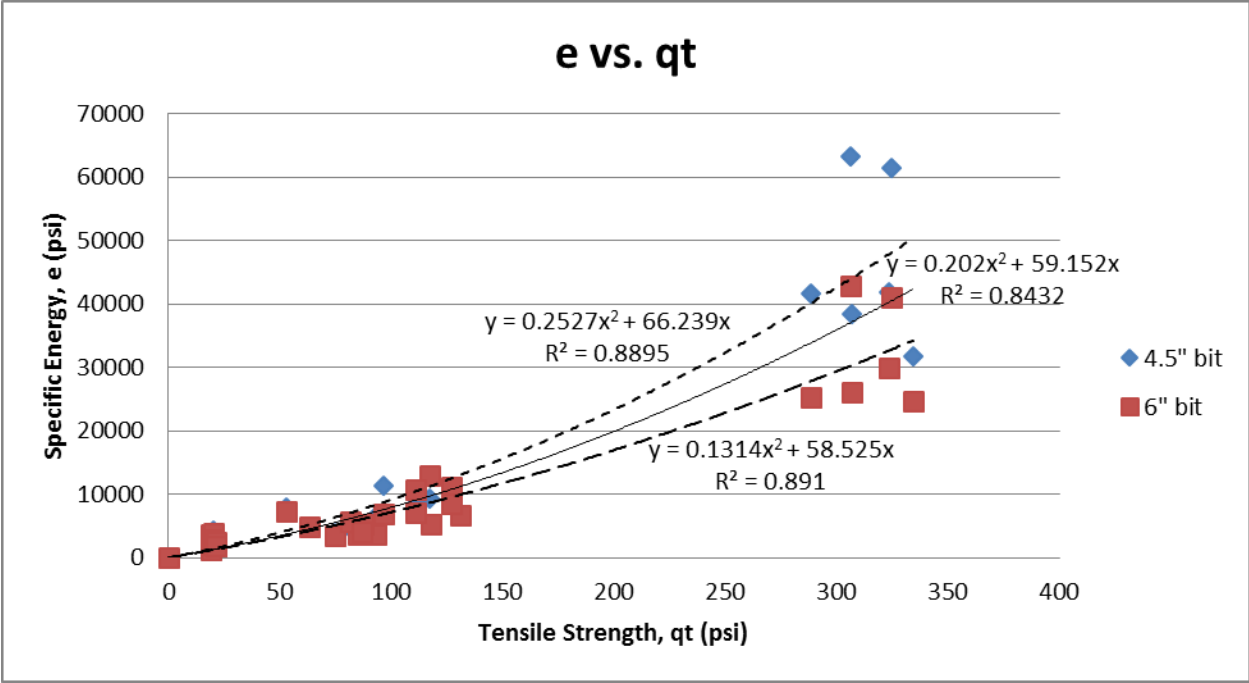


Figure 52 - Specific energy vs tensile strength

As seen in both figures, plotting specific energy vs. compressive and tensile strength provided a better result than Karasawa's drillability equations when analyzing both bit sizes separately and as a whole. Comparing R² values for both compressive and

tensile strengths, Teale produced the better fit, thus explaining more of the variation ($R^2 = 0.8529 > 0.5854$ for compressive, $R^2 = 0.8432 > 0.576$ for tensile).

2.3.8 Comparing Teale and Karasawa

After comparing Teale and Karasawa's equations on the basis of bit diameter, comparisons were then made on the basis of rotational speed and penetration rate.

2.3.8.1 Comparisons Based on Rotational Speed

The following provides comparison of Karasawa's and Teale's equations based on rotational speed groupings (i.e., 20 RPM drillings are grouped together and 40 RPM drillings are grouped together, regardless of bit diameter or penetration rate. Note: the small dashed lines are for 20 RPM, the large dashed lines for 40 RPM and the solid lines for both):

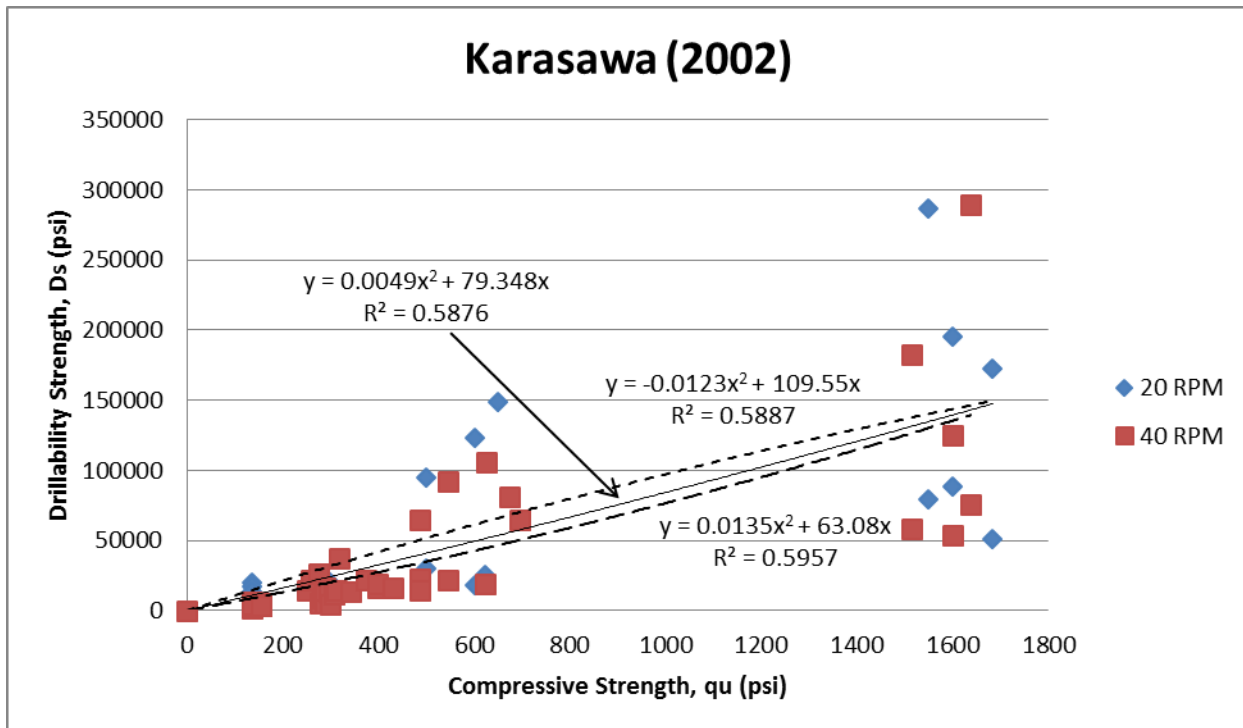


Figure 53 - D_s vs q_u (grouped by rotational speeds)

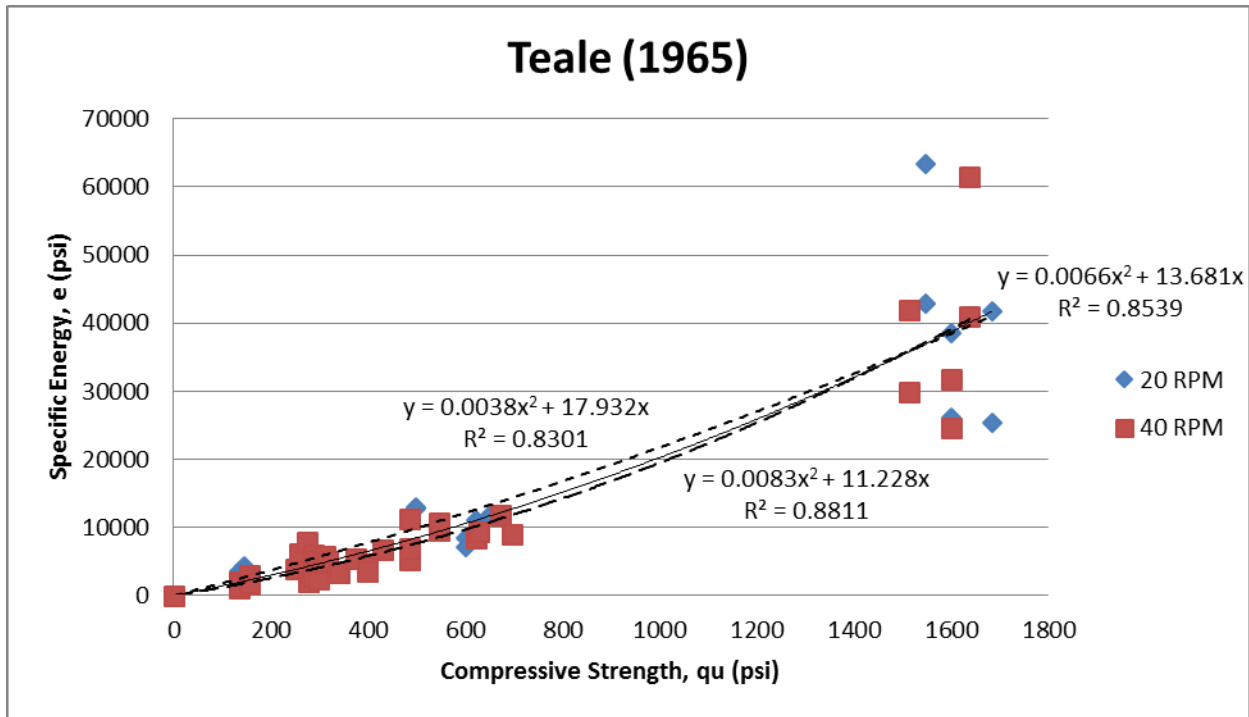


Figure 54 - e vs q_u (grouped by rotational speeds)

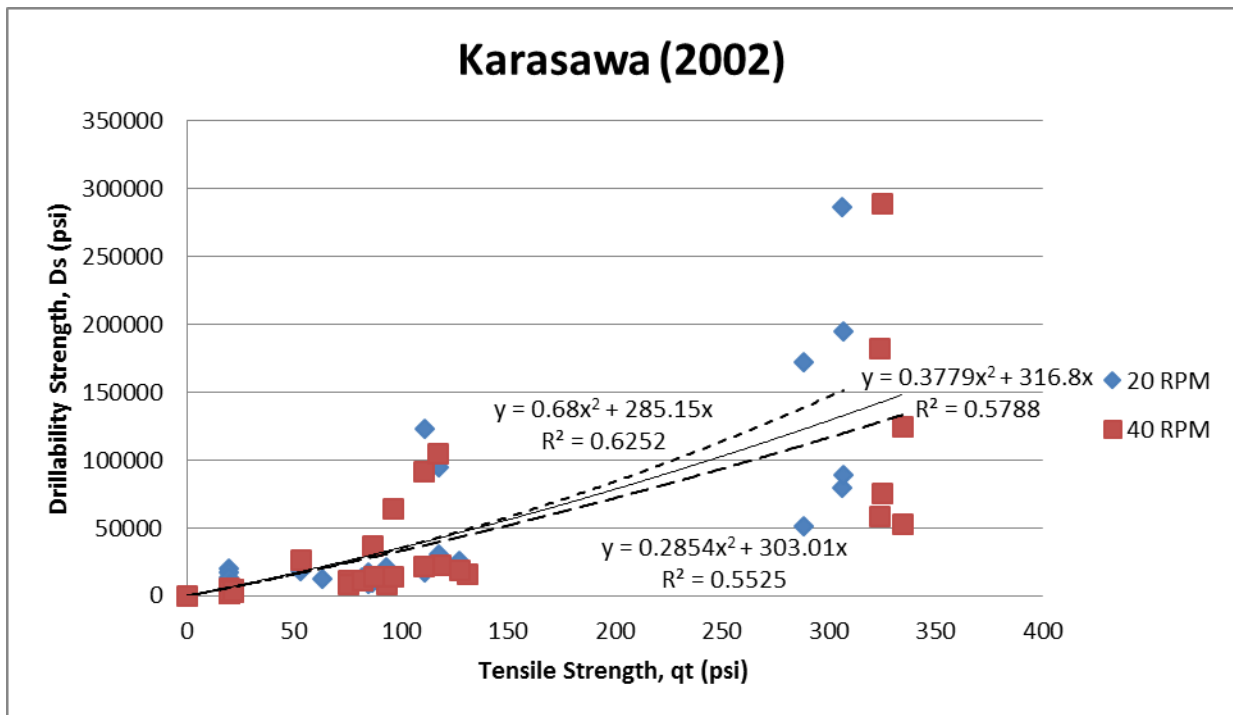


Figure 55 - D_s vs q_t (grouped by rotational speeds)

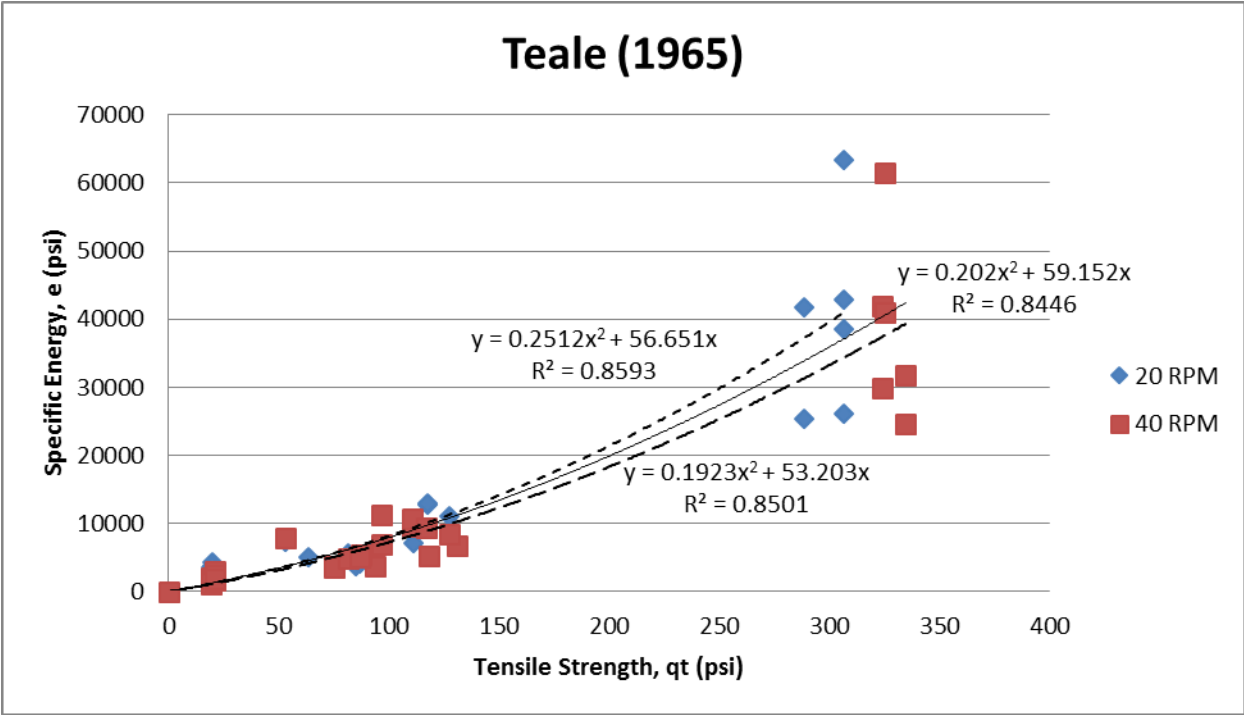


Figure 56 - e vs qt (grouped by rotational speeds)

In comparing the two equations based on rotational speed groupings, it is evident (R^2) that Teale’s equation is superior in describing the variability.

2.3.8.2 Comparisons Based on Penetration Rates

The next comparison shows groupings based on penetration rates for each rotational speed (This was done to reduce the plots from being far to cluttered with 6 different penetration rates). The comparisons can be seen here (Note: curve equations and R^2 values for all penetration rates combined are displayed atop the legend):

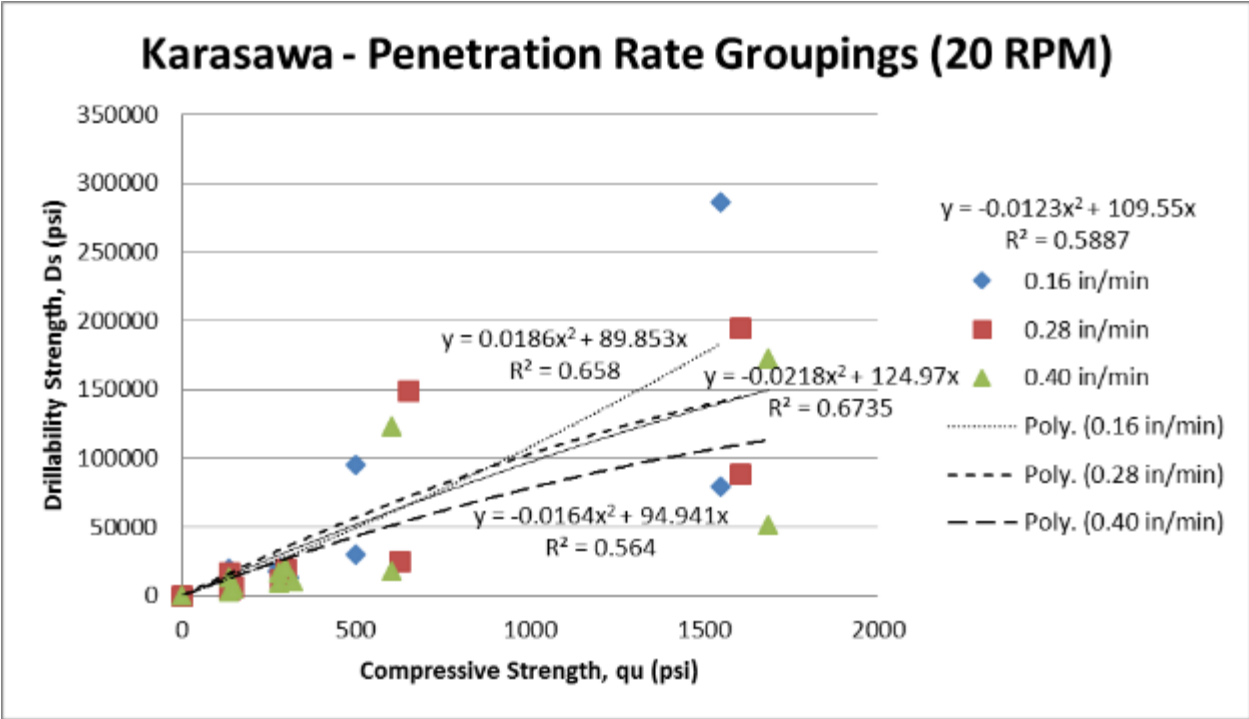


Figure 57 - D_s vs q_u (grouped by penetration rates for 20 RPM drillings)

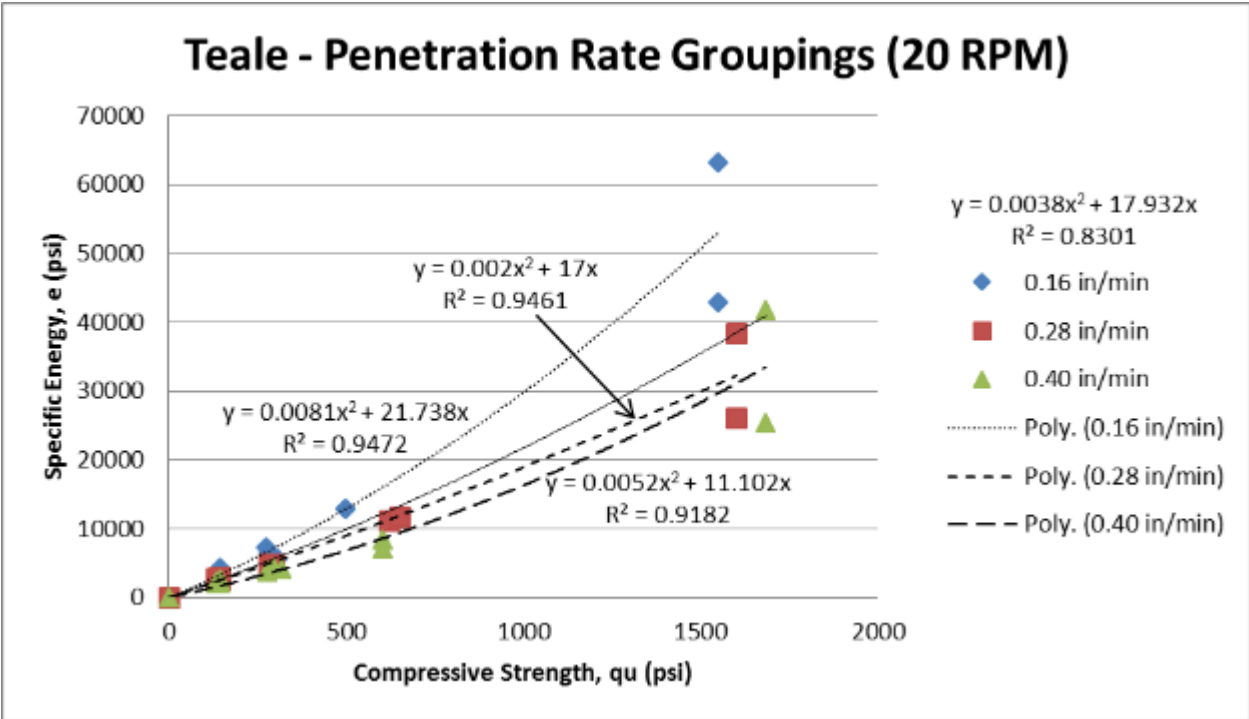


Figure 58 - e vs q_u (grouped by penetration rates for 20 RPM drillings)

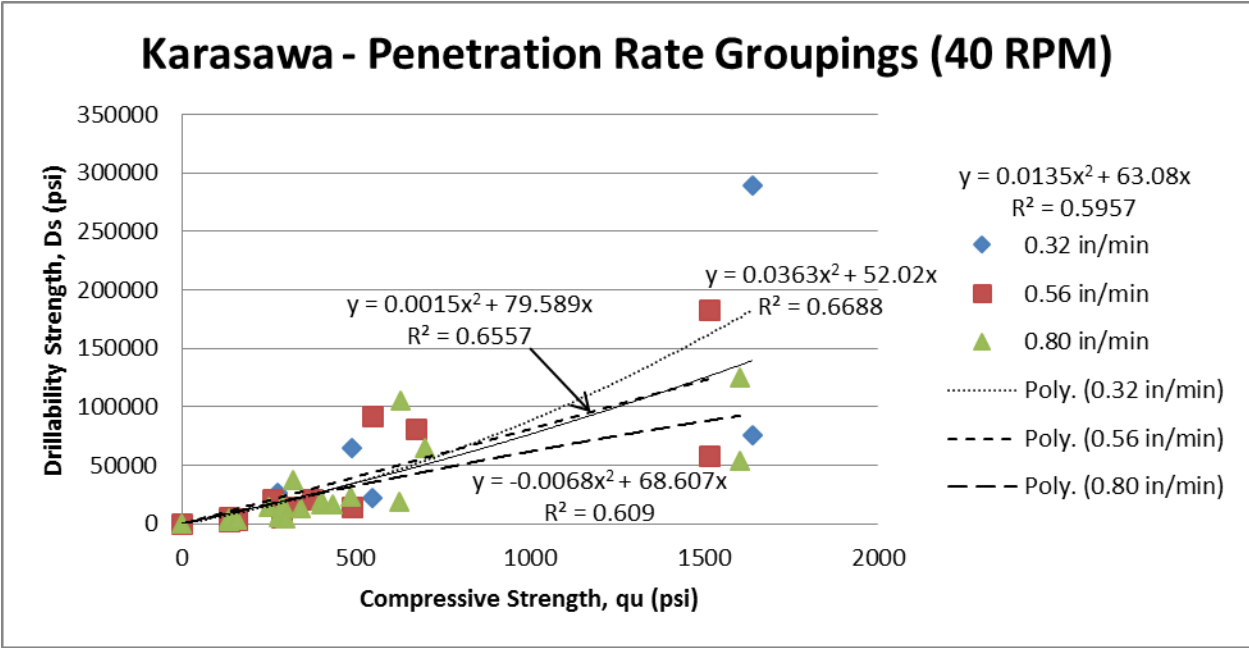


Figure 59 - D_s vs q_u (grouped by penetration rates for 40 RPM drillings)

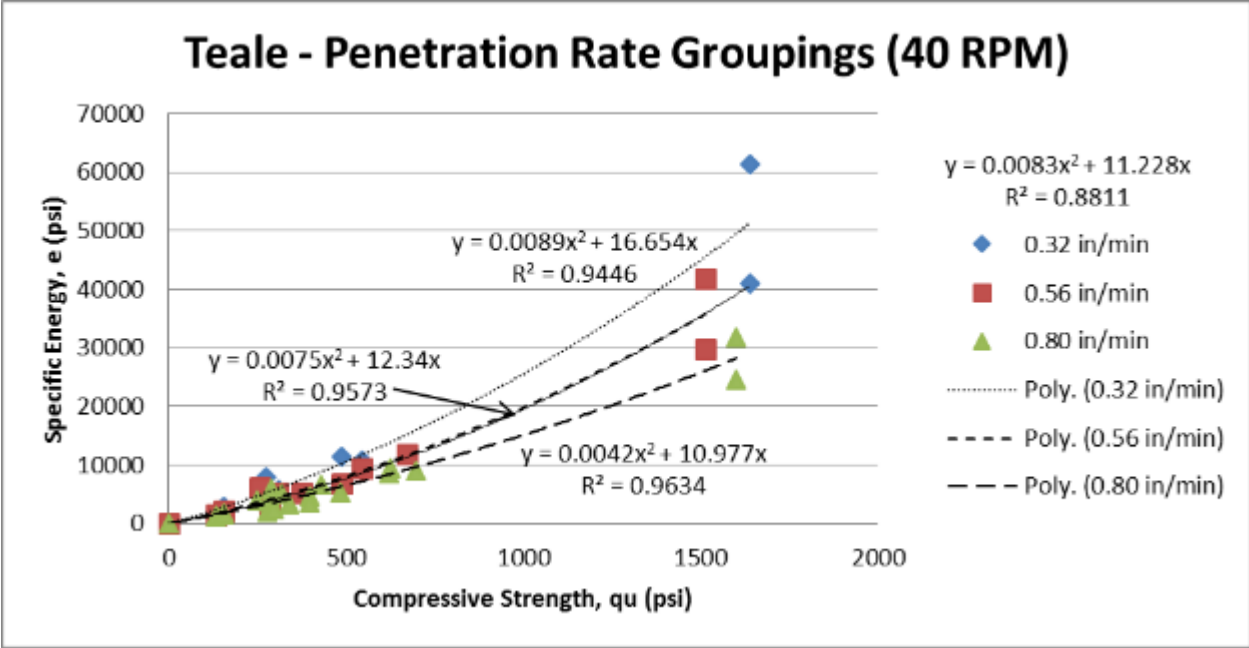


Figure 60 - e vs q_u (grouped by penetration rates for 40 RPM drillings)

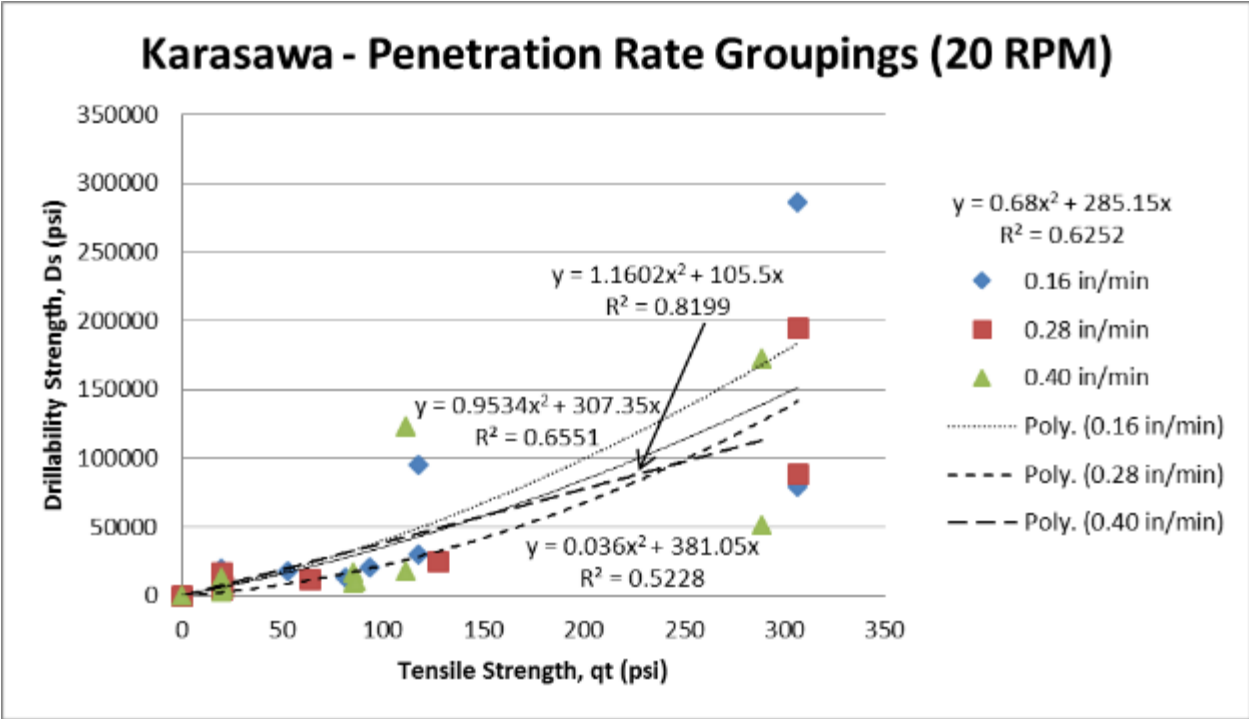


Figure 61 - D_s vs q_t (grouped by penetration rates for 20 RPM drillings)

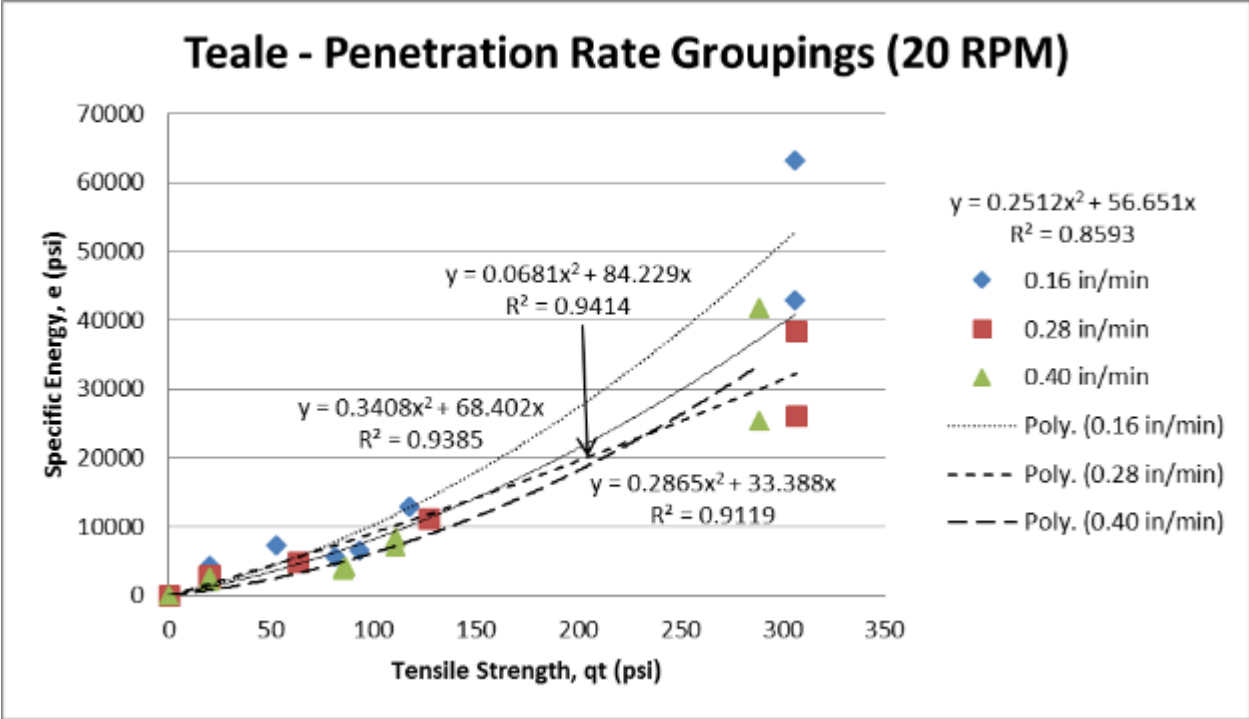


Figure 62 - e vs q_t (grouped by penetration rates for 20 RPM drillings)

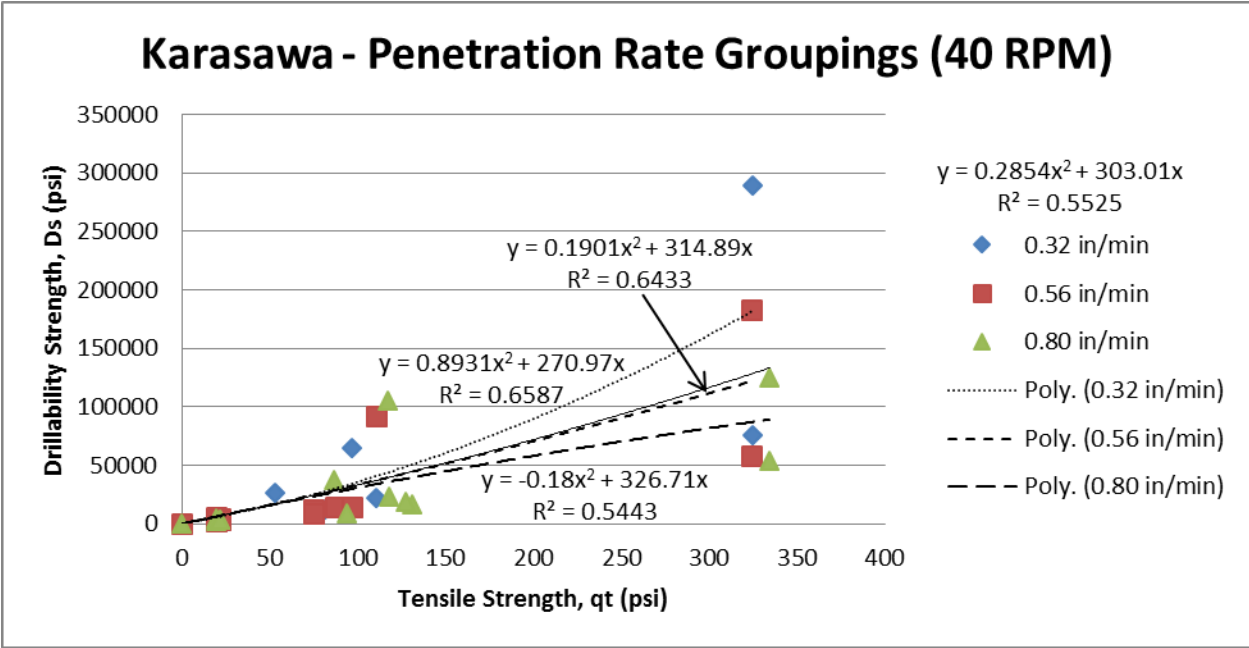


Figure 63 - D_s vs q_t (grouped by penetration rates for 40 RPM drillings)

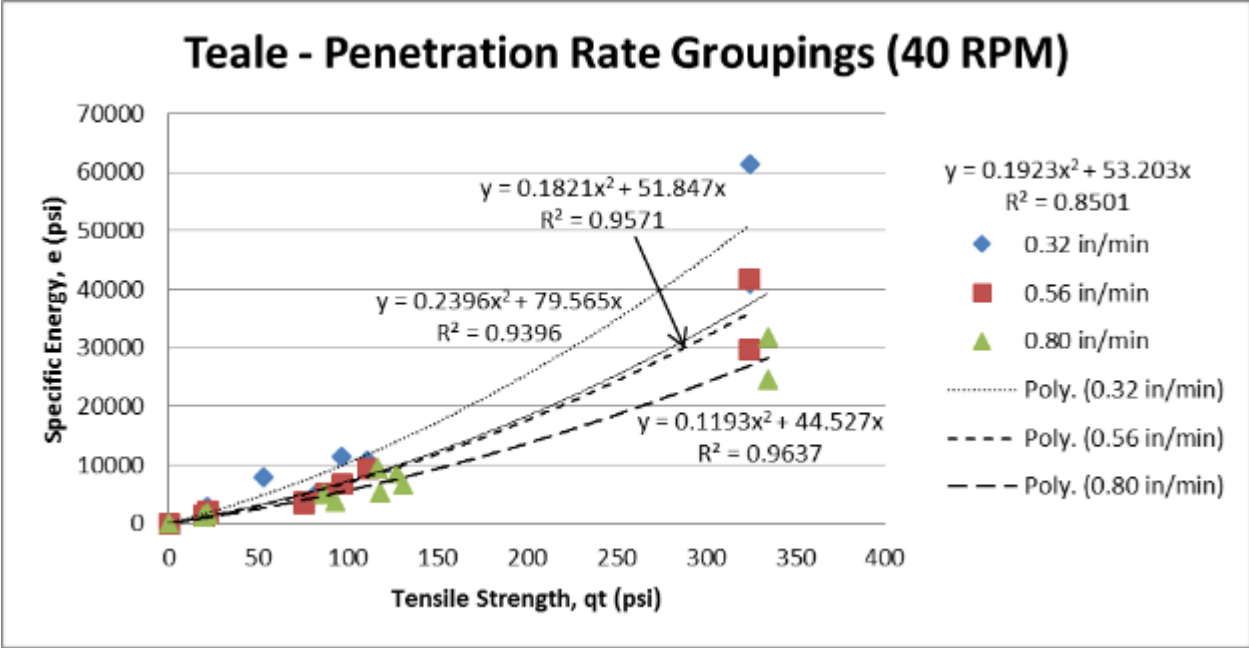


Figure 64 - e vs q_t (grouped by penetration rates for 40 RPM drillings)

From the provided comparisons, again it is evident that Teale's equation is superior when grouping results by penetration rates.

From all comparisons between the 2 developed equations, it is apparent that Teale's equation is superior to Karasawa's equation for describing variability of the results based on bit diameter, rotational speed and penetration rate. Moving forward it appeared Teale's equation would likely be the equation that provided the best results.

It is important to note that predicting both q_u and q_t was needed to use the recommended skin friction equation from the FDOT's Soils and Foundations Handbook, SFH, developed by McVay et al. (1992). The equation is presented here:

$$f_s = 1/2 \times q_u^{0.5} \times q_t^{0.5} \dots\dots\dots \text{Eq 6}$$

Using both q_u and q_t to calculate skin friction allows for adjustments to be made based on material formation, q_t/q_u . Johnson's criteria (1985), explains that the q_t/q_u ratio for various geomaterials is not the same. For example, Johnston's findings showed the split tension strength for carbonate materials, such as limestone and dolomite, is higher than that of lithified argillaceous materials, such as clay and mudstone, with the same compressive strength. Therefore, it was assumed that some form of q_t adjustment would be needed to accurately predict skin friction in the field; as the material formation, q_t/q_u , of concrete provides greater tensile strength compared to limestone with the same compressive strength (Anoglu, 2006). Since Gatorock was designed as a CLSM, a form of concrete, the assumption seemed reasonable. Johnston's criteria will be discussed in detail in Section 3.5.

CHAPTER 3 PRELIMINARY MONITORING OF FIELD DRILLING (PILOT PROJECTS)

3.1 Development of Equipment for Shaft Installation Monitoring in Real Time

In addition to a thorough laboratory investigation, field monitoring equipment was needed to monitor shaft installations in the field. However, information regarding the types of drill rigs and tooling used for shaft installations in Florida was scarce. It was important to understand what was being used in the field before developing equipment to mount on the drill rig and monitor the shaft installations. Therefore, an investigation took place to provide more insight. The following section briefly covers the investigation.

3.1.1 Surveying Florida Contractors and District Geotechnical Engineers

In order to gain a better understanding of what types of drill rigs and tooling were being used in the field to install drilled shafts; a survey was created and presented to leading contractors and district geotechnical engineers from Florida, Alabama, and Georgia that practice in the state of Florida. The intent of the survey was to develop a better understanding of drilled shaft equipment, as well as typical operating parameters of the rigs used in Florida. From the results of the survey, field monitoring equipment would be developed to create a monitoring system capable of being used on a variety of rig types. The following is a summary of the survey results:

Table 18 - Summary of the drilled shaft survey results

Rig Type	Truck – Mounted	Carrier – Mounted	Crane – Mounted	Crawler – Mounted
% of rigs used	27%	9%	18%	46%
Power Unit	Hydraulic	Hydraulic	Hydraulic	Hydraulic
Kelly System	Telescoping	Telescoping	Telescoping	Telescoping
Crowd System	Hydraulic pull-down	Hydraulic pull-down	Hydraulic pull-down	Hydraulic pull-down
Crowd Monitoring	67% In-cab monitor	100% In-cab monitor	50% In-cab monitor	60% 75% In-cab monitor 25% Digital monitor
Torque Monitoring	67% In-cab monitor	100% In-cab monitor	100% 50% In-cab monitor 50% Torque multiplier	80% 50% In-cab monitor 25% Torque multiplier 25% Digital Monitor
RPM Monitoring	100% In-cab monitor	100% In-cab monitor	100% 50% In-cab monitor 50% Laser eye sensor	100% 60% In-cab monitor 20% Laser eye sensor 20% Digital monitor
Depth (ft) Monitoring	100% 100% Weighted tape 50% In-cab monitor	100% Weighted tape	100% 100% Weighted tape 50% In-cab monitor	100% 100% Weighted tape 80% In-cab monitor 20% Digital Monitor

From the compiled data, a trend toward the use of hydraulic powered rigs was observed. Also observed was that for European rigs where efficiency in drilling is important, hydraulically powered rigs are more prevalent. The results also showed that recorded monitoring is rare and typically only found in European rigs (used for efficiency). Therefore, a monitoring system would be needed to record drilling parameters torque, crowd, rotational speed, and penetration rate.

3.1.2 Monitoring Equipment

After a thorough investigation, two monitoring systems were compared. A system built from the ground up by UF researchers and a commercially available system produced by Jean Lutz. The following comparisons were made:

Table 19 - Field monitoring system comparison

Jean Lutz System	UF Developed System
All products from same vendor and designed for drilled shaft monitoring with 30+ years of experience backing them.	Will consist of multiple products from various vendors, none were specifically designed for this type of application.
Requires minimal programming to get the system to operational status.	Programming time is unknown, estimated to be several months.
Top and bottom hole parameters can be recorded through the same junction box. Rock strength and strain equations can be preloaded into software by Jean Lutz. Real time visuals only available on BAP, cannot be seen on computer in real time.	Top and bottom hole parameters will be recorded through same junction box. All equations will be programmed by researchers. Real time visuals will be available. Can be programmed to be an executable program.
Technical support is available for troubleshooting problems.	Technical support available from vendor of each separate component.
Experienced field technicians available for rig installation, calibration and training.	Installation and calibration will be done by researchers. (Instructions will be provided in Final Report)
All sensors have an IP66 rating.	Rotation and depth sensors have IP50 rating. Torque and crowd sensors have and IP65 rating. Most sensors will require waterproof housing.
Mounting equipment included with diagrams available.	Mounting equipment will need to be designed and manufactured.
No sensor/control module compatibility issues.	Possible compatibility issues due to various vendor's products being used.
Graphical results built into software. Not available on computer in real time.	Graphical results will need to be programmed into software. Could be available on computer in real time.
Void and decompressed zone detection built in.	N/A
Versatile system that could be used for different future project applications. (i.e., driven piles, vibrodriving, etc.)	Will strictly be used for drilled shaft monitoring.

From the comparative analysis, it was decided to acquire the Jean Lutz monitoring system, Figure 65.



Figure 65 - Jean Lutz monitoring system.

With the Jean Lutz monitoring equipment acquired, the focus of the research turned to field monitoring. The field investigation began by monitoring drilled shaft projects where load testing was planned. The remainder of this chapters covers the research effort and findings from the preliminary field monitoring trials, termed “pilot projects”.

3.2 Pilot Project Overview

During the course of the research project, two field monitoring opportunities were presented which provided the first field monitoring trials (pilot projects). The locations were in Quincy, Florida (Little River Bridge) and Jacksonville, FL (Overland Bridge), where each location had planned drilled shaft installations with subsequent load testing. In addition, all the test shafts were instrumented with strain gauges along their length to assess skin friction by layer. This provided a means to directly compare the estimated shaft capacity, obtained from monitoring, with the actual measured capacity, using conventional load test methods, over specified portions of the shaft. Additionally, each location used a different type of load testing, O-cell testing at Little River and Statnamic testing at Overland. This in combination with the static load test (Kanapaha), discussed in Chapter 4, provided direct comparative data from three of the most conventional load testing methods used throughout the state. This also provided field monitoring with three variations in the following categories: location, shaft diameter, drill rigs used to install the shafts, drilling crews, drill bits and drill bit tooth configurations. These variable drilling parameters provided great insight as to how laboratory drilling equations held up when drilling conditions and rig configurations change. The remainder of this chapter

will mostly focus on the Little River monitoring as more comparative data was able to be obtained. However, results from both locations are provided where a rock auger bit was used to drill through limestone.

3.3 Little River

From the available comparable data provided by the O-cell results at Little River, a 33 foot section (Elevation +45.6' to +12.6') of the installed shaft was used for comparison. This 33 foot section was used because it was the only portion of the shaft that appeared to have been fully mobilized or was approaching mobilization. This was also a location where a rock auger was continuously used and the drilling media was similar to that used in the laboratory drillings (i.e., Limestone). The analysis process and results are discussed throughout this section. The strain gauge load distribution and boring log for the O-cell test shaft is provided.



Strain Gauge Load Distribution

Test Shaft 1 - US 90 over Little River - Gadsden County, FL

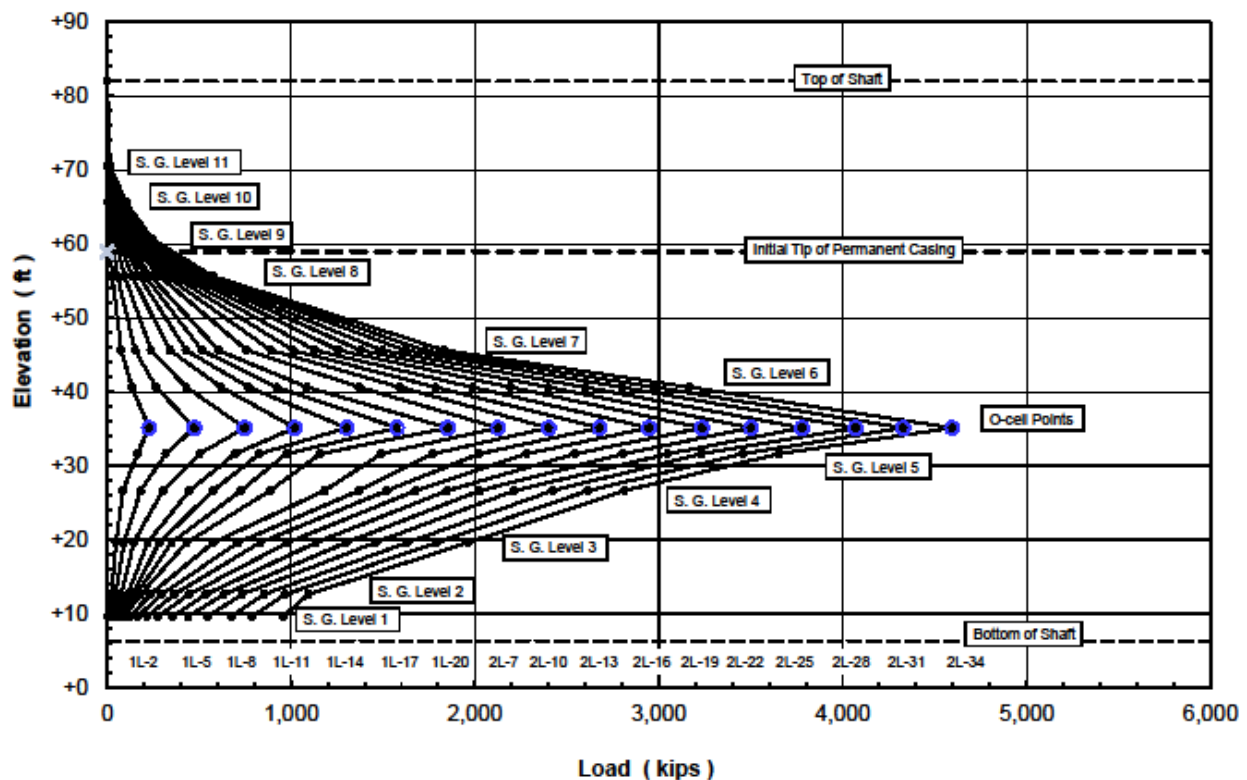


Figure 66 - O-cell strain gauge load distribution from Little River

Evident from the slopes of the load test results, some of the segments reached failure (i.e., parallel) whereas other zones did not. Of interest are the zones or layers which reached failure vs. the predicted capacity from the monitored drilling process.

	UNIVERSAL ENGINEERING SCIENCES	PROJECT NO.: 2030.1300057.0000
	BORING LOG	REPORT NO.:
		PAGE: 1

PROJECT: T3417 - SR 10 (US 90) Over Little River & Hurricane Creek - Pilot Borings Quincy, Gadsden County, Florida	BORING DESIGNATION: LS-1 SECTION: TOWNSHIP:	SHEET: 1 of 1 RANGE:
CLIENT: Anderson Columbia Company	G.S. ELEVATION (ft): 79.7	DATE STARTED: 10/22/13
LOCATION: Per Boring Location Plan	WATER TABLE (ft): 5	DATE FINISHED: 10/25/13
REMARKS: Little River Load Test Shaft	DATE OF READING: 10/26/2013	DRILLED BY: R. Woodard
	EST. W.S.W.T. (ft):	TYPE OF SAMPLING: SPT/Core

Elev. (ft)	SAMPLING	BLOWS PER 5' INCREMENT	N (BLOWS/FT.)	W.T.	SYMBOL	DESCRIPTION	-200 (%)	MC (%)	ATTERBERG LIMITS		K (FT./DAY)	ORG. CONT. (%)
									LL	PI		
0		3-3-3	6			Brown to Gray Very Loose to Loose Silty Sand (SP-SM, SM)						
5		2-2-1	3									
10		2-5-6	10									
15		3-1-1	2									
20		1-2-2	4									
25		2-3-3	5									
30		16-31-41	72			Brown to Gray Very Loose to Loose Silty Sand with Wood (SP-SM, SM)						
35		16-25-35	50			Gray Very Dense Silty Clayey Sand (SM, SC)						
40		17-22-30	52									
45		7-17-24	44			Light Gray Hard Cemented Sandy Silty Clay (CL/CH, ML/MH)						
50		5-50/2"	50/2"									
55		50/2.5"	50/2.5"			Gray Stiff to Hard Silty Clay (CL/CH)						
60		23-37-44	81									
65		16-13-18	31			Gray Very Dense Silty Clayey Sand (SM, SC)						
70		14-18-22	40			Light Gray Stiff to Very Stiff Sandy Silty Clay with Weathered Limestone (CL/CH, ML/MH)						
75		3-4-5	9									
80		50/2"	50/2"									
85		8-6-12	18									
90		6-12-24	36			Light Gray Hard Sandy Silty Clay with Weathered Limestone (CL/CH, ML/MH)						
95		50/5"	50/5"									
100		12-16-16	32									
105		6-27-36	63									
110		29-50/3"	50/3"									
115		38-50/5.5"	50/5.5"									
120		50/5.5"	50/5.5"			Hard Weathered Limestone						
125		27-43-28	71			Light Gray Hard Sandy Silty Clay with Weathered Limestone (CL/CH, ML/MH)						
130		50/4"	50/4"									
135		50/1"	50/1"									

Figure 67 - Little River boring in the footprint of the O-cell test shaft

3.3.1 Converting the Raw Data

When field drilling data was first collected, the units of measure had to be converted to match the laboratory drilling data for further analysis. The rotational speeds did not require any conversion and the penetration rate conversion was simply converting from ft/hr to in/min. However, for the torque and crowd conversions, the process required taking measures of pressure (obtained by tapping into hydraulic lines) and converting them into physical measures (i.e., lbf for force and in-lbs for torque). This required rig specific equations to make the conversions. These transformation equations were provided by IMT rig engineers, since an IMT AF250 drill rig was used. The following displays the raw and converted frequency distributions for each of the monitored drilling parameters within the investigated portion of the shaft:

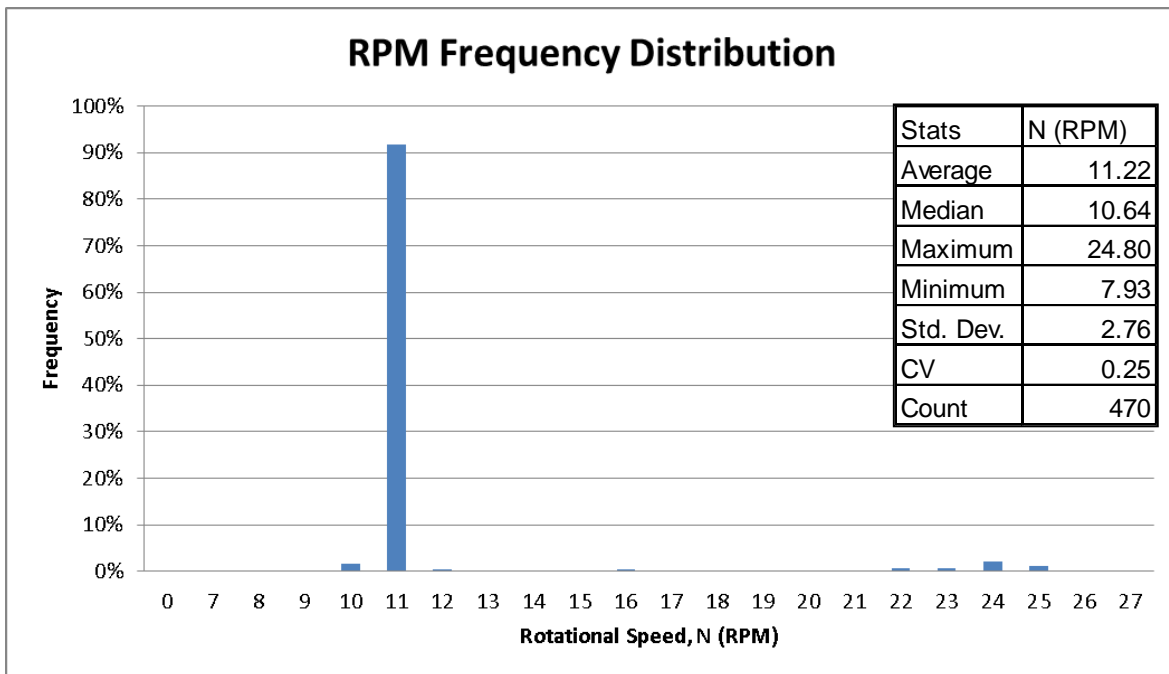


Figure 68 - RPM frequency distribution

From the rotational speed frequency distribution two main groupings were noticed; one grouping around 11 RPM and the other around 24 RPM. The lower rotational speed grouping was from using 1st gear and the higher rotational speed grouping was from using 2nd gear (This was confirmed by an IMT rig specialist). This was important as torque transformation equations are dependent and different based on which gear was being used (Only torque requires transformation based on the gear used) by the operator during the drilling process. From conversation with the drill rig operator, it was indicated that only 1st and 2nd gears were used (3rd gear available but wasn't used). Therefore, torque transformation was based on only using 1st and 2nd gear. Also noticed was a smaller 3rd grouping around 16 RPM, this was the typical rotational speed

recorded when shifting between 1st and 2nd gear. This can be seen in the raw data when transitioning occurred between higher and lower rotational speeds:

Table 20 - Rotational speeds for transitioning between gears

N (RPM)	N (RPM)	N (RPM)	N (RPM)
22.58	10.60	10.65	10.68
22.65	10.54	10.54	10.66
22.64	10.51	10.55	10.59
22.04	10.56	9.59	10.23
16.05	15.06	15.77	15.44
10.65	23.64	22.77	22.40
10.49	23.28	24.64	22.20
10.57	24.08	24.55	21.58
10.56	23.88	24.80	21.74

When transitioning from the higher to lower gear, the rotational speed was typically 16 RPM and above. When transitioning from the lower to higher gear, the rotational speed was typically 15 RPM and below. Therefore, torque values with a rotational speed below 16 RPM were designated 1st gear and assigned the respective transformation equation. Torque values with a rotational speed above 16 RPM were designated 2nd gear and assigned the respective transformation equation. Determining which gear was being used by means of rotational speed was necessary because each gear shift was not recorded as researchers were unaware this would be necessary at the time of monitoring.

The following provides torque frequency distributions for the raw and converted data using all rotational speeds:

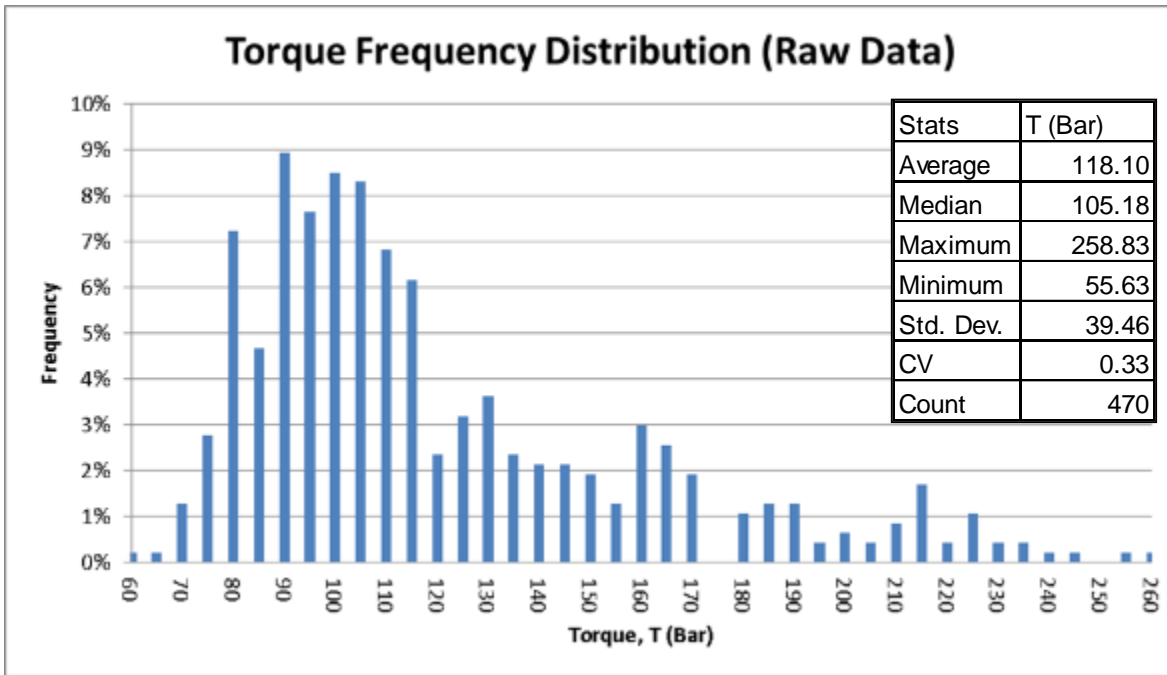


Figure 69 - Raw data torque frequency distribution

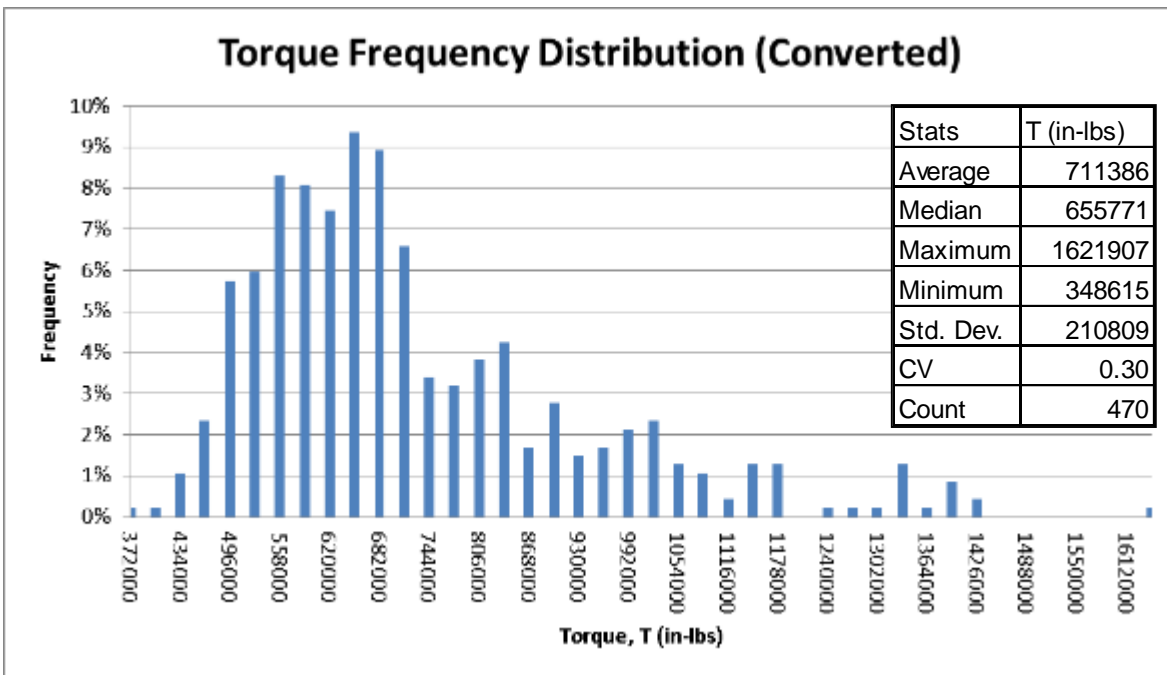


Figure 70 - Converted torque frequency distribution

Next, torque frequency distributions are provided for the raw and converted data showing the distributions for all rotational speeds and rotational speeds separated based on gear selection (represented by rotational speed designation)

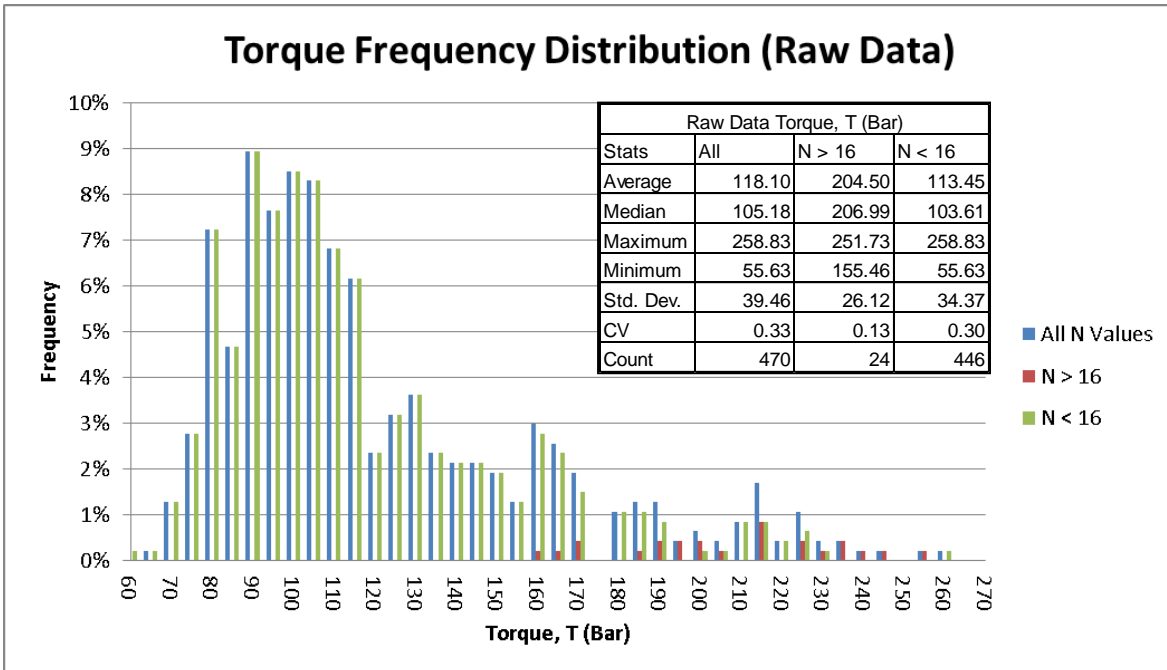


Figure 71 - Raw data torque frequency distribution with rotational speed breakdown

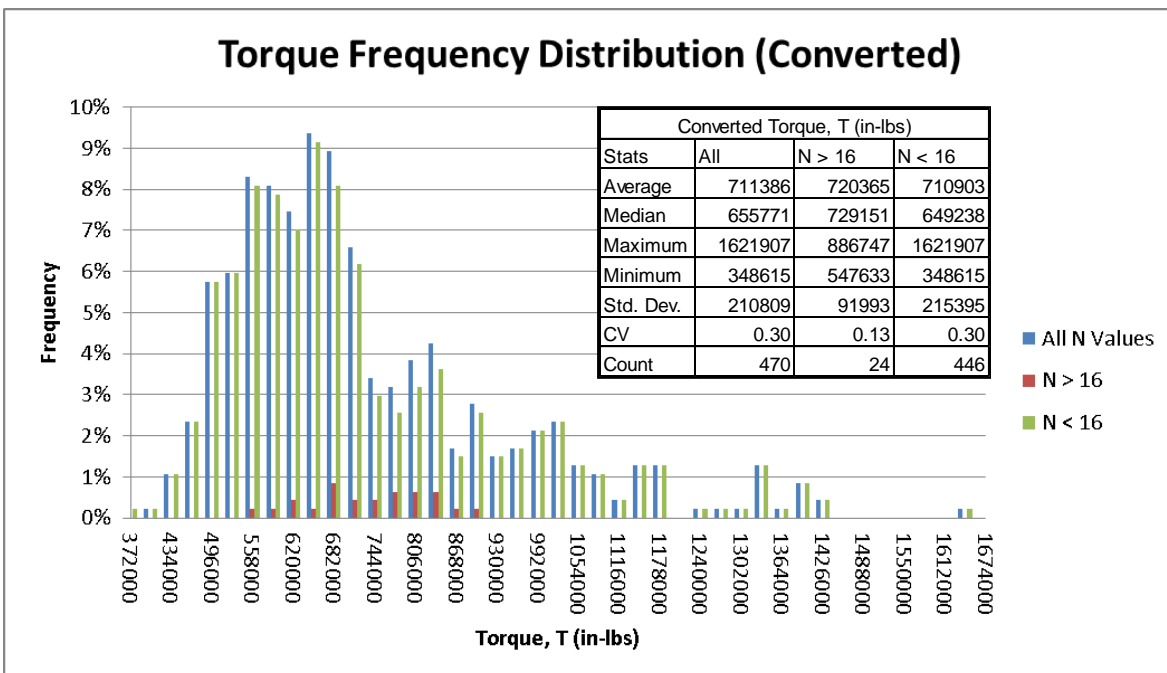


Figure 72 - Converted torque frequency distribution with rotational speed breakdown

The following provides frequency distributions for raw data and converted penetration rates:

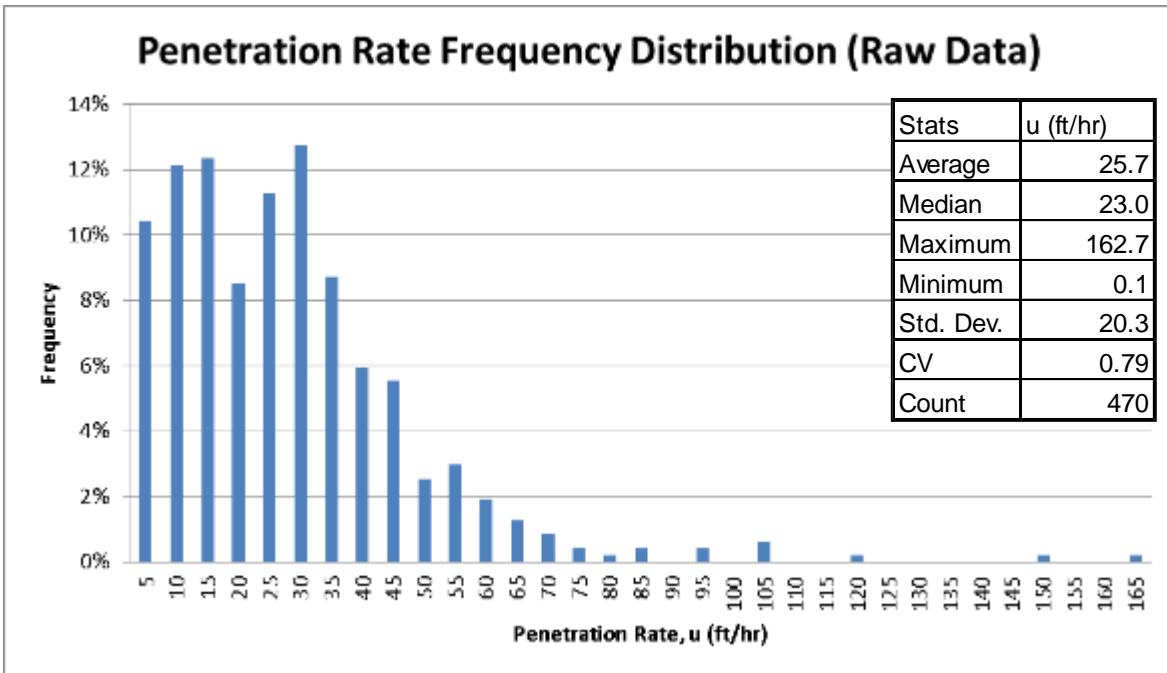


Figure 73 - Raw data penetration rate frequency distribution

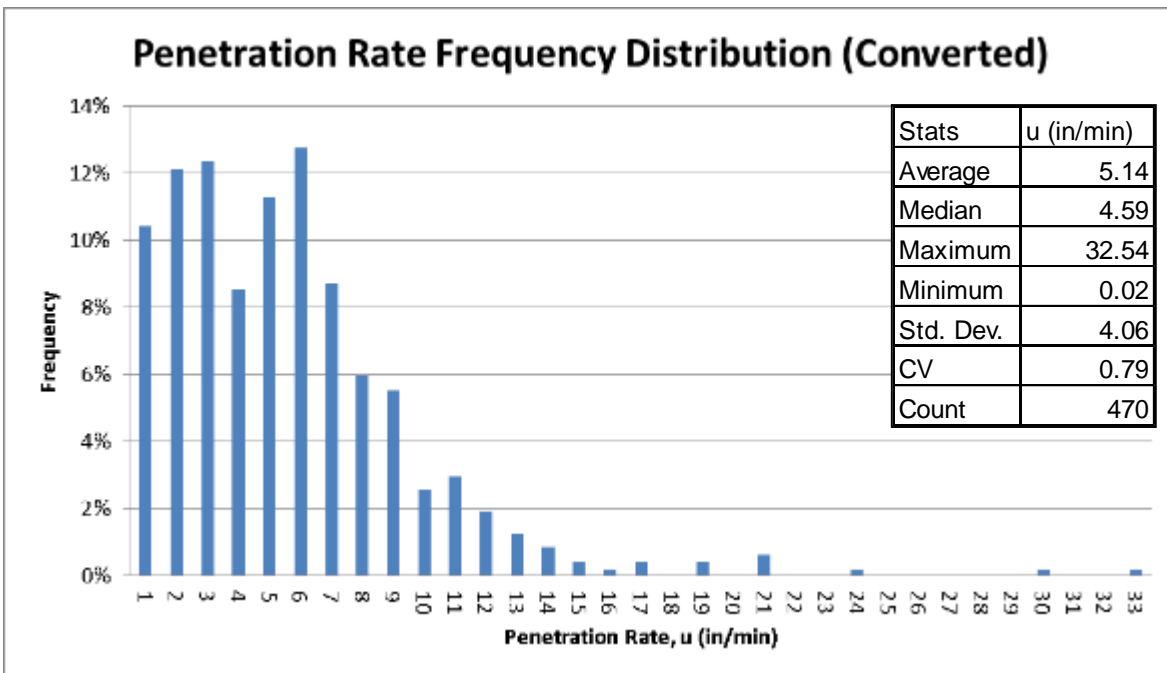


Figure 74 - Converted penetration rate frequency distribution

The following provides frequency distributions for raw data and converted crowd:

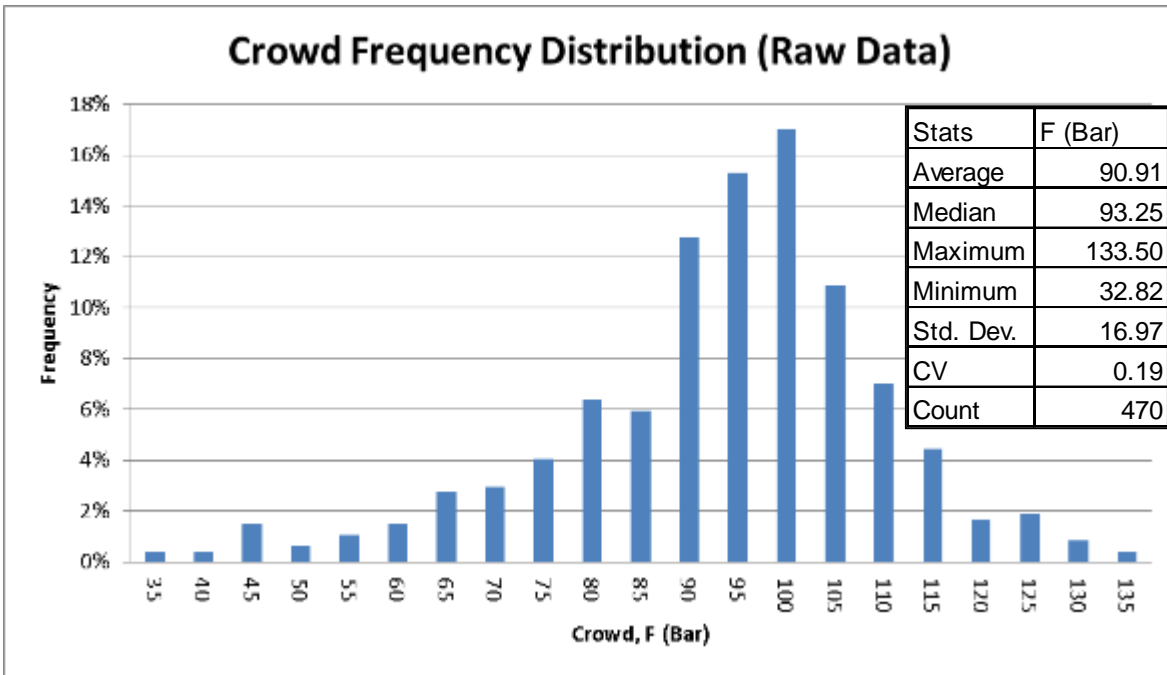


Figure 75 - Raw data crowd frequency distribution

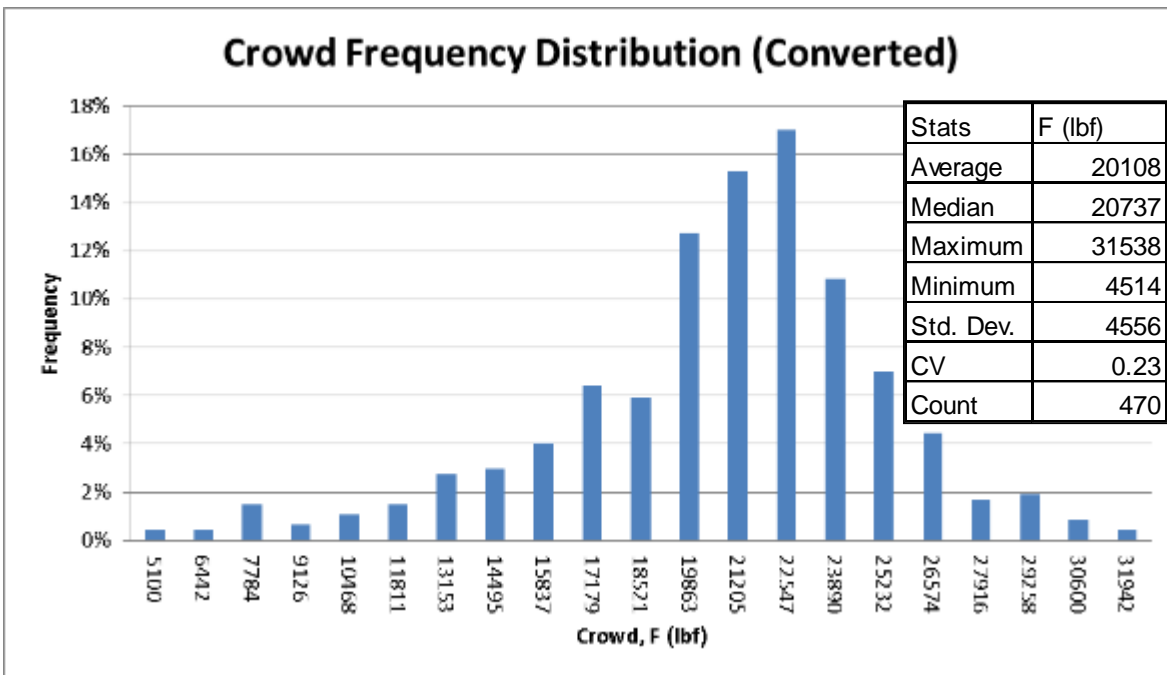


Figure 76 - Converted crowd frequency distribution

Also of interest is plotting the recorded (converted) drilling parameters vs. elevation. The following shows each data point recorded for each drilling parameter plotted vs. elevation:

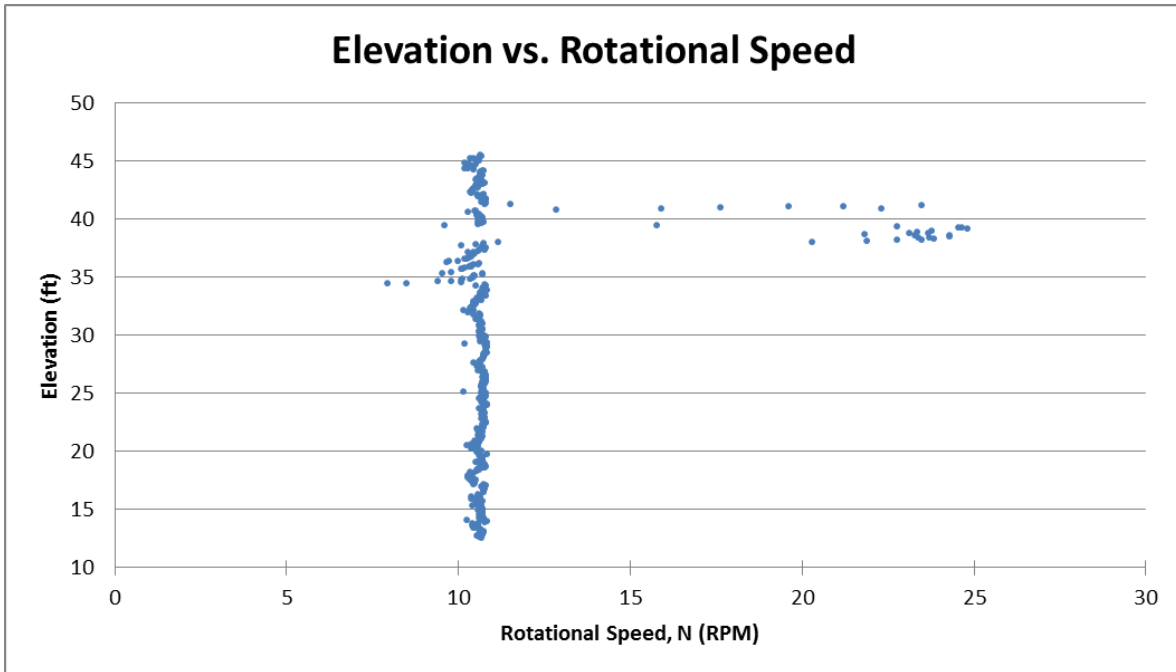


Figure 77 - Rotational speed vs. elevation plot

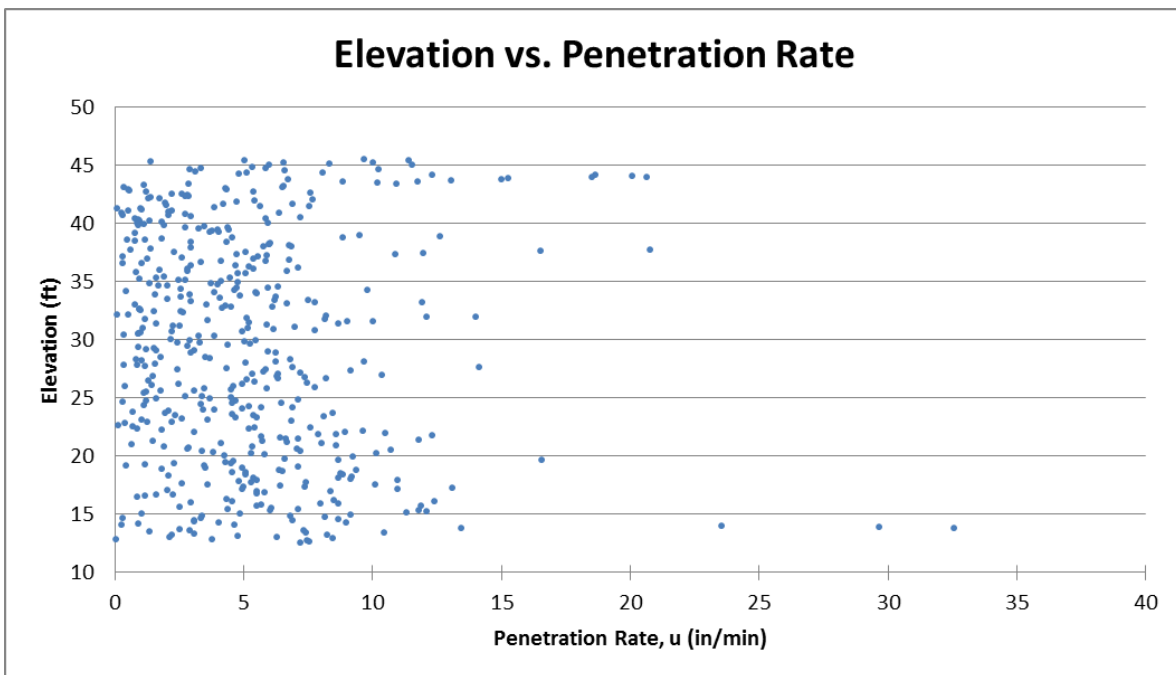


Figure 78 - Penetration Rate vs. elevation plot

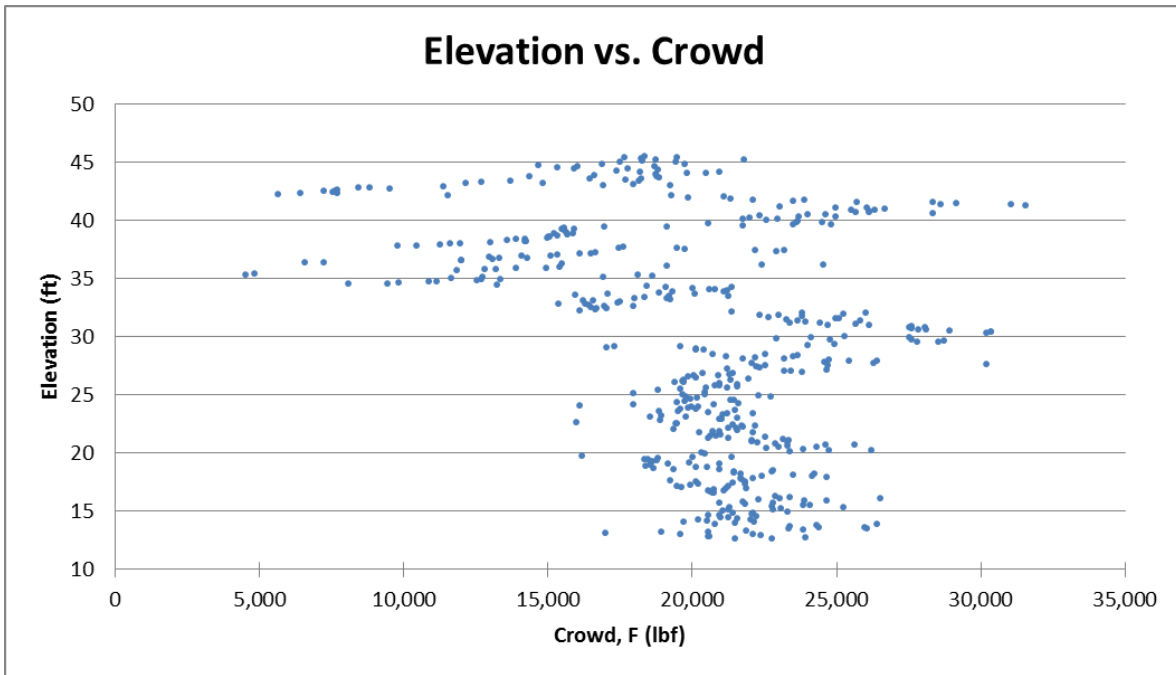


Figure 79 - Crowd vs. elevation plot

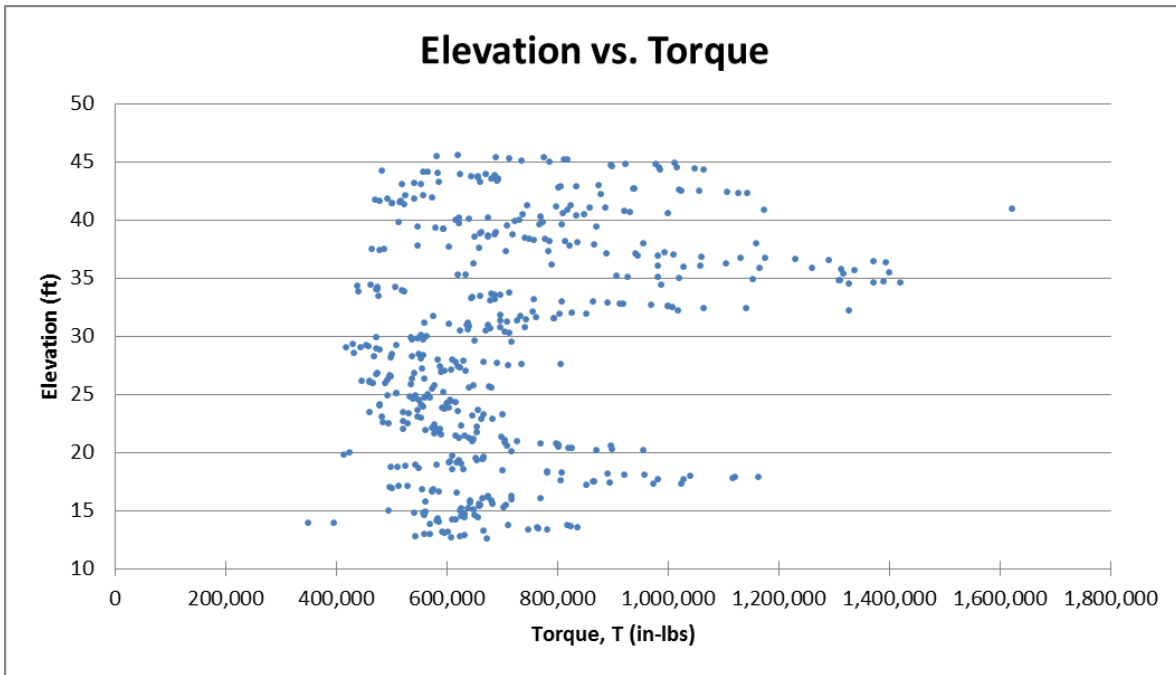


Figure 80 - Torque vs. elevation plot

Once the drilling parameters were properly converted for comparison with lab data, drilling equations derived using Karasawa and Teale's methods were employed. Preliminary results confirmed that Karasawa's method was too dependent on the

diameter of the bit, resulting in upscaling issues and producing large overestimations. Therefore, Teal's specific energy method was used to conduct a thorough analysis of the field drilling at Little River. Preliminary analysis results using Karasawa's method can be seen here:

Table 21 - Karasawa preliminary analysis of O-cell test shaft

Arithmetic Mean (Raw Data) - Karasawa					
Shaft Section (Strain Gauge Levels)	Elevation Range (ft)		Measured Mean (O-cell) (ksf)	Predicted Mean (Monitoring) (ksf)	Percent Difference
SG7 to SG6	45.60	40.60	21.10	52.07	146.78%
SG6 to O-cell	40.60	35.10	20.60	64.30	212.14%
O-cell to SG5	35.10	31.60	21.40	54.36	154.02%
SG5 to SG4	31.60	26.60	13.60	16.51	21.40%
SG4 to SG3	26.60	19.60	9.70	20.02	106.39%
SG3 to SG2	19.60	12.60	9.90	23.81	140.51%
Average Skin Friction (ksf)			15.12	36.17	139.26%
Total Load (kips)			6269	15000	139.26%

Using Teale's specific energy method the following q_u vs. elevation plot was developed:

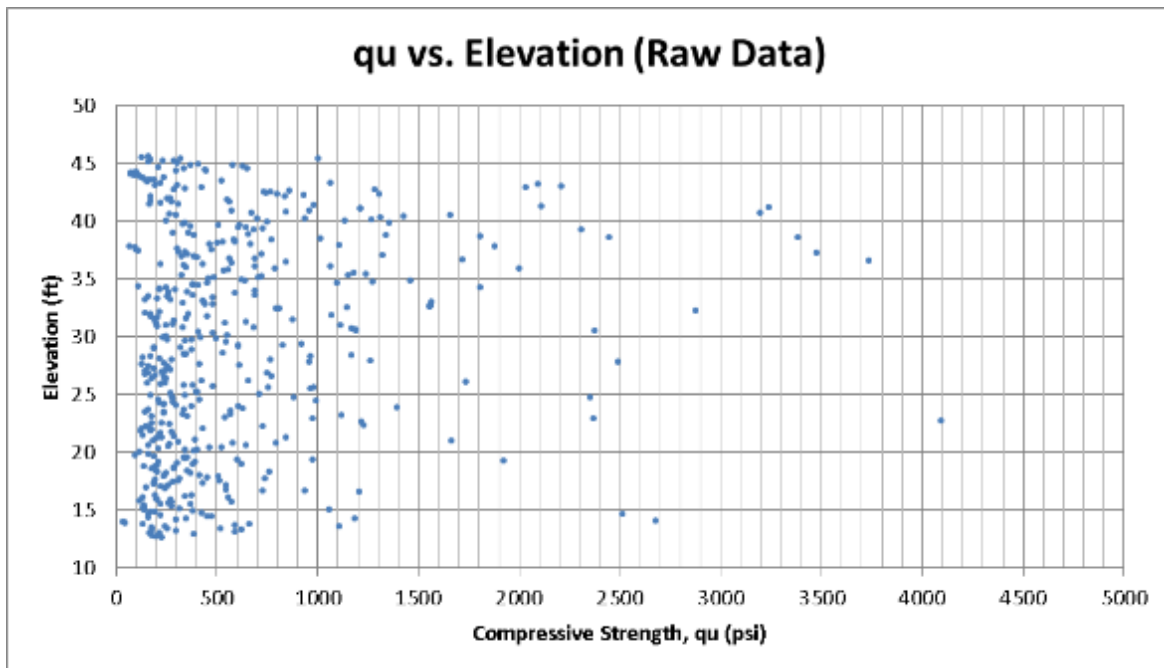


Figure 81 - Raw data compressive strength vs. elevation plot

Next, raw data q_u and f_s (skin friction) frequency distributions were created for the entire span of the investigated portion of the shaft (El. +45.6 to +12.6, strain gauges 7 to 2 or SG7 to SG2), results were developed in tsf:

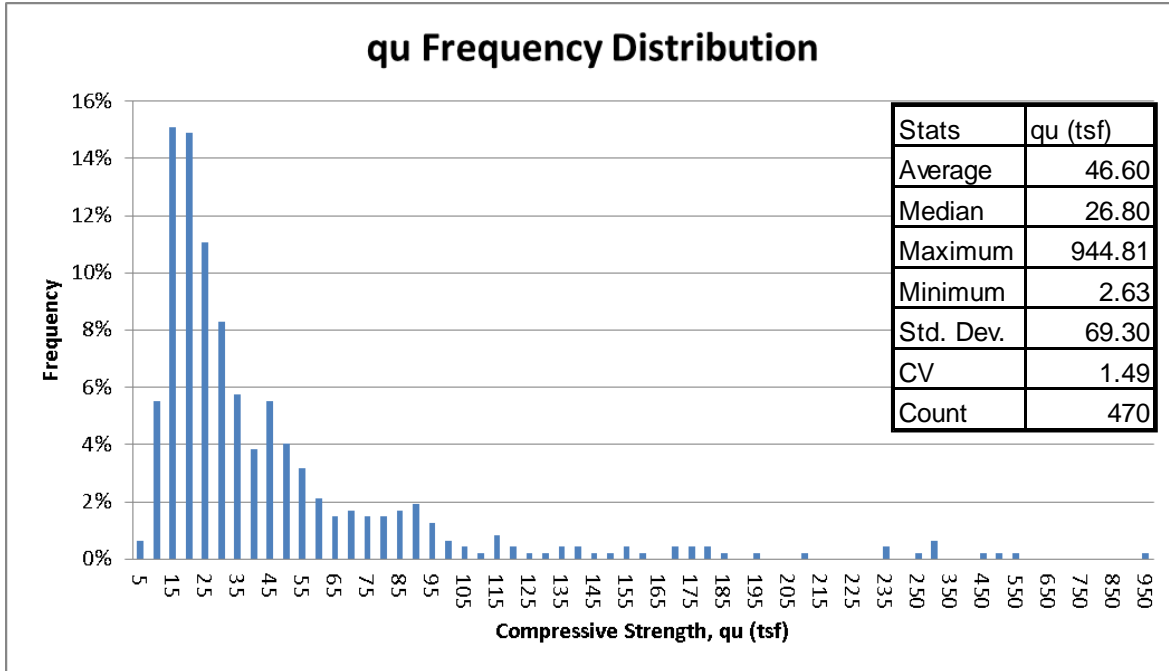


Figure 82 - Raw data compressive strength frequency distribution

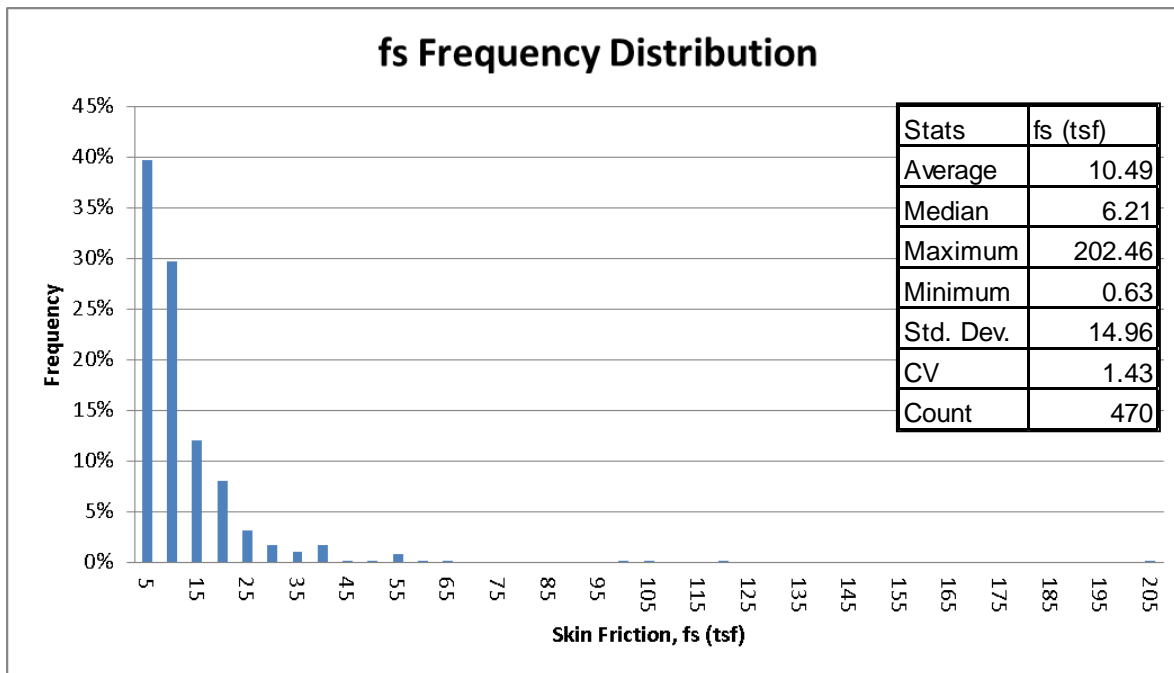


Figure 83 - Raw data skin friction frequency distribution

Note: Skin Friction, $f_s = \frac{1}{2} * \text{sqrt}(q_u) * \text{sqrt}(q_t) * \text{REC}\%$, where REC% is assumed to be 1 (100%) because the test cylinders used to develop compressive and tensile strengths for the drilling equations were completely intact and no voids during drill monitoring were observed. For the analysis of skin friction, the α and β methods were considered but ruled out because the α method is generally used solely for clay soils, based on the undrained shear strength and the β method is largely dependent on effective stress and lacks data for determining β in limestone or rock.

From the frequency distributions, a log-normal trend was noticed as expected. Probability plots for q_u and f_s using z-transformations were then created using the natural logarithm of the raw data (Note: results are reported in tsf):

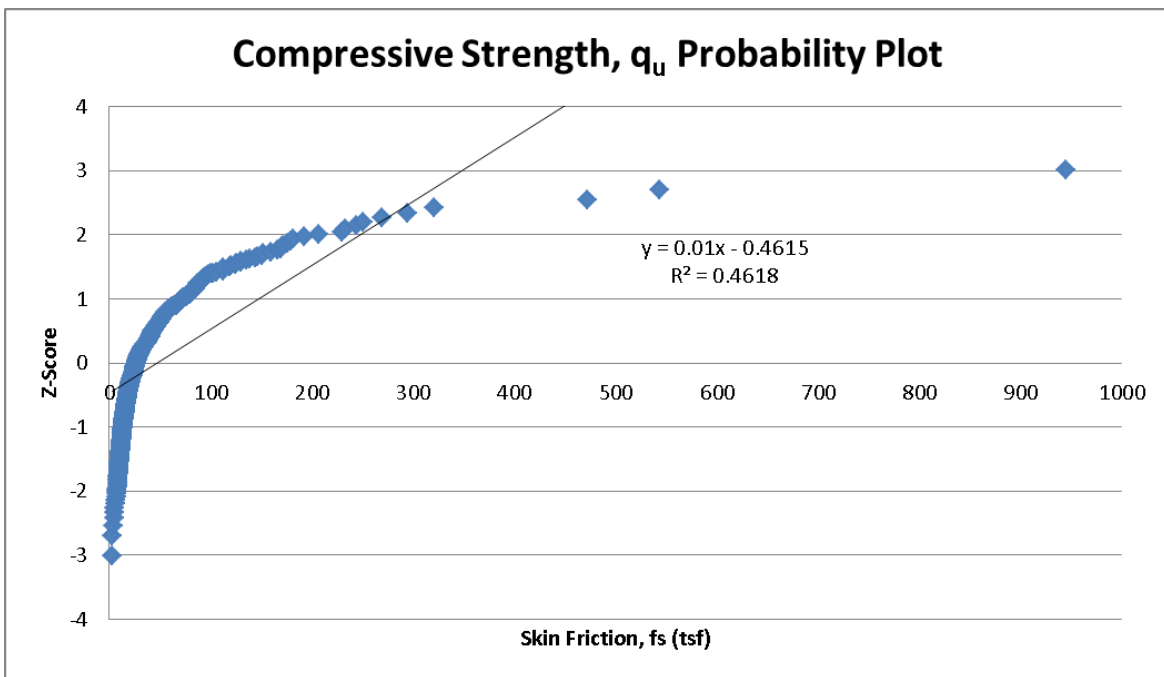


Figure 84 - Raw data compressive strength probability plot for Normal Distribution

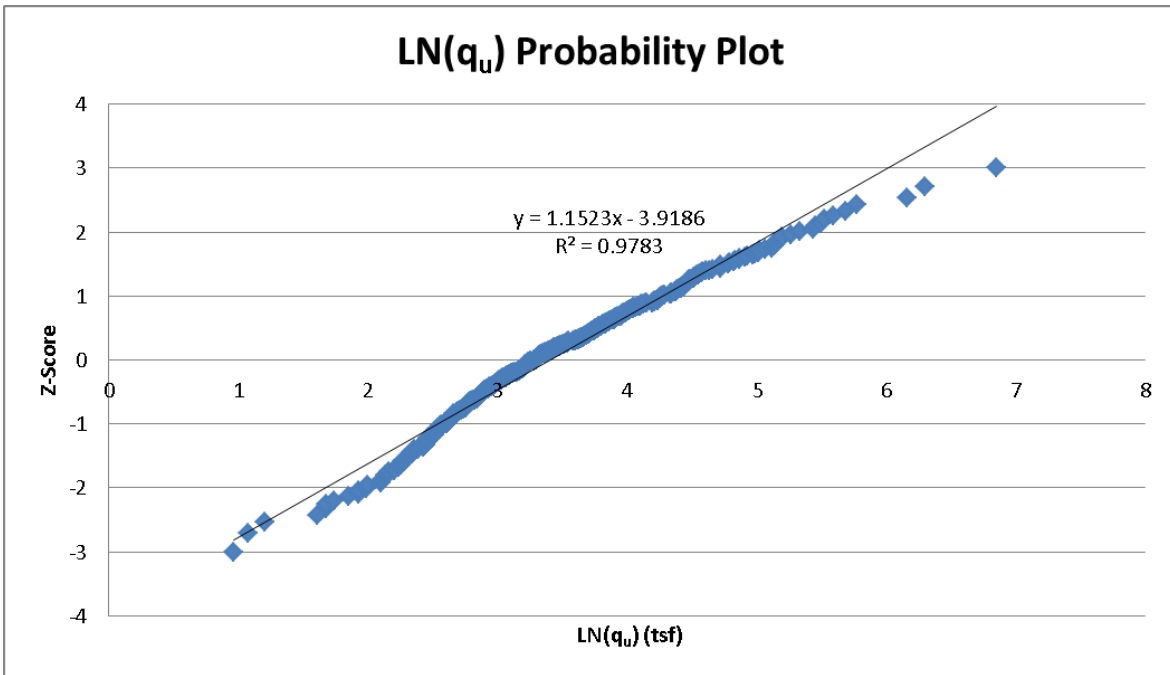


Figure 85 - Compressive strength natural log probability plot

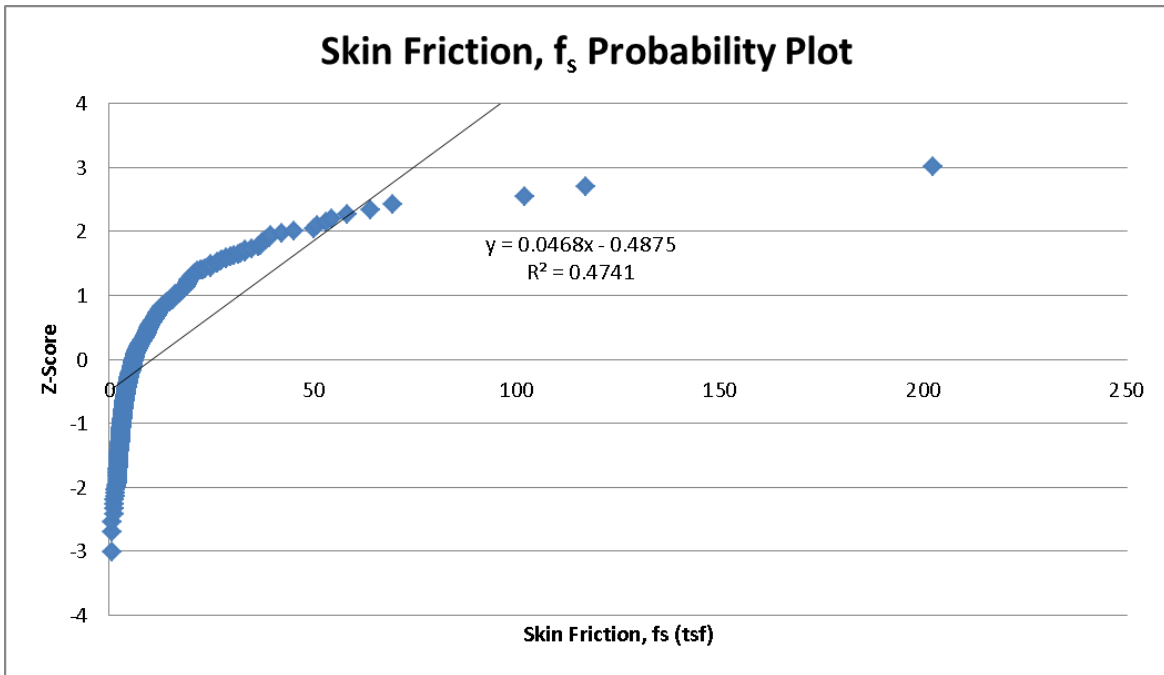


Figure 86 - Raw data skin friction probability plot for Normal Distribution

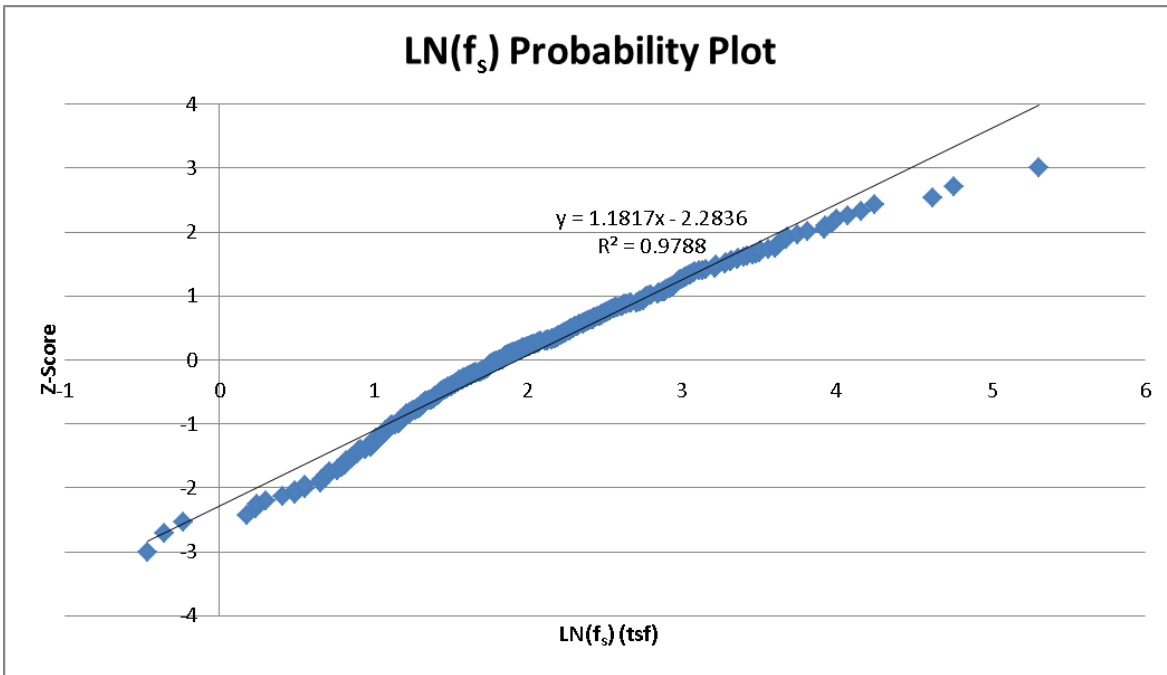


Figure 87 - Skin friction natural log probability plot

From the probability plots using z-transformations, it was shown that taking the natural logarithm of the raw data and creating a frequency distribution produced a more normal distribution. This was confirmed by creating frequency distributions for the natural logarithms of the q_u and f_s raw data:

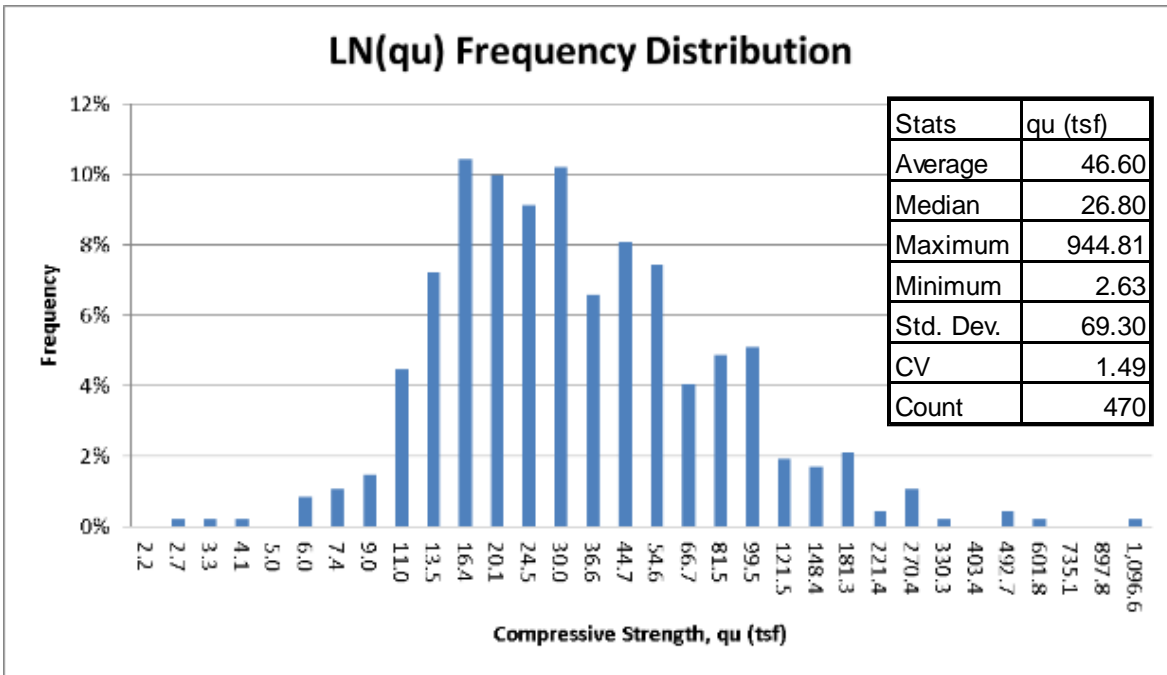


Figure 88 - Compressive strength natural log frequency distribution

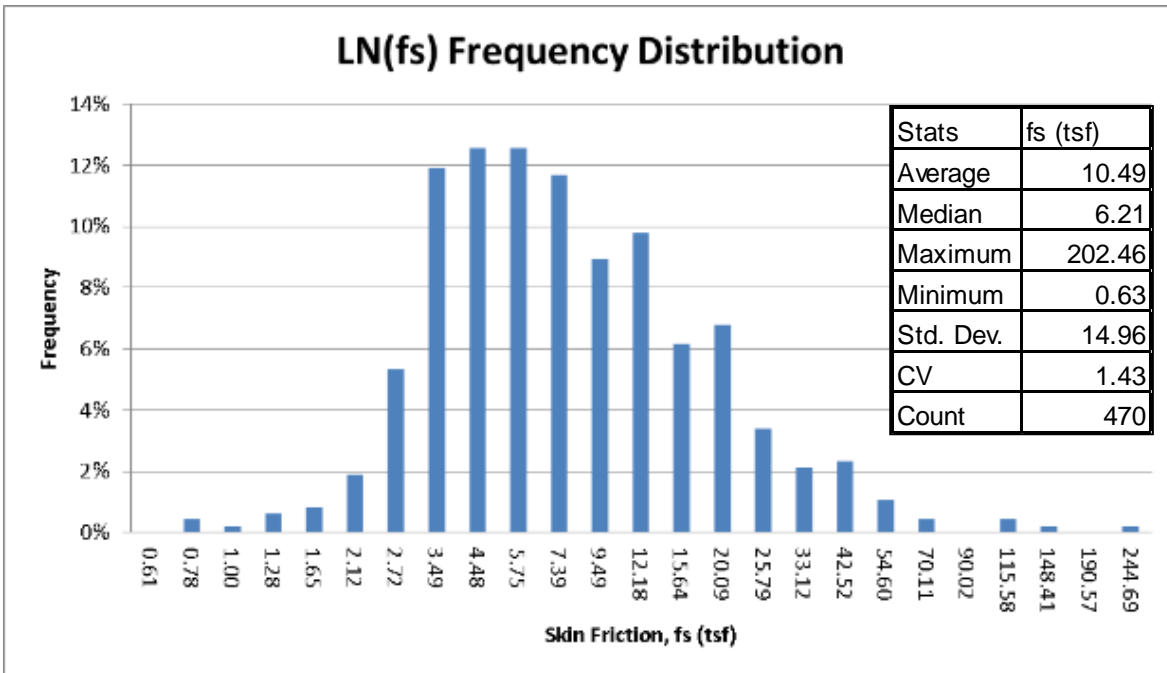


Figure 89 - Skin friction natural log frequency distribution

3.3.2 Preliminary Field Monitoring Analysis

From the previous analysis, it was evident that the raw analyzed data followed a log-normal trend with outlying values that may need to be eliminated or limited through additional methods. However, it was proposed that eliminating or limiting values may result in underestimates because the higher end values provide significant strength and greatly add to the shafts true capacity. Therefore, it was important to include the raw data set, without elimination or limitation, in further analysis. The following provides four methods used for additional analysis in attempt to remove or limit the outlying values.

Limiting Method:

Limits the recorded value based on an expected limiting adhesion, with the following ultimate limits:

$$\begin{aligned}q_u &= 120 \text{ tsf} \\q_t &= 20 \text{ tsf} \\f_s &= 25 \text{ tsf}\end{aligned}$$

Raw data values outside of the limits are not thrown out. If the raw data value exceeds the limit, it is set to the limit value and still used in the final averaging.

FDOT Method:

The arithmetic mean and standard deviation are found for all values in the investigated range of the shaft (+45.6' to +12.6'). Values that fall outside of one standard deviation from the mean are thrown out. A new arithmetic mean and standard deviation are then found using the remaining data.

FDOT* Method:

The arithmetic mean and standard deviation are found for each section of the investigated range of the shaft (i.e., between strain gauges). Values that fall outside of one standard deviation from the mean are thrown out. A new arithmetic mean and standard deviation are then found using the remaining data.

LN Transform Method:

The log space mean and standard deviation are found using the predetermined arithmetic mean and standard deviation from the raw data set (Elevation +45.6' to +12.6'). The entire raw data set is then converted into log-space using the natural logarithm. Any value in the converted data set that falls outside of one standard deviation (plus or minus) in log-space is thrown out. The remaining values are then used to determine the new mean and standard deviation in normal-space.

The following provides probability density function, PDF, plots for each method as well as the raw data:

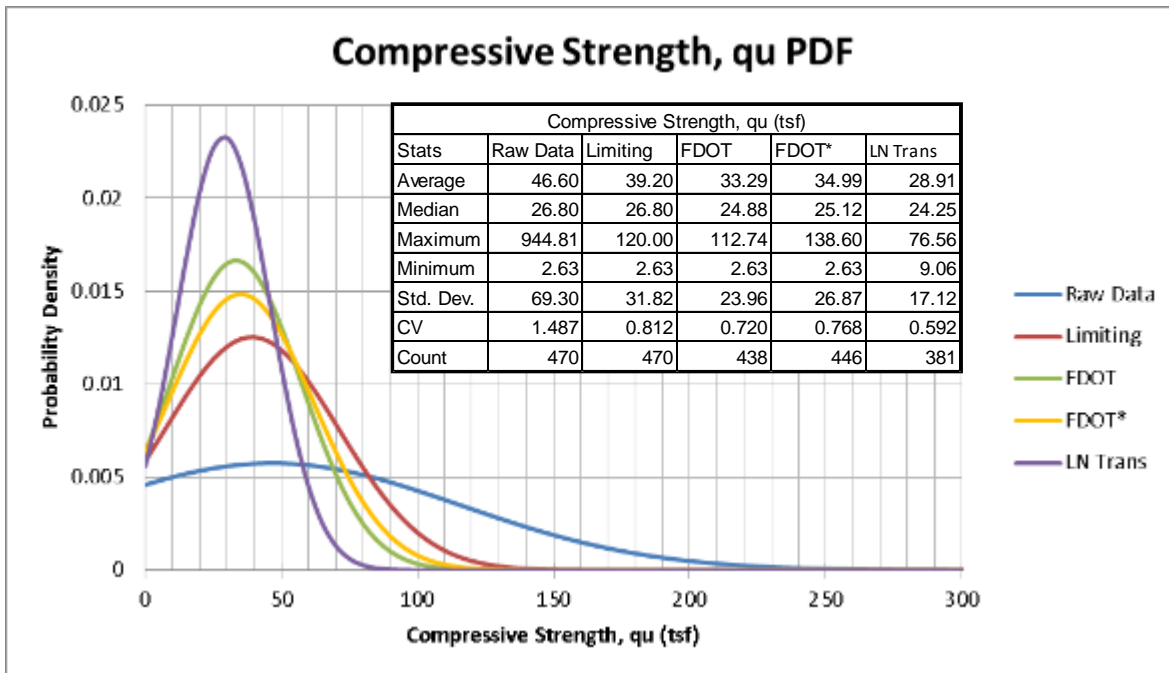


Figure 90 - Compressive strength probability density function

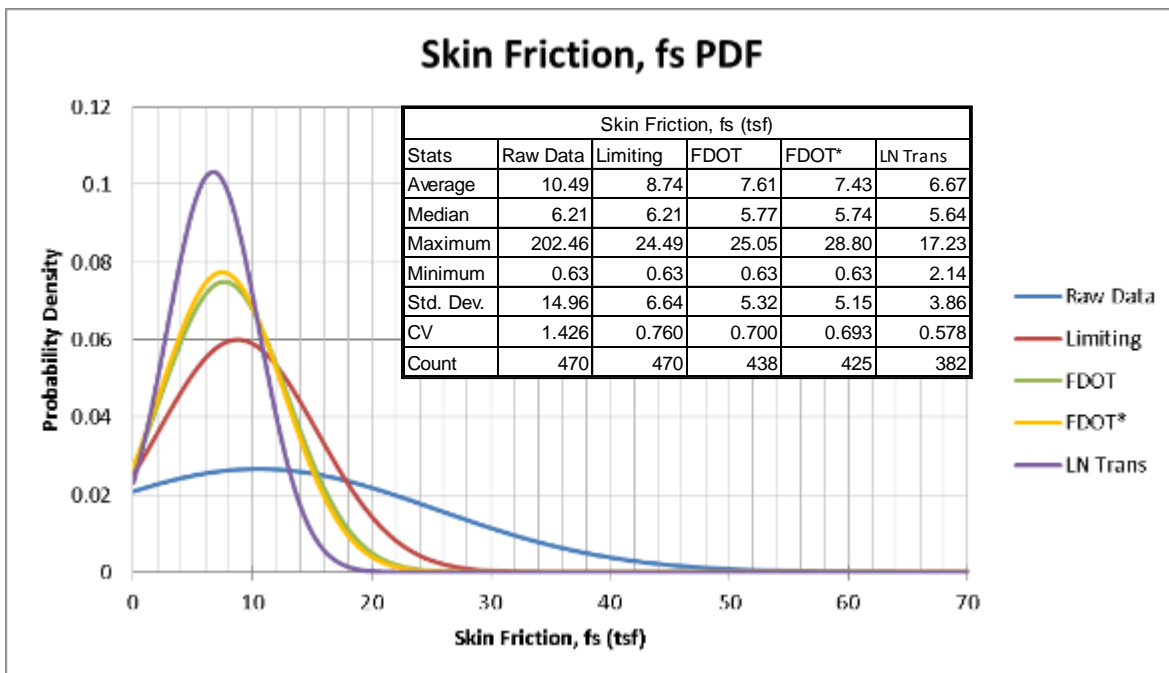


Figure 91 - Skin friction probability density function

Also investigated was the geometric mean to provide a better understanding of the central tendency of the data. The calculated geometric mean for q_u was 30 tsf, and 6.92 tsf for f_s . Looking at the q_u and f_s PDFs in Figure 90Figure 91, it is noticed that the methods used for analysis have reduced the spread of the raw data and reduced the mean values closer to the geometric mean which was the desired effect for each method. Next, frequency distributions were created and investigated for each section between strain gauges of the investigated portion of the shaft. The following provides the frequency distributions for each analysis method between strain gauges (for O-cell comparison) in the investigated portion of the shaft:

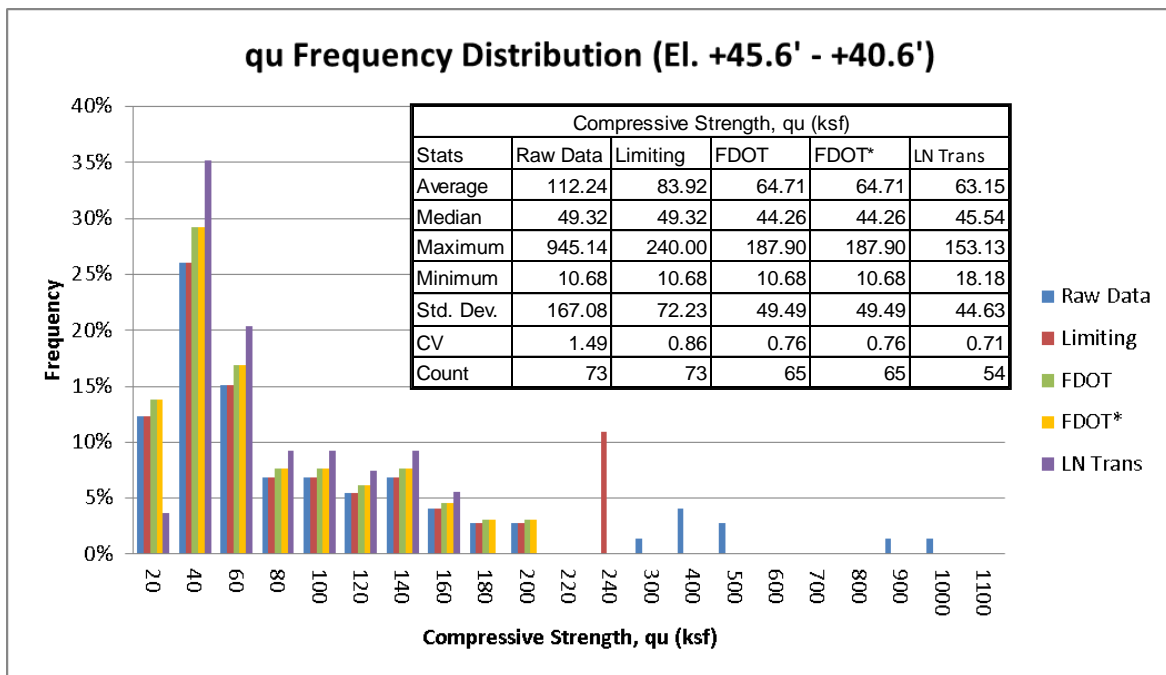


Figure 92 - Compressive strength frequency distribution, SG 7 to SG6

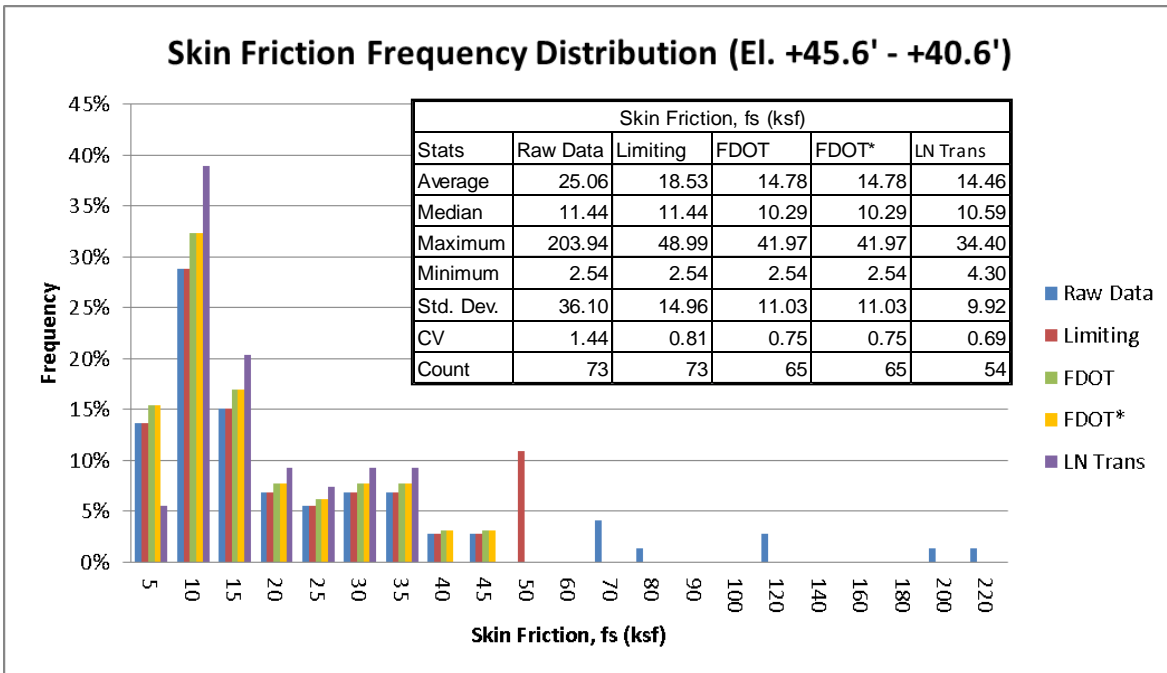


Figure 93 - Skin friction frequency distribution, SG 7 to SG6

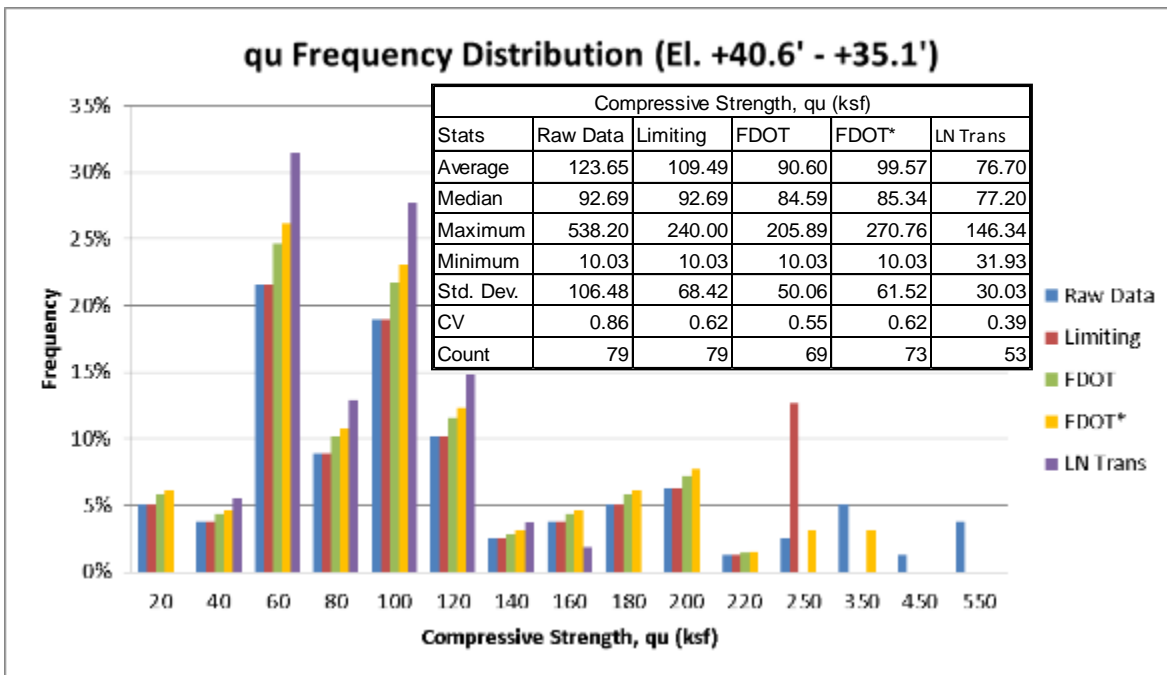


Figure 94 - Compressive strength frequency distribution, SG 6 to O-cell

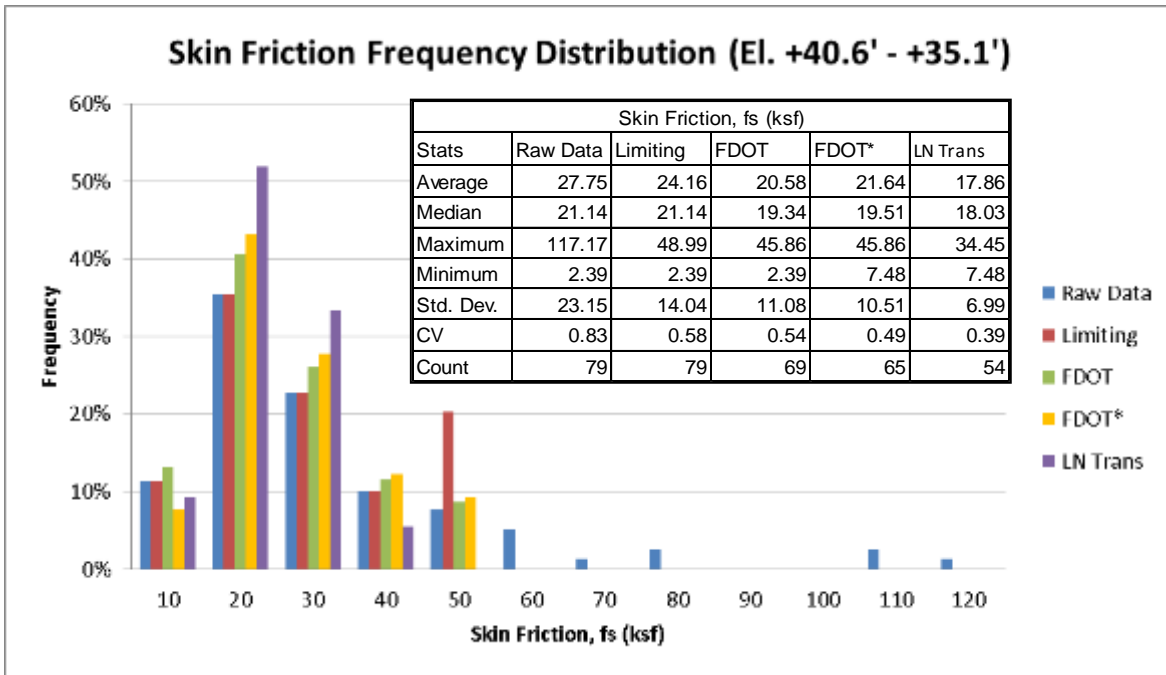


Figure 95 - Skin friction frequency distribution, SG 6 to O-cell

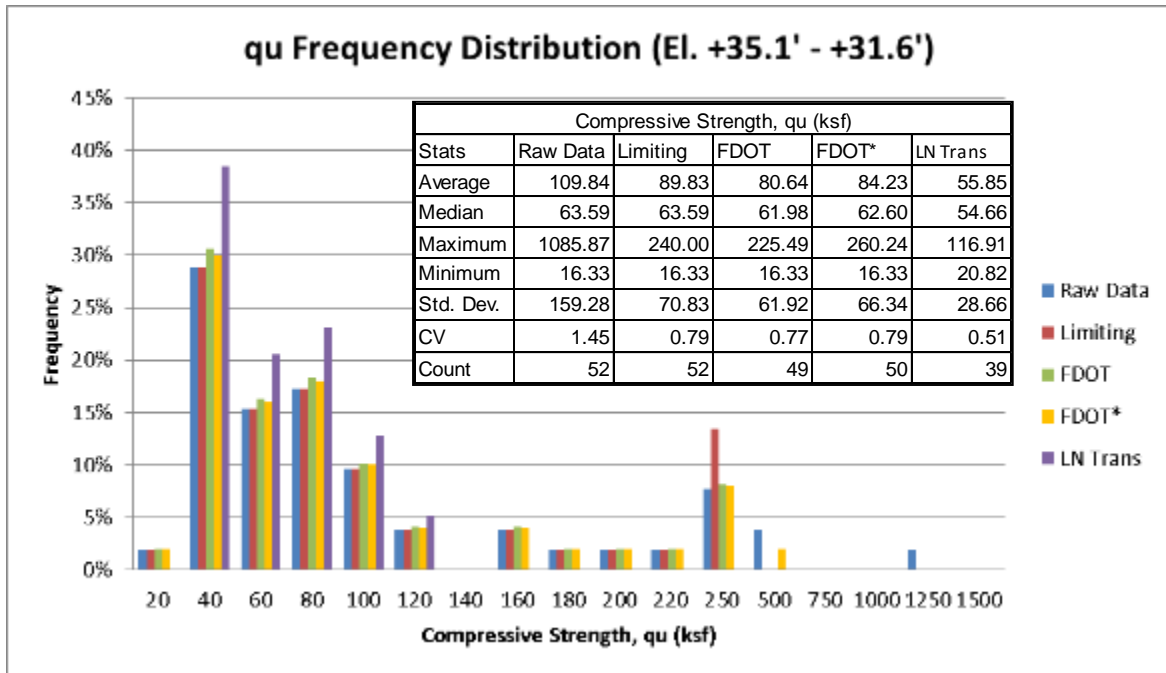


Figure 96 - Compressive strength frequency distribution, O-cell to SG 5

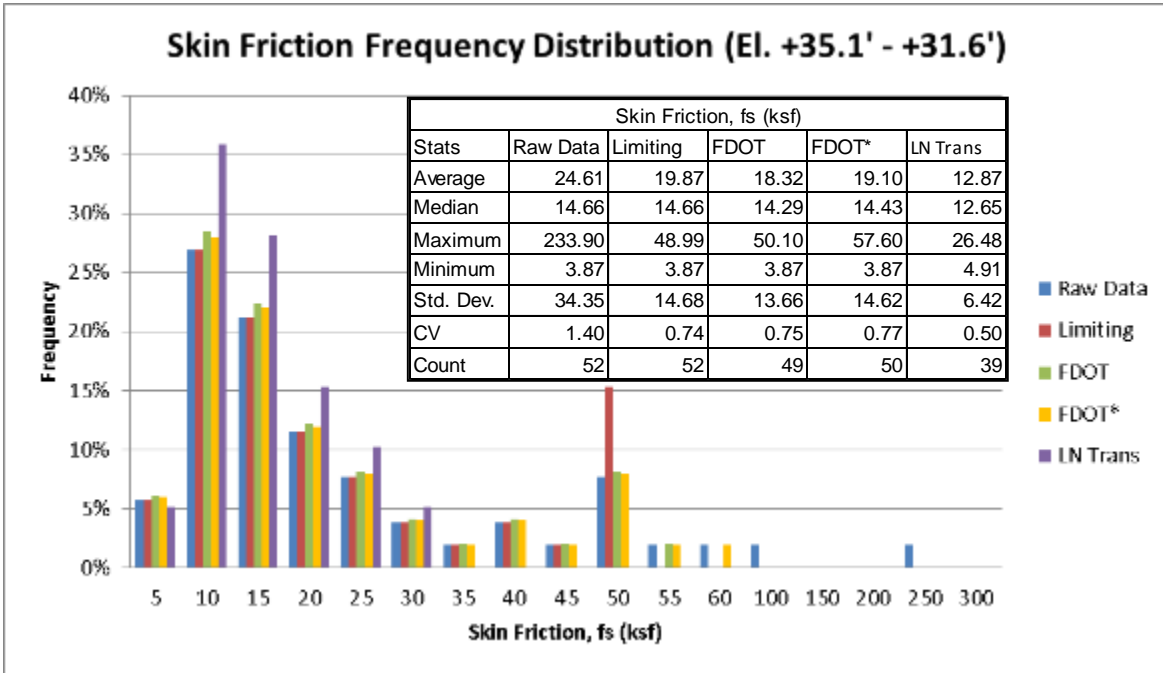


Figure 97 - Skin friction frequency distribution, O-cell to SG 5

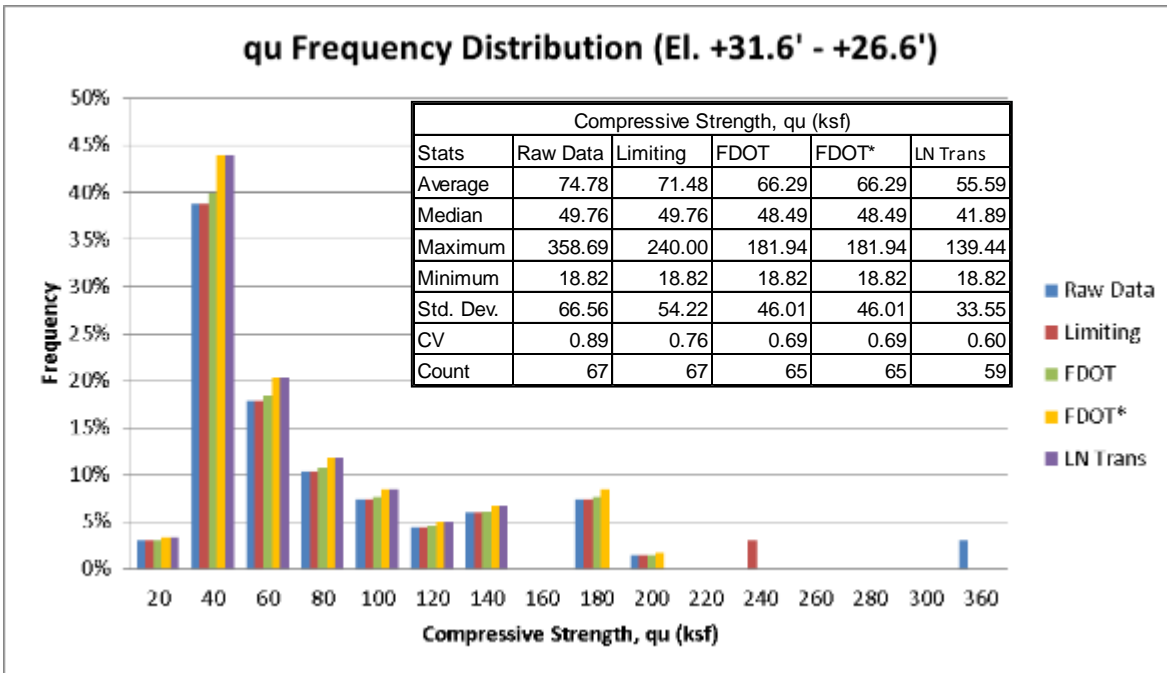


Figure 98 - Compressive strength frequency distribution, SG 5 to SG 4

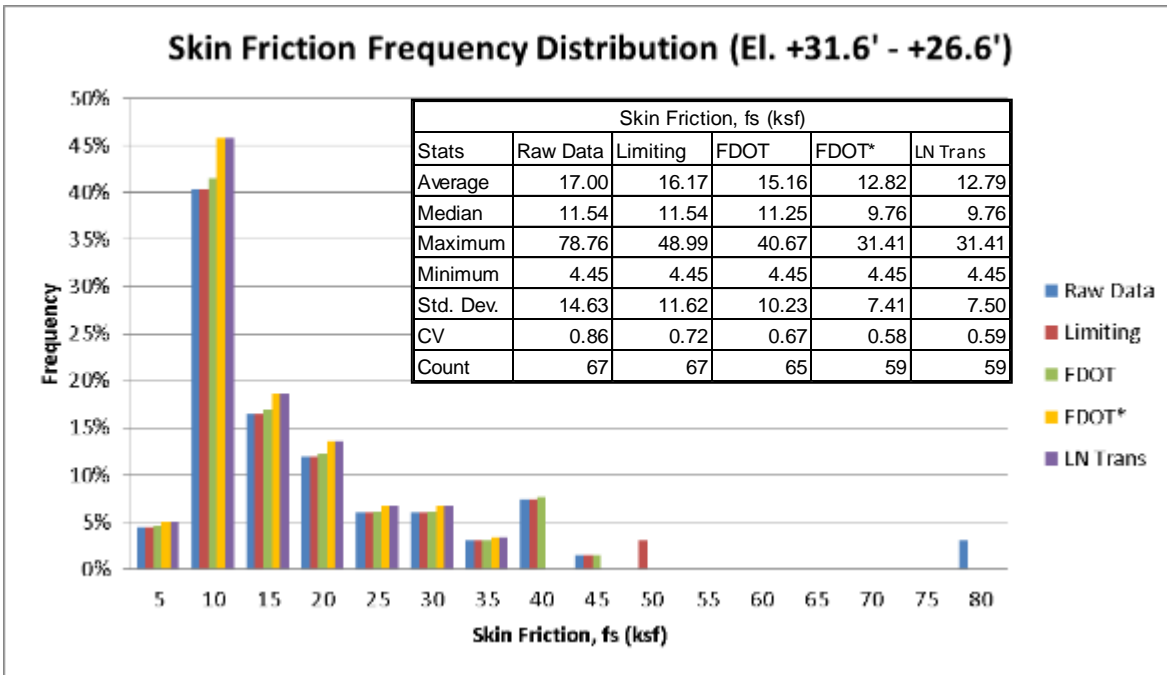


Figure 99 - Skin friction frequency distribution, SG 5 to SG 4

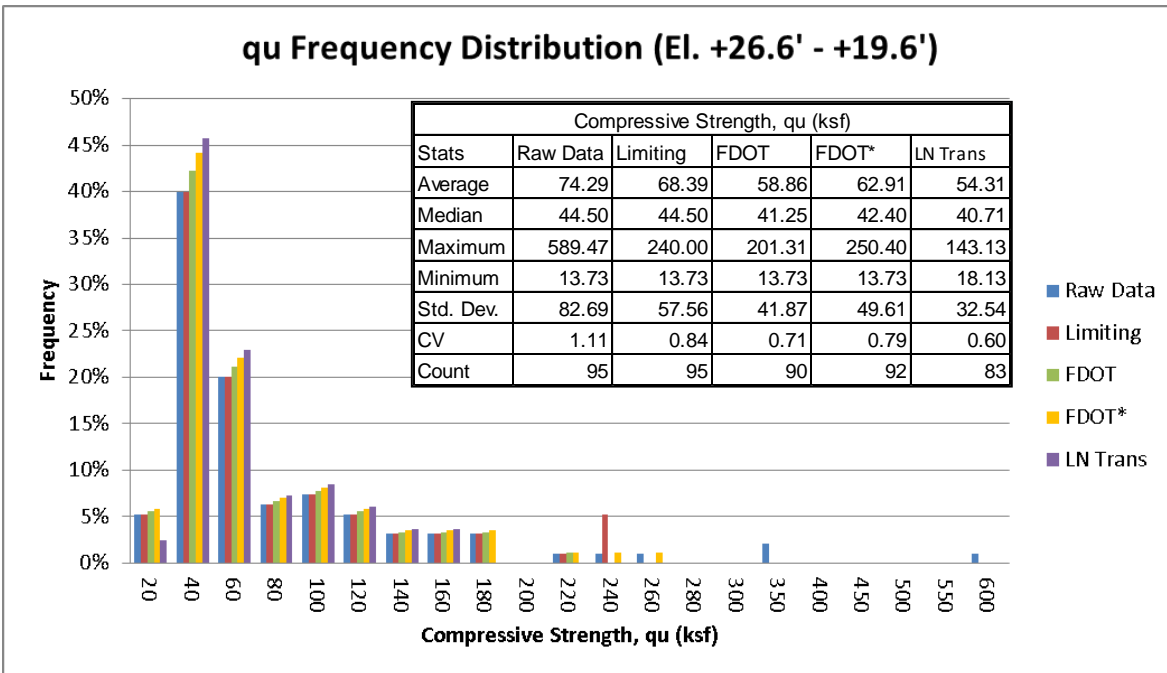


Figure 100 - Compressive strength frequency distribution, SG 4 to SG 3

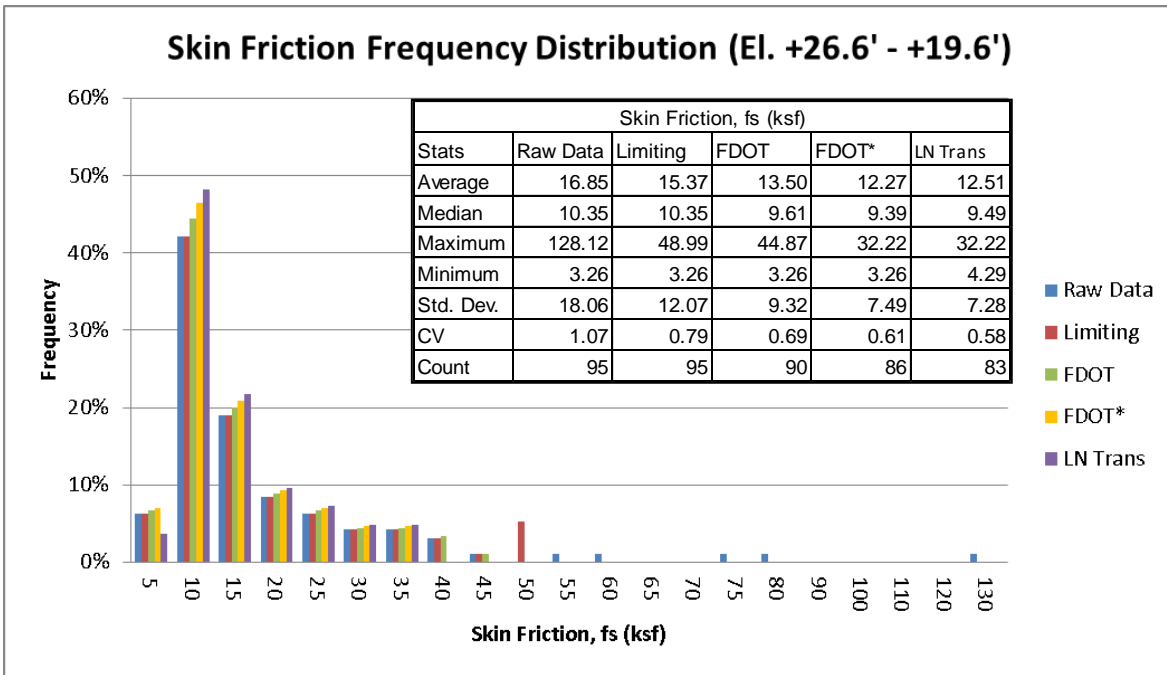


Figure 101 - Skin friction frequency distribution, SG 4 to SG 3

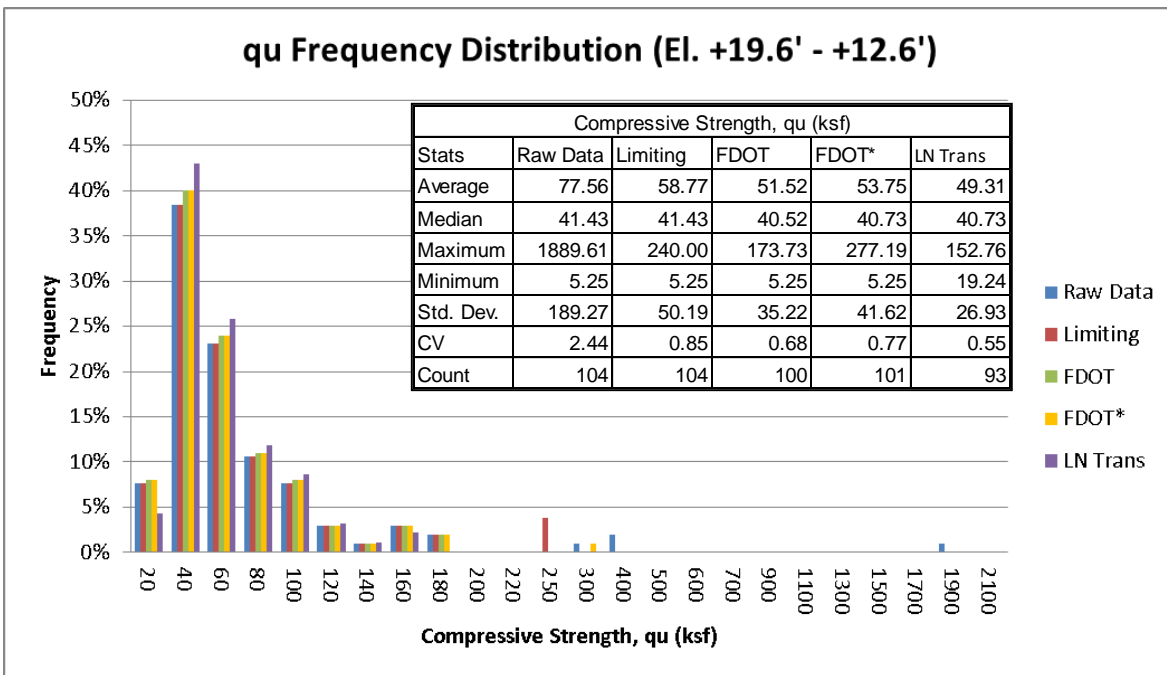


Figure 102 - Compressive strength frequency distribution, SG 3 to SG 2

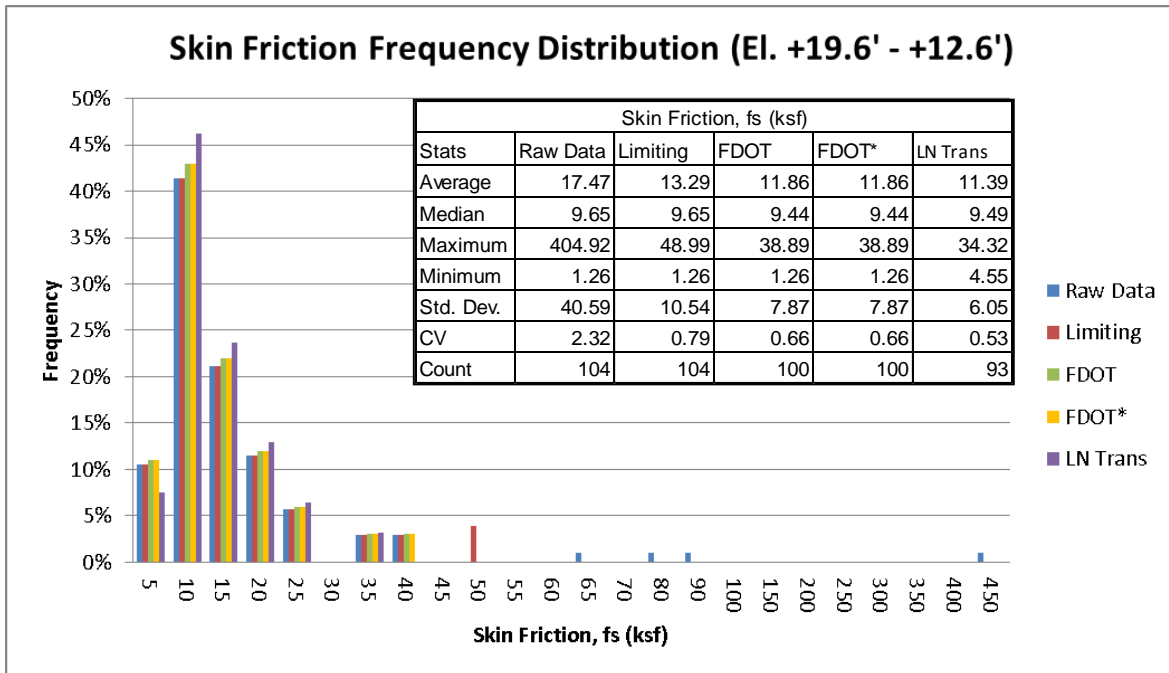


Figure 103 - Skin friction frequency distribution, SG 3 to SG 2

Next, for the investigated portion of the shaft (El. +45.6' to +12.6'), the average skin friction (ksf) was computed and compared to the O-cell results for each section between strain gauges. An overall skin friction average is provided and determined using the lengths of each section to proportion the averaging. This was also done for the total predicted load over the entire 33 foot section and provided for comparison. The following provides the final results using the raw data, geometric mean, and the four additional methods of analysis (Note: Strain gauge levels SG4 to SG3 and SG3 to SG2 were not approaching mobilization):

Table 22 - O-cell test shaft analysis raw data results

Arithmetic Mean (Raw Data)										
Shaft Section (Strain Gauge Levels)	Elevation Range (ft)		Measured Mean (O-cell) (ksf)	Predicted Mean (Monitoring) (ksf)	Percent Difference	Predicted Maximum (Monitoring) (ksf)	Predicted Minimum (Monitoring) (ksf)	Predicted Standard Deviation (Monitoring)	Predicted CV (Monitoring)	Count
SG7 to SG6	45.6	40.6	21.10	25.06	18.75%	203.94	2.54	36.10	1.44	73
SG6 to O-cell	40.6	35.1	20.60	27.75	34.69%	117.17	2.39	23.15	0.83	79
O-cell to SG5	35.1	31.6	21.40	24.61	15.00%	233.90	3.87	34.35	1.40	52
SG5 to SG4	31.6	26.6	13.60	17.00	25.02%	78.76	4.45	14.63	0.86	67
SG4 to SG3	26.6	19.6	9.70	16.85	73.76%	128.12	3.26	18.06	1.07	95
SG3 to SG2	19.6	12.6	9.90	17.47	76.42%	404.92	1.26	40.59	2.32	104
Average Skin Friction (ksf)			15.12	20.89	38.16%	200.24	2.83	27.63	1.36	78.33
Total Load (kips)			6269	8662	38.16%	Totals not needed for these values				

Table 23 - O-cell test shaft analysis geometric mean results

Geometric Mean (Raw Data)						
Shaft Section (Strain Gauge Levels)	Elevation Range (ft)		Measured Mean (O-cell) (ksf)	Predicted Mean (Monitoring) (ksf)	Percent Difference	Count
SG7 to SG6	45.6	40.6	21.10	14.12	-33.10%	73
SG6 to O-cell	40.6	35.1	20.60	20.91	1.51%	79
O-cell to SG5	35.1	31.6	21.40	16.13	-24.62%	52
SG5 to SG4	31.6	26.6	13.60	13.07	-3.91%	67
SG4 to SG3	26.6	19.6	9.70	11.49	18.44%	95
SG3 to SG2	19.6	12.6	9.90	10.74	8.53%	104
Average Skin Friction (ksf)			15.12	14.03	-7.19%	78.33
Total Load (kips)			6269	5819	-7.19%	N/A

Table 24 - O-cell test shaft analysis limiting method results

Limiting Ultimate Values										
Shaft Section (Strain Gauge Levels)	Elevation Range (ft)		Measured Mean (O-cell) (ksf)	Predicted Mean (Monitoring) (ksf)	Percent Difference	Predicted Maximum (Monitoring) (ksf)	Predicted Minimum (Monitoring) (ksf)	Predicted Standard Deviation (Monitoring)	Predicted CV (Monitoring)	Count
SG7 to SG6	45.6	40.6	21.10	18.53	-12.20%	48.99	2.54	14.96	0.81	73
SG6 to O-cell	40.6	35.1	20.60	24.16	17.30%	48.99	2.39	14.04	0.58	79
O-cell to SG5	35.1	31.6	21.40	19.87	-7.14%	48.99	3.87	14.68	0.74	52
SG5 to SG4	31.6	26.6	13.60	16.17	18.87%	48.99	4.45	11.62	0.72	67
SG4 to SG3	26.6	19.6	9.70	15.37	58.41%	48.99	3.26	12.07	0.79	95
SG3 to SG2	19.6	12.6	9.90	13.29	34.25%	48.99	1.26	10.54	0.79	104
Average Skin Friction (ksf)			15.12	17.47	15.56%	48.99	2.83	12.72	0.74	78.33
Total Load (kips)			6269	7245	15.56%	Totals not needed for these values				

Table 25 - O-cell test shaft analysis FDOT method results

FDOT Method										
Shaft Section (Strain Gauge Levels)	Elevation Range (ft)		Measured Mean (O-cell) (ksf)	Predicted Mean (Monitoring) (ksf)	Percent Difference	Predicted Maximum (Monitoring) (ksf)	Predicted Minimum (Monitoring) (ksf)	Predicted Standard Deviation (Monitoring)	Predicted CV (Monitoring)	Count
SG7 to SG6	45.6	40.6	21.10	14.78	-29.97%	41.97	2.54	11.03	0.75	65
SG6 to O-cell	40.6	35.1	20.60	20.58	-0.12%	45.86	2.39	11.08	0.54	69
O-cell to SG5	35.1	31.6	21.40	18.32	-14.40%	50.10	3.87	13.66	0.75	49
SG5 to SG4	31.6	26.6	13.60	15.16	11.44%	40.67	4.45	10.23	0.67	65
SG4 to SG3	26.6	19.6	9.70	13.50	39.15%	44.87	3.26	9.32	0.69	90
SG3 to SG2	19.6	12.6	9.90	11.86	19.82%	38.89	1.26	7.87	0.66	100
Average Skin Friction (ksf)			15.12	15.29	1.11%	43.25	2.83	10.16	0.67	73.00
Total Load (kips)			6269	6339	1.11%	Totals not needed for these values				

Table 26 - O-cell test shaft analysis FDOT* method results

FDOT* Method (Each Section)										
Shaft Section (Strain Gauge Levels)	Elevation Range (ft)		Measured Mean (O-cell) (ksf)	Predicted Mean (Monitoring) (ksf)	Percent Difference	Predicted Maximum (Monitoring) (ksf)	Predicted Minimum (Monitoring) (ksf)	Predicted Standard Deviation (Monitoring)	Predicted CV (Monitoring)	Count
SG7 to SG6	45.6	40.6	21.10	14.78	-29.97%	41.97	2.54	11.03	0.75	65
SG6 to O-cell	40.6	35.1	20.60	21.64	5.05%	45.86	7.48	10.51	0.49	65
O-cell to SG5	35.1	31.6	21.40	19.10	-10.73%	57.60	3.87	14.62	0.77	50
SG5 to SG4	31.6	26.6	13.60	12.82	-5.76%	31.41	4.45	7.41	0.58	59
SG4 to SG3	26.6	19.6	9.70	12.27	26.47%	32.22	3.26	7.49	0.61	86
SG3 to SG2	19.6	12.6	9.90	11.86	19.82%	38.89	1.26	7.87	0.66	100
Average Skin Friction (ksf)			15.12	14.93	-1.23%	39.95	3.67	9.35	0.63	70.83
Total Load (kips)			6269	6192	-1.23%	Totals not needed for these values				

Table 27 - O-cell test shaft LN transformed method results

LN Transform Method										
Shaft Section (Strain Gauge Levels)	Elevation Range (ft)		Measured Mean (O-cell) (ksf)	Predicted Mean (Monitoring) (ksf)	Percent Difference	Predicted Maximum (Monitoring) (ksf)	Predicted Minimum (Monitoring) (ksf)	Predicted Standard Deviation (Monitoring)	Predicted CV (Monitoring)	Count
SG7 to SG6	45.6	40.6	21.10	14.28	-32.31%	34.40	4.00	10.02	0.70	55
SG6 to O-cell	40.6	35.1	20.60	18.18	-11.75%	35.78	7.48	7.33	0.40	55
O-cell to SG5	35.1	31.6	21.40	13.91	-34.98%	35.44	4.91	7.75	0.56	41
SG5 to SG4	31.6	26.6	13.60	13.17	-3.18%	36.01	4.45	7.99	0.61	60
SG4 to SG3	26.6	19.6	9.70	12.58	29.69%	36.09	3.99	7.74	0.62	86
SG3 to SG2	19.6	12.6	9.90	11.55	16.70%	35.85	4.07	6.42	0.56	95
Average Skin Friction (ksf)			15.12	13.78	-8.82%	35.65	4.76	7.78	0.57	65.33
Total Load (kips)			6269	5716	-8.82%	Totals not needed for these values				

From the tabular results, it can be seen that several methods provide shaft capacity estimations close to what the O-cell results provided. The FDOT and FDOT* methods provided the closest estimations as both were within 2% difference of the measured O-cell result. However, these predictions were made using split tension strengths derived from the e vs. q_t curve developed during the laboratory investigation, Figure 52. Investigating the q_t/q_u ratios developed in the lab and obtained at Little River shows that the material formation of the Gatorock used for lab drillings was translated to the field data. This was determined by plotting q_t vs. q_u for both data sets and comparing the trends of the data. Figure 104, provides the q_t vs. q_u plot obtained from the Gatorock cast cylinders which were used as a reference of strength for each drilled block.

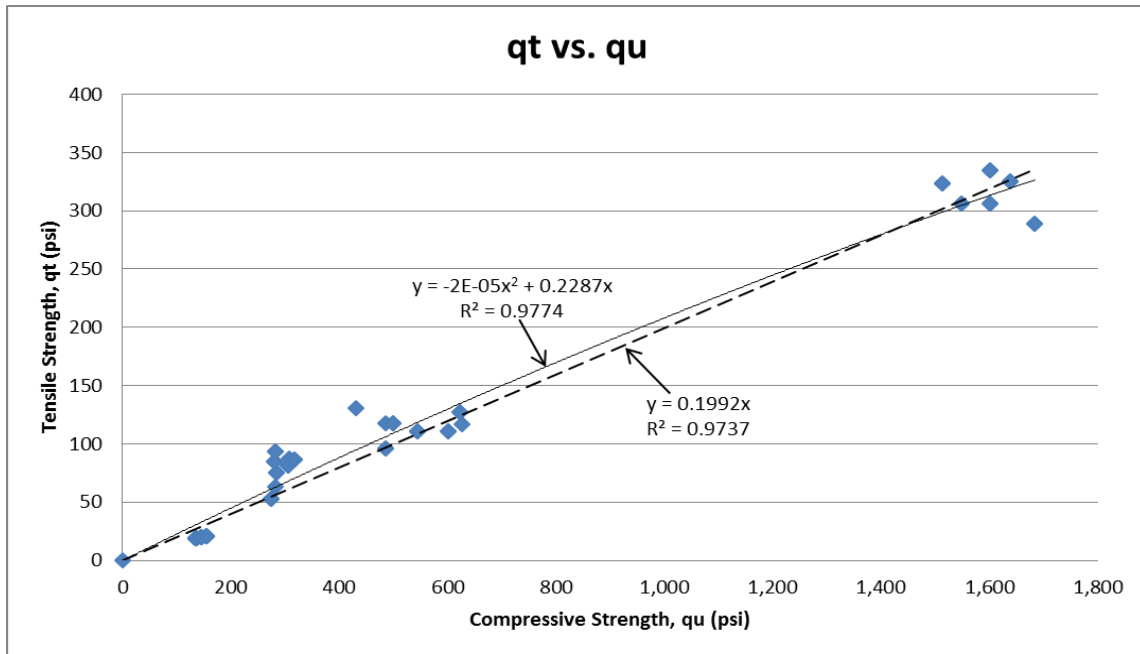


Figure 104 - Lab drilling q_u vs q_t plot to show q_t/q_u slope

As seen in Figure 104, the second order polynomial provides a better fit for q_t/q_u as q_u increases. This indicates the Gatorock q_t/q_u ratio is declining as compressive strength increases. Figure 105, provides even better visualization where q_t and q_u are plotted vs. specific energy using the previously developed e vs. q_u and e vs. q_t curves. As specific energy increases, q_u increases at far more rapid rate than q_t .

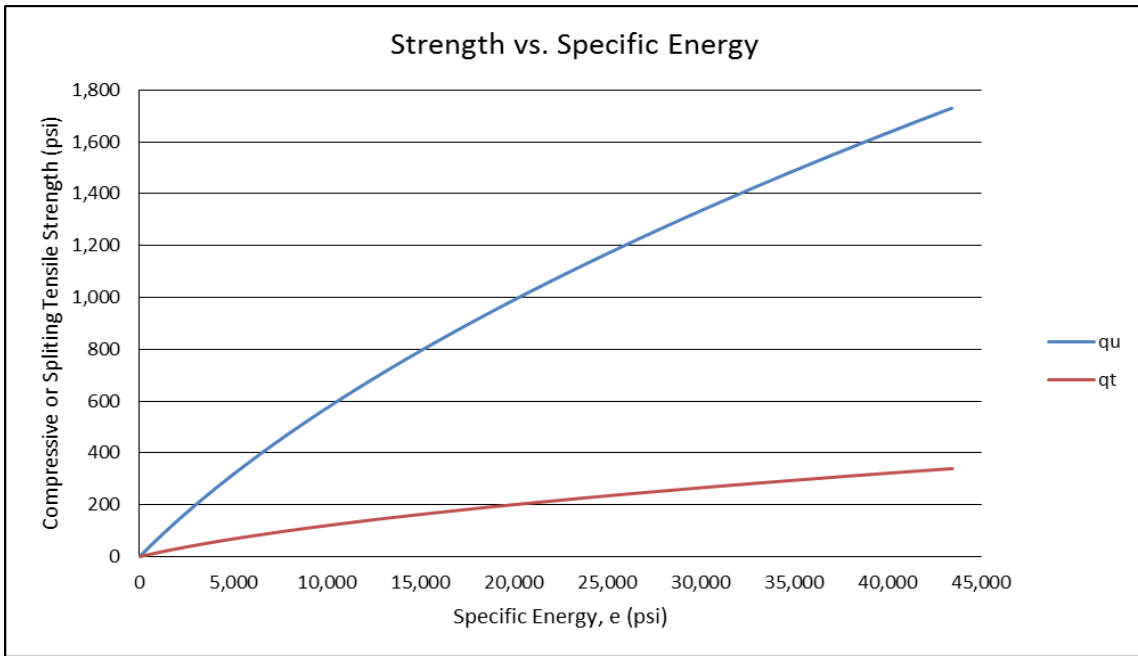


Figure 105 – Strength vs. specific energy

However, the average q_t/q_u ratio, determined by the linear regression slope in Figure 104, is approximately 0.2. This same “average slope” can be seen in Figure 106 when q_u and q_t values, recorded during field drilling at Little River, are plotted against one another.

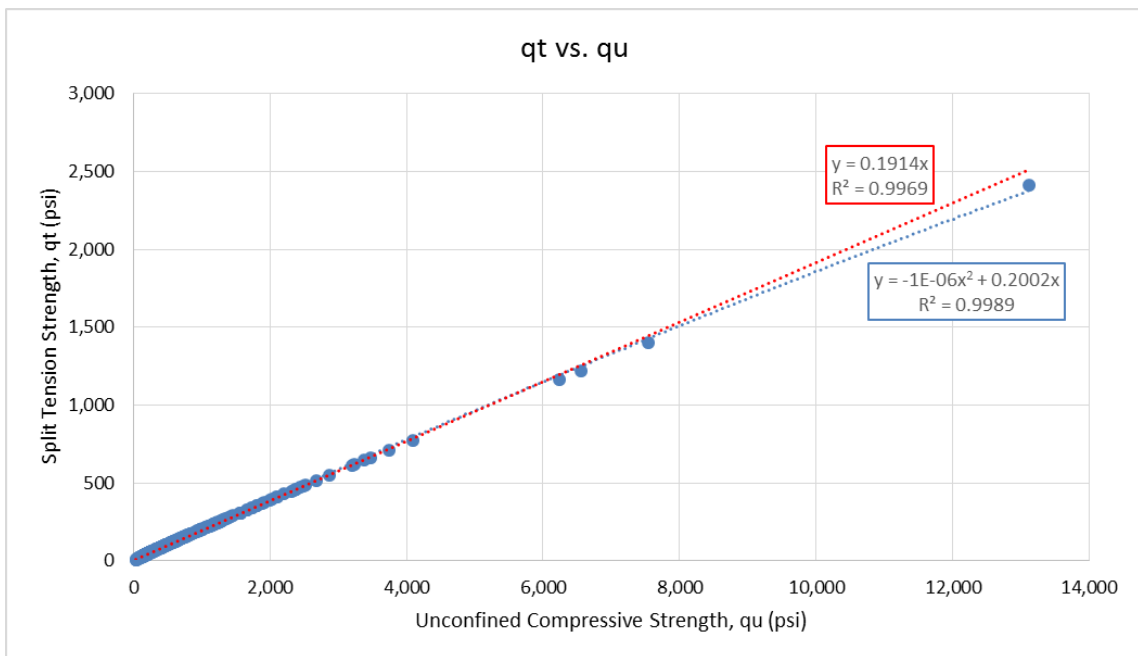


Figure 106 - Little River q_u vs. q_t plot to show q_t/q_u slope

The q_t/q_u plots in Figure 104 and Figure 106, produced regression equations that are nearly identical. Also, the Little River data points are almost perfectly aligned which was a strong indicator the Gatorock material formation was translated to the field data. Therefore, tensile strengths would need to be adjusted based on the q_t/q_u relationship of the site being monitored. The following section investigates adjusting the q_t values based on obtained q_u and q_t core data at Little River.

3.2.2.1 Investigating q_t Slope Adjustments

As discussed, tensile strength values will need to be adjusted based on the monitoring site q_t/q_u relationship. At Little River, seven boring locations were available for comparison. However, the closest boring, B8, with q_u and q_t data in the same elevation range as the investigated portion of the test shaft was located 76.5 ft away and may not be comparable. Consequently, multiple methods were used to investigate how the data is affected by adjusting q_t based on site conditions.

Each method grouped pairs of q_u and q_t values within one vertical foot of each other (above and below) for each individual boring. This was done in an attempt to provide a range of q_t values for each recorded q_u value. Once all the pairs were created, the q_t/q_u ratio was found for each pair. Any q_t/q_u value that fell outside of one standard deviation was removed. Remaining pairs were then used to create a new q_u vs q_t slope at each boring location. Remaining pairs were also combined from every boring location, removing the outliers, and used to plot q_u vs. q_t to determine the q_t/q_u ratio for the entire site.

The first method used all available data at all elevations.

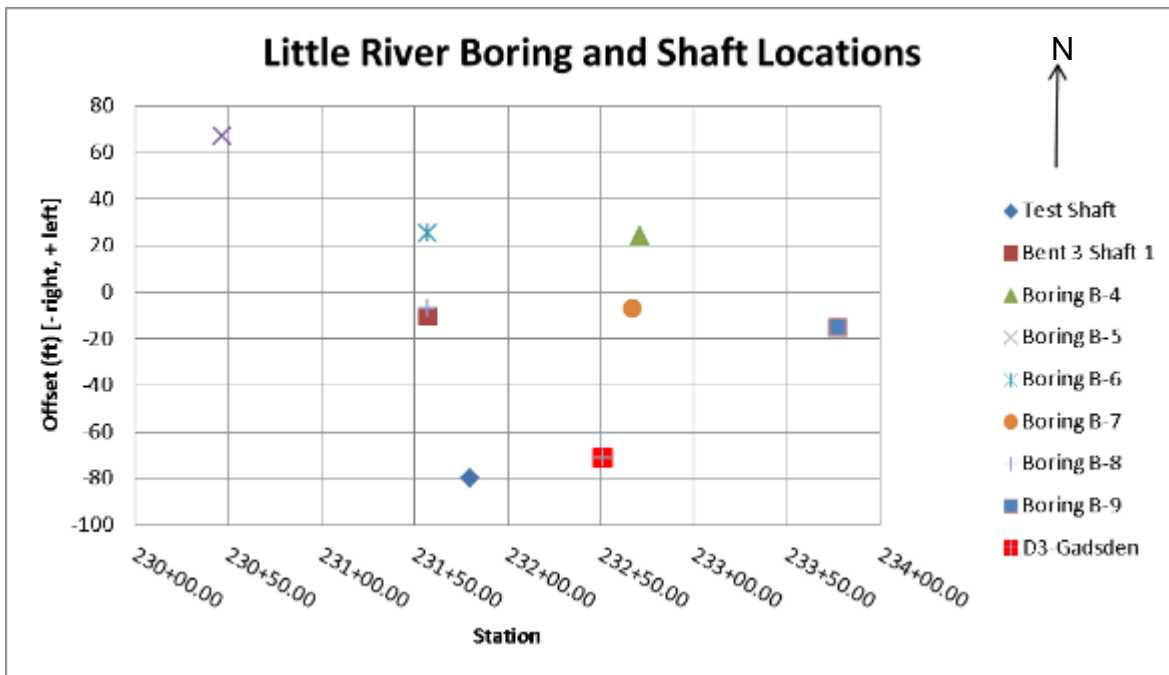


Figure 107 - Little River boring and shaft locations

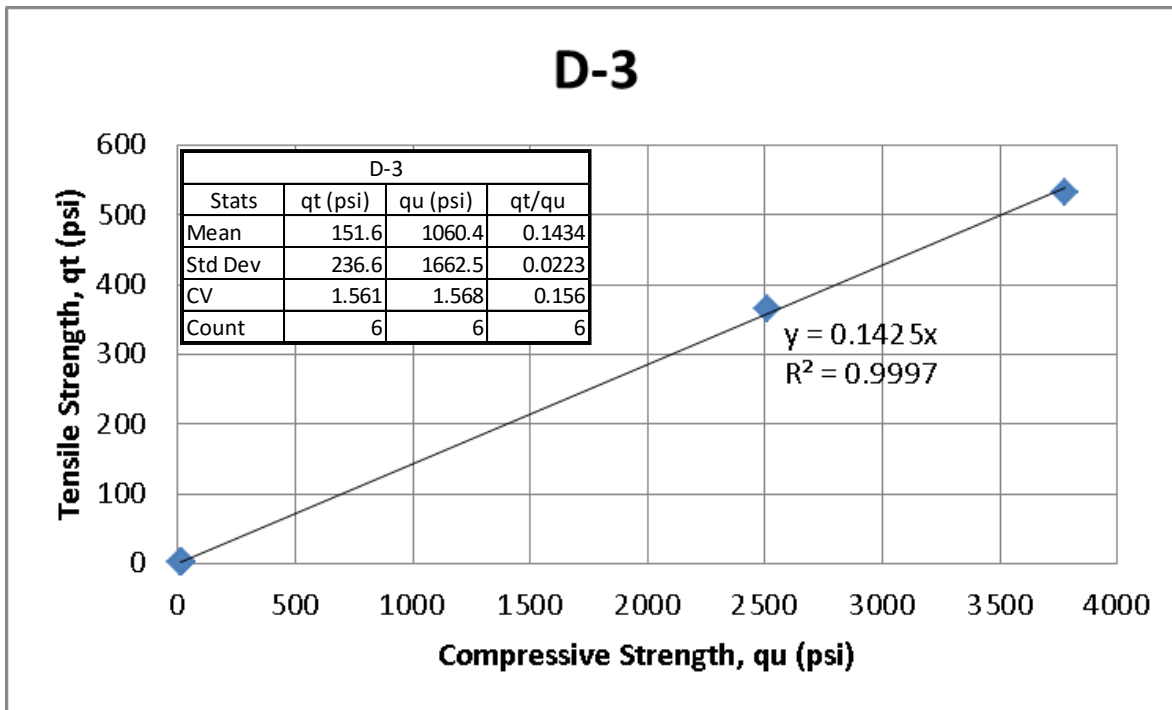


Figure 108 - Little River boring D3 q_t/q_u analysis using all elevations

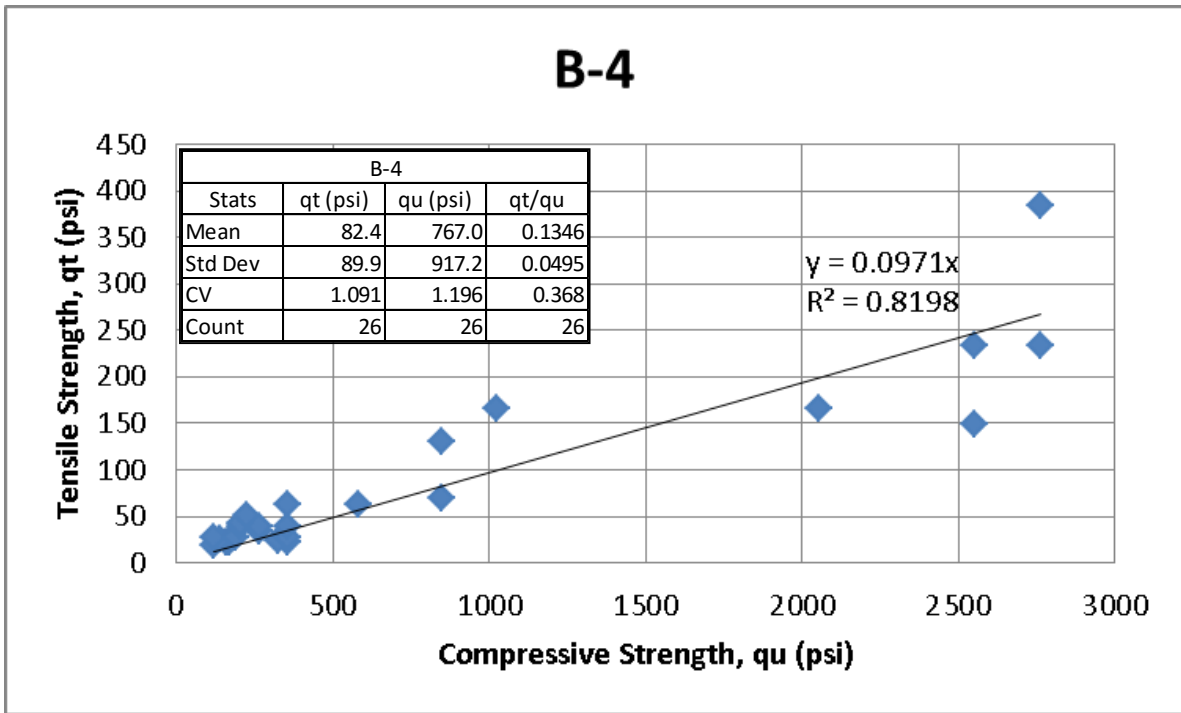


Figure 109 - Little River boring B4 q_t/q_u analysis using all elevations

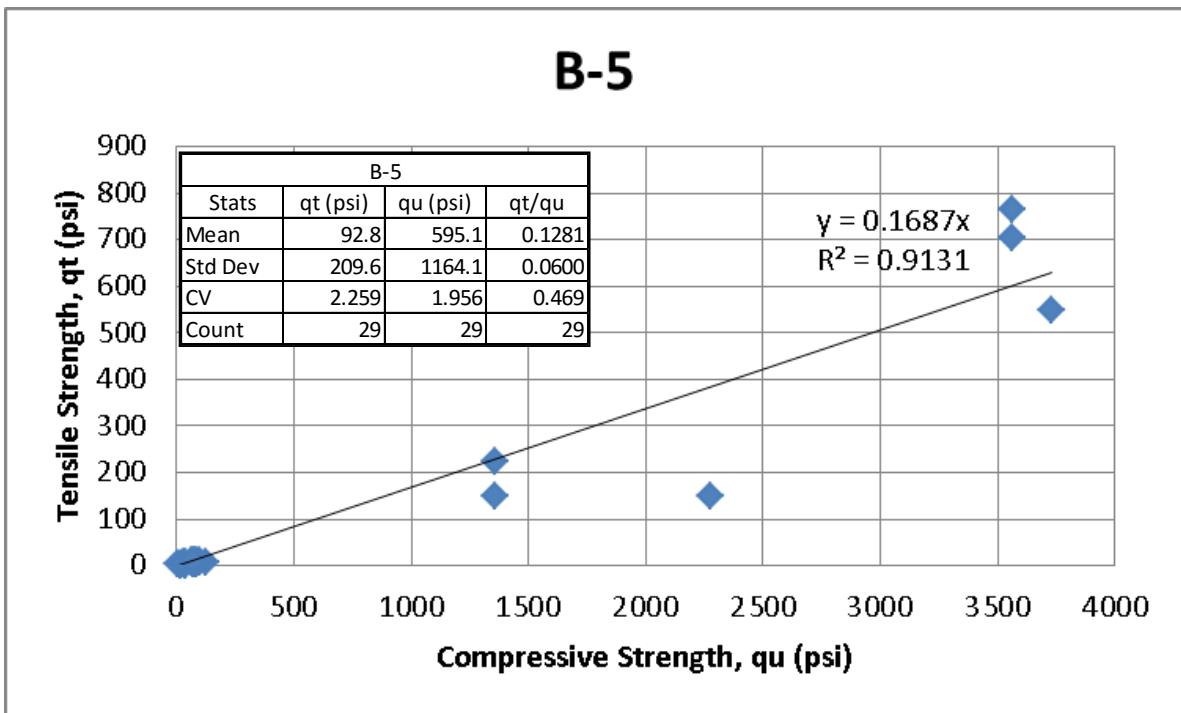


Figure 110 - Little River boring B5 q_t/q_u analysis using all elevations

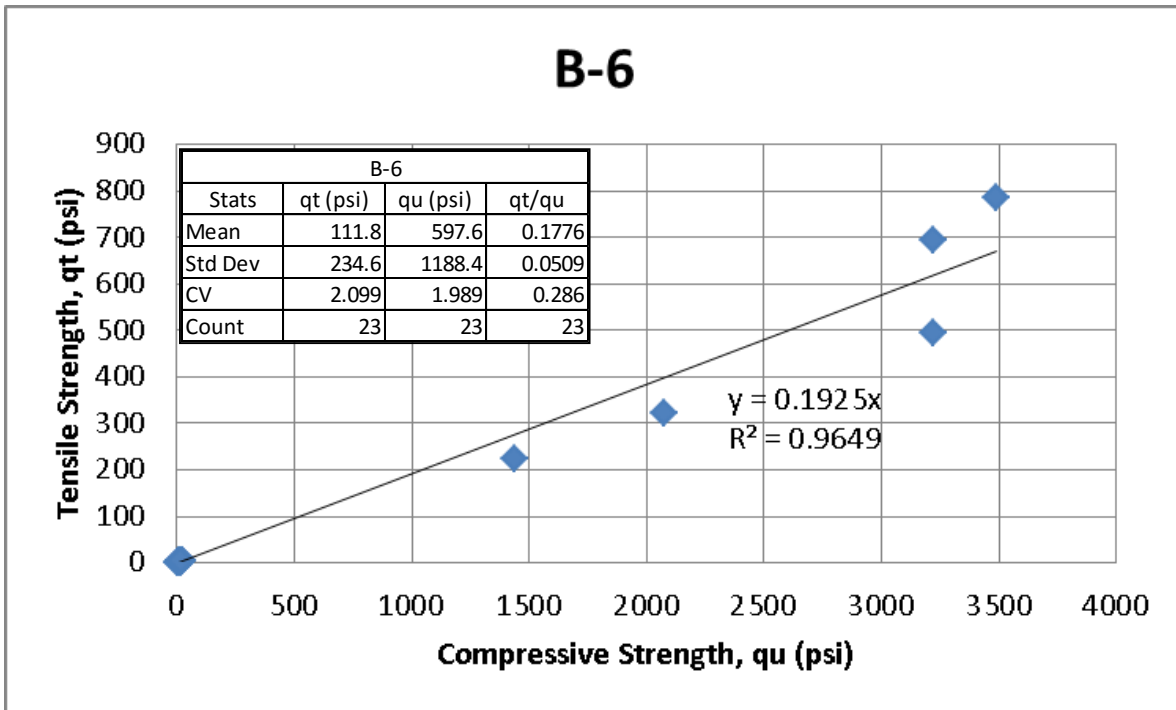


Figure 111 - Little River boring B6 q_t/q_u analysis using all elevations

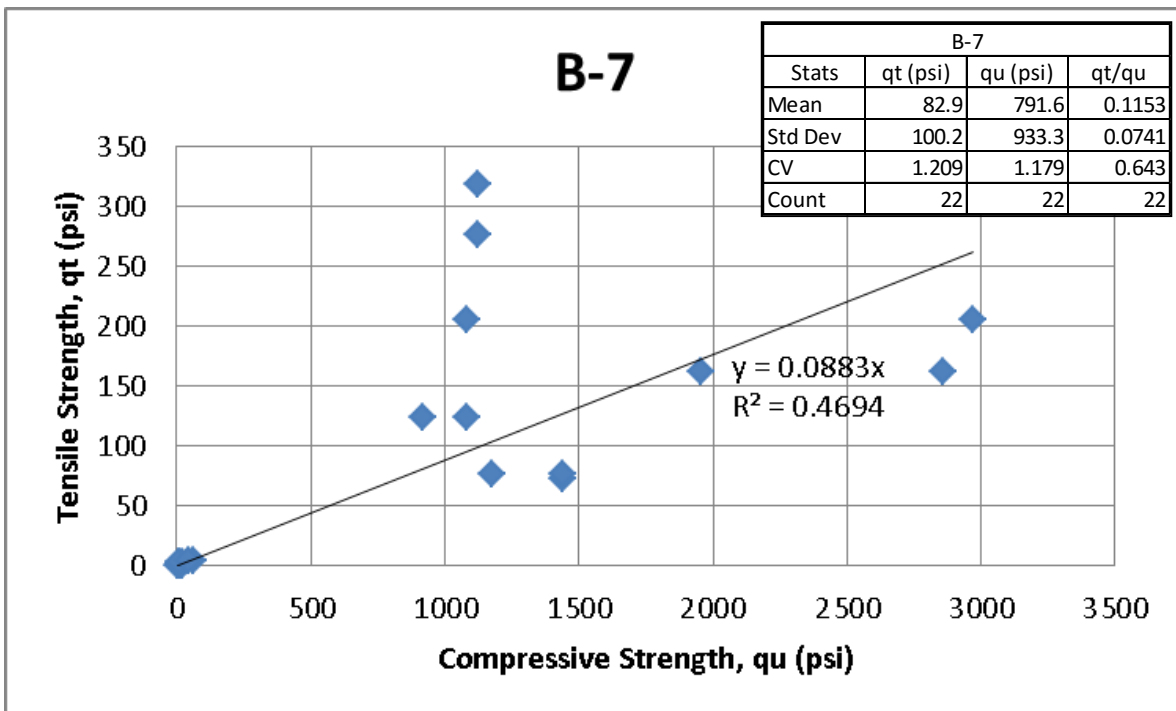


Figure 112 - Little River boring B7 q_t/q_u analysis using all elevations

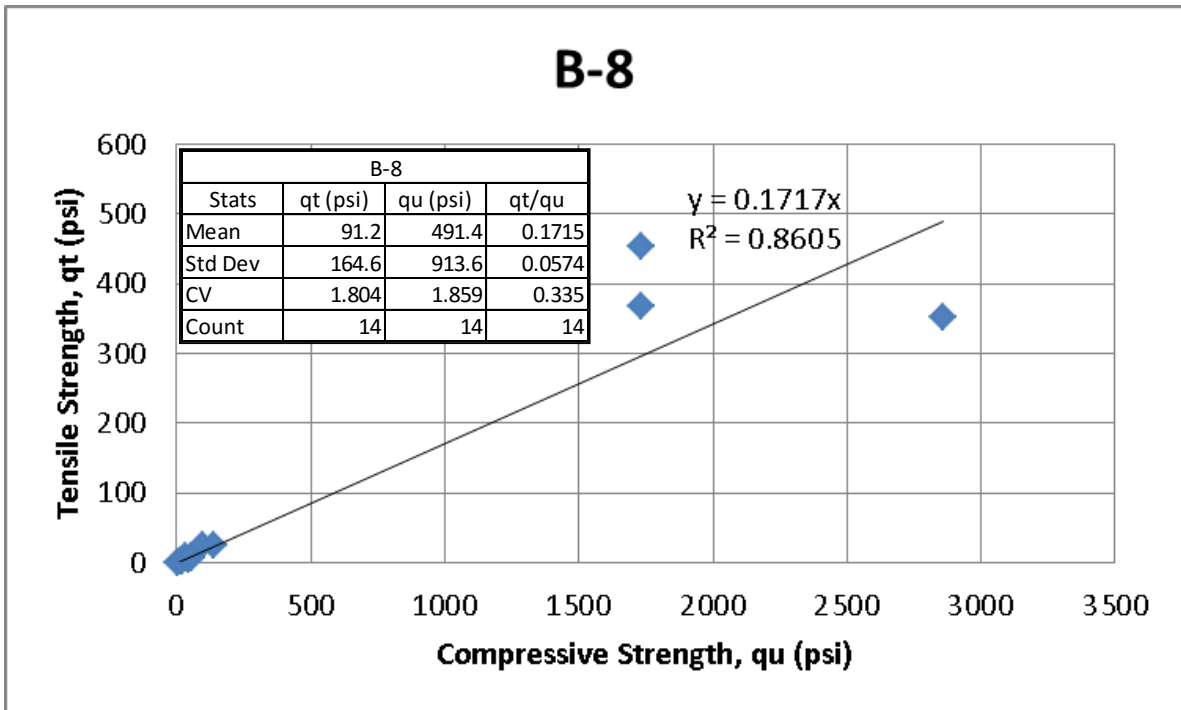


Figure 113 - Little River boring B8 q_t/q_u analysis using all elevations

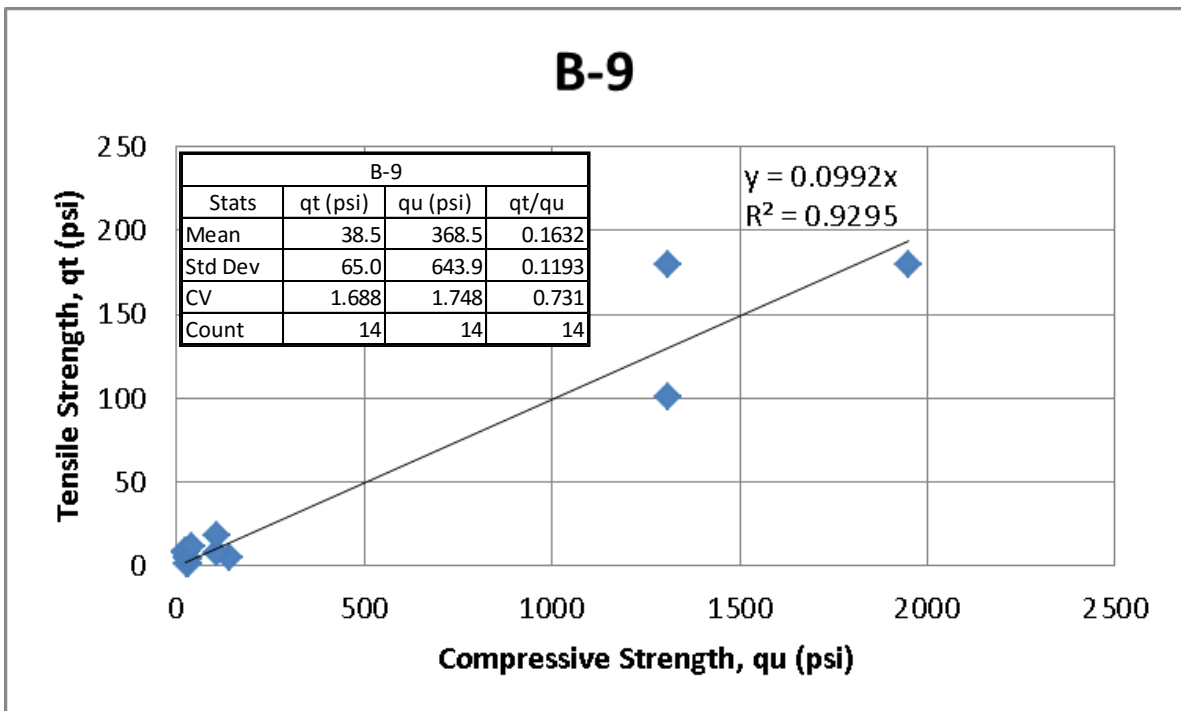


Figure 114 - Little River boring B9 q_t/q_u analysis using all elevations

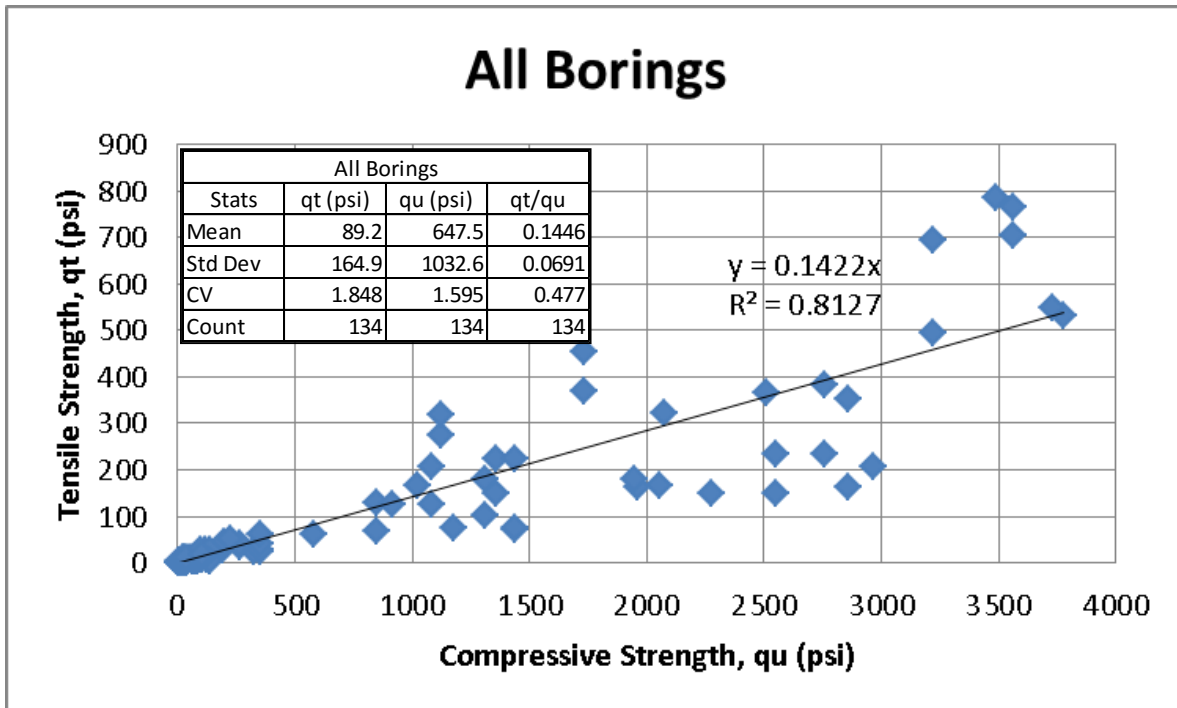


Figure 115 - Little River boring q_t/q_u analysis using all elevations and boring locations

Once all remaining pairs were grouped using all boring locations, any q_t/q_u value that fell outside of one standard deviation was removed and a new q_t/q_u slope was found:

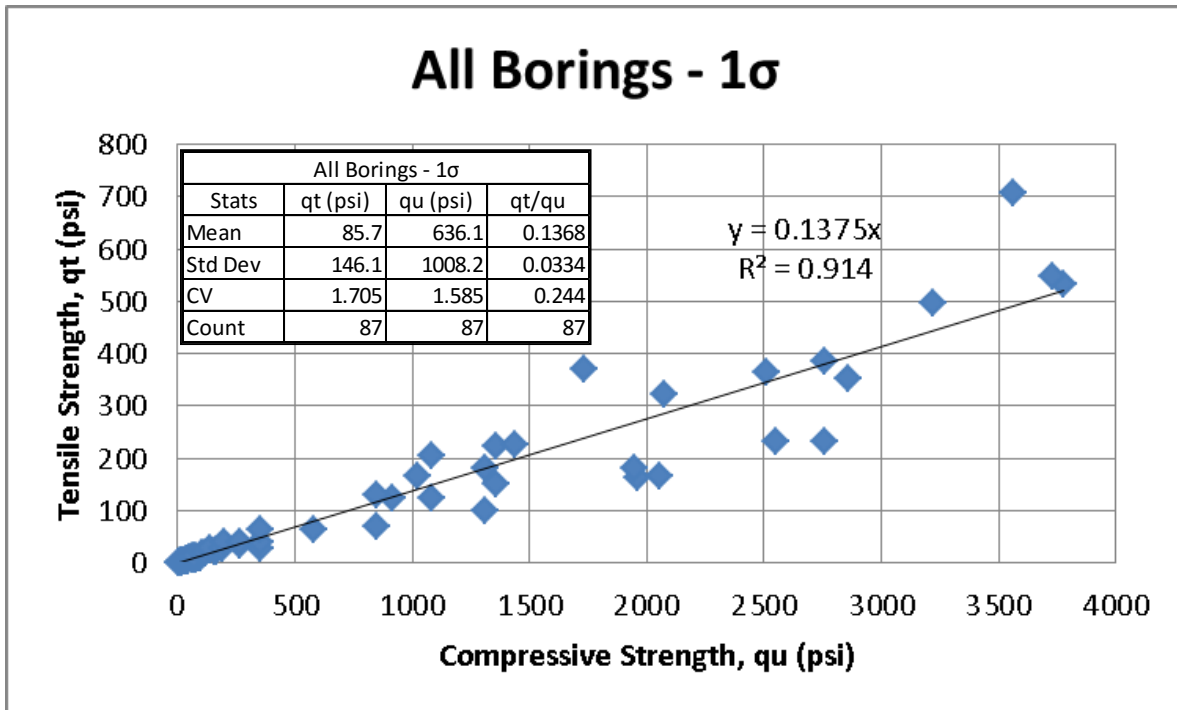


Figure 116 - Little River q_t/q_u analysis using all depths and boring locations, outliers removed

The following are the results using all depths and boring locations to adjust the q_t values:

Table 28 - O-cell test shaft analysis raw data results

Arithmetic Mean (Raw Data)										
Shaft Section (Strain Gauge Levels)	Elevation Range (ft)		Measured Mean (O-cell) (ksf)	Predicted Mean (Monitoring) (ksf)	Percent Difference	Predicted Maximum (Monitoring) (ksf)	Predicted Minimum (Monitoring) (ksf)	Predicted Standard Deviation (Monitoring)	Predicted CV (Monitoring)	Count
SG7 to SG6	45.6	40.6	21.10	20.81	-1.38%	175.23	1.98	30.98	1.49	73
SG6 to O-cell	40.6	35.1	20.60	22.93	11.29%	99.78	1.86	19.74	0.86	79
O-cell to SG5	35.1	31.6	21.40	20.37	-4.83%	201.32	3.03	29.53	1.45	52
SG5 to SG4	31.6	26.6	13.60	13.86	1.94%	66.50	3.49	12.34	0.89	67
SG4 to SG3	26.6	19.6	9.70	13.77	41.99%	109.29	2.55	15.33	1.11	95
SG3 to SG2	19.6	12.6	9.90	14.38	45.25%	350.34	0.97	35.09	2.44	104
Average Skin Friction (ksf)			15.12	17.21	13.81%	172.11	2.21	23.68	1.41	78.33
Total Load (kips)			6269	7135	13.81%	Totals not needed for these values				

Table 29 - O-cell test shaft analysis geometric mean results

Geometric Mean (Raw Data)						
Shaft Section (Strain Gauge Levels)	Elevation Range (ft)		Measured Mean (O-cell) (ksf)	Predicted Mean (Monitoring) (ksf)	Percent Difference	Count
SG7 to SG6	45.6	40.6	21.10	11.38	-46.09%	73
SG6 to O-cell	40.6	35.1	20.60	17.01	-17.40%	79
O-cell to SG5	35.1	31.6	21.40	13.03	-39.11%	52
SG5 to SG4	31.6	26.6	13.60	10.50	-22.81%	67
SG4 to SG3	26.6	19.6	9.70	9.20	-5.13%	95
SG3 to SG2	19.6	12.6	9.90	8.59	-13.22%	104
Average Skin Friction (ksf)			15.12	11.31	-25.21%	78.33
Total Load (kips)			6269	4689	-25.21%	N/A

Table 30 - O-cell test shaft analysis limiting method results

Limiting Ultimate Values										
Shaft Section (Strain Gauge Levels)	Elevation Range (ft)		Measured Mean (O-cell) (ksf)	Predicted Mean (Monitoring) (ksf)	Percent Difference	Predicted Maximum (Monitoring) (ksf)	Predicted Minimum (Monitoring) (ksf)	Predicted Standard Deviation (Monitoring)	Predicted CV (Monitoring)	Count
SG7 to SG6	45.6	40.6	21.10	16.05	-23.93%	48.99	1.98	14.50	0.90	73
SG6 to O-cell	40.6	35.1	20.60	20.71	0.52%	48.99	1.86	13.50	0.65	79
O-cell to SG5	35.1	31.6	21.40	16.86	-21.20%	48.99	3.03	13.60	0.81	52
SG5 to SG4	31.6	26.6	13.60	13.39	-1.57%	48.99	3.49	10.50	0.78	67
SG4 to SG3	26.6	19.6	9.70	12.83	32.28%	48.99	2.55	11.15	0.87	95
SG3 to SG2	19.6	12.6	9.90	11.06	11.69%	48.99	0.97	9.91	0.90	104
Average Skin Friction (ksf)			15.12	14.77	-2.32%	48.99	2.21	11.95	0.82	78.33
Total Load (kips)			6269	6124	-2.32%	Totals not needed for these values				

Table 31 - O-cell test shaft analysis FDOT method results

FDOT Method										
Shaft Section (Strain Gauge Levels)	Elevation Range (ft)		Measured Mean (O-cell) (ksf)	Predicted Mean (Monitoring) (ksf)	Percent Difference	Predicted Maximum (Monitoring) (ksf)	Predicted Minimum (Monitoring) (ksf)	Predicted Standard Deviation (Monitoring)	Predicted CV (Monitoring)	Count
SG7 to SG6	45.6	40.6	21.10	12.00	-43.14%	34.84	1.98	9.18	0.76	65
SG6 to O-cell	40.6	35.1	20.60	16.80	-18.46%	38.17	1.86	9.28	0.55	69
O-cell to SG5	35.1	31.6	21.40	14.95	-30.14%	41.81	3.03	11.48	0.77	49
SG5 to SG4	31.6	26.6	13.60	12.29	-9.63%	33.73	3.49	8.53	0.69	65
SG4 to SG3	26.6	19.6	9.70	10.91	12.50%	37.32	2.55	7.76	0.71	90
SG3 to SG2	19.6	12.6	9.90	9.55	-3.52%	32.21	0.97	6.53	0.68	100
Average Skin Friction (ksf)			15.12	12.41	-17.94%	35.94	2.21	8.48	0.69	73.00
Total Load (kips)			6269	5145	-17.94%	Totals not needed for these values				

Table 32 - O-cell test shaft analysis FDOT* method results

FDOT* Method (Each Section)										
Shaft Section (Strain Gauge Levels)	Elevation Range (ft)		Measured Mean (O-cell) (ksf)	Predicted Mean (Monitoring) (ksf)	Percent Difference	Predicted Maximum (Monitoring) (ksf)	Predicted Minimum (Monitoring) (ksf)	Predicted Standard Deviation (Monitoring)	Predicted CV (Monitoring)	Count
SG7 to SG6	45.6	40.6	21.10	12.00	-43.14%	34.84	1.98	9.18	0.76	65
SG6 to O-cell	40.6	35.1	20.60	17.67	-14.20%	38.17	5.92	8.83	0.50	65
O-cell to SG5	35.1	31.6	21.40	15.62	-27.02%	48.25	3.03	12.30	0.79	50
SG5 to SG4	31.6	26.6	13.60	10.33	-24.06%	25.85	3.49	6.14	0.59	59
SG4 to SG3	26.6	19.6	9.70	9.88	1.85%	26.54	2.55	6.20	0.63	86
SG3 to SG2	19.6	12.6	9.90	9.55	-3.52%	32.21	0.97	6.53	0.68	100
Average Skin Friction (ksf)			15.12	12.11	-19.92%	33.14	2.88	7.80	0.65	70.83
Total Load (kips)			6269	5020	-19.92%	Totals not needed for these values				

Table 33 - O-cell test shaft LN transformed method results

LN Transform Method										
Shaft Section (Strain Gauge Levels)	Elevation Range (ft)		Measured Mean (O-cell) (ksf)	Predicted Mean (Monitoring) (ksf)	Percent Difference	Predicted Maximum (Monitoring) (ksf)	Predicted Minimum (Monitoring) (ksf)	Predicted Standard Deviation (Monitoring)	Predicted CV (Monitoring)	Count
SG7 to SG6	45.6	40.6	21.10	11.41	-45.90%	28.39	3.02	8.43	0.74	56
SG6 to O-cell	40.6	35.1	20.60	15.19	-26.27%	30.81	3.05	7.40	0.49	58
O-cell to SG5	35.1	31.6	21.40	11.51	-46.22%	30.67	3.03	7.26	0.63	43
SG5 to SG4	31.6	26.6	13.60	10.62	-21.92%	29.76	3.49	6.64	0.63	60
SG4 to SG3	26.6	19.6	9.70	10.13	4.48%	29.83	3.12	6.42	0.63	86
SG3 to SG2	19.6	12.6	9.90	9.28	-6.28%	29.63	3.19	5.30	0.57	95
Average Skin Friction (ksf)			15.12	11.21	-25.86%	29.81	3.16	6.77	0.61	66.33
Total Load (kips)			6269	4648	-25.86%	Totals not needed for these values				

The second method was based on trends noticed during the preliminary site investigation of the borings. Seen in Figure 117, there appears to be three different subsurface layers based on laboratory q_u data:

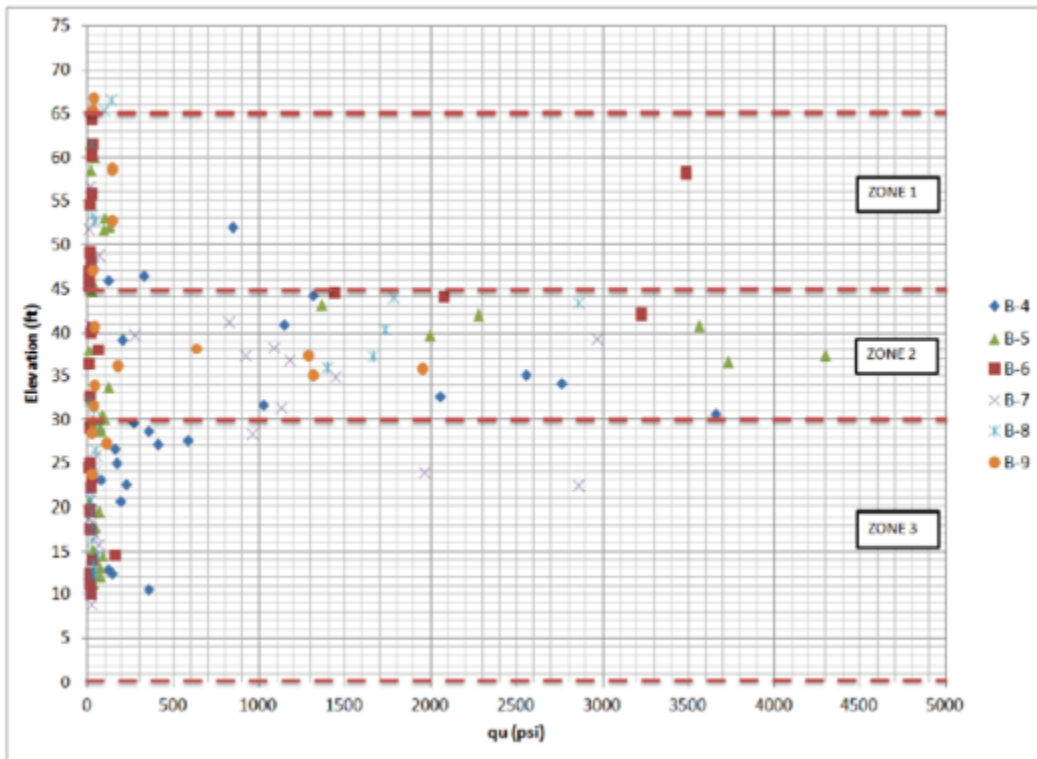


Figure 117 - Little River q_u stratification, indicating zones

Of interest are zones 2 and 3, where the shaft investigation took place. For both of these zones, a new q_t/q_u slope was determined using data available from all borings in each of the zones. The following provides the results:

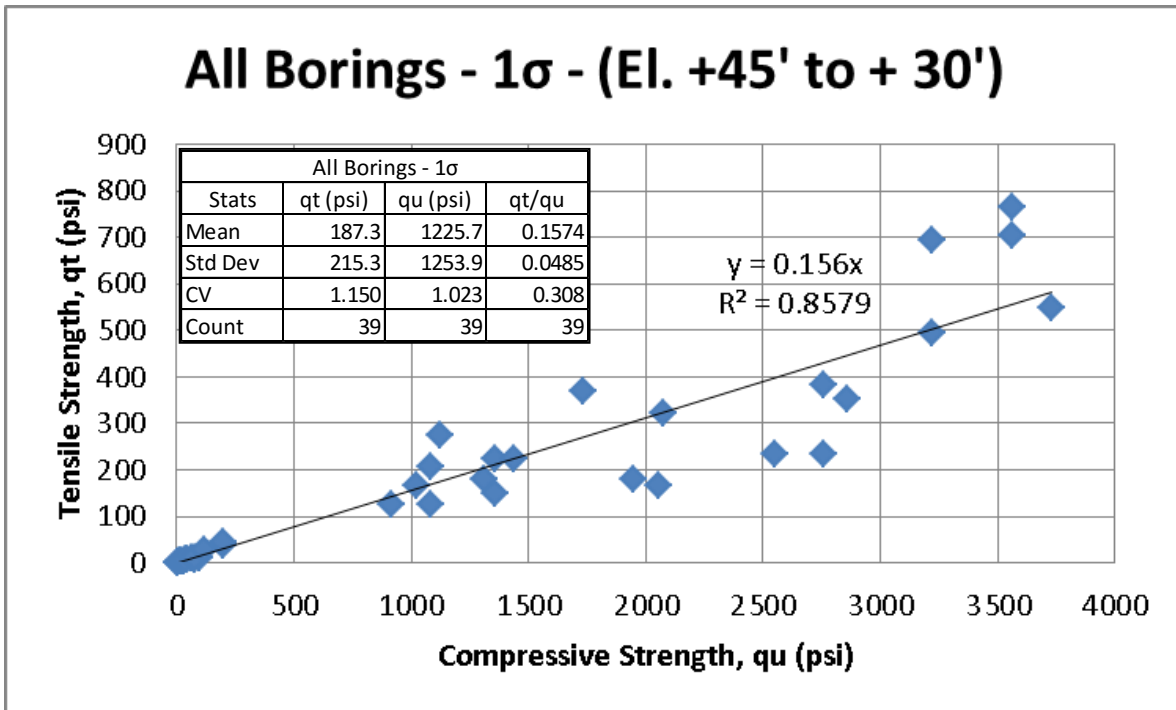


Figure 118 - Little River q_t/q_u analysis using data from elevations +45' to +30' at all locations

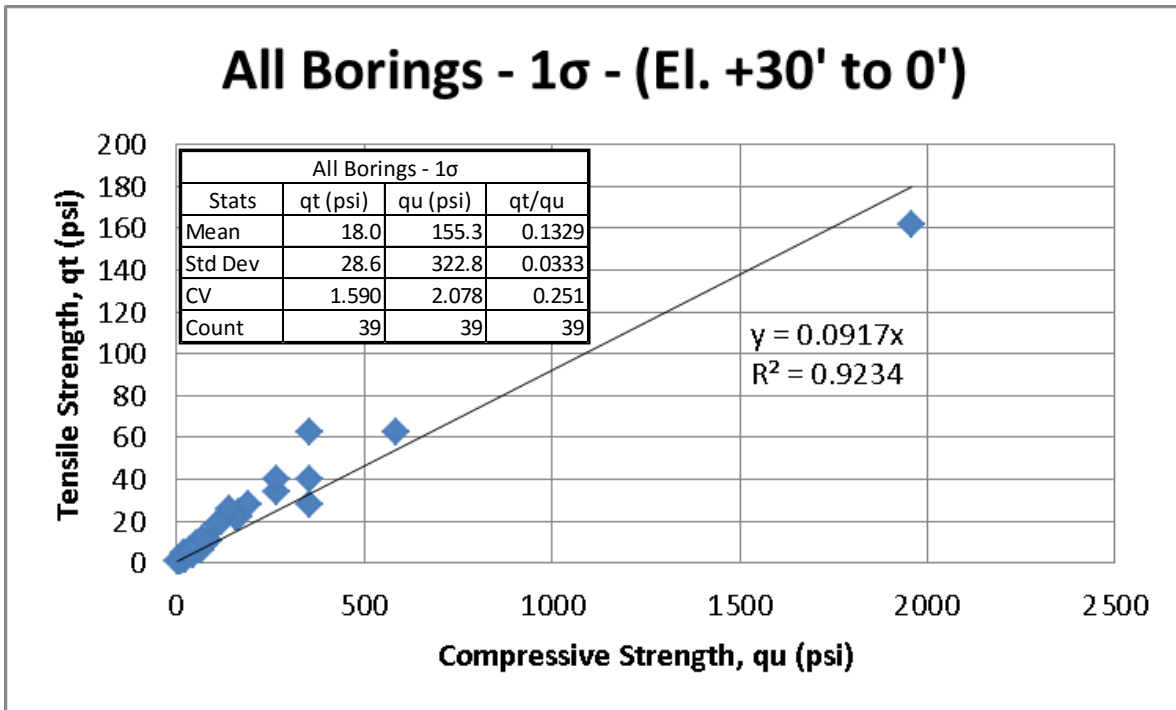


Figure 119 - Little River q_t/q_u analysis, elevations +30' to 0' at all locations, outliers removed

The following provides the analysis results using the second method for adjusting qt:

Table 34 - O-cell test shaft analysis raw data results

Arithmetic Mean (Raw Data)										
Shaft Section (Strain Gauge Levels)	Elevation Range (ft)		Measured Mean (O-cell) (ksf)	Predicted Mean (Monitoring) (ksf)	Percent Difference	Predicted Maximum (Monitoring) (ksf)	Predicted Minimum (Monitoring) (ksf)	Predicted Standard Deviation (Monitoring)	Predicted CV (Monitoring)	Count
SG7 to SG6	45.6	40.6	21.10	22.17	5.05%	186.65	2.11	33.00	1.49	73
SG6 to O-cell	40.6	35.1	20.60	24.42	18.54%	106.29	1.98	21.03	0.86	79
O-cell to SG5	35.1	31.6	21.40	21.69	1.37%	214.44	3.23	31.46	1.45	52
SG5 to SG4	31.6	26.6	13.40	11.32	-15.51%	54.31	2.85	10.08	0.89	67
SG4 to SG3	26.6	19.6	9.70	11.25	15.96%	89.25	2.08	12.52	1.11	95
SG3 to SG2	19.6	12.6	9.90	11.74	18.62%	286.11	0.80	28.66	2.44	104
Average Skin Friction (ksf)			15.09	16.32	8.18%	156.59	2.03	22.10	1.41	78.33
Total Load (kips)			6257	6768	8.18%	Totals not needed for these values				

Table 35 - O-cell test shaft analysis geometric mean results

Geometric Mean (Raw Data)						
Shaft Section (Strain Gauge Levels)	Elevation Range (ft)		Measured Mean (O-cell) (ksf)	Predicted Mean (Monitoring) (ksf)	Percent Difference	Count
SG7 to SG6	45.6	40.6	21.10	12.12	-42.57%	73
SG6 to O-cell	40.6	35.1	20.60	18.12	-12.02%	79
O-cell to SG5	35.1	31.6	21.40	13.88	-35.14%	52
SG5 to SG4	31.6	26.6	13.40	8.57	-36.02%	67
SG4 to SG3	26.6	19.6	9.70	7.51	-22.53%	95
SG3 to SG2	19.6	12.6	9.90	7.02	-29.13%	104
Average Skin Friction (ksf)			15.09	10.71	-29.02%	78.33
Total Load (kips)			6257	4441	-29.02%	N/A

Table 36 - O-cell test shaft analysis limiting method results

Limiting Ultimate Values										
Shaft Section (Strain Gauge Levels)	Elevation Range (ft)		Measured Mean (O-cell) (ksf)	Predicted Mean (Monitoring) (ksf)	Percent Difference	Predicted Maximum (Monitoring) (ksf)	Predicted Minimum (Monitoring) (ksf)	Predicted Standard Deviation (Monitoring)	Predicted CV (Monitoring)	Count
SG7 to SG6	45.6	40.6	21.10	16.75	-20.63%	48.99	2.11	14.65	0.87	73
SG6 to O-cell	40.6	35.1	20.60	21.79	5.80%	48.99	1.98	13.85	0.64	79
O-cell to SG5	35.1	31.6	21.40	17.83	-16.67%	48.99	3.23	14.19	0.80	52
SG5 to SG4	31.6	26.6	13.40	11.05	-17.55%	44.42	2.85	8.99	0.81	67
SG4 to SG3	26.6	19.6	9.70	10.64	9.71%	48.99	2.08	9.68	0.91	95
SG3 to SG2	19.6	12.6	9.90	9.22	-6.88%	48.99	0.80	8.87	0.96	104
Average Skin Friction (ksf)			15.09	13.95	-7.55%	48.30	2.03	11.33	0.84	78.33
Total Load (kips)			6257	5784	-7.55%	Totals not needed for these values				

Table 37 - O-cell test shaft analysis FDOT method results

FDOT Method										
Shaft Section (Strain Gauge Levels)	Elevation Range (ft)		Measured Mean (O-cell) (ksf)	Predicted Mean (Monitoring) (ksf)	Percent Difference	Predicted Maximum (Monitoring) (ksf)	Predicted Minimum (Monitoring) (ksf)	Predicted Standard Deviation (Monitoring)	Predicted CV (Monitoring)	Count
SG7 to SG6	45.6	40.6	21.10	12.78	-39.44%	37.11	2.11	9.77	0.76	65
SG6 to O-cell	40.6	35.1	20.60	16.93	-17.84%	37.58	1.98	8.97	0.53	66
O-cell to SG5	35.1	31.6	21.40	12.75	-40.41%	36.26	3.23	8.12	0.64	44
SG5 to SG4	31.6	26.6	13.40	10.04	-25.09%	27.55	2.85	6.97	0.69	65
SG4 to SG3	26.6	19.6	9.70	8.91	-8.13%	30.48	2.08	6.34	0.71	90
SG3 to SG2	19.6	12.6	9.90	7.80	-21.21%	26.30	0.80	5.33	0.68	100
Average Skin Friction (ksf)			15.09	11.18	-25.93%	31.95	2.03	7.37	0.67	71.67
Total Load (kips)			6257	4634	-25.93%	Totals not needed for these values				

Table 38 - O-cell test shaft analysis FDOT* method results

FDOT* Method (Each Section)										
Shaft Section (Strain Gauge Levels)	Elevation Range (ft)		Measured Mean (O-cell) (ksf)	Predicted Mean (Monitoring) (ksf)	Percent Difference	Predicted Maximum (Monitoring) (ksf)	Predicted Minimum (Monitoring) (ksf)	Predicted Standard Deviation (Monitoring)	Predicted CV (Monitoring)	Count
SG7 to SG6	45.6	40.6	21.10	12.78	-39.44%	37.11	2.11	9.77	0.76	65
SG6 to O-cell	40.6	35.1	20.60	18.83	-8.62%	40.66	6.31	9.41	0.50	65
O-cell to SG5	35.1	31.6	21.40	16.63	-22.27%	51.39	3.23	13.10	0.79	50
SG5 to SG4	31.6	26.6	13.40	8.43	-37.06%	21.11	2.85	5.01	0.59	59
SG4 to SG3	26.6	19.6	9.70	8.07	-16.83%	21.67	2.08	5.07	0.63	86
SG3 to SG2	19.6	12.6	9.90	7.80	-21.21%	26.30	0.80	5.33	0.68	100
Average Skin Friction (ksf)			15.09	11.48	-23.90%	31.23	2.75	7.40	0.65	70.83
Total Load (kips)			6257	4761	-23.90%	Totals not needed for these values				

Table 39 - O-cell test shaft LN transformed method results

LN Transform Method										
Shaft Section (Strain Gauge Levels)	Elevation Range (ft)		Measured Mean (O-cell) (ksf)	Predicted Mean (Monitoring) (ksf)	Percent Difference	Predicted Maximum (Monitoring) (ksf)	Predicted Minimum (Monitoring) (ksf)	Predicted Standard Deviation (Monitoring)	Predicted CV (Monitoring)	Count
SG7 to SG6	45.6	40.6	21.10	11.67	-44.69%	28.61	2.91	8.64	0.74	56
SG6 to O-cell	40.6	35.1	20.60	14.90	-27.68%	28.90	2.89	7.40	0.50	55
O-cell to SG5	35.1	31.6	21.40	10.86	-49.25%	23.09	3.23	5.90	0.54	40
SG5 to SG4	31.6	26.6	13.40	10.00	-25.38%	27.55	2.85	7.22	0.72	65
SG4 to SG3	26.6	19.6	9.70	8.88	-8.48%	26.81	2.89	5.71	0.64	85
SG3 to SG2	19.6	12.6	9.90	7.98	-19.41%	26.30	2.91	4.80	0.60	96
Average Skin Friction (ksf)			15.09	10.49	-30.45%	27.04	2.93	6.49	0.63	66.17
Total Load (kips)			6257	4352	-30.45%	Totals not needed for these values				

The third method was completed in the same manner as the second method but only used data from boring B8, the closest boring to the test shaft. This was done because boring locations with similar distances away from the river (moving east) provided similar q_t/q_u ratios (boring B8, B6 and D3). Borings B4, B7 and B9, the furthest borings from the river, all showed much lower q_t/q_u slopes.

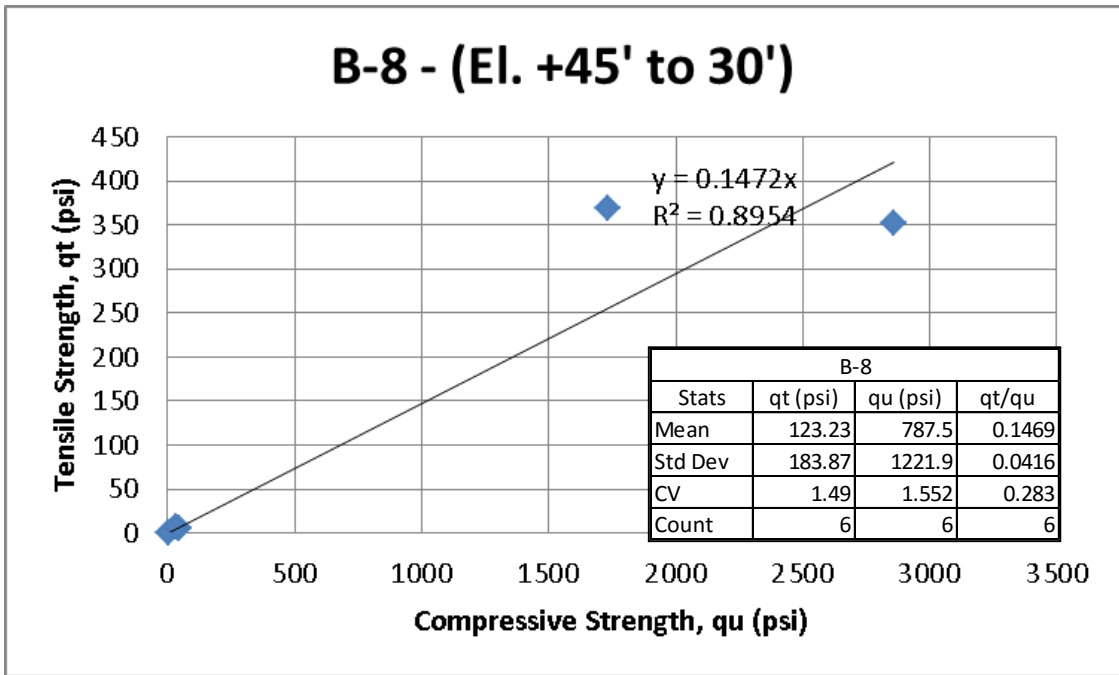


Figure 120 - Little River qt/qu analysis using data from elevations +45' to +30' from boring B8

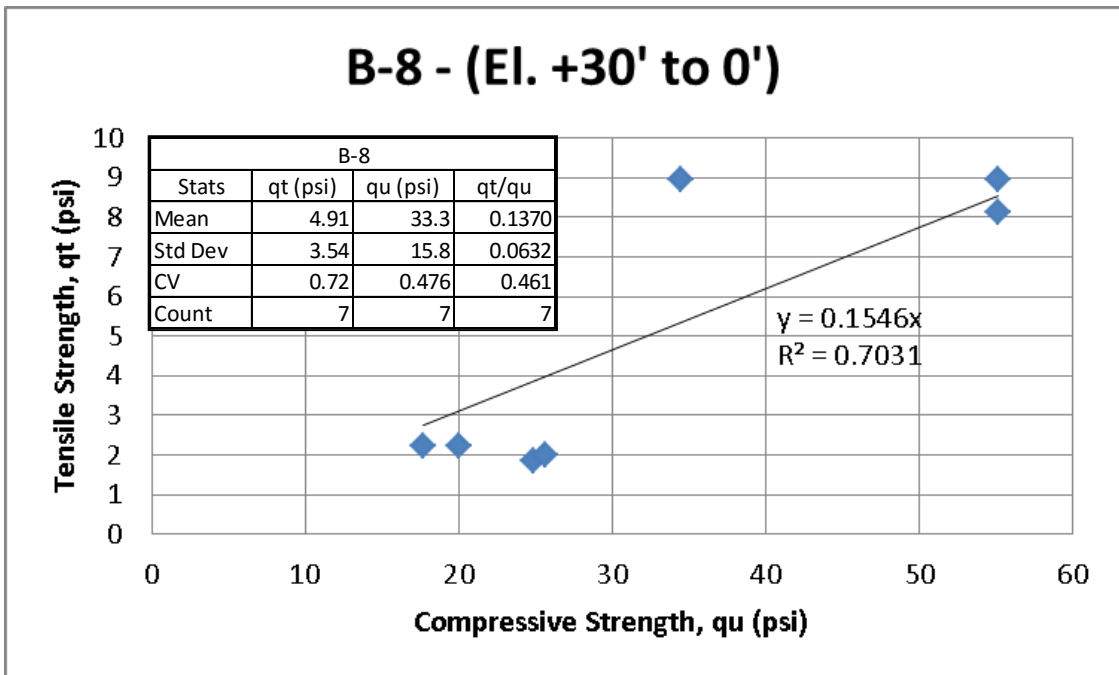


Figure 121 - Little River qt/qu analysis using data from elevations +30' to 0' from boring B8

Table 40 - O-cell test shaft analysis raw data results

Arithmetic Mean (Raw Data)										
Shaft Section (Strain Gauge Levels)	Elevation Range (ft)		Measured Mean (O-cell) (ksf)	Predicted Mean (Monitoring) (ksf)	Percent Difference	Predicted Maximum (Monitoring) (ksf)	Predicted Minimum (Monitoring) (ksf)	Predicted Standard Deviation (Monitoring)	Predicted CV (Monitoring)	Count
SG7 to SG6	45.6	40.6	21.10	21.53	2.04%	181.31	2.05	32.05	1.49	73
SG6 to O-cell	40.6	35.1	20.60	23.72	15.15%	103.24	1.92	20.43	0.86	79
O-cell to SG5	35.1	31.6	21.40	21.07	-1.53%	208.31	3.13	30.56	1.45	52
SG5 to SG4	31.6	26.6	13.60	14.70	8.10%	70.52	3.70	13.09	0.89	67
SG4 to SG3	26.6	19.6	9.70	14.60	50.56%	115.89	2.70	16.26	1.11	95
SG3 to SG2	19.6	12.6	9.90	15.25	54.02%	371.49	1.03	37.21	2.44	104
Average Skin Friction (ksf)			15.12	18.01	19.13%	180.84	2.32	24.83	1.41	78.33
Total Load (kips)			6269	7469	19.13%	Totals not needed for these values				

Table 41 - O-cell test shaft analysis geometric mean results

Geometric Mean (Raw Data)						
Shaft Section (Strain Gauge Levels)	Elevation Range (ft)		Measured Mean (O-cell) (ksf)	Predicted Mean (Monitoring) (ksf)	Percent Difference	Count
SG7 to SG6	45.6	40.6	21.10	11.77	-44.22%	73
SG6 to O-cell	40.6	35.1	20.60	17.60	-14.54%	79
O-cell to SG5	35.1	31.6	21.40	13.48	-37.00%	52
SG5 to SG4	31.6	26.6	13.60	11.13	-18.15%	67
SG4 to SG3	26.6	19.6	9.70	9.76	0.59%	95
SG3 to SG2	19.6	12.6	9.90	9.11	-7.98%	104
Average Skin Friction (ksf)			15.12	11.84	-21.71%	78.33
Total Load (kips)			6269	4908	-21.71%	N/A

Table 42 - O-cell test shaft analysis limiting method results

Limiting Ultimate Values										
Shaft Section (Strain Gauge Levels)	Elevation Range (ft)		Measured Mean (O-cell) (ksf)	Predicted Mean (Monitoring) (ksf)	Percent Difference	Predicted Maximum (Monitoring) (ksf)	Predicted Minimum (Monitoring) (ksf)	Predicted Standard Deviation (Monitoring)	Predicted CV (Monitoring)	Count
SG7 to SG6	45.6	40.6	21.10	16.42	-22.17%	48.99	2.05	14.58	0.89	73
SG6 to O-cell	40.6	35.1	20.60	21.30	3.39%	48.99	1.92	13.71	0.64	79
O-cell to SG5	35.1	31.6	21.40	17.38	-18.77%	48.99	3.13	13.92	0.80	52
SG5 to SG4	31.6	26.6	13.60	14.11	3.72%	48.99	3.70	10.83	0.77	67
SG4 to SG3	26.6	19.6	9.70	13.51	39.31%	48.99	2.70	11.52	0.85	95
SG3 to SG2	19.6	12.6	9.90	11.62	17.40%	48.99	1.03	10.12	0.87	104
Average Skin Friction (ksf)			15.12	15.35	1.54%	48.99	2.32	12.20	0.81	78.33
Total Load (kips)			6269	6366	1.54%	Totals not needed for these values				

Table 43 - O-cell test shaft analysis FDOT method results

FDOT Method										
Shaft Section (Strain Gauge Levels)	Elevation Range (ft)		Measured Mean (O-cell) (ksf)	Predicted Mean (Monitoring) (ksf)	Percent Difference	Predicted Maximum (Monitoring) (ksf)	Predicted Minimum (Monitoring) (ksf)	Predicted Standard Deviation (Monitoring)	Predicted CV (Monitoring)	Count
SG7 to SG6	45.6	40.6	21.10	12.41	-41.17%	36.05	2.05	9.49	0.76	65
SG6 to O-cell	40.6	35.1	20.60	17.38	-15.64%	39.50	1.92	9.60	0.55	69
O-cell to SG5	35.1	31.6	21.40	15.47	-27.71%	43.26	3.13	11.88	0.77	49
SG5 to SG4	31.6	26.6	13.60	13.03	-4.17%	35.77	3.70	9.05	0.69	65
SG4 to SG3	26.6	19.6	9.70	11.57	19.29%	39.58	2.70	8.23	0.71	90
SG3 to SG2	19.6	12.6	9.90	10.13	2.30%	34.16	1.03	6.92	0.68	100
Average Skin Friction (ksf)			15.12	13.00	-14.04%	37.69	2.32	8.88	0.69	73.00
Total Load (kips)			6269	5389	-14.04%	Totals not needed for these values				

Table 44 - O-cell test shaft analysis FDOT* method results

FDOT* Method (Each Section)										
Shaft Section (Strain Gauge Levels)	Elevation Range (ft)		Measured Mean (O-cell) (ksf)	Predicted Mean (Monitoring) (ksf)	Percent Difference	Predicted Maximum (Monitoring) (ksf)	Predicted Minimum (Monitoring) (ksf)	Predicted Standard Deviation (Monitoring)	Predicted CV (Monitoring)	Count
SG7 to SG6	45.6	40.6	21.10	12.41	-41.17%	36.05	2.05	9.49	0.76	65
SG6 to O-cell	40.6	35.1	20.60	18.29	-11.23%	39.50	6.13	9.14	0.50	65
O-cell to SG5	35.1	31.6	21.40	16.16	-24.49%	49.92	3.13	12.73	0.79	50
SG5 to SG4	31.6	26.6	13.60	10.95	-19.47%	27.41	3.70	6.51	0.59	59
SG4 to SG3	26.6	19.6	9.70	10.48	8.00%	28.14	2.70	6.58	0.63	86
SG3 to SG2	19.6	12.6	9.90	10.13	2.30%	34.16	1.03	6.92	0.68	100
Average Skin Friction (ksf)			15.12	12.67	-16.18%	34.71	3.02	8.16	0.65	70.83
Total Load (kips)			6269	5255	-16.18%	Totals not needed for these values				

Table 45 - O-cell test shaft LN transformed method results

LN Transform Method										
Shaft Section (Strain Gauge Levels)	Elevation Range (ft)		Measured Mean (O-cell) (ksf)	Predicted Mean (Monitoring) (ksf)	Percent Difference	Predicted Maximum (Monitoring) (ksf)	Predicted Minimum (Monitoring) (ksf)	Predicted Standard Deviation (Monitoring)	Predicted CV (Monitoring)	Count
SG7 to SG6	45.6	40.6	21.10	11.96	-43.32%	29.37	3.24	8.64	0.72	55
SG6 to O-cell	40.6	35.1	20.60	15.71	-23.72%	31.87	3.16	7.66	0.49	58
O-cell to SG5	35.1	31.6	21.40	12.09	-43.52%	31.73	3.99	7.27	0.60	42
SG5 to SG4	31.6	26.6	13.60	11.26	-17.20%	31.55	3.70	7.04	0.63	60
SG4 to SG3	26.6	19.6	9.70	10.75	10.79%	31.63	3.31	6.81	0.63	86
SG3 to SG2	19.6	12.6	9.90	9.84	-0.62%	31.41	3.38	5.62	0.57	95
Average Skin Friction (ksf)			15.12	11.79	-22.04%	31.28	3.42	7.06	0.60	66.00
Total Load (kips)			6269	4887	-22.04%	Totals not needed for these values				

Once the results were investigated based on q_t adjustments, the data was then analyzed again making adjustments based on average REC%. This approach was developed in case very limited or no core data was available to make q_t adjustments. Therefore, REC% adjustments were made for each zone previously indicated without using the q_t adjustments. The average REC% for each zone was created using all

boring locations with data within the designated zone. This was done to investigate the affect REC% adjustments had without the influence of the q_t adjustments. For zone 2, REC% = 86.4 and zone 3 REC% = 84.4. The results are provided here:

Table 46 - O-cell test shaft analysis raw data results

Arithmetic Mean (Raw Data)										
Shaft Section (Strain Gauge Levels)	Elevation Range (ft)		Measured Mean (O-cell) (ksf)	Predicted Mean (Monitoring) (ksf)	Percent Difference	Predicted Maximum (Monitoring) (ksf)	Predicted Minimum (Monitoring) (ksf)	Predicted Standard Deviation (Monitoring)	Predicted CV (Monitoring)	Count
SG7 to SG6	45.6	40.6	21.10	21.65	2.60%	176.20	2.20	31.19	1.44	73
SG6 to O-cell	40.6	35.1	20.60	23.97	16.37%	101.23	2.06	20.00	0.83	79
O-cell to SG5	35.1	31.6	21.40	21.26	-0.64%	202.09	3.34	29.68	1.40	52
SG5 to SG4	31.6	26.6	13.60	14.35	5.51%	66.47	3.75	12.35	0.86	67
SG4 to SG3	26.6	19.6	9.70	14.23	46.65%	108.13	2.75	15.24	1.07	95
SG3 to SG2	19.6	12.6	9.90	14.74	48.90%	341.75	1.06	34.25	2.32	104
Average Skin Friction (ksf)			15.12	17.85	18.07%	170.50	2.41	23.58	1.36	78.33
Total Load (kips)			6269	7402	18.07%	Totals not needed for these values				

Table 47 - O-cell test shaft analysis geometric mean results

Geometric Mean (Raw Data)						
Shaft Section (Strain Gauge Levels)	Elevation Range (ft)		Measured Mean (O-cell) (ksf)	Predicted Mean (Monitoring) (ksf)	Percent Difference	Count
SG7 to SG6	45.6	40.6	21.10	12.20	-42.20%	73
SG6 to O-cell	40.6	35.1	20.60	18.07	-12.29%	79
O-cell to SG5	35.1	31.6	21.40	13.94	-34.87%	52
SG5 to SG4	31.6	26.6	13.60	11.03	-18.90%	67
SG4 to SG3	26.6	19.6	9.70	9.70	-0.03%	95
SG3 to SG2	19.6	12.6	9.90	9.07	-8.40%	104
Average Skin Friction (ksf)			15.12	11.99	-20.70%	78.33
Total Load (kips)			6269	4972	-20.70%	N/A

Table 48 - O-cell test shaft analysis limiting method results

Limiting Ultimate Values										
Shaft Section (Strain Gauge Levels)	Elevation Range (ft)		Measured Mean (O-cell) (ksf)	Predicted Mean (Monitoring) (ksf)	Percent Difference	Predicted Maximum (Monitoring) (ksf)	Predicted Minimum (Monitoring) (ksf)	Predicted Standard Deviation (Monitoring)	Predicted CV (Monitoring)	Count
SG7 to SG6	45.6	40.6	21.10	16.01	-24.14%	42.33	2.20	12.93	0.81	73
SG6 to O-cell	40.6	35.1	20.60	20.88	1.35%	42.33	2.06	12.13	0.58	79
O-cell to SG5	35.1	31.6	21.40	17.17	-19.77%	42.33	3.34	12.68	0.74	52
SG5 to SG4	31.6	26.6	13.60	13.64	0.32%	41.35	3.75	9.81	0.72	67
SG4 to SG3	26.6	19.6	9.70	12.97	33.70%	41.35	2.75	10.19	0.79	95
SG3 to SG2	19.6	12.6	9.90	11.22	13.30%	41.35	1.06	8.89	0.79	104
Average Skin Friction (ksf)			15.12	14.92	-1.29%	41.76	2.41	10.86	0.74	78.33
Total Load (kips)			6269	6189	-1.29%	Totals not needed for these values				

Table 49 - O-cell test shaft analysis FDOT method results

FDOT Method										
Shaft Section (Strain Gauge Levels)	Elevation Range (ft)		Measured Mean (O-cell) (ksf)	Predicted Mean (Monitoring) (ksf)	Percent Difference	Predicted Maximum (Monitoring) (ksf)	Predicted Minimum (Monitoring) (ksf)	Predicted Standard Deviation (Monitoring)	Predicted CV (Monitoring)	Count
SG7 to SG6	45.6	40.6	21.10	12.77	-39.49%	36.26	2.20	9.53	0.75	65
SG6 to O-cell	40.6	35.1	20.60	17.78	-13.70%	39.63	2.06	9.57	0.54	69
O-cell to SG5	35.1	31.6	21.40	15.83	-26.05%	43.29	3.34	11.81	0.75	49
SG5 to SG4	31.6	26.6	13.60	12.79	-5.94%	34.33	3.75	8.63	0.67	65
SG4 to SG3	26.6	19.6	9.70	11.39	17.45%	37.87	2.75	7.87	0.69	90
SG3 to SG2	19.6	12.6	9.90	10.01	1.13%	32.82	1.06	6.64	0.66	100
Average Skin Friction (ksf)			15.12	13.05	-13.65%	36.89	2.41	8.68	0.67	73.00
Total Load (kips)			6269	5413	-13.65%	Totals not needed for these values				

Table 50 - O-cell test shaft analysis FDOT* method results

FDOT* Method (Each Section)										
Shaft Section (Strain Gauge Levels)	Elevation Range (ft)		Measured Mean (O-cell) (ksf)	Predicted Mean (Monitoring) (ksf)	Percent Difference	Predicted Maximum (Monitoring) (ksf)	Predicted Minimum (Monitoring) (ksf)	Predicted Standard Deviation (Monitoring)	Predicted CV (Monitoring)	Count
SG7 to SG6	45.6	40.6	21.10	12.77	-39.49%	36.26	2.20	9.53	0.75	65
SG6 to O-cell	40.6	35.1	20.60	18.70	-9.23%	39.63	6.46	9.08	0.49	65
O-cell to SG5	35.1	31.6	21.40	16.50	-22.87%	49.77	3.34	12.63	0.77	50
SG5 to SG4	31.6	26.6	13.60	10.82	-20.46%	26.51	3.75	6.26	0.58	59
SG4 to SG3	26.6	19.6	9.70	10.35	6.74%	27.19	2.75	6.32	0.61	86
SG3 to SG2	19.6	12.6	9.90	10.01	1.13%	32.82	1.06	6.64	0.66	100
Average Skin Friction (ksf)			15.12	12.76	-15.60%	34.12	3.14	8.00	0.63	70.83
Total Load (kips)			6269	5292	-15.60%	Totals not needed for these values				

Table 51 - O-cell test shaft LN transformed method results

LN Transform Method										
Shaft Section (Strain Gauge Levels)	Elevation Range (ft)		Measured Mean (O-cell) (ksf)	Predicted Mean (Monitoring) (ksf)	Percent Difference	Predicted Maximum (Monitoring) (ksf)	Predicted Minimum (Monitoring) (ksf)	Predicted Standard Deviation (Monitoring)	Predicted CV (Monitoring)	Count
SG7 to SG6	45.6	40.6	21.10	12.34	-41.51%	29.72	3.46	8.65	0.70	55
SG6 to O-cell	40.6	35.1	20.60	15.71	-23.75%	30.91	6.46	6.34	0.40	55
O-cell to SG5	35.1	31.6	21.40	12.02	-43.82%	30.62	4.25	6.70	0.56	41
SG5 to SG4	31.6	26.6	13.60	11.11	-18.29%	30.39	3.75	6.75	0.61	60
SG4 to SG3	26.6	19.6	9.70	10.70	10.30%	30.46	3.46	6.49	0.61	85
SG3 to SG2	19.6	12.6	9.90	9.75	-1.51%	30.26	3.44	5.42	0.56	95
Average Skin Friction (ksf)			15.12	11.78	-22.05%	30.39	4.08	6.63	0.57	65.17
Total Load (kips)			6269	4887	-22.05%	Totals not needed for these values				

Next, a REC% adjustment was made using a REC% = 81.22, which is an average from all REC% values for all borings and elevations. As well, a $q_t/q_u = 0.1375$ (from q_t adjustment method 1) was used in combination with the new REC%. The following provides the results:

Table 52 - O-cell test shaft analysis raw data results

Arithmetic Mean (Raw Data)										
Shaft Section (Strain Gauge Levels)	Elevation Range (ft)		Measured Mean (O-cell) (ksf)	Predicted Mean (Monitoring) (ksf)	Percent Difference	Predicted Maximum (Monitoring) (ksf)	Predicted Minimum (Monitoring) (ksf)	Predicted Standard Deviation (Monitoring)	Predicted CV (Monitoring)	Count
SG7 to SG6	45.6	40.6	21.10	16.90	-19.90%	142.32	1.61	25.16	1.49	73
SG6 to O-cell	40.6	35.1	20.60	18.62	-9.61%	81.04	1.51	16.03	0.86	79
O-cell to SG5	35.1	31.6	21.40	16.54	-22.71%	163.52	2.46	23.99	1.45	52
SG5 to SG4	31.6	26.6	13.60	11.26	-17.20%	54.01	2.83	10.02	0.89	67
SG4 to SG3	26.6	19.6	9.70	11.19	15.33%	88.77	2.07	12.45	1.11	95
SG3 to SG2	19.6	12.6	9.90	11.68	17.98%	284.55	0.79	28.50	2.44	104
Average Skin Friction (ksf)			15.12	13.98	-7.56%	139.79	1.79	19.23	1.41	78.33
Total Load (kips)			6269	5795	-7.56%	Totals not needed for these values				

Table 53 - O-cell test shaft analysis geometric mean results

Geometric Mean (Raw Data)						
Shaft Section (Strain Gauge Levels)	Elevation Range (ft)		Measured Mean (O-cell) (ksf)	Predicted Mean (Monitoring) (ksf)	Percent Difference	Count
SG7 to SG6	45.6	40.6	21.10	9.24	-56.21%	73
SG6 to O-cell	40.6	35.1	20.60	13.82	-32.92%	79
O-cell to SG5	35.1	31.6	21.40	10.58	-50.55%	52
SG5 to SG4	31.6	26.6	13.60	8.53	-37.31%	67
SG4 to SG3	26.6	19.6	9.70	7.47	-22.95%	95
SG3 to SG2	19.6	12.6	9.90	6.98	-29.52%	104
Average Skin Friction (ksf)			15.12	9.18	-39.26%	78.33
Total Load (kips)			6269	3808	-39.26%	N/A

Table 54 - O-cell test shaft analysis limiting method results

Limiting Ultimate Values										
Shaft Section (Strain Gauge Levels)	Elevation Range (ft)		Measured Mean (O-cell) (ksf)	Predicted Mean (Monitoring) (ksf)	Percent Difference	Predicted Maximum (Monitoring) (ksf)	Predicted Minimum (Monitoring) (ksf)	Predicted Standard Deviation (Monitoring)	Predicted CV (Monitoring)	Count
SG7 to SG6	45.6	40.6	21.10	13.04	-38.21%	39.79	1.61	11.78	0.90	73
SG6 to O-cell	40.6	35.1	20.60	16.82	-18.36%	39.79	1.51	10.97	0.65	79
O-cell to SG5	35.1	31.6	21.40	13.70	-36.00%	39.79	2.46	11.05	0.81	52
SG5 to SG4	31.6	26.6	13.60	10.87	-20.06%	39.79	2.83	8.52	0.78	67
SG4 to SG3	26.6	19.6	9.70	10.42	7.44%	39.79	2.07	9.05	0.87	95
SG3 to SG2	19.6	12.6	9.90	8.98	-9.29%	39.79	0.79	8.05	0.90	104
Average Skin Friction (ksf)			15.12	11.99	-20.67%	39.79	1.79	9.70	0.82	78.33
Total Load (kips)			6269	4974	-20.67%	Totals not needed for these values				

Table 55 - O-cell test shaft analysis FDOT method results

FDOT Method										
Shaft Section (Strain Gauge Levels)	Elevation Range (ft)		Measured Mean (O-cell) (ksf)	Predicted Mean (Monitoring) (ksf)	Percent Difference	Predicted Maximum (Monitoring) (ksf)	Predicted Minimum (Monitoring) (ksf)	Predicted Standard Deviation (Monitoring)	Predicted CV (Monitoring)	Count
SG7 to SG6	45.6	40.6	21.10	9.74	-53.82%	28.30	1.61	7.45	0.76	65
SG6 to O-cell	40.6	35.1	20.60	13.64	-33.77%	31.00	1.51	7.54	0.55	69
O-cell to SG5	35.1	31.6	21.40	12.14	-43.26%	33.96	2.46	9.32	0.77	49
SG5 to SG4	31.6	26.6	13.60	9.98	-26.60%	27.40	2.83	6.93	0.69	65
SG4 to SG3	26.6	19.6	9.70	8.86	-8.63%	30.31	2.07	6.31	0.71	90
SG3 to SG2	19.6	12.6	9.90	7.76	-21.64%	26.16	0.79	5.30	0.68	100
Average Skin Friction (ksf)			15.12	10.08	-33.35%	29.19	1.79	6.89	0.69	73.00
Total Load (kips)			6269	4178	-33.35%	Totals not needed for these values				

Table 56 - O-cell test shaft analysis FDOT* method results

FDOT* Method (Each Section)										
Shaft Section (Strain Gauge Levels)	Elevation Range (ft)		Measured Mean (O-cell) (ksf)	Predicted Mean (Monitoring) (ksf)	Percent Difference	Predicted Maximum (Monitoring) (ksf)	Predicted Minimum (Monitoring) (ksf)	Predicted Standard Deviation (Monitoring)	Predicted CV (Monitoring)	Count
SG7 to SG6	45.6	40.6	21.10	9.74	-53.82%	28.30	1.61	7.45	0.76	65
SG6 to O-cell	40.6	35.1	20.60	14.35	-30.32%	31.00	4.81	7.18	0.50	65
O-cell to SG5	35.1	31.6	21.40	12.68	-40.73%	39.19	2.46	9.99	0.79	50
SG5 to SG4	31.6	26.6	13.60	8.39	-38.32%	21.00	2.83	4.99	0.59	59
SG4 to SG3	26.6	19.6	9.70	8.02	-17.28%	21.55	2.07	5.04	0.63	86
SG3 to SG2	19.6	12.6	9.90	7.76	-21.64%	26.16	0.79	5.30	0.68	100
Average Skin Friction (ksf)			15.12	9.83	-34.96%	26.91	2.34	6.33	0.65	70.83
Total Load (kips)			6269	4078	-34.96%	Totals not needed for these values				

Table 57 - O-cell test shaft LN transformed method results

LN Transform Method										
Shaft Section (Strain Gauge Levels)	Elevation Range (ft)		Measured Mean (O-cell) (ksf)	Predicted Mean (Monitoring) (ksf)	Percent Difference	Predicted Maximum (Monitoring) (ksf)	Predicted Minimum (Monitoring) (ksf)	Predicted Standard Deviation (Monitoring)	Predicted CV (Monitoring)	Count
SG7 to SG6	45.6	40.6	21.10	9.27	-56.06%	23.06	2.46	6.85	0.74	56
SG6 to O-cell	40.6	35.1	20.60	12.34	-40.12%	25.02	2.48	6.01	0.49	58
O-cell to SG5	35.1	31.6	21.40	9.35	-56.32%	24.91	2.46	5.89	0.63	43
SG5 to SG4	31.6	26.6	13.60	8.63	-36.58%	24.17	2.83	5.39	0.63	60
SG4 to SG3	26.6	19.6	9.70	8.23	-15.14%	24.23	2.54	5.22	0.63	86
SG3 to SG2	19.6	12.6	9.90	7.54	-23.88%	24.06	2.59	4.31	0.57	95
Average Skin Friction (ksf)			15.12	9.10	-39.78%	24.21	2.56	5.50	0.61	66.33
Total Load (kips)			6269	3775	-39.78%	Totals not needed for these values				

Next, REC% adjustments were made for each zone and used in combination with q_t/q_u ratios previously developed for each respective zone (q_t adjustment method 2). The results are displayed here:

Table 58 - O-cell test shaft analysis raw data results

Arithmetic Mean (Raw Data)										
Shaft Section (Strain Gauge Levels)	Elevation Range (ft)		Measured Mean (O-cell) (ksf)	Predicted Mean (Monitoring) (ksf)	Percent Difference	Predicted Maximum (Monitoring) (ksf)	Predicted Minimum (Monitoring) (ksf)	Predicted Standard Deviation (Monitoring)	Predicted CV (Monitoring)	Count
SG7 to SG6	45.6	40.6	21.10	19.15	-9.24%	161.27	1.82	28.51	1.49	73
SG6 to O-cell	40.6	35.1	20.60	21.10	2.42%	91.83	1.71	18.17	0.86	79
O-cell to SG5	35.1	31.6	21.40	18.74	-12.42%	185.28	2.79	27.18	1.45	52
SG5 to SG4	31.6	26.6	13.60	9.56	-29.74%	45.84	2.40	8.51	0.89	67
SG4 to SG3	26.6	19.6	9.70	9.49	-2.13%	75.33	1.75	10.57	1.11	95
SG3 to SG2	19.6	12.6	9.90	9.91	0.12%	241.47	0.67	24.19	2.44	104
Average Skin Friction (ksf)			15.12	13.97	-7.60%	133.54	1.74	18.89	1.41	78.33
Total Load (kips)			6269	5793	-7.60%	Totals not needed for these values				

Table 59 - O-cell test shaft analysis geometric mean results

Geometric Mean (Raw Data)						
Shaft Section (Strain Gauge Levels)	Elevation Range (ft)		Measured Mean (O-cell) (ksf)	Predicted Mean (Monitoring) (ksf)	Percent Difference	Count
SG7 to SG6	45.6	40.6	21.10	10.47	-50.38%	73
SG6 to O-cell	40.6	35.1	20.60	15.66	-23.99%	79
O-cell to SG5	35.1	31.6	21.40	11.99	-43.96%	52
SG5 to SG4	31.6	26.6	13.60	7.24	-46.80%	67
SG4 to SG3	26.6	19.6	9.70	6.34	-34.61%	95
SG3 to SG2	19.6	12.6	9.90	5.92	-40.19%	104
Average Skin Friction (ksf)			15.12	9.17	-39.37%	78.33
Total Load (kips)			6269	3801	-39.37%	N/A

Table 60 - O-cell test shaft analysis limiting method results

Limiting Ultimate Values										
Shaft Section (Strain Gauge Levels)	Elevation Range (ft)		Measured Mean (O-cell) (ksf)	Predicted Mean (Monitoring) (ksf)	Percent Difference	Predicted Maximum (Monitoring) (ksf)	Predicted Minimum (Monitoring) (ksf)	Predicted Standard Deviation (Monitoring)	Predicted CV (Monitoring)	Count
SG7 to SG6	45.6	40.6	21.10	14.47	-31.42%	42.33	1.82	12.66	0.87	73
SG6 to O-cell	40.6	35.1	20.60	18.83	-8.59%	42.33	1.71	11.96	0.64	79
O-cell to SG5	35.1	31.6	21.40	15.41	-28.00%	42.33	2.79	12.26	0.80	52
SG5 to SG4	31.6	26.6	13.60	9.33	-31.43%	37.49	2.40	7.59	0.81	67
SG4 to SG3	26.6	19.6	9.70	8.98	-7.40%	41.35	1.75	8.17	0.91	95
SG3 to SG2	19.6	12.6	9.90	7.78	-21.41%	41.35	0.67	7.48	0.96	104
Average Skin Friction (ksf)			15.12	11.93	-21.07%	41.18	1.74	9.68	0.84	78.33
Total Load (kips)			6269	4949	-21.07%	Totals not needed for these values				

Table 61 - O-cell test shaft analysis FDOT method results

FDOT Method										
Shaft Section (Strain Gauge Levels)	Elevation Range (ft)		Measured Mean (O-cell) (ksf)	Predicted Mean (Monitoring) (ksf)	Percent Difference	Predicted Maximum (Monitoring) (ksf)	Predicted Minimum (Monitoring) (ksf)	Predicted Standard Deviation (Monitoring)	Predicted CV (Monitoring)	Count
SG7 to SG6	45.6	40.6	21.10	11.04	-47.67%	32.06	1.82	8.44	0.76	65
SG6 to O-cell	40.6	35.1	20.60	14.62	-29.01%	32.47	1.71	7.75	0.53	66
O-cell to SG5	35.1	31.6	21.40	11.02	-48.51%	31.33	2.79	7.01	0.64	44
SG5 to SG4	31.6	26.6	13.60	8.47	-37.71%	23.25	2.40	5.88	0.69	65
SG4 to SG3	26.6	19.6	9.70	7.52	-22.46%	25.72	1.75	5.35	0.71	90
SG3 to SG2	19.6	12.6	9.90	6.58	-33.50%	22.20	0.67	4.50	0.68	100
Average Skin Friction (ksf)			15.12	9.55	-36.80%	27.28	1.74	6.29	0.67	71.67
Total Load (kips)			6269	3962	-36.80%	Totals not needed for these values				

Table 62 - O-cell test shaft analysis FDOT* method results

FDOT* Method (Each Section)										
Shaft Section (Strain Gauge Levels)	Elevation Range (ft)		Measured Mean (O-cell) (ksf)	Predicted Mean (Monitoring) (ksf)	Percent Difference	Predicted Maximum (Monitoring) (ksf)	Predicted Minimum (Monitoring) (ksf)	Predicted Standard Deviation (Monitoring)	Predicted CV (Monitoring)	Count
SG7 to SG6	45.6	40.6	21.10	11.04	-47.67%	32.06	1.82	8.44	0.76	65
SG6 to O-cell	40.6	35.1	20.60	16.27	-21.04%	35.13	5.45	8.13	0.50	65
O-cell to SG5	35.1	31.6	21.40	14.37	-32.84%	44.40	2.79	11.32	0.79	50
SG5 to SG4	31.6	26.6	13.60	7.12	-47.66%	17.82	2.40	4.23	0.59	59
SG4 to SG3	26.6	19.6	9.70	6.81	-29.80%	18.29	1.75	4.28	0.63	86
SG3 to SG2	19.6	12.6	9.90	6.58	-33.50%	22.20	0.67	4.50	0.68	100
Average Skin Friction (ksf)			15.12	9.83	-35.00%	26.71	2.36	6.34	0.65	70.83
Total Load (kips)			6269	4075	-35.00%	Totals not needed for these values				

Table 63 - O-cell test shaft LN transformed method results

LN Transform Method										
Shaft Section (Strain Gauge Levels)	Elevation Range (ft)		Measured Mean (O-cell) (ksf)	Predicted Mean (Monitoring) (ksf)	Percent Difference	Predicted Maximum (Monitoring) (ksf)	Predicted Minimum (Monitoring) (ksf)	Predicted Standard Deviation (Monitoring)	Predicted CV (Monitoring)	Count
SG7 to SG6	45.6	40.6	21.10	10.08	-52.21%	24.72	2.51	7.47	0.74	56
SG6 to O-cell	40.6	35.1	20.60	12.87	-37.51%	24.97	2.50	6.39	0.50	55
O-cell to SG5	35.1	31.6	21.40	9.38	-56.15%	19.95	2.79	5.10	0.54	40
SG5 to SG4	31.6	26.6	13.60	8.44	-37.95%	23.25	2.40	6.10	0.72	65
SG4 to SG3	26.6	19.6	9.70	7.49	-22.76%	22.62	2.44	4.82	0.64	85
SG3 to SG2	19.6	12.6	9.90	6.73	-31.98%	22.20	2.46	4.05	0.60	96
Average Skin Friction (ksf)			15.12	8.96	-40.70%	23.05	2.50	5.54	0.63	66.17
Total Load (kips)			6269	3718	-40.70%	Totals not needed for these values				

Finally, the last method used REC% and q_t/q_u adjustments for each zone based on data from boring B8 (closest boring location, q_t adjustment method 3) for analysis. The following provides the results:

Table 64 - O-cell test shaft analysis raw data results

Arithmetic Mean (Raw Data)										
Shaft Section (Strain Gauge Levels)	Elevation Range (ft)		Measured Mean (O-cell) (ksf)	Predicted Mean (Monitoring) (ksf)	Percent Difference	Predicted Maximum (Monitoring) (ksf)	Predicted Minimum (Monitoring) (ksf)	Predicted Standard Deviation (Monitoring)	Predicted CV (Monitoring)	Count
SG7 to SG6	45.6	40.6	21.10	18.88	-10.51%	159.01	1.80	28.11	1.49	73
SG6 to O-cell	40.6	35.1	20.60	20.80	0.98%	90.55	1.69	17.91	0.86	79
O-cell to SG5	35.1	31.6	21.40	18.48	-13.65%	182.68	2.75	26.80	1.45	52
SG5 to SG4	31.6	26.6	13.60	13.97	2.69%	66.99	3.51	12.43	0.89	67
SG4 to SG3	26.6	19.6	9.70	13.87	43.03%	110.09	2.56	15.44	1.11	95
SG3 to SG2	19.6	12.6	9.90	14.49	46.32%	352.92	0.98	35.35	2.44	104
Average Skin Friction (ksf)			15.12	16.42	8.61%	166.92	2.13	22.74	1.41	78.33
Total Load (kips)			6269	6809	8.61%	Totals not needed for these values				

Table 65 - O-cell test shaft analysis geometric mean results

Geometric Mean (Raw Data)						
Shaft Section (Strain Gauge Levels)	Elevation Range (ft)		Measured Mean (O-cell) (ksf)	Predicted Mean (Monitoring) (ksf)	Percent Difference	Count
SG7 to SG6	45.6	40.6	21.10	10.32	-51.08%	73
SG6 to O-cell	40.6	35.1	20.60	15.44	-25.05%	79
O-cell to SG5	35.1	31.6	21.40	11.82	-44.75%	52
SG5 to SG4	31.6	26.6	13.60	10.58	-22.24%	67
SG4 to SG3	26.6	19.6	9.70	9.27	-4.44%	95
SG3 to SG2	19.6	12.6	9.90	8.65	-12.59%	104
Average Skin Friction (ksf)			15.12	10.80	-28.59%	78.33
Total Load (kips)			6269	4477	-28.59%	N/A

Table 66 - O-cell test shaft analysis limiting method results

Limiting Ultimate Values										
Shaft Section (Strain Gauge Levels)	Elevation Range (ft)		Measured Mean (O-cell) (ksf)	Predicted Mean (Monitoring) (ksf)	Percent Difference	Predicted Maximum (Monitoring) (ksf)	Predicted Minimum (Monitoring) (ksf)	Predicted Standard Deviation (Monitoring)	Predicted CV (Monitoring)	Count
SG7 to SG6	45.6	40.6	21.10	14.40	-31.75%	42.96	1.80	12.78	0.89	73
SG6 to O-cell	40.6	35.1	20.60	18.68	-9.33%	42.96	1.69	12.02	0.64	79
O-cell to SG5	35.1	31.6	21.40	15.24	-28.76%	42.96	2.75	12.21	0.80	52
SG5 to SG4	31.6	26.6	13.60	13.40	-1.46%	46.54	3.51	10.29	0.77	67
SG4 to SG3	26.6	19.6	9.70	12.84	32.34%	46.54	2.56	10.95	0.85	95
SG3 to SG2	19.6	12.6	9.90	11.04	11.53%	46.54	0.98	9.62	0.87	104
Average Skin Friction (ksf)			15.12	14.01	-7.35%	45.02	2.13	11.16	0.81	78.33
Total Load (kips)			6269	5809	-7.35%	Totals not needed for these values				

Table 67 - O-cell test shaft analysis FDOT method results

FDOT Method										
Shaft Section (Strain Gauge Levels)	Elevation Range (ft)		Measured Mean (O-cell) (ksf)	Predicted Mean (Monitoring) (ksf)	Percent Difference	Predicted Maximum (Monitoring) (ksf)	Predicted Minimum (Monitoring) (ksf)	Predicted Standard Deviation (Monitoring)	Predicted CV (Monitoring)	Count
SG7 to SG6	45.6	40.6	21.10	10.89	-48.41%	31.61	1.80	8.33	0.76	65
SG6 to O-cell	40.6	35.1	20.60	15.24	-26.01%	34.64	1.69	8.42	0.55	69
O-cell to SG5	35.1	31.6	21.40	13.57	-36.61%	37.94	2.75	10.42	0.77	49
SG5 to SG4	31.6	26.6	13.60	12.38	-8.96%	33.98	3.51	8.59	0.69	65
SG4 to SG3	26.6	19.6	9.70	10.99	13.33%	37.60	2.56	7.82	0.71	90
SG3 to SG2	19.6	12.6	9.90	9.62	-2.81%	32.45	0.98	6.58	0.68	100
Average Skin Friction (ksf)			15.12	11.88	-21.44%	34.59	2.13	8.13	0.69	73.00
Total Load (kips)			6269	4925	-21.44%	Totals not needed for these values				

Table 68 - O-cell test shaft analysis FDOT* method results

FDOT* Method (Each Section)										
Shaft Section (Strain Gauge Levels)	Elevation Range (ft)		Measured Mean (O-cell) (ksf)	Predicted Mean (Monitoring) (ksf)	Percent Difference	Predicted Maximum (Monitoring) (ksf)	Predicted Minimum (Monitoring) (ksf)	Predicted Standard Deviation (Monitoring)	Predicted CV (Monitoring)	Count
SG7 to SG6	45.6	40.6	21.10	10.89	-48.41%	31.61	1.80	8.33	0.76	65
SG6 to O-cell	40.6	35.1	20.60	16.04	-22.15%	34.64	5.37	8.02	0.50	65
O-cell to SG5	35.1	31.6	21.40	14.17	-33.78%	43.78	2.75	11.16	0.79	50
SG5 to SG4	31.6	26.6	13.60	10.40	-23.50%	26.04	3.51	6.19	0.59	59
SG4 to SG3	26.6	19.6	9.70	9.95	2.60%	26.73	2.56	6.25	0.63	86
SG3 to SG2	19.6	12.6	9.90	9.62	-2.81%	32.45	0.98	6.58	0.68	100
Average Skin Friction (ksf)			15.12	11.55	-23.58%	31.71	2.74	7.44	0.65	70.83
Total Load (kips)			6269	4791	-23.58%	Totals not needed for these values				

Table 69 - O-cell test shaft LN transformed method results

LN Transform Method										
Shaft Section (Strain Gauge Levels)	Elevation Range (ft)		Measured Mean (O-cell) (ksf)	Predicted Mean (Monitoring) (ksf)	Percent Difference	Predicted Maximum (Monitoring) (ksf)	Predicted Minimum (Monitoring) (ksf)	Predicted Standard Deviation (Monitoring)	Predicted CV (Monitoring)	Count
SG7 to SG6	45.6	40.6	21.10	11.17	-47.08%	29.42	2.84	8.52	0.76	57
SG6 to O-cell	40.6	35.1	20.60	14.14	-31.35%	28.54	5.37	6.36	0.45	58
O-cell to SG5	35.1	31.6	21.40	10.60	-50.47%	27.83	3.50	6.37	0.60	42
SG5 to SG4	31.6	26.6	13.60	10.38	-23.66%	26.04	3.51	6.27	0.60	59
SG4 to SG3	26.6	19.6	9.70	9.99	2.95%	26.73	3.15	6.16	0.62	85
SG3 to SG2	19.6	12.6	9.90	9.15	-7.60%	28.53	3.21	5.06	0.55	94
Average Skin Friction (ksf)			15.12	10.80	-28.53%	27.83	3.58	6.36	0.59	65.83
Total Load (kips)			6269	4481	-28.53%	Totals not needed for these values				

From the entire analysis, it was found that the raw data method typically provided the best result when used with q_t adjustments. The FDOT* and Limiting method provided some of the most accurate total estimations but produced a more streamlined result and did not follow the trends of the data for each individual layer. It was also determined that the geometric mean and LN transform methods were far too conservative in their

estimations, and that the FDOT* method typically produced better results than the FDOT method. As a result, the geometric mean, LN transform, and FDOT methods were abandoned for future field drilling analysis.

3.4 Overland Test Shaft Preliminary Analysis

Overland shaft monitoring provided limited comparative data. The lack of comparative data was a combination of the Statnamic load testing not fully mobilizing the entire shaft and the majority of limestone layers being drilled with a rock drilling bucket. In drilled shaft installations, a rock auger bit is typically used when drilling into layers of rock and was therefore the focus of developing drilling equations. However, drilling buckets are sometimes used in softer weathered rock where they tend to be more efficient than rock augers in removing drilled debris. Consequently, it is expected that some form of bit coefficient will need to be developed for drilling buckets based on the newly developed rock auger bit equations. This should be possible as the cutting action provided by conical carbide teeth is the same for both bits types. Although, it is expected that drilling buckets will produce higher side resistances due to a larger surface area in contact with side walls of the shaft and drilling buckets are not tapered like an auger bit. Regardless, the main focus of this research was to develop drilling equations for use with rock augers, since these are the drill bit types generally used.

In light of the repeated use of drilling buckets at Overland, small sections of test shaft 1 and 2 were brought to complete failure. Fortunately, one of these failed sections was in limestone where a rock auger was used, providing comparable data. Hydraulic conversions were made using spec sheet data available from Bauer. The following explains the crowd and torque conversions made to provide the preliminary analysis.

3.4.1 Developing Drill Rig Equations for Crowd and Torque Conversion

The Bauer BG 30 drill rig used at Overland was confirmed to use a multi drive system with two available gears. However, second gear provides higher rotational speeds with less available torque and is only used for spinning off material from the auger bit. For the analysis, only first gear needed to be considered as this was the gear used for drilling (confirmed by the contractors lead drill rig operator). Once the gear setup was confirmed, the next step was to determine the maximum torque, crowd, and hydraulic pressures available within the system. From spec sheets provided by Bauer for the exact rig, these parameters were able to be determined and confirmed from rig inspection. The maximum crowd was determined to be 330 kN using an operating pressure of 320 bar (32 MPa). The maximum torque was determined to be 300 kN-m using an operating pressure of 350 bar (35 MPa). The following shows how the values were determined:



Figure 122 - Bauer BG 30 crowd specs from serial plate, max crowd and operating pressure



Figure 123 - Bauer BG 30 specs from serial plate, showing model type and operating pressure

Technical data

Overall height	26,5 m
Weight without attachment (approx.)	94 t
Rotary drive	KDK 300 K
Torque (nominal) at 350 bar	295 kNm
Speed of rotation (max.)	31 U/min (rpm)
Crowd winch	
Crowd force push / pull (effective)	330 / 330 kN

Figure 124 - Bauer BG 30 spec sheet, showing torque operating pressure and maximum crowd

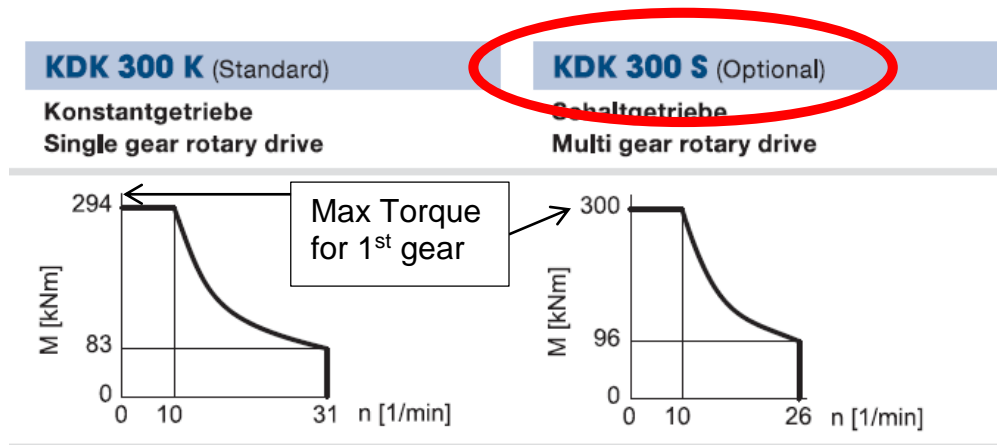


Figure 125 - Bauer BG 30 specs, showing model type and maximum torque

Once the needed parameters were determined, the conversions could be made using the following equation:

$$\text{Torque or Crowd} = K * (\text{Operating Pressure} - \text{Threshold Pressure}) \dots \dots \dots \text{Eq 7}$$

The theoretical threshold pressure for the Bauer BG30 rigs was 5 Bar, according to a Jean Lutz representative. This provided a single equation with a single unknown and could be solved straightforward. The following are the known parameters:

Maximum Torque = 300 kN-m
 Maximum Crowd = 330 kN
 Operating Pressure for Torque = 350 Bar
 Operating Pressure for Crowd = 320 Bar
 Threshold Pressure = 5 Bar

For Crowd:

$$330 \text{ kN} = K * (320 \text{ bar} - 5 \text{ bar}), \text{ solving for K provides, } K = 1.0476$$

For Torque:

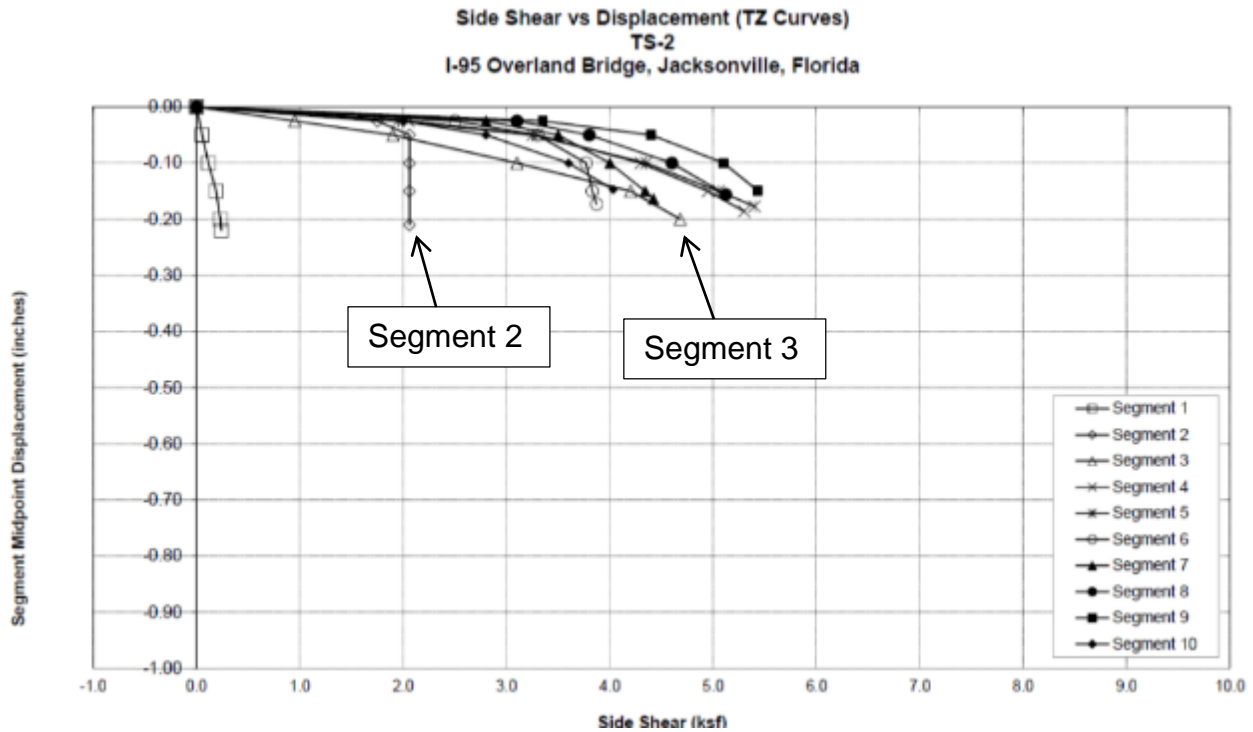
$$300 \text{ kN-m} = K * (350 \text{ bar} - 5 \text{ bar}), \text{ solving for K provides, } K = 0.8696$$

The derived K coefficients were very similar to the equations provided by IMT engineers for the rig used at Little River. For the IMT AF250 rig, $K_{\text{crowd}} = 1.194$ and in 1st gear $K_{\text{Torque}} = 0.708$. Both of these coefficients were used in the general equation, torque or crowd = K * Pressure. Using the theoretical K coefficients the following preliminary analysis was completed.

Presented below is the load transfer summary and T-Z curve data for test shaft 2 at Overland:

Table 70 - Load transfer summary for Overland test shaft 2

Location	Segment Top / Segment Bottom Elevation (feet)	Soil Type	Layer Displacement (inches)	Maximum Mobilized Unit Side Shear Resistance (ksf)
Segment 1	Ground Surface +6 to -18 Feet	Overburden Sands	0.220	0.24
Segment 2	-18 Feet to -23 Feet	Limestone	0.210	2.06
Segment 3	-23 Feet to -28 Feet	Limestone	0.200	4.68
Segment 4	-28 Feet to -33 Feet	Limestone	0.186	5.30
Segment 5	-33 Feet to -38 Feet	Limestone	0.177	5.40
Segment 6	-38 Feet to -43 Feet	Limestone	0.173	3.87
Segment 7	-43 Feet to -48 Feet	Clayey Sand "Marl"	0.164	4.42
Segment 8	-48 Feet to -53 Feet	Clayey Sand "Marl"	0.156	5.12
Segment 9	-53 Feet to -58 Feet	Clayey Sand "Marl"	0.149	5.43
Segment 10	-58 Feet to -63 Feet	Clayey Sand "Marl"	0.145	4.03
Toe Segment	-63 Feet to -65.32 Feet	Clayey Sand "Marl"	0.142	4.03
End Bearing		Clayey Sand "Marl"	0.142	42.4 ksf @ displacement of 0.24% of shaft diameter



Seen from the two data sheets, segments 2 and 3 were in limestone, or representative limestone material. The side shear was fully mobilized in segment 2 and was approaching mobilization in segment 3. Both of these sections were also drilled using a rock auger. Therefore, analysis was completed for both segments using q_u estimated from monitoring, q_t adjustments made using available core within the elevation range of each segment, and f_s derived using the SFH recommended equation. The preliminary results are presented here:

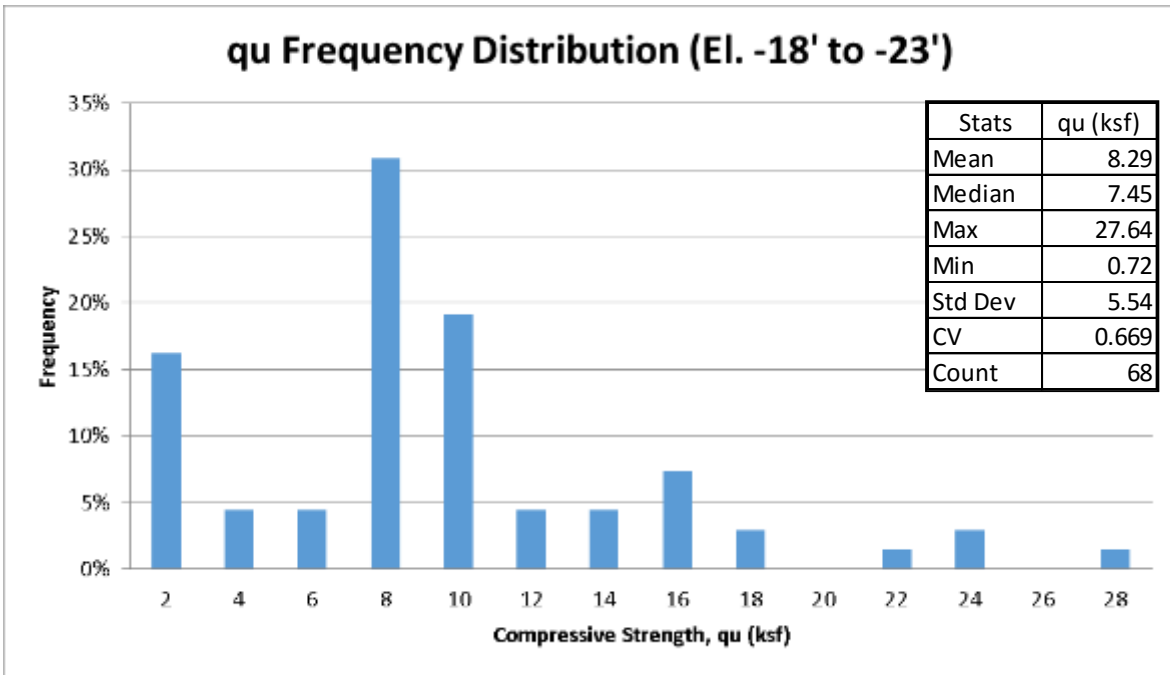


Figure 127 - Overland test shaft 2 compressive strength frequency distribution for segment 2

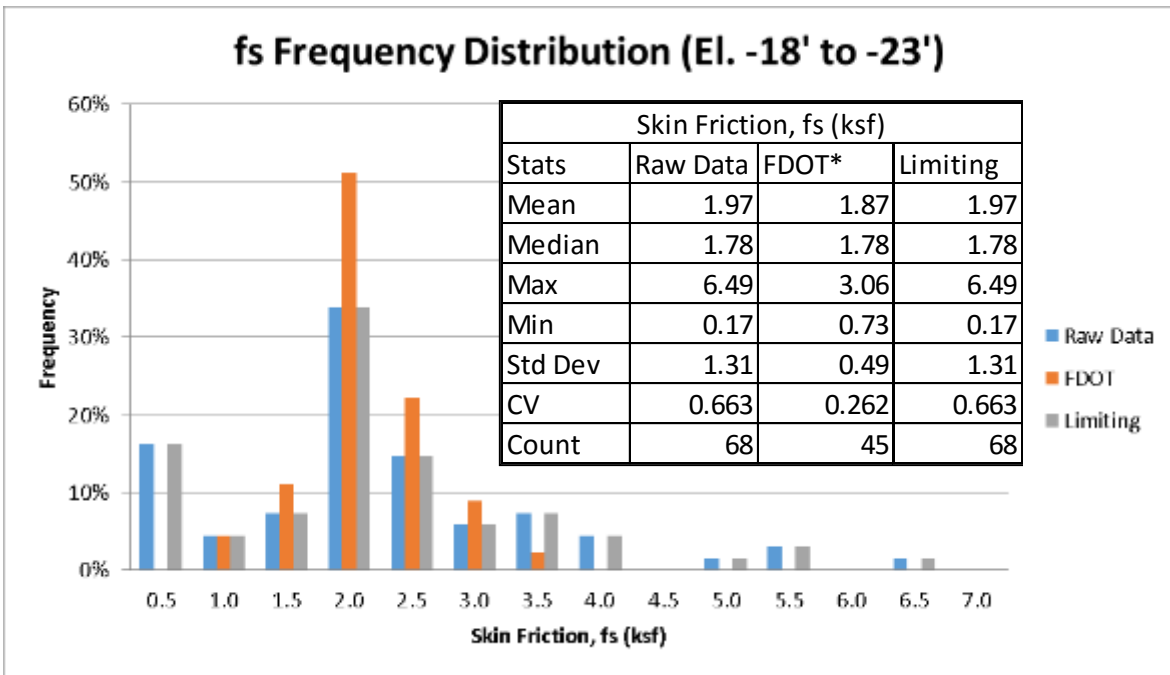


Figure 128 - Overland test shaft 2 skin friction frequency distribution for segment 2

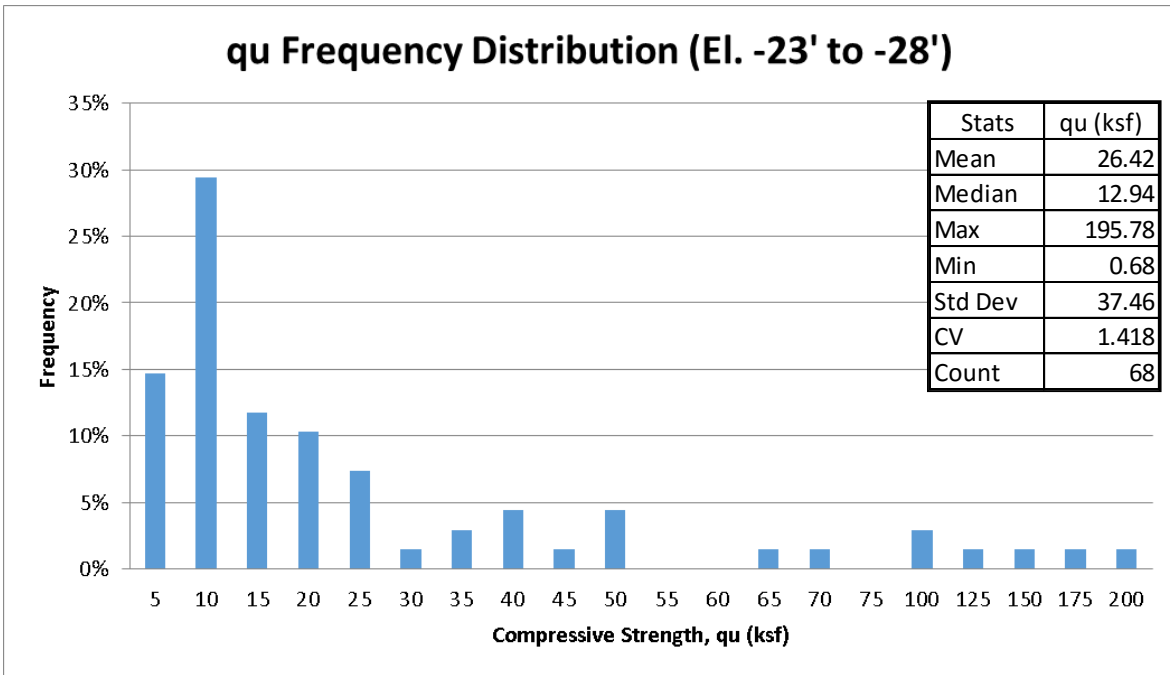


Figure 129 - Overland test shaft 2 compressive strength frequency distribution for segment 3

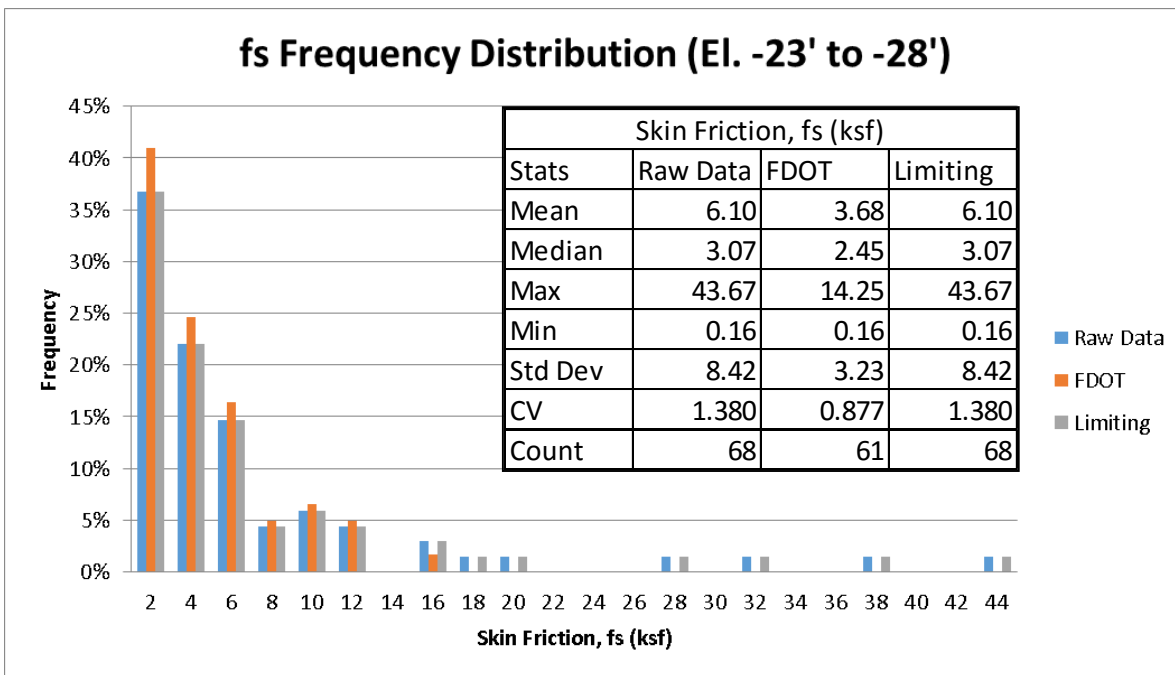


Figure 130 - Overland test shaft 2 skin friction frequency distribution for segment 3

Table 71 - Test shaft 2 preliminary analysis results

Segment	Status	Statnamic	Raw Data		FDOT		Limiting	
		fs (ksf)	fs (ksf)	% Diff	fs (ksf)	% Diff	fs (ksf)	% Diff
2	Fully Mobilized	2.06	1.97	-4.32	1.87	-9.31	1.97	-4.32
3	Approaching Mobilization	4.68	6.10	68.86	3.68	-48.59	6.10	68.86

From the results it can be seen that for segment 2 (fully mobilized), the monitoring predictions were within 5 – 10% difference of the Statnamic results. This proved that Teale’s specific energy equation, used at both locations, was able to accurately predict the capacity of both shafts. Therefore, Teale’s equation was used for the remaining analyses and the Kanapaha load test.

3.5 Johnston’s Criteria

Preliminary analysis verified the drilled shaft monitoring methods were capable of estimating compressive strength in real time quite accurately. However, in order to estimate skin friction and shaft capacity in real time, using the SFH recommended method, split tension data was also needed. The previous sections presented multiple methods of adjusting the q_t/q_u ratios based on site specific conditions, post monitoring, to determine the needed split tension strengths for determining skin friction. However, the efficiency and validity of this approach was in question. Using this approach, skin friction could not be estimated in real time and compressive strength values may be paired with split tension values from two dissimilar materials. The latter may provide inaccurate q_t/q_u ratios and shaft capacity estimates in other locations with less available core data. For example, in Table 72 the red box indicates a q_t - q_u pair that would be used to determine the average q_t/q_u ratio for a layer or site to make q_t adjustments. However, looking at the dry unit weights and moisture contents of the two test results, it is clear that these are dissimilar materials and should not be combined and used to determine an average q_t/q_u ratio.

Table 72 - Core data from Little River indicating dissimilar materials

Boring/ Shaft-Core	Sample No.	Test Type	Moisture (%)	Dry Density (pcf)	Max Load (lbs)	S.T. Strength (psi)	q(u) (psi)	Displ. @ Fail. (in)	Strain @ Fail. (%)
(38)									
2/1-1	1	T	15.6	106.5	79.3	13.9		0.0344	
(48)									
2/1-2	1	T	59.8	63.3	39.6	6.5		0.0863	
	2	U	58.2	64.7	128.6		38.1	0.1904	3.67
	3	T	60.1	63.2	66.0	8.1		0.0655	
	4	U	69.0	59.7	61.1		16.9	0.1679	3.34
	5	T	3.2	156.0	9,520.2	975.2		0.0682	
	6	T	3.8	135.0	3,180.6	327.3		0.0489	
	7	U	5.1	134.4	5,319.1		1,116.9	0.0553	1.08
	8	T	7.6	131.5	2,077.8	218.1		0.0335	
	9	T	4.8	149.9	1,031.9	107.3		0.0228	
	10	T	61.3	63.2	39.3	4.0		0.0624	
	11	T	28.8	91.6	54.5	5.2		0.1934	

Based on this logic, new criteria were developed to produce “valid” q_t - q_u pairs. The new criteria was set to only match pairs if the dry densities (dry unit weight) were within 10 pcf of one another and if the moisture contents were within 4% of one another. The thought behind this was that similar materials should have similar dry unit weights and also a similar void structure which would satisfy the $G_w = S_e$ condition for geomaterials. The dry unit weight indicates that similar materials make up the rock mass and the water content is representative of the void ratio and porosity of the material which should be indicative of the void structure. However, enforcing the pairing criterion provided very few q_t - q_u pairs at each site to determine the q_t/q_u ratio needed to make the proper q_t adjustments. This was more relevant at Overland where fewer than five “valid” pairs were able to be created for each distinct layer that was monitored; even though additional core data was obtained in four separate locations, all within 10 feet of the monitored shaft. This led to a more theoretical approach to develop q_t adjustments.

Based on Johnston’s criterion (1985) for geomaterials, a q_t/q_u vs. q_u plot was developed by Anoglu et al. (2006) for the concrete industry, indicating q_t/q_u ratios decrease as compressive strength increases and that the trend is nonlinear (Gatorock trending was in agreement). Anoglu tested various concrete samples that were developed using different water-to-cement ratios, binders, additives, cure times, and curing conditions. This is similar to the various limestone formations found throughout Florida. Each formation comprises different binding materials found within the rock matrix, such as clay found in north Florida that is not found in south Florida, various formation ages ranging from less than 1 million years to over 35 million years, various curing conditions such as changing sea level or the amount of overburden present above the formation, as well as different skeletal remains left behind that act as the aggregate and provide

the main source of the binder from calcite precipitate. Figure 131 presents Anoglu's developed concrete plot.

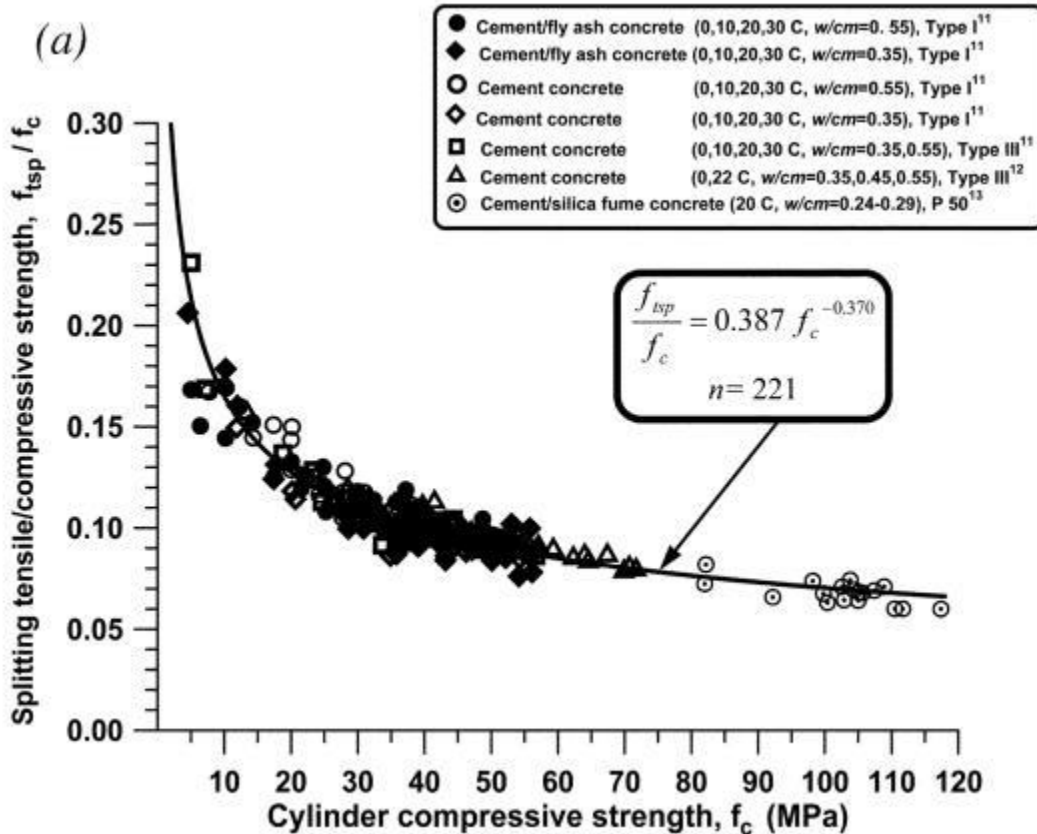


Figure 131 - q_t/q_u vs q_u for concrete (Anoglu et al., 2006)

In Johnston's report, he indicated that a similar relationship for splitting tensile strength and compressive strength can be determined for all geomaterials ranging from lightly over-consolidated clay to very hard rock. Using Johnston's proposed criterion, an equation similar to Anoglu's was developed for Florida geomaterials. The equation development began using Anoglu's relationship for q_t/q_u ratios, based on Johnston's criterion.

$$q_t/q_u = B/M \dots \dots \dots \text{Eq 8}$$

where,

- q_t = Uniaxial tensile strength (direct tension)
- q_u = Uniaxial compression strength (unconfined compression)

- B is a material parameter developed by Johnston that defines the nonlinearity of the Mohr-Coulomb failure envelope and is a measure of confinement effectiveness. B is independent of material type.
- M is also a Johnston material parameter and defines the changes in failure stresses associated with different geomaterial types (i.e., The relationship between Φ' and q_u)

Johnston developed a single equation for B,

$$B = 1 - (\log 0.0172q_u)^2 \dots\dots\dots \text{Eq 9}$$

where q_u is measured in kilopascals (kPa), and developed multiple equations for M based on material groupings such as; carbonate materials with well-developed crystal cleavage (e.g., limestone and dolomite),

$$M = 2.065 + 0.170(\log q_u)^2 \dots\dots\dots \text{Eq 10}$$

and lithified argillaceous materials with strong crystals and poorly developed crystal cleavage (e.g., clay, claystone, and mudstone),

$$M = 2.065 + 0.231(\log q_u)^2 \dots\dots\dots \text{Eq 11}$$

With the understanding that Florida field drilling would likely pass through varying layers of over-consolidated clays, IGMs, and limestone, both M equations were considered for the development of the Florida geomaterials, q_t/q_u vs. q_u relationship. Therefore, using Johnston's equations for M and B, the following relationships, Figure 132, were developed using q_u values ranging from 1 to 10,000 psi, with data points plotted for q_u in increments of 10 psi (e.g. 10 psi, 20 psi, 30 psi, etc.). The respective q_t values were generated using the relationship $q_t = q_u \times (B/M)$. Note, the carbonate materials are labeled limestone and the lithified argillaceous materials are labeled clay.

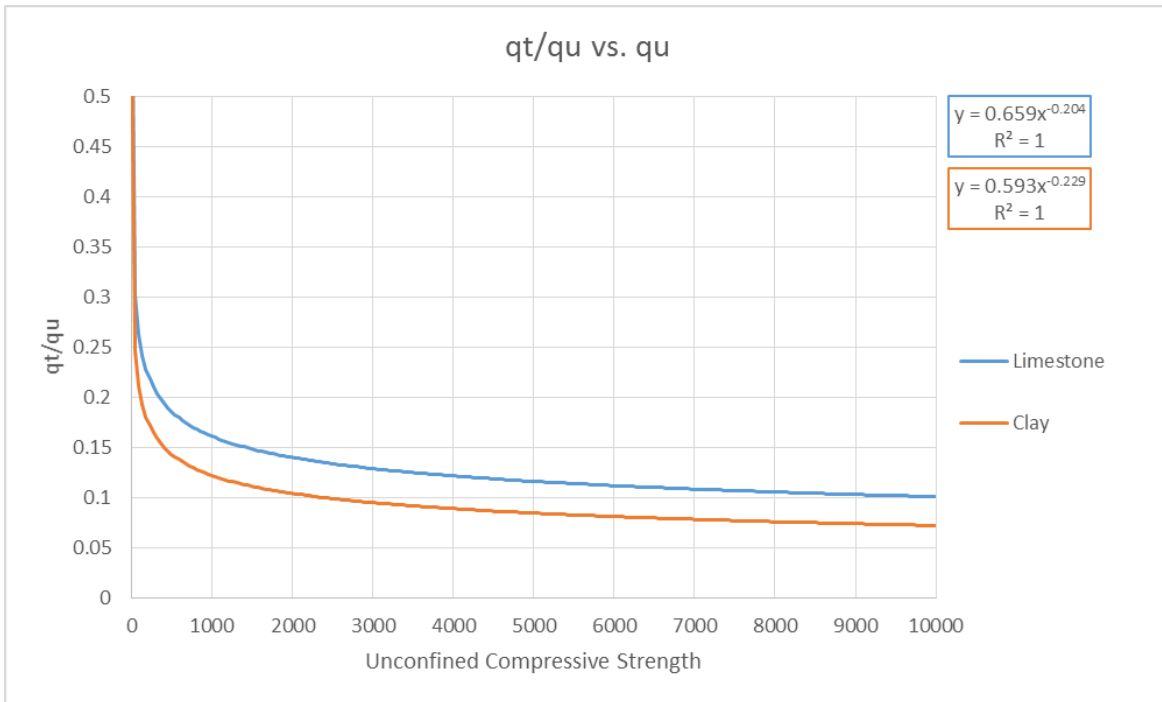


Figure 132 – q_t/q_u vs. q_u for clay and limestone using Johnston's criteria

Evident from the developed regression equations, the shape of the two curves are different and the new curve developed for Florida geomaterials needed to account for this. It was proposed that by using the q_u data set from Little River, the shape of the two curves could be combined. At Little River, there was a high degree of variability within the q_u core samples that were collected ($CV = 1.81$). The high degree of variability was a result of the multiple materials types present at the site (three distinct layers indicated in Figure 117). This included over-consolidated clays, IGMs, and limestone with a large q_u range ($q_u = 4.3$ to $4,300$ psi). Therefore, by using the reported q_u values from Little River, more emphasis would be placed in different portions of the q_u range. This would be more representative of actual Florida site conditions instead of using equally spaced increments of q_u to establish the relationship. For example, it is highly unlikely that there would be an equal number of core samples obtained in the 9,000 to 10,000 psi q_u range and the 1 to 1,000 psi q_u range and the developed curve needed to account for this. As well, by placing more emphasis on low end q_u values, from clays and IGMs, the approach should reshape the curve to better represent both material groupings. Since the focus of the study is on limestone, the M equation for limestone was used as the basis for development and the following presents the developed curve.

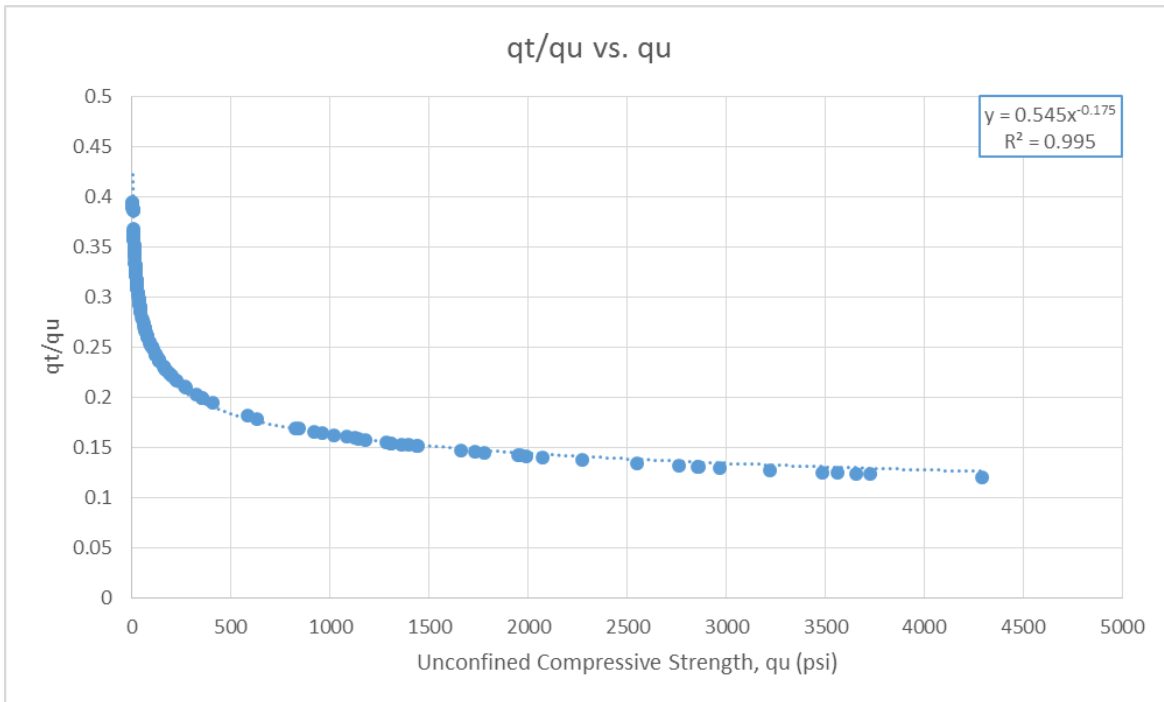


Figure 133 – q_t/q_u vs. q_u developed using only Little River q_u data

The new Florida geomaterials curve was then compared to the previously developed clay and limestone curves.

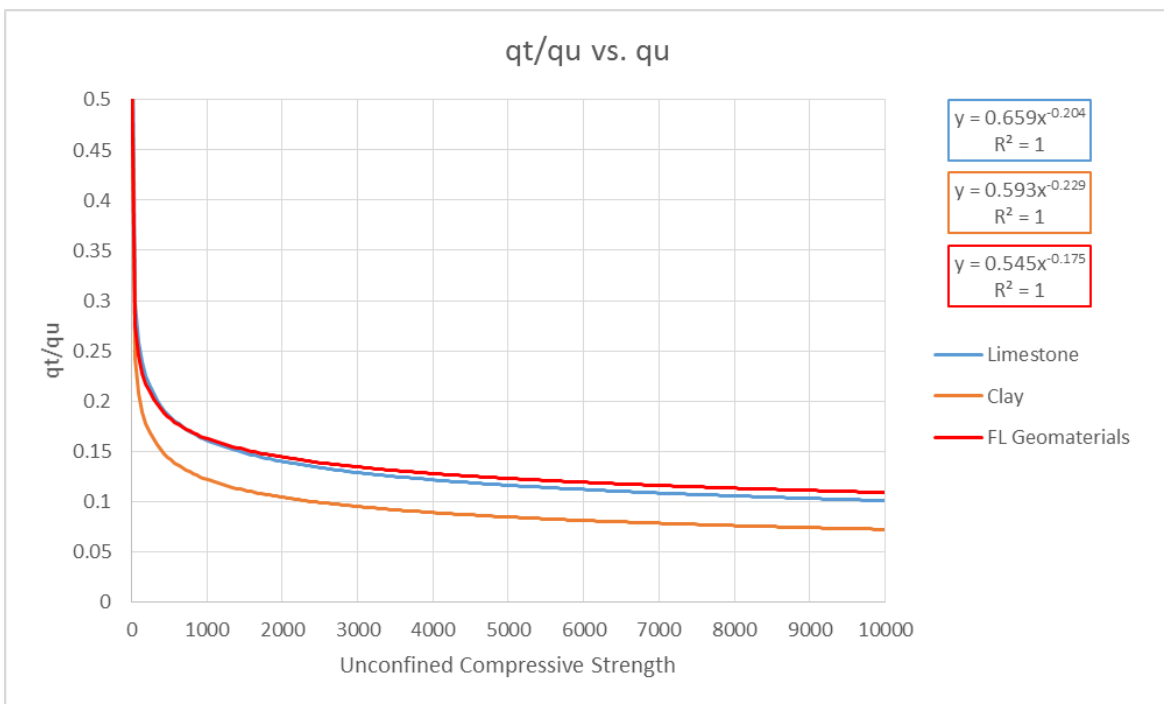


Figure 134 – Comparison of q_t/q_u vs. q_u curves

As seen in Figure 134, the shape of the limestone curve changed. However, the curve provided q_t/q_u ratios much higher than the clay and IGM curve, and were higher than the original limestone curve for $q_u > 1,000$ psi. This was thought to be a result of Johnston's data set not including any limestone samples from Florida to establish the M equations. Therefore, a correction factor would need to be applied to account for the differences in material formation of Florida limestone compared to limestone found elsewhere throughout the nation. In Florida, for the design of highway pavement materials; the Limerock Bearing Ratio, LBR, is used instead of the California Bearing Ratio, CBR, which is used nationwide. The only difference between the two tests is the compressive strength used to define the standard strength of limestone. For the CBR, $q_u = 1,000$ psi and for the LBR, $q_u = 800$ psi. This same reduction was then applied to establish the correction factor,

$$\text{Correction Factor} = q_{u\text{LBR}}/q_{u\text{CBR}} = 800 \text{ psi}/1,000 \text{ psi} = 0.80 \dots \text{Eq 12}$$

applying the correction factor to q_u ,

$$q_t/(0.8 \times q_u) = B/M \dots \dots \dots \text{Eq 13}$$

and rearranging the equation to solve for q_t ,

$$q_t = 0.8 \times q_u \times (B/M) \dots \dots \dots \text{Eq 14}$$

Therefore, the new equation would be,

$$q_t/q_u = 0.8 \times 0.545 \times q_u^{-0.175} = 0.436 \times q_u^{-0.175} \dots \dots \dots \text{Eq 15}$$

The new Florida geomaterials equation, with the correction factor applied, Eq 15, was then compared to the original limestone and clay equations again, Figure 135.

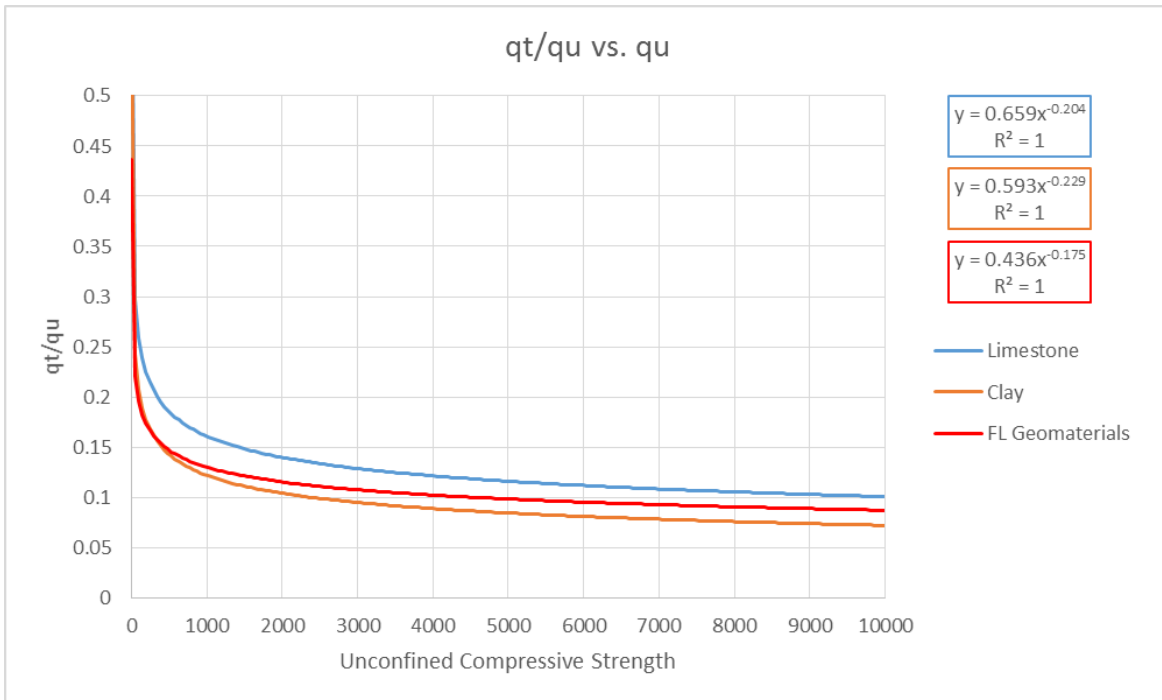


Figure 135 - Comparison of q_t/q_u vs. q_u curves with the new Florida geomaterials curve

Evident in Figure 135, the correction factor appeared to work well. The q_t/q_u ratios for the lower end q_u values were quite representative of the clay and IGM curve, and as q_u increases the q_t/q_u ratios become more representative of the original limestone curve. Therefore, by only using the q_u values obtained from Little River and applying the correction factor, a curve that represents both material groupings was developed. Interestingly, the q_t/q_u range is approximately 0.29 to 0.09 for q_u ranging from 10 to 10,000 psi, and is close to what UF and FDOT investigators felt the range should be (The range was thought to be 0.3 to 0.1).

To simplify deriving q_t using q_u with the newly developed equation, q_t was plotted vs. q_u , Figure 136, and another equation was derived to calculate q_t directly.

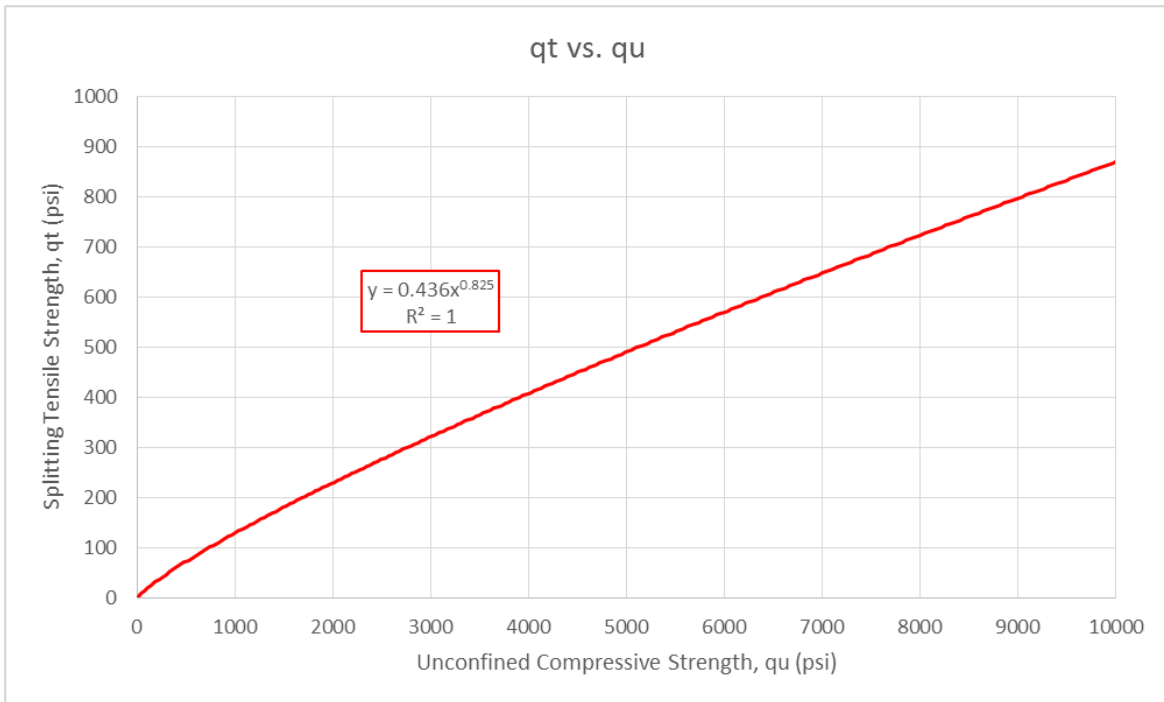


Figure 136 – Florida geomaterials q_t equation

From Figure 136, estimates for q_t can now be derived directly using the following equation,

$$q_t = 0.436 \times q_u^{0.825} \dots\dots\dots \text{Eq 16}$$

where the units for q_u and q_t are in psi.

Using the new Florida geomaterials equation, q_t values were estimated using measured q_u values and compared to measured q_t core data from around the state. The basis of the comparison was dry unit weight and water content (pairing criteria parameters) plotted versus q_t . If the predicted q_t values were accurate, they should plot in accordance with the measured q_t values obtained from actual split tension testing. Figure 137 and Figure 138 provide the comparisons using 1223 measured q_t values and 739 predicted q_t values derived using the Florida geomaterials equation with the available 739 compressive strength values from the following project sites.

- 17th Street Causeway
- Acosta Bridge
- BR720153 SR-9 (I-95) Overland
- CR-326 @ Waccasa River
- HEFT / SR 874 PD&E

- I-295 Buckman Bridge
- I-295 Dames Point Bridge
- I-95 @ I-295 Cloverleaf
- I-95 Fuller Warren Bridge
- Jewfish Creek
- MIC- People Mover Project
- NW 12th Ave (SR 933) Miami River Bridge
- NW 36th Street Bridge
- Pump Station at Bal Harbour (96th St & Indian Creek)
- Radio Tower Everglades Academy (Florida City)
- SR-10 @ CSX RR (Beaver St. Viaduct), Duval Co.
- SR-20 @ Lochloosa Creek, Alachua Co.
- SR-25 @ Santa Fe River
- SR30/US98 @ Aucilla River (District 3)
- SR-9 (I-95) Overland Bridge
- US-90 Victory Bridge (District 3)
- Verona Ave Bridge Over Grand Canal
- Wall At Service Road South of Snake Creek

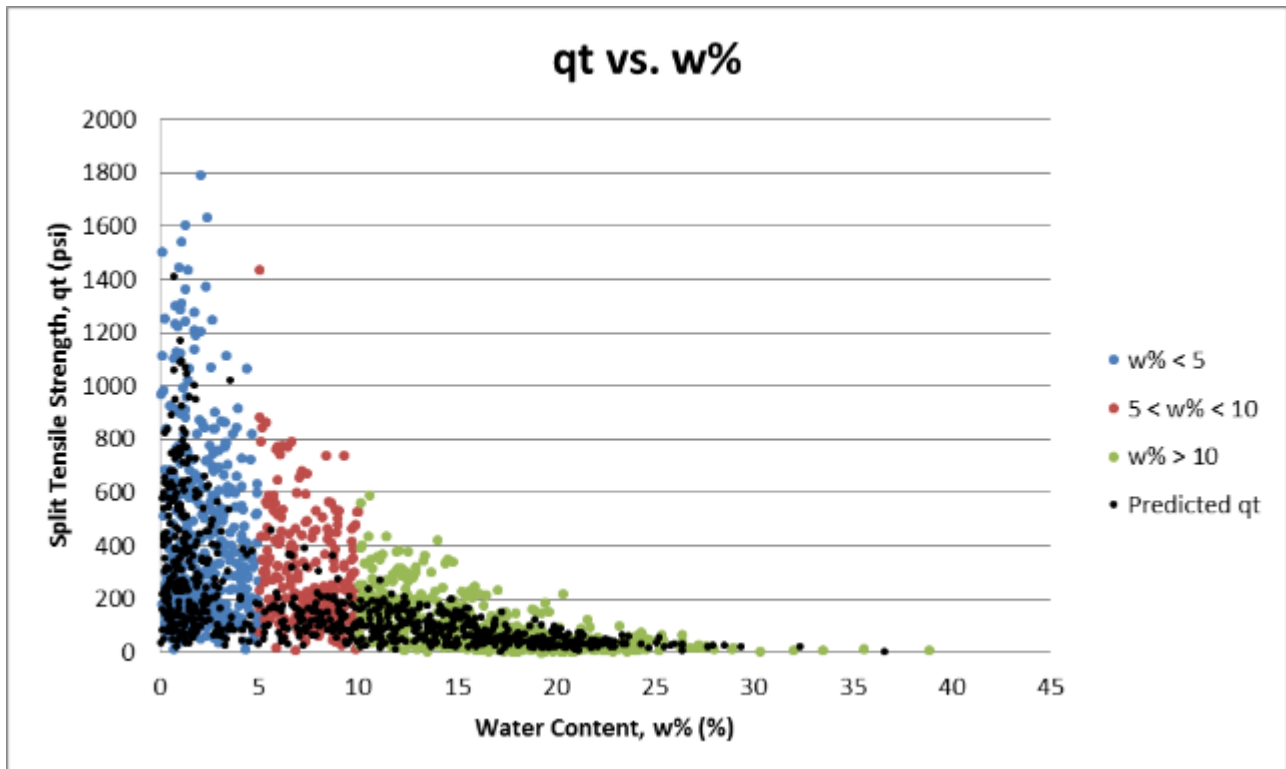


Figure 137 - split tension strength vs. water content with predicted q_t values for 23 Florida sites

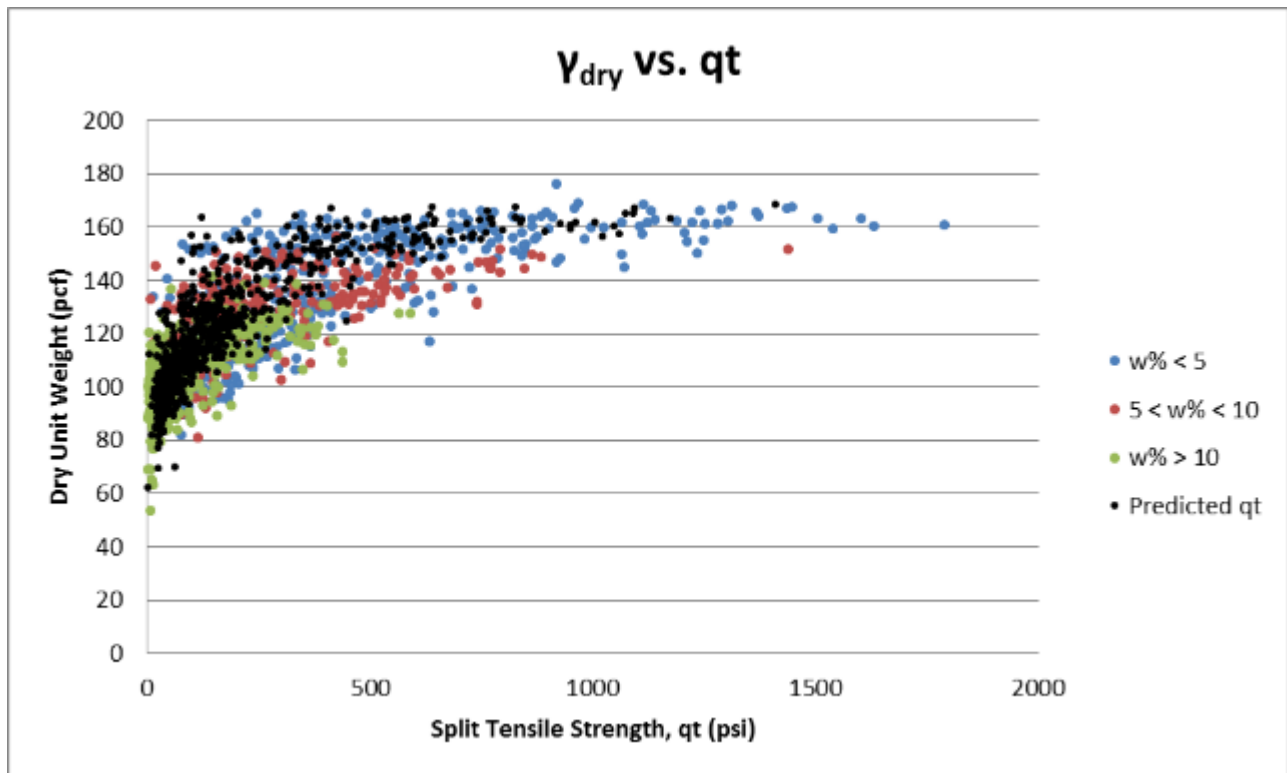


Figure 138 - Dry unit weight vs. split tension strength with predicted and measured q_t values from 23 Florida sites

Figure 137 and Figure 138, show the predicted q_t values fit the measured q_t data very well for all of Florida. The dry unit weight versus split tension plot provided better trending and a more thorough investigation was conducted.

For the investigation, measured q_t values were grouped by dry unit weight within a 5 pcf range (e.g., 105 to 110 pcf, 110 to 115 pcf, etc.). Next, the mean and standard deviation were calculated for q_t values within each unit weight range. The standard deviation was used to establish an “acceptable” strength range, one standard deviation above and below the mean, for predicted q_t values within each respective unit weight range. The predicted q_t values were grouped and averaged the same way as the measured values. The measured and predicted q_t values were then compared on the basis of dry unit weight versus splitting tensile strength. The results are provided in Figure 139.

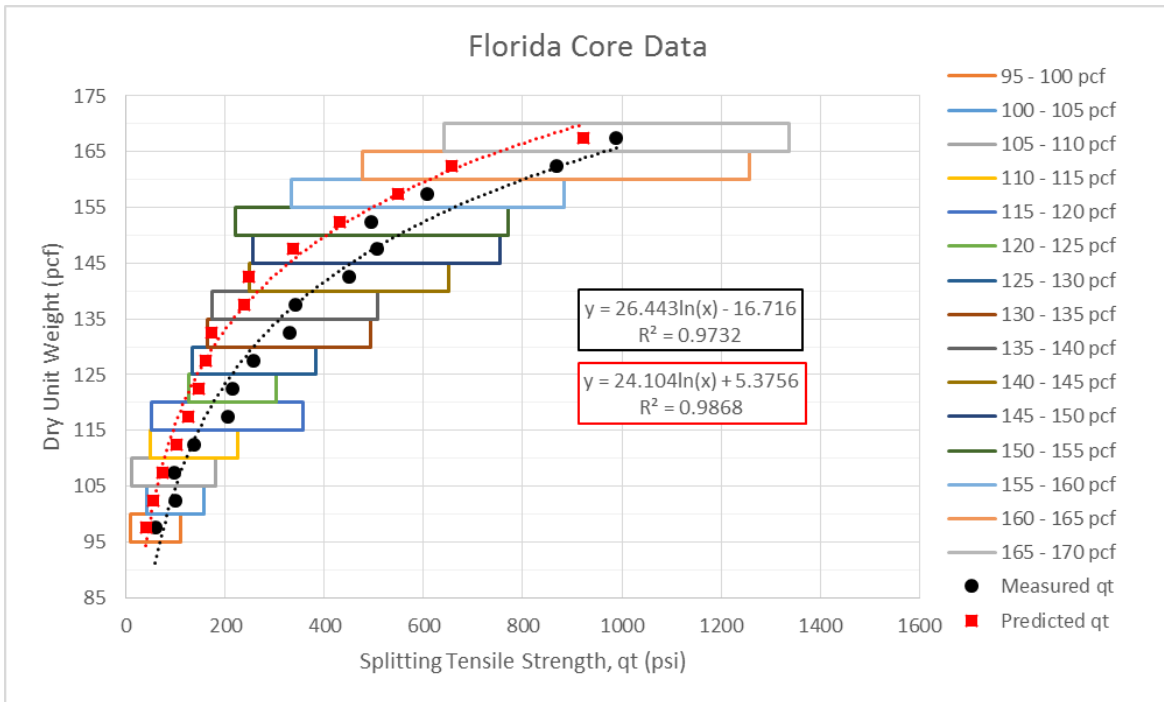


Figure 139 - Dry unit weight vs. split tension strength with average predicted and measured q_t values from 23 Florida sites

As seen in Figure 139, the predicted q_t values all fall within one standard deviation from the mean measured q_t values. Therefore, the Florida geomaterials equation, Eq 16, for predicting q_t using q_u should be fairly accurate. Although, it should be noted that the q_t used in Johnston's criteria is for uniaxial tension (direct tension), not split tension. Anoglu used the following to transform uniaxial tension to split tension;

$$\text{Uniaxial Tension} = \lambda \times \text{Split Tension} \dots \text{Eq 17}$$

where $\lambda = 0.9$.

However, the value of λ used by Anoglu was derived for concrete, and the value of λ for Florida limestone and IGM is unknown. Therefore, λ was assumed to be 1, as the current Florida geomaterials equation provided a good conservative estimate for splitting tensile strength.

The next step was to reanalyze the Little River and Overland monitoring using q_t derived from monitored q_u values with the new Florida geomaterials equation, Eq 16, and making a skin friction prediction using SFH recommended method. The preliminary analysis included using the limestone and Florida geomaterials equations to determine which performed best in locations where side shear was mobilized. The correction factor, 0.8, used to develop the Florida geomaterials equation, was also applied to the

general limestone equation and considered for the analysis as well. The “general limestone equation” is referencing the regression equation for limestone in Figure 132Figure 134, rearranged to solve for q_t directly, $q_t =$

$$0.659q_u^{0.796} \dots\dots\dots \text{Equation 18.}$$

$$q_t = 0.659q_u^{0.796} \dots\dots\dots \text{Equation 18}$$

The analysis included four sections at Little River, SG7 to SG4, and segment 2 from Overland using the raw data method. The results are provided in Table 73Table 75.

Table 73 - Pilot projects reanalyzed using the limestone equation, Eq 18

Limestone Equation, Eq 18					
Location	Section	Thickness (ft)	Measured (ksf)	Predicted (ksf)	% Difference
Little River	SG7 to SG6	5.0	21.10	21.79	3.27%
Little River	SG6 to O-cell	5.5	20.60	24.54	19.13%
Little River	O-cell to SG5	3.5	21.40	21.59	0.89%
Little River	SG5 to SG4	5.0	13.60	15.61	14.78%
Overland	Segment 2	5.0	2.06	2.20	6.80%
Average	All	4.9	15.50	17.02	9.69%

Table 74 - Pilot projects reanalyzed using Eq 18, for limestone, with correction factor

Limestone Equation, Eq 18, with Correction Factor Applied					
Location	Section	Thickness (ft)	Measured (ksf)	Predicted (ksf)	% Difference
Little River	SG7 to SG6	5.0	21.10	19.49	-7.63%
Little River	SG6 to O-cell	5.5	20.60	21.95	6.55%
Little River	O-cell to SG5	3.5	21.40	19.32	-9.72%
Little River	SG5 to SG4	5.0	13.60	13.97	2.72%
Overland	Segment 2	5.0	2.06	1.97	-4.37%
Average	All	4.9	15.50	15.23	-1.75%

Table 75 - Pilot projects reanalyzed using the Florida geomaterials equation, Eq 16

Florida Geomaterials Equation, Eq 16					
Location	Section	Thickness (ft)	Measured (ksf)	Predicted (ksf)	% Difference
Little River	SG7 to SG6	5.0	21.10	19.67	-6.78%
Little River	SG6 to O-cell	5.5	20.60	22.09	7.23%
Little River	O-cell to SG5	3.5	21.40	19.46	-9.07%
Little River	SG5 to SG4	5.0	13.60	13.95	2.57%
Overland	Segment 2	5.0	2.06	1.90	-7.77%
Average	All	4.9	15.50	15.30	-1.29%

Evident from the tables, the Florida geomaterials equation, Eq 16, provided the most accurate results. Although, the limestone equation, Eq 18, with the correction applied

also provided very good estimates. It was thought the Florida geomaterials equation may have outperformed the limestone equation because the majority of the comparative data was from Little River and the Florida geomaterials equation was developed using only Little River data, creating a bias. The results from Overland supported the idea, as the limestone equation with the correction factor provided the best result. Therefore, the limestone equation with the correction factor was also considered for the final analysis at Kanapaha.

The following presents the newly analyzed monitoring results using the Florida geomaterials equation, Eq 16, to predict q_t at both Little River and Overland, as well as the results using q_t slope adjustments with the pairing criteria for both locations. Again, the pairing criteria only matched q_t with q_u if both samples had dry unit weights within 10 pcf of one another and water contents within 4% of one other. The slope adjustments, using the average q_t/q_u for a defined thickness, were made for each individual layer at Overland and for each soil zone at Little River (zones 2 and 3), Figure 117. Only the raw data method is provided for the Little River analysis as this produced the best result. Similar results were found using the FDOT*, Limiting, and Raw Data methods at Overland. However, the raw data method once again provided the best result.

Table 76 - Little River monitoring results using the FL geomaterials equation, Eq 16

Arithmetic Mean (Raw Data)										
Shaft Section (Strain Gauge Levels)	Elevation Range (ft)		Measured Mean (O-cell) (ksf)	Predicted Mean (Monitoring) (ksf)	Percent Difference	Predicted Maximum (Monitoring) (ksf)	Predicted Minimum (Monitoring) (ksf)	Predicted Standard Deviation (Monitoring)	Predicted CV (Monitoring)	Count
SG7 to SG6	45.6	40.6	21.10	19.67	-6.79%	144.61	2.42	25.88	1.32	73
SG6 to O-cell	40.6	35.1	20.60	22.09	7.21%	86.51	2.28	17.10	0.77	79
O-cell to SG5	35.1	31.6	21.40	19.46	-9.08%	164.14	3.56	24.33	1.25	52
SG5 to SG4	31.6	26.6	13.60	13.95	2.60%	59.74	4.06	11.11	0.80	67
SG4 to SG3	26.6	19.6	9.70	13.77	41.95%	94.00	3.04	13.46	0.98	95
SG3 to SG2	19.6	12.6	9.90	13.89	40.28%	272.12	1.27	27.47	1.98	104
Average Skin Friction (ksf)			15.12	16.71	10.50%	140.45	2.65	19.72	1.21	78.33
Total Load (kips)			6269	6928	10.50%	Totals not needed for these values				

Table 77 - Overland monitoring results using the FL geomaterials equation, Eq 16

Segment	Status	Statnamic	Raw Data		FDOT*		Limiting	
		fs (ksf)	fs (ksf)	% Diff	fs (ksf)	% Diff	fs (ksf)	% Diff
2	Fully Mobilized	2.06	1.90	-7.77	1.86	-9.56	1.90	-7.73
3	Approaching Mobilization	4.68	5.55	18.48	1.77	-62.10	5.30	13.34

Table 78 - Little River monitoring results using q_t slope adjustments with pairing criteria

Arithmetic Mean (Raw Data)										
Shaft Section (Strain Gauge Levels)	Elevation Range (ft)		Measured Mean (O-cell) (ksf)	Predicted Mean (Monitoring) (ksf)	Percent Difference	Predicted Maximum (Monitoring) (ksf)	Predicted Minimum (Monitoring) (ksf)	Predicted Standard Deviation (Monitoring)	Predicted CV (Monitoring)	Count
SG7 to SG6	45.6	40.6	21.10	20.81	-1.38%	175.23	1.98	30.98	1.49	73
SG6 to O-cell	40.6	35.1	20.60	24.42	18.54%	106.29	1.98	21.03	0.86	79
O-cell to SG5	35.1	31.6	21.40	21.69	1.37%	214.44	3.23	31.46	1.45	52
SG5 to SG4	31.6	26.6	13.60	12.69	-6.71%	67.62	2.85	11.88	0.94	67
SG4 to SG3	26.6	19.6	9.70	11.25	15.96%	89.25	2.08	12.52	1.11	95
SG3 to SG2	19.6	12.6	9.90	11.74	18.62%	286.11	0.80	28.66	2.44	104
Average Skin Friction (ksf)			15.12	16.32	7.97%	156.87	2.01	22.07	1.42	78.33
Total Load (kips)			6269	6769	7.97%	Totals not needed for these values				

Table 79 - Overland monitoring results using q_t slope adjustments with pairing criteria

Segment	Status	Statnamic	Raw Data		FDOT*		Limiting	
		fs (ksf)	fs (ksf)	% Diff	fs (ksf)	% Diff	fs (ksf)	% Diff
2	Fully Mobilized	2.06	1.95	-5.34	1.88	-8.56	1.95	-5.34
3	Approaching Mobilization	4.68	5.62	20.09	3.72	-20.53	5.62	20.09

Using either approach to predict q_t worked very well at both locations and produced similar results. However, the benefit of using Florida geomaterials to predict q_t and skin friction is the ability to make real time predictions. Using the Florida geomaterials equation would also be largely beneficial for sites where core data is limited for individual layer q_t adjustments.

Additional Little River analysis was also completed using the Florida geomaterials equation. The analysis took place in strain gauge zone 8 (SG8 to SG7), Figure 140. Analysis was not previously completed because half of the layer was indicated as clay and initial monitoring efforts were solely focused on layers of limestone. However, based on Johnston's criteria, monitoring layers of over-consolidated clays should be possible.

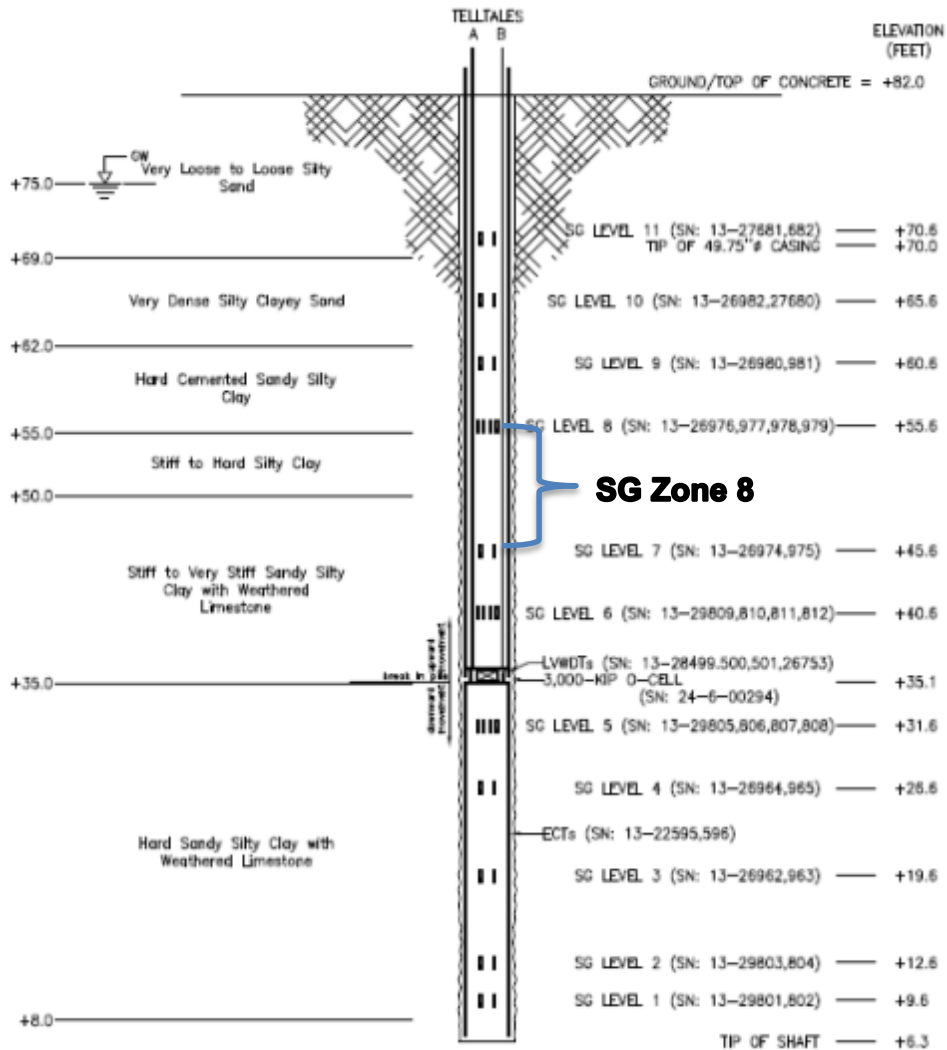


Figure 140 - Little River O-cell shaft profile, indicating strain gauge zone 8

Monitoring results indicated the unit side shear to be 11.15 ksf, where the O-cell measured 9.9 ksf. It is important to note that strain gauge zone 8 appears to be approaching mobilization based on the T-Z curves and strain gauge load distribution "Figure 66", but was not fully mobilized. The following includes an updated table with new monitoring results added and a bar graph providing visualization of the results.

Table 80 - Updated monitoring results including strain gauge zone 8

Arithmetic Mean (Raw Data)					
Shaft Section (Strain Gauge Levels)	Elevation Range (ft)		Measured Mean (O-cell) (ksf)	Predicted Mean (Monitoring) (ksf)	Percent Difference
SG8 to SG7	55.6	45.6	9.90	11.15	12.63%
SG7 to SG6	45.6	40.6	21.10	19.67	-6.78%
SG6 to O-cell	40.6	35.1	20.60	22.09	7.23%
O-cell to SG5	35.1	31.6	21.40	19.46	-9.07%
SG5 to SG4	31.6	26.6	13.60	13.95	2.57%
SG4 to SG3	26.6	19.6	9.70	13.77	41.96%
SG3 to SG2	19.6	12.6	9.90	13.89	40.30%
Average - SG8 to SG4			15.89	16.18	1.85%
Total Load (kips) - SG8 to SG4			5789	5896	1.85%
Average - SG8 to SG2			13.90	15.41	10.86%
Total Load (kips) - SG8 to SG2			7513	8329	10.86%

Note: The highlighted sections are zones where T-Z curve and strain gauge load distribution data indicate side shear is not approaching full mobilization. Zones that are not highlighted indicate side shear has been mobilized or is approaching mobilization.

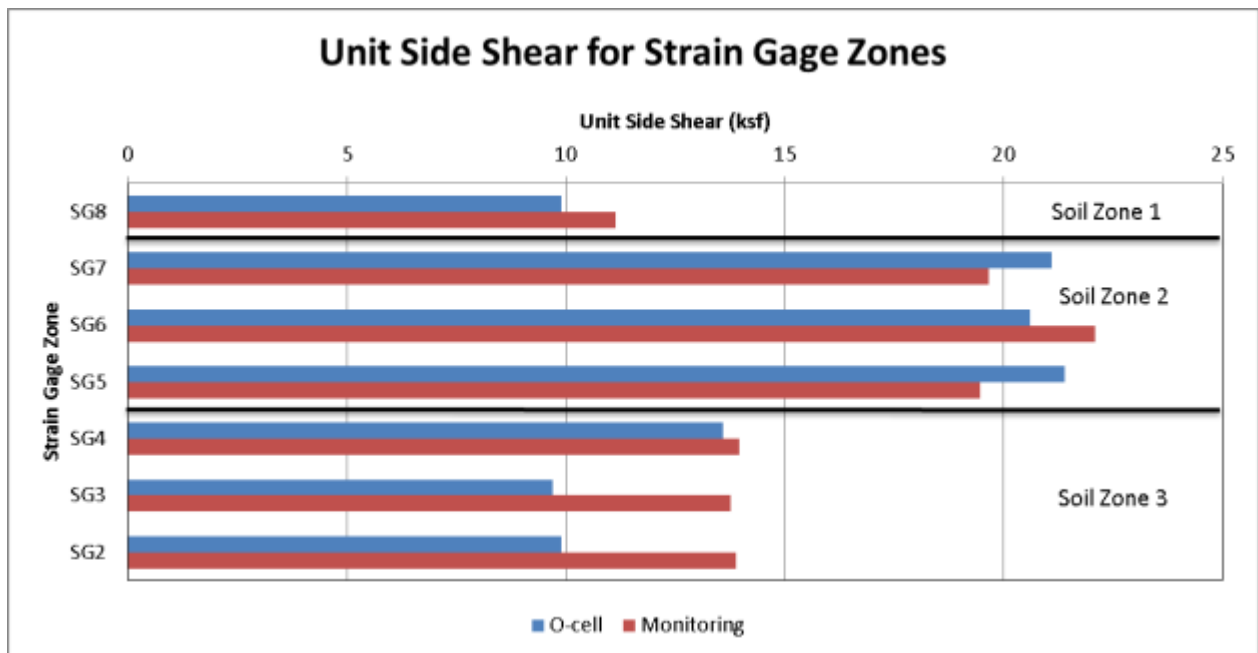


Figure 141 - Unit side shear for each monitored strain gauge zone

Figure 141, shows monitoring results in all three of soil zones indicated in the geotechnical report. The results follow the same trend as the q_u soil stratification in Figure 117, from the geotechnical report.

With the success of the preliminary monitoring trials at both Overland and Little River, researchers felt the drilling equations and the raw data method of analysis, which consistently provided the best results, could be used for the top down static load test. Consequently, the final monitoring efforts would use the raw data method of analysis with the q_u equation developed in the lab using Teale's equation, Eq 20, the Florida geomaterials q_t equation, Eq 16, developed using Johnston's criteria and the skin friction equation developed by McVay et al, Eq 6. For convenience, the equations were combined so f_s could be solved directly from q_u :

Substituting the Florida geomaterials equation,

$$q_t = 0.436 \times q_u^{0.825} \quad q_t = 0.436 \times q_u^{0.825} \dots\dots\dots \text{Eq 16}$$

into the skin friction equation developed by McVay et al.,

$$f_s = 1/2 \times q_u^{0.5} \times q_t^{0.5} \quad f_s = 1/2 \times q_u^{0.5} \times q_t^{0.5} \dots\dots\dots \text{Eq 6}$$

f_s can be solved directly using only q_u ,

$$f_s = 0.3302 \times q_u^{0.9125} \dots\dots\dots \text{Eq 19}$$

where,

$$q_u = \frac{-13.68 + \sqrt{187.2 - 0.0264 * \left(-\frac{F}{A} - \left(\frac{2\pi}{A} \right) \left(\frac{NT}{u} \right) \right)}}{0.0132} \dots\dots\dots \text{Eq 20}$$

which is the drilling equation developed in the lab.

CHAPTER 4 FULL-SCALE DRILLED SHAFT INSTALLATION WITH CAPACITY ESTIMATED REAL TIME FROM DRILLING PARAMETERS FOLLOWED BY STATIC LOAD TESTING

4.1 Kanapaha Overview

The site designated for the final load test was FDOT’s Kanapaha site located in Gainesville, Florida. The Kanapaha site was chosen for the final test because previous site investigation indicated the limestone was highly variable and highly weathered, and core samples were hard to recover (i.e., poor recoveries in most locations). Both parties, FDOT and UF, felt that a successful result at Kanapaha would prove the true benefit of drilled shaft monitoring.

4.2 Kanapaha Site Investigation

From previous site investigation completed at Kanapaha, a host of CPT, SPT, auger boring, and core boring data was available to begin the search for an ideal load test location. Previous load test data obtained in 1993 was also available. Throughout the course of the new site investigation, 12 seismic test lines, over 20 CPTs, 15 core borings, and 5 SPTs were completed in the search for a viable location “Figure 142”.

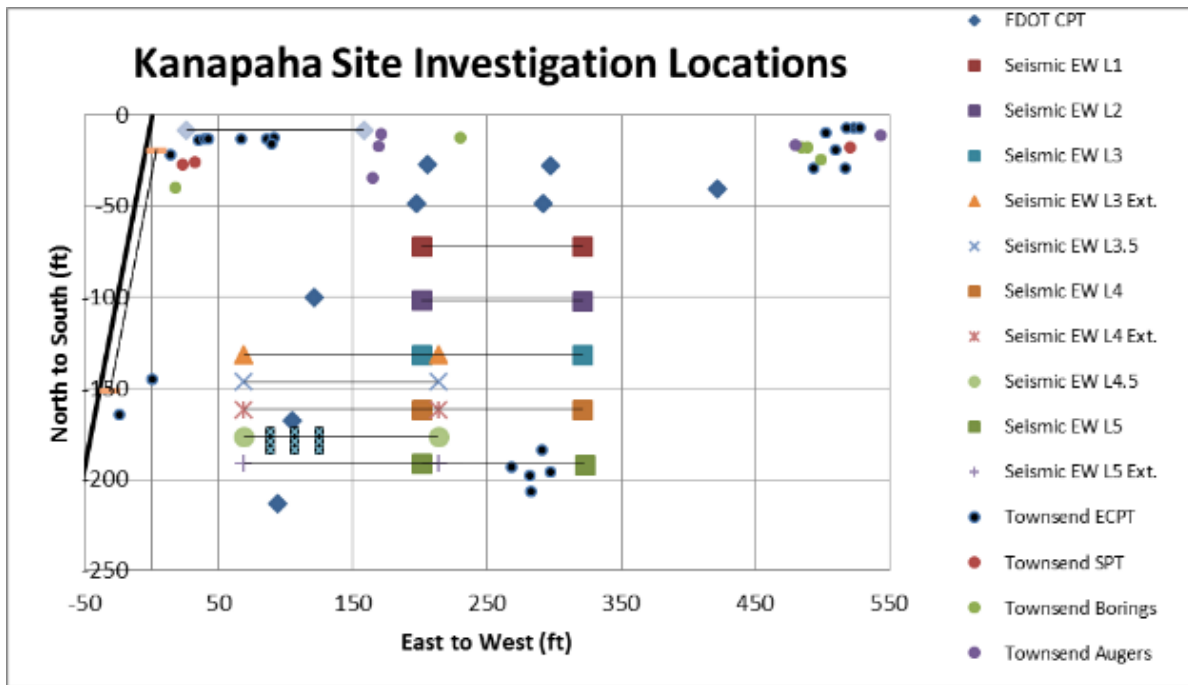


Figure 142 - Kanapaha site investigation locations

The incredible amount of site investigation performed was mainly due to the highly variable and highly weathered nature of the limestone. At the Kanapaha site, the Ocala Limestone formation is encountered, which is one of the oldest formations found in

Florida. Additionally, the site is located within the Ocala uplift which provides a karst landscape that is very cavernous due to a high degree of weathering. In most locations where seismic testing indicated rock was present, SPT and core runs indicated the same. However, the extracted limestone was mostly in a granular form due to the high degree of weathering. For example, the seismic results for EW line 3 (Figure 143) indicated limestone should be encountered between depths 30 to 35 feet.

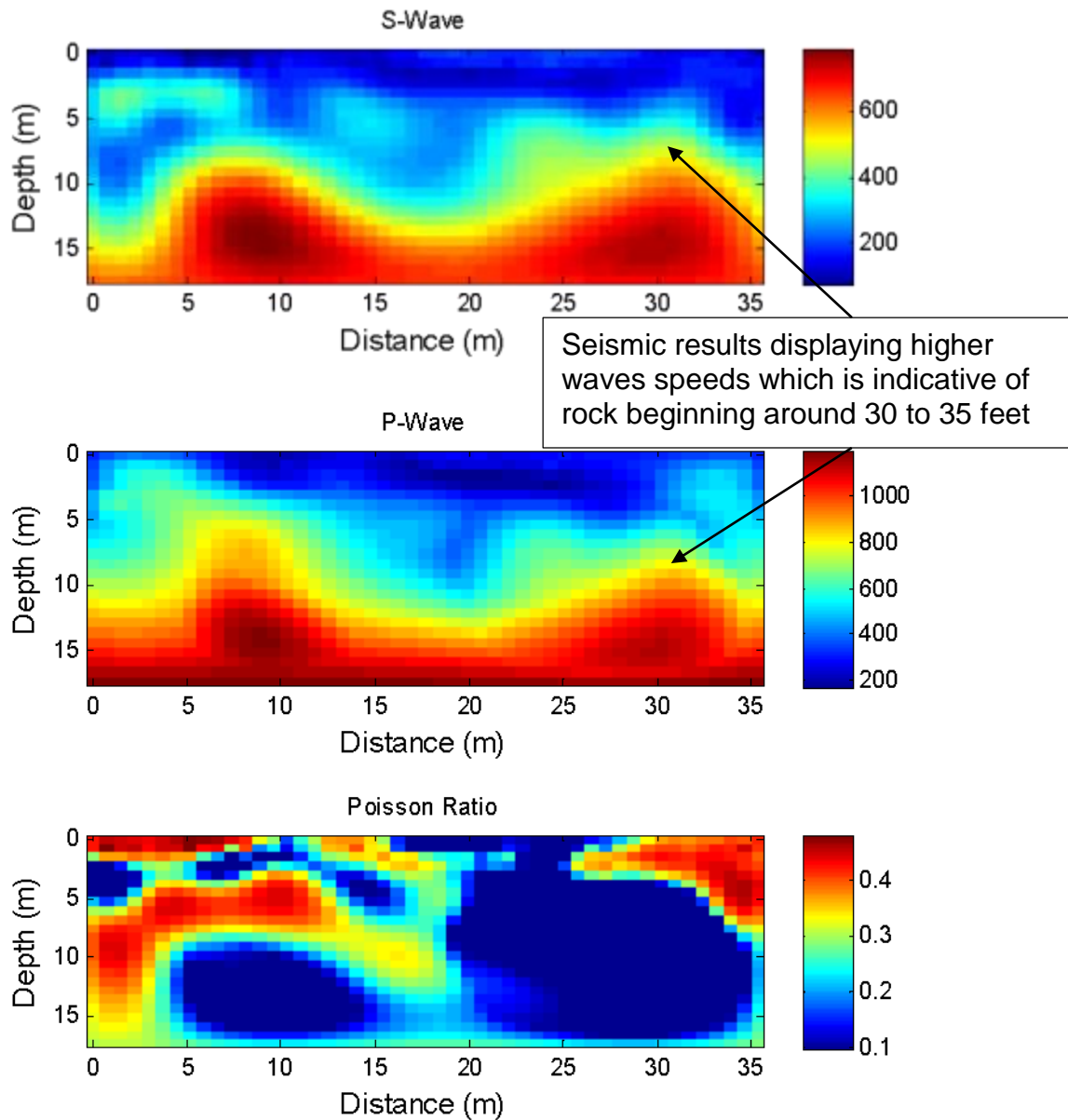


Figure 143 - Seismic line EW 3 results for P-wave, S-wave, and Poisson ratio

From the SPT run, limestone was encountered at the predicted depth, however the limestone was highly weathered with the recovered samples obtained in a granular form

rather than an intact rock mass as previously discussed. This can be seen in Figure 144 and Figure 145.



Figure 144 - Limestone recovered at a depth of 30 feet (grey clay at the top of the spoon)



Figure 145 - Highly weathered limestone at a depth of 30 feet

In addition to poor intact specimen recoveries encountered throughout the site, the planned load test shaft diameters were 36 inches (3 feet). This meant that in order to adhere to ASTM guidelines for a top down static load test, the clear distance between shafts needed to be 15 feet to provide the needed 5D spacing. In total this called for a 39 foot span of competent limestone at nearly the same depth with a similar layer thickness in all three shaft locations.

It was not until nearly a year of thorough site investigation was completed until such a location was found in the south east corner of the site. Displayed in Figure 146, borings 23, 24 and 25 were designated the shaft locations. The reaction shafts are indicated in green and the test shaft is indicated in red.

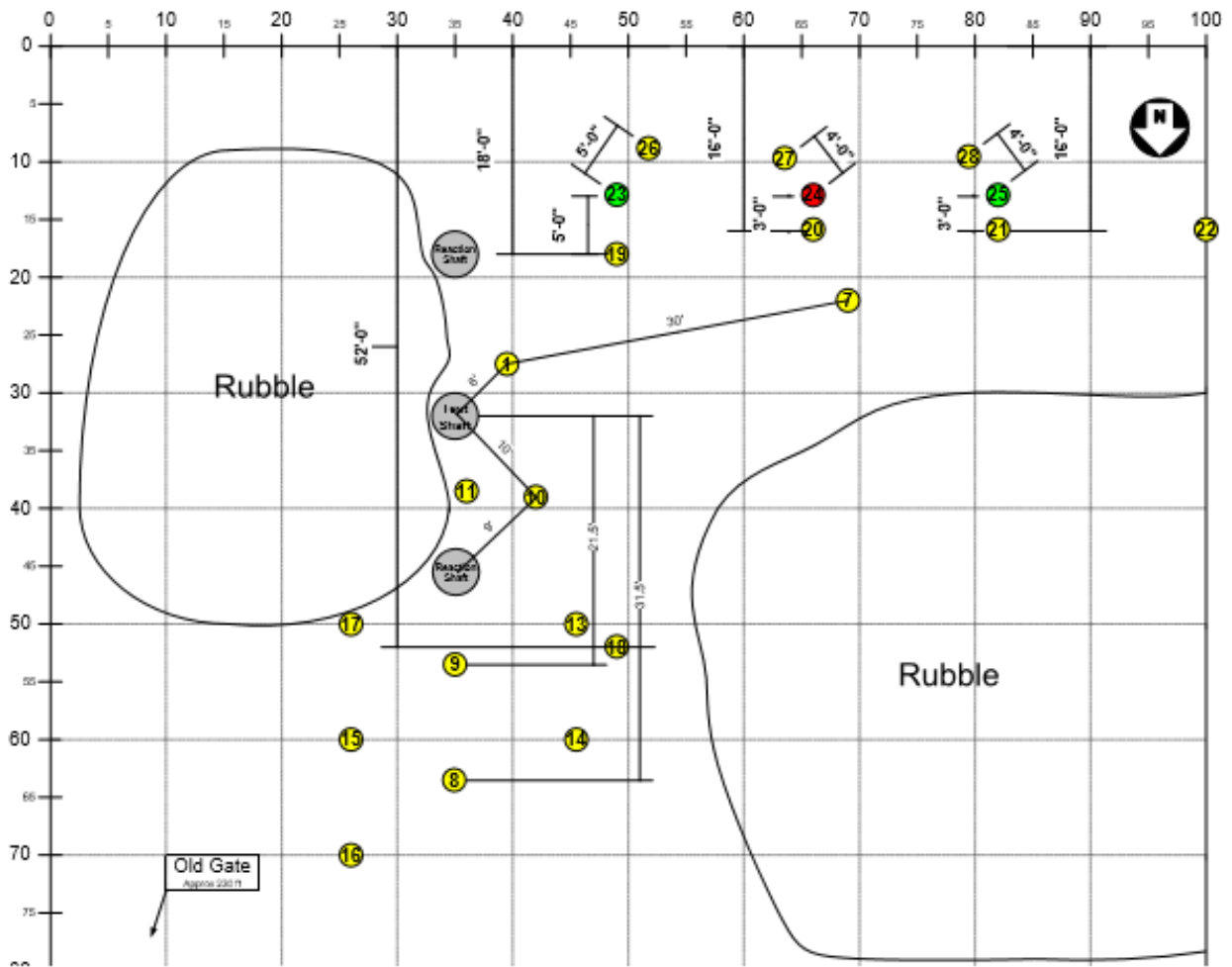


Figure 146 - Kanapaha boring locations



Figure 147 - Displays the first competent rock cores recovered at the site.

4.3 Core Data Analysis

As discussed in the previous section, the necessary core data to design the shafts for the final load test was obtained in the southeast corner of the site. The core data indicated that competent limestone should be present from 40 to 50 feet below the surface in all three shaft locations. From the core data, frequency distributions were created for compressive and split tension strength, Figure 148 through Figure 151, for the aforementioned depths from all 9 borings in and around the footprint of the shafts. Johnston's criteria (Florida geomaterials equation), was used to provide additional data for comparison. Using Johnston's criteria, compressive strength was estimated using each split tension result and split tension strength was estimated using each compressive strength result, doubling the amount of data available for analysis.

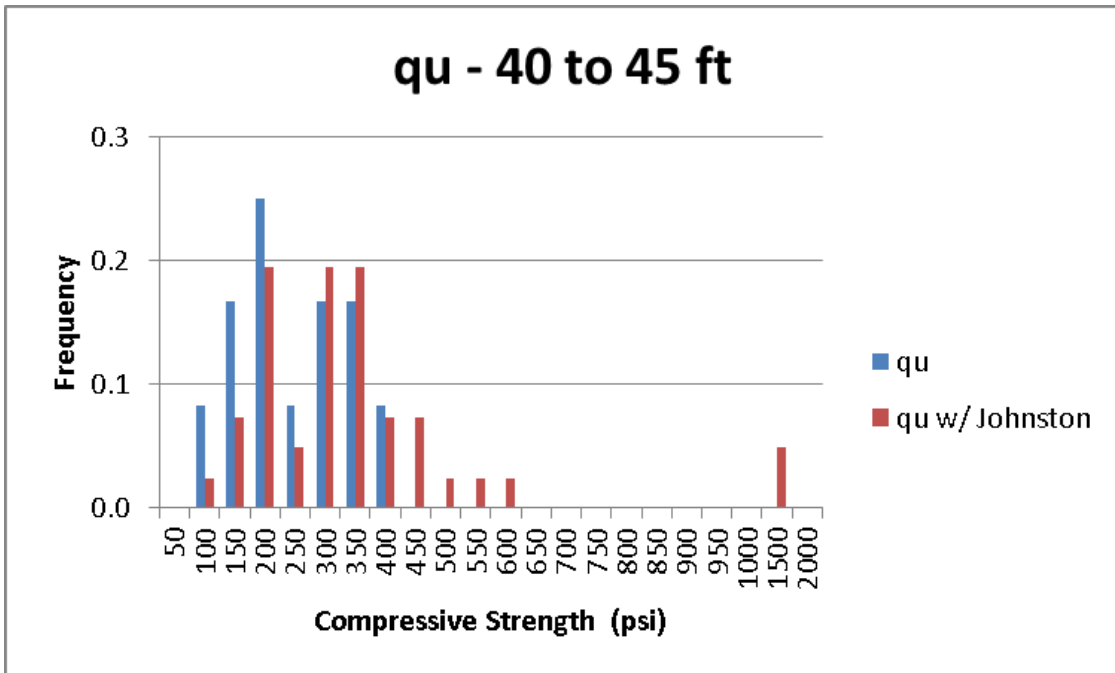


Figure 148 - q_u frequency distribution for depths 40 to 45 feet

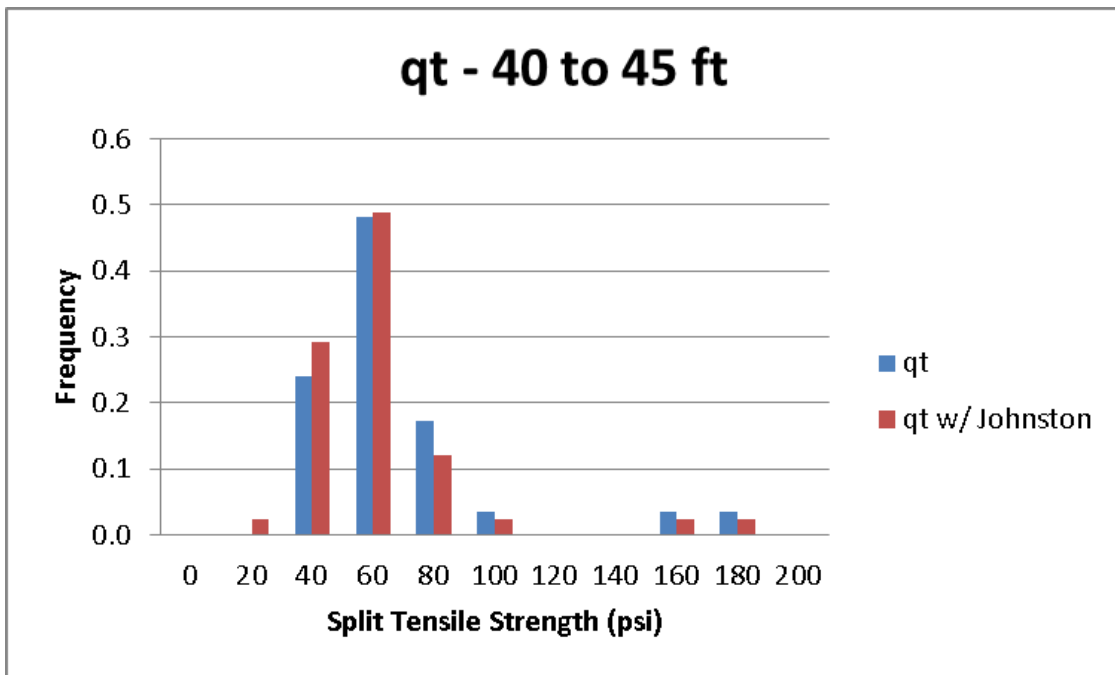


Figure 149 - q_t frequency distribution for depths 40 to 45 feet

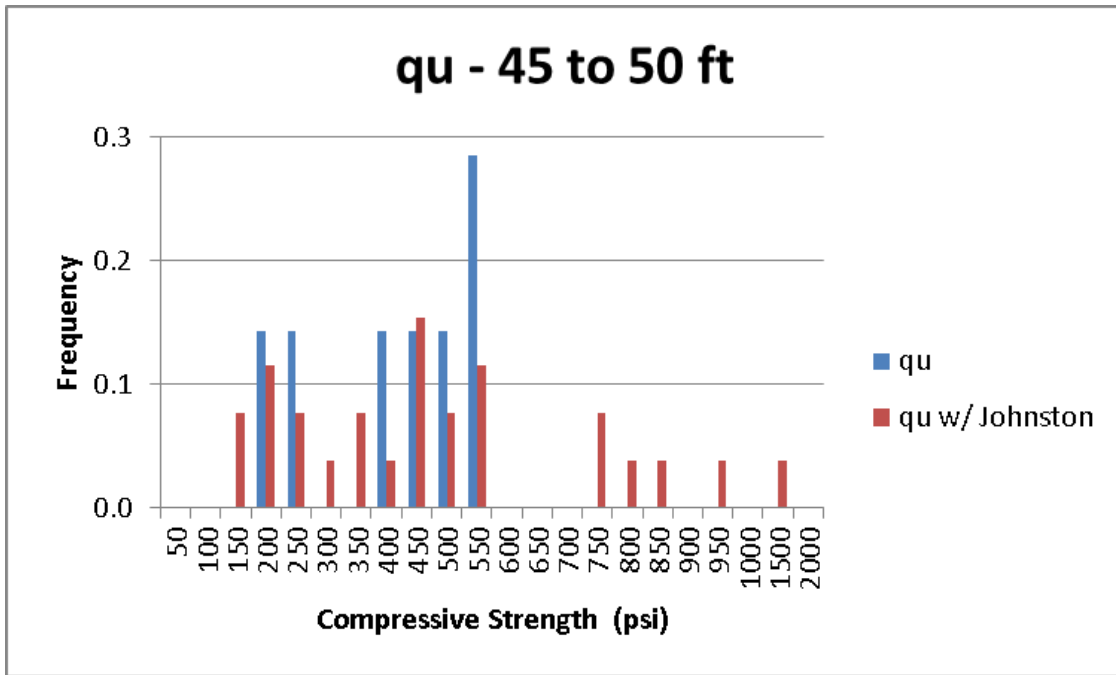


Figure 150 - q_u frequency distribution for depths 45 to 50 feet

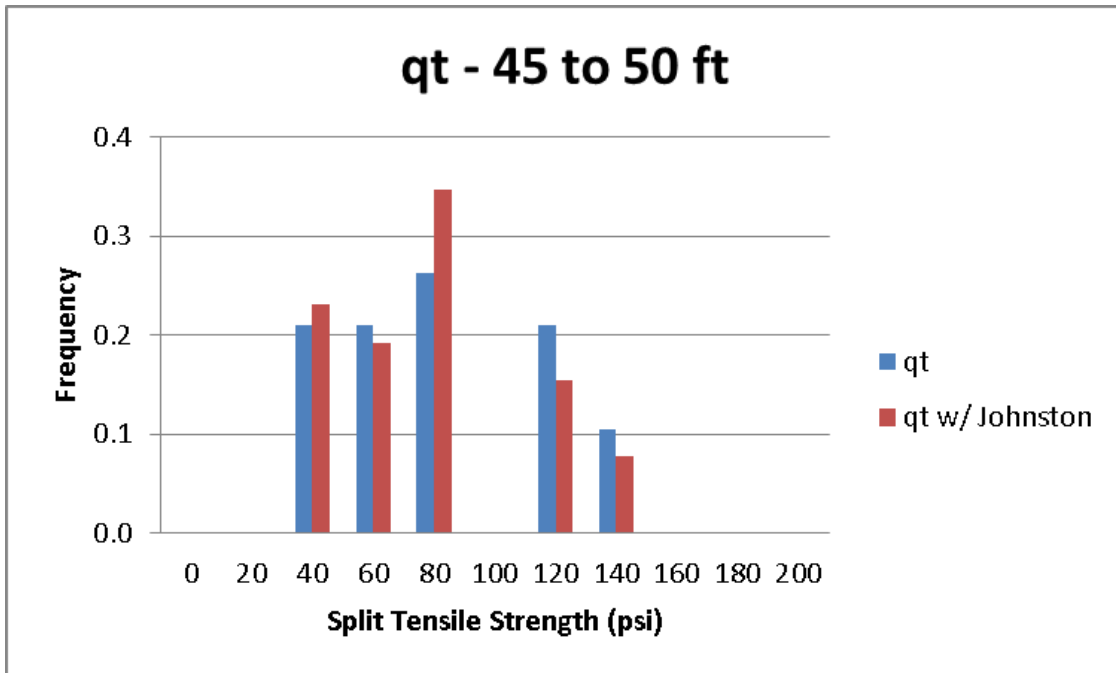


Figure 151 - q_t frequency distribution for depths 45 to 50 feet

Of interest, is the comparison of the frequency distributions where only measured q_u values are considered and the distributions where predicted q_u values using Johnston's criteria are combined with the measured q_u values. The q_u distributions using

Johnston's criteria indicated higher strength limestone may be present. The reason for the increase in strength is likely a result of the failure mode during the compression test. Johnston noted in his report that his most important condition to satisfy his criteria was that compression test results had to be in reasonable agreement with all other test methods, particularly triaxial tests on similar specimens. This is because quite often, the failure mode associated with compression testing is axial splitting, shown in Figure 152-a. A compressive failure mode should ideally involve a shear plane inclined to the sample axis, as displayed in Figure 152-b. However, rarely is the ideal shear plane ever achieved in unconfined compression testing.

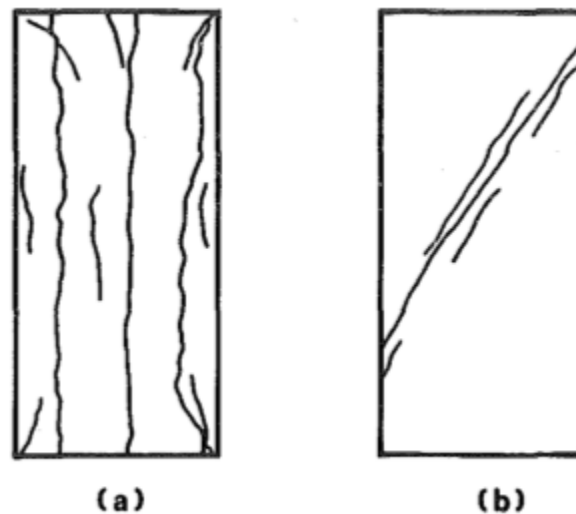


Figure 152 - Failure modes in compression tests: (a) Axial splitting, (b) shearing

The axial splitting mode may be caused by platen friction effects, which induce the development of tensile stresses within the tested sample. This ultimately leads to a failure controlled by the smaller tensile strength of the material. Therefore, the failure involving tensile splitting will give a result that can significantly underestimate the likely compressive shear strength. The tested cores were investigated for axial splitting and this was found to be the case for several samples. Therefore, higher end q_u values obtained using Johnston's criteria were considered during the shaft designs. Frequency distributions for skin friction in each layer are presented in Figure 153 and Figure 154.

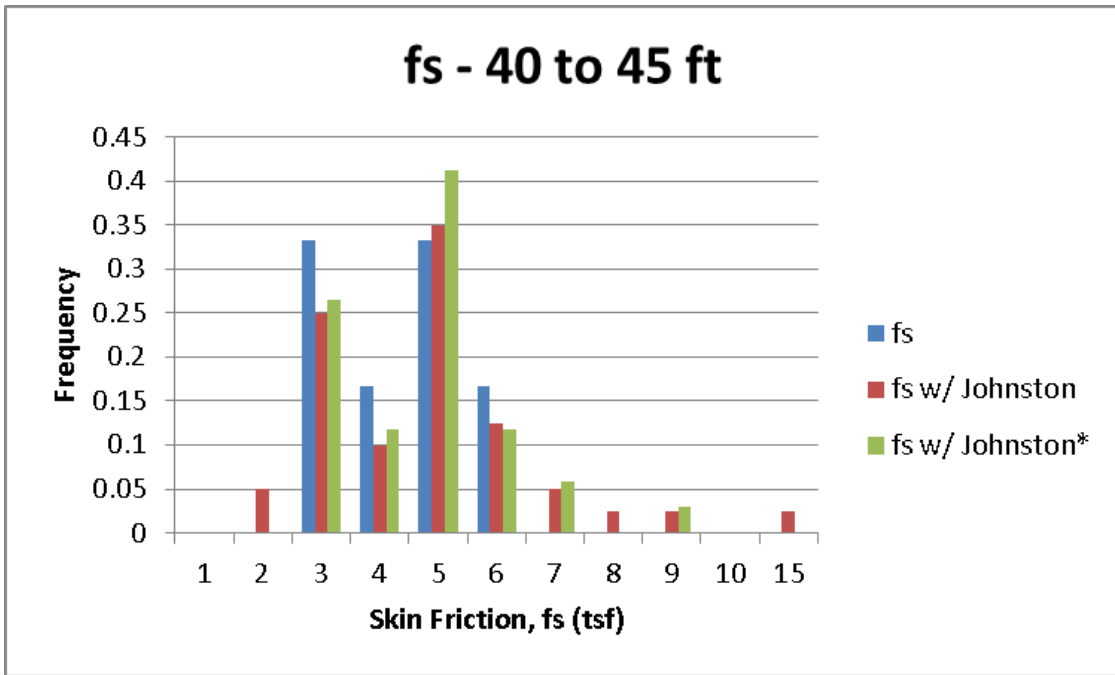


Figure 153 - Skin friction frequency distribution for depths 40 to 45 feet

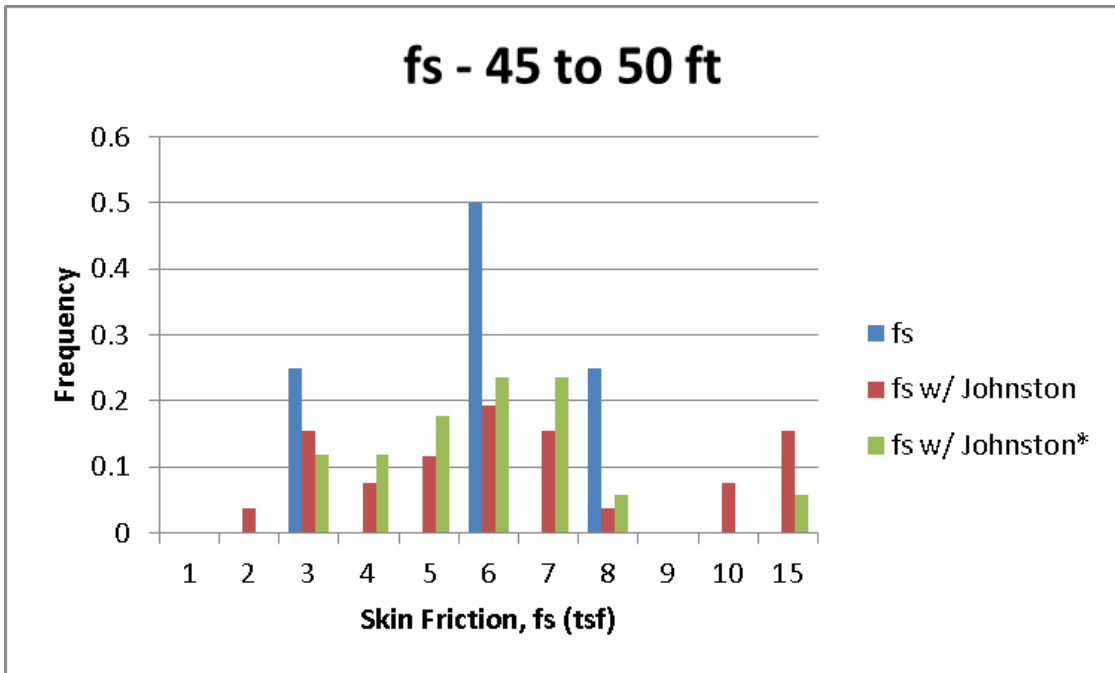


Figure 154 - Skin friction frequency distribution for depths 45 to 50 feet

After investigating the frequency distributions three methods for estimating skin friction were implemented: average skin friction using measured values, average skin friction including predicted Johnston values and using measured and Johnston generated

values to determine an average and eliminating values that fell above or below one standard deviation from the mean (f_s w/ Johnston* in Figure 153). Average skin friction values were determined for each shaft by only using core data obtained from the 3 closest borings, all within five feet from the center of the shaft (i.e., East shaft only considered borings 19, 23 and 26 to determine the average skin friction using each method of analysis). The results are displayed in the following tables.

Table 81 - Estimated skin friction for depths 40 to 45 feet

Shaft	Skin Friction, f_s (tsf)		
	Average	Avg w/ Johnston	Avg w/ Johnston*
East Shaft	3.5	3.9	3.7
Test Shaft	2.9	3.9	3.9
West Shaft	4.8	5.5	4.6

Table 82 - Estimated skin friction for depths 45 to 50 feet

Depth = 45 - 50 ft	Skin Friction, f_s (tsf)		
	Average	Avg w/ Johnston	Avg w/ Johnston*
East Shaft	3.3	3.7	2.9
Test Shaft	6.5	6.2	6.4
West Shaft	6.6	6.9	5.9

The average and Johnston* values were chosen to use for MultiPier simulations. As well, variable recoveries, REC%, were considered for the simulations. This was done to account for the high degree of weathering encountered with the recovered cores. Researchers were unsure if the actual recoveries were representative of the field conditions. Due to the high degree of weathering it is likely the limited rock matrix, providing the cementation, was compromised during recovery. Using variable recoveries, higher than the actual recovery, in the simulations should account for this. The average recoveries from 40 to 45 feet for the east, test, and west shaft were 36%, 44%, and 54.7%, respectively. From 45 to 50 feet the average recoveries were 20%, 28.3%, and 42.3%, respectively. The following tables provide all of the skin friction and compressive strength values that were used in the MultiPier simulations.

Table 83 - Limestone properties used in MultiPier simulations for the east shaft

East Reaction Shaft			
Unit Weight (pcf)	105	105	105
qu (psi)	128.8	265.9	250.5
Depth	35 - 40 feet	40 - 45 feet	45 - 50 feet
REC %	fs (tsf)	fs (tsf)	fs (tsf)
100%	2	3.5	3.3
80%	1.6	2.8	2.64
50%	1	1.75	1.65
Actual Avg. REC%	0.84	1.2	0.66
100% w/ Johnston*	2	3.7	2.9

Table 84 - Limestone properties used in MultiPier simulations for the test shaft

Test Shaft			
Unit Weight (pcf)	105	105	105
qu (psi)	128.8	133.7	505.6
Depth	35 - 40 feet	40 - 45 feet	45 - 50 feet
REC %	fs (tsf)	fs (tsf)	fs (tsf)
100%	2	2.9	6.5
80%	1.6	2.32	5.2
50%	1	1.45	3.25
Actual Avg. REC%	0.734	0.995	1.3
100% w/ Johnston*	2	3.9	6.4

Table 85 - Limestone properties used in MultiPier simulations for the west shaft

West Reaction Shaft			
Unit Weight (pcf)	105	105	105
qu (psi)	128.8	250	458
Depth	35 - 40 feet	40 - 45 feet	45 - 50 feet
REC %	fs (tsf)	fs (tsf)	fs (tsf)
100%	2	4.8	6.6
80%	1.6	3.84	5.28
50%	1	2.4	3.3
Actual Avg. REC%	0.42	2.63	1.39
100% w/ Johnston*	2	4.6	5.9

The strengths for the layer between depths 35 to 40 feet were assumed values. This was included in the analysis because recoveries were made at these depths. However, only two split tension tests were able to be performed. Both q_t values were approximately 240 psi which equates to a compressive strength of approximately 2100 psi using Johnston's criteria. Because rock was present within this layer, researchers felt it appropriate to model this layer as rock rather than a clay layer. Therefore, a skin friction value of 2 tsf (very soft or weathered rock) was designated for this layer in all three shaft locations and the estimated compressive strength was a product of using the skin friction equation developed by McVay et al. with Johnston criteria, solving for q_u .

$$f_s = 2 \text{ tsf} = 27.8 \text{ psi} = \frac{1}{2} \times \sqrt{q_u} \times \sqrt{q_t} = \frac{1}{2} \times \sqrt{q_u} \times \sqrt{0.436q_u^{0.825}}$$

Therefore, $q_u = 128.8 \text{ psi}$ and $q_t = 24.0 \text{ psi}$.

Above the rock layers, two separate layers were modeled. From depths 0 to 15 feet, a sandy to silty sand layer with $\gamma = 110 \text{ pcf}$ and $\phi = 30^\circ$ was modeled. From depths 15 to 35 feet a silty clay to clay layer with $\gamma = 120 \text{ pcf}$, $C_u = 2000 \text{ psf}$ and $f_s = 1 \text{ tsf}$ was modeled. The layering was used in all three shaft locations. This completed modeling the soil profile for the MultiPier simulations.

Next, the lengths of the shafts needed to be determined. This was done by running simulations for depths 45, 47.5 and 50 feet for the reaction shafts and depths 48, 50 and 52 feet for the test shaft. As well, eccentric loading due to a possible offset of the rebar cage during placement was investigated. This is a common occurrence as the rebar cage is rarely perfectly aligned within the center of the shaft and the effects needed to be considered. Therefore, simulations at each depth in the reaction shaft were performed using no offset, a 0.5" offset and a 1" offset. Moments created by offsetting the cage, Figure 155, were investigated and recorded for each simulation as well as the demand to capacity, D/C, ratios which indicate the factor of safety associated with the design. The induced load, top and bottom axial displacement, and the top lateral displacement were also recorded.

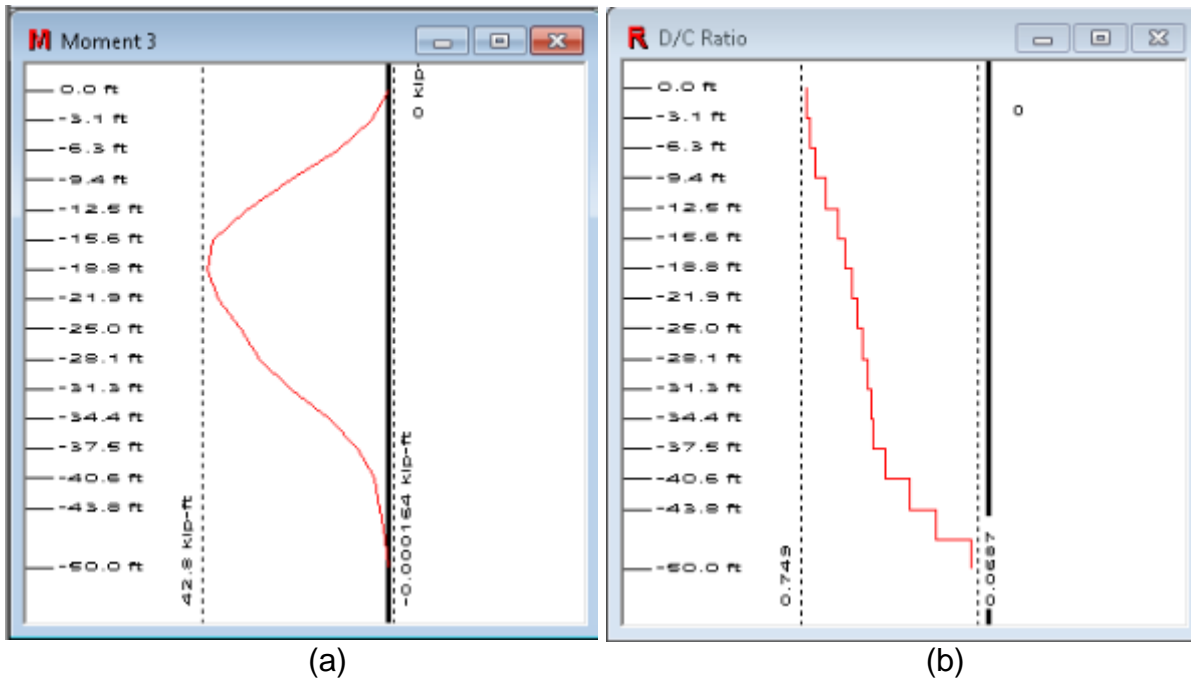


Figure 155 - MultiPier result showing (a) the induced moment by offsetting the rebar cage and (b) the demand to capacity ratio, D/C, which is used to determine the factor of safety.

Accounting for all of the variations resulted in 105 simulations that were required to complete the analysis. In total, close to 200 MultiPier simulations were performed. From these simulations the worst case scenario was investigated. This would result in the two reaction shafts having the weakest estimated capacities possible and the test shaft having the strongest estimated capacity possible. The axial displacements at the top of the reaction shafts were limited to 0.35 inches. The following are the associated loads that would result in this displacement if the reaction shafts were at the weakest capacity estimates:

$$P_{ERS} = 610 \text{ kips}$$

$$P_{WRS} = 744 \text{ kips}$$

The test shaft simulations were limited to 1 inch of axial displacement at the top of the shaft. This was done because the resulting displacement at the bottom of the shaft for the estimated soil conditions resulted in an axial displacement that typically ranged from 0.8" to 0.9". The typical displacement range for mobilizing drilled shafts in limestone is generally 0.2" to 0.4" therefore a displacement between 0.8" and 0.9" ensures full mobilization with a factor of safety of nearly two. Modeling the limestone with the strongest estimated rock strength would require a load of 1460 kips to provide an axial displacement of 0.835" at the bottom of the shaft. The combined load from the reaction shafts (weakest estimate) only provided a load of 1354 kips. However, applying the

combined load from the reaction shafts of 1354 kips to the test shaft would result in an axial displacement of 0.734" at the bottom of the test shaft and still provided a factor of safety close to two for fully mobilizing the test shaft.

It was thought the test shaft would not require a load this high and therefore some of the strength in the reaction shafts may not be necessary. Therefore, the plan was to install the east shaft first since it was estimated to be the weakest. The test shaft would then be installed. Based on the monitoring results for the east reaction shaft and the test shaft, the west reaction shaft length may be able to be reduced as the associated strength with the 50 foot embedment may not be needed. If the west reaction shaft was only embedded to 45 feet the available load would be 628 kips with an estimated axial displacement 0.233" at the bottom of the shaft (0.35" at the top). This would be nearly identical to the east reaction shaft, embedded 50 feet, with an available load of 610 kips and an estimated displacement of 0.245"; providing similar displacements in both reaction shafts and sufficient data to compare with monitoring results obtained for the reaction shafts. Based on the MultiPier simulations, the following shaft profiles and cross-sections were developed:

East Reaction Shaft

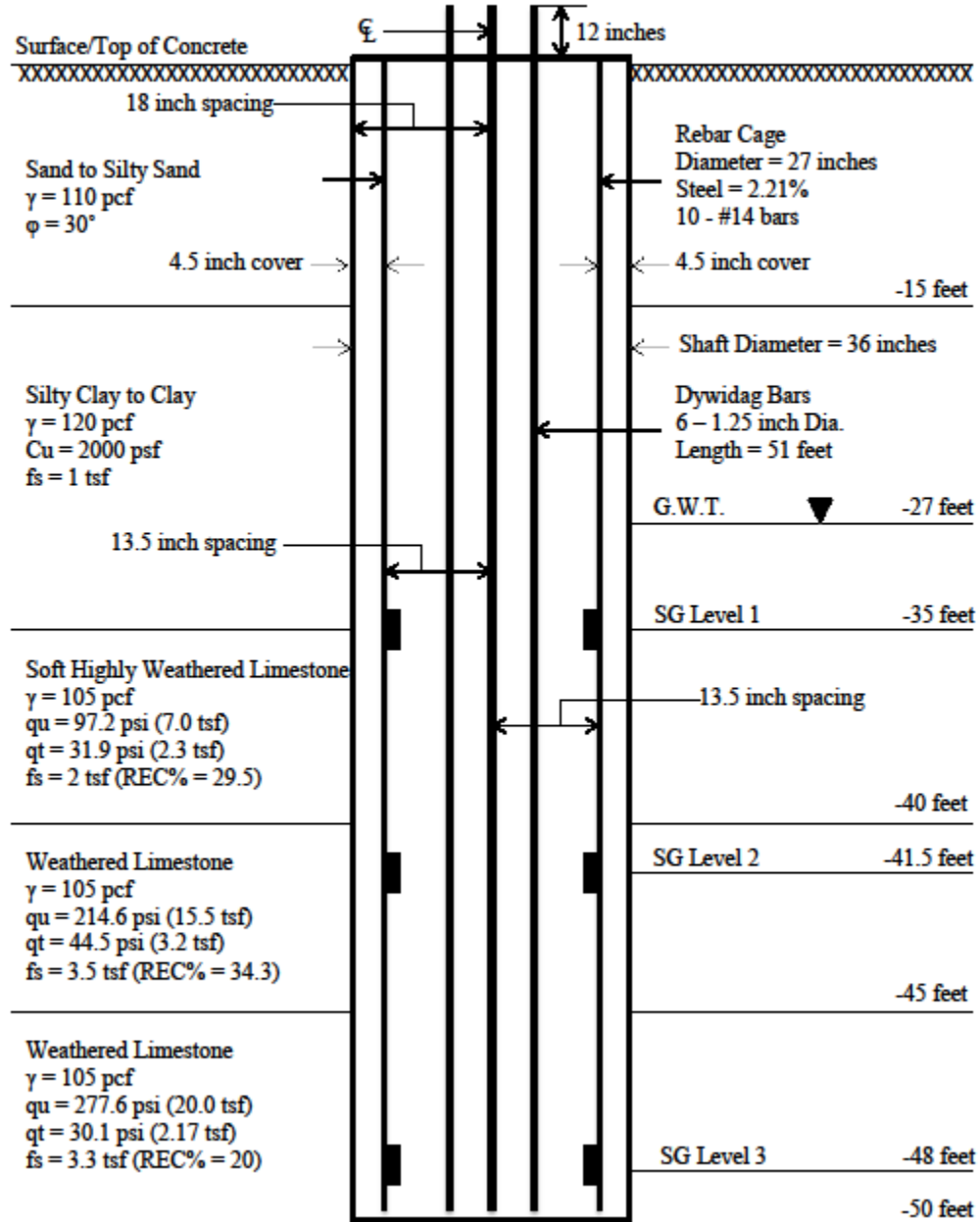


Figure 156 - East reaction shaft profile

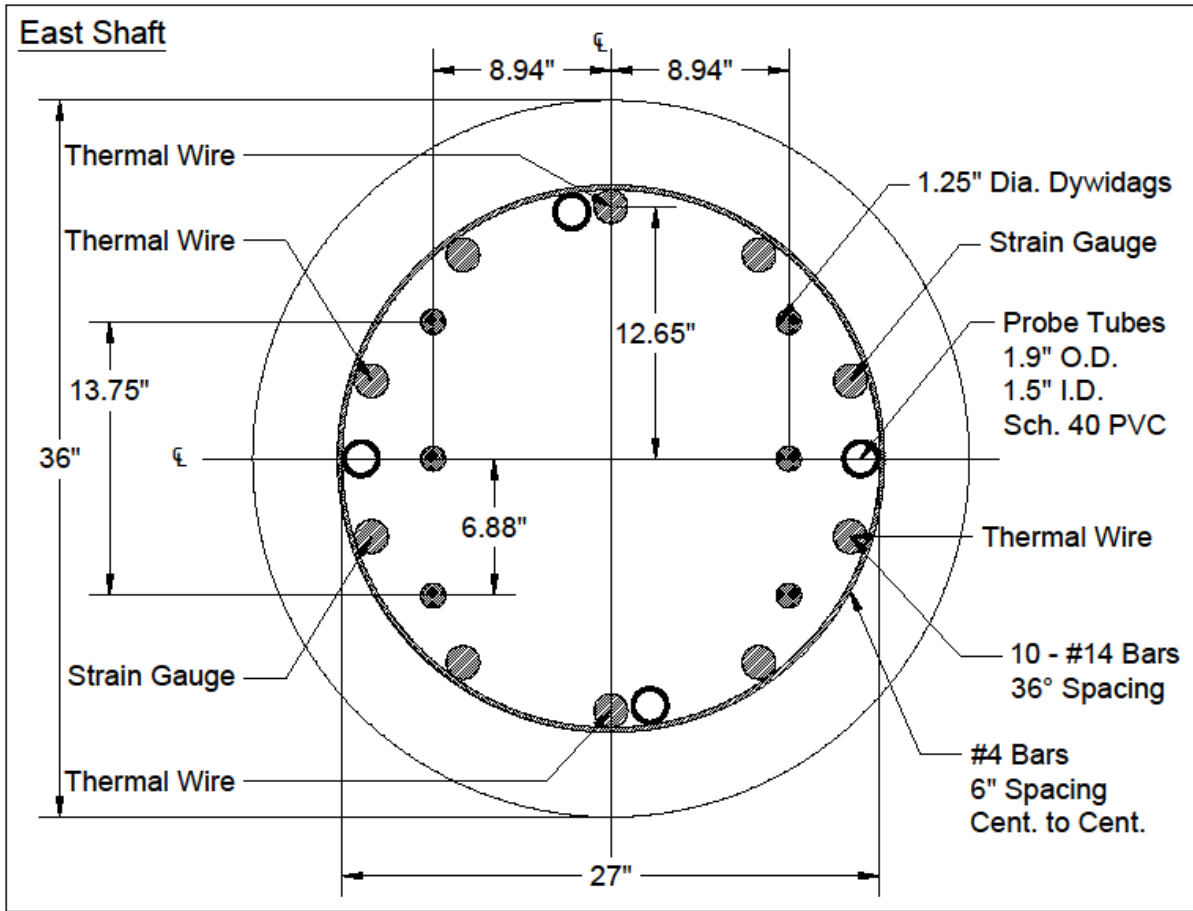


Figure 157 - East reaction shaft steel cross-section – layout 1

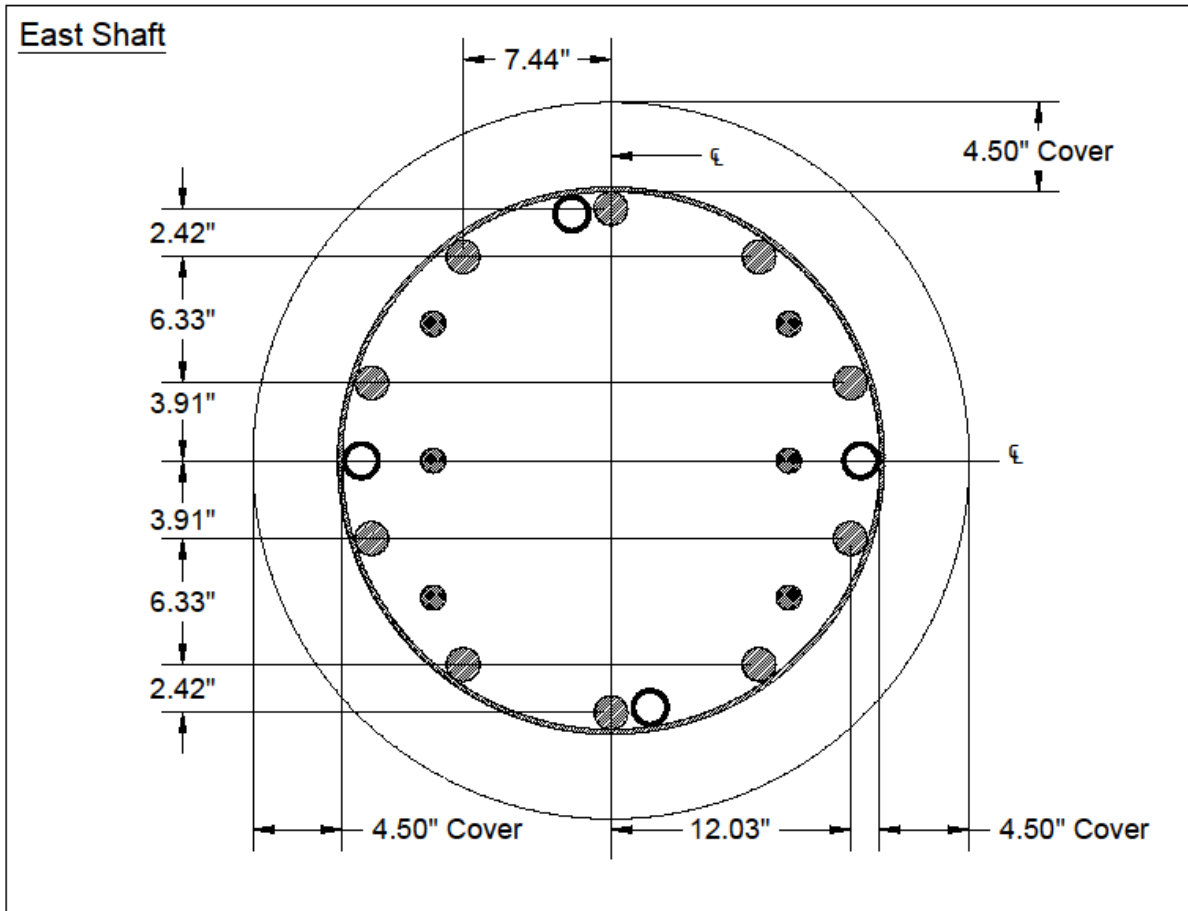


Figure 158 - East reaction shaft steel cross-section – layout 2

Test Shaft

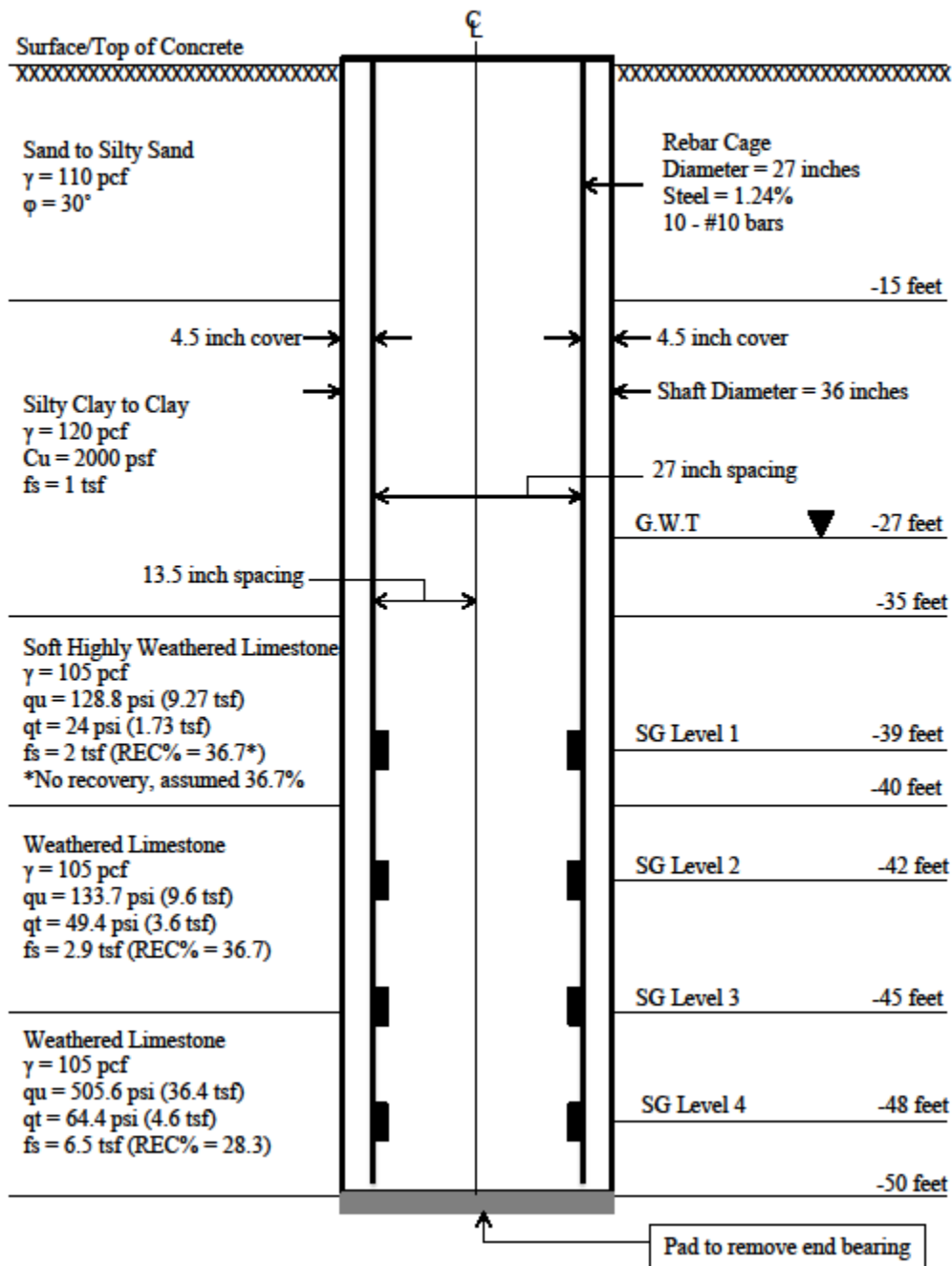


Figure 159 - Test shaft profile

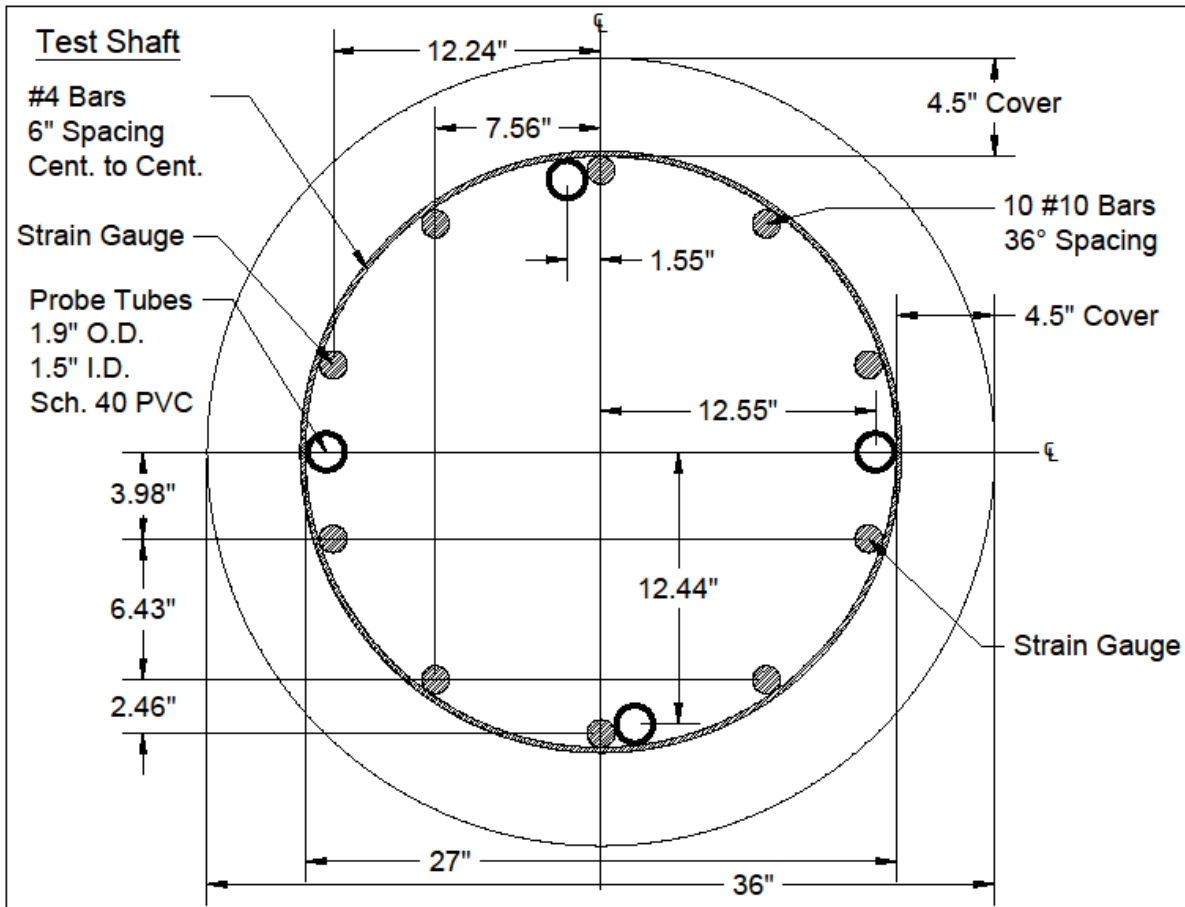


Figure 160 - Test shaft steel cross-section

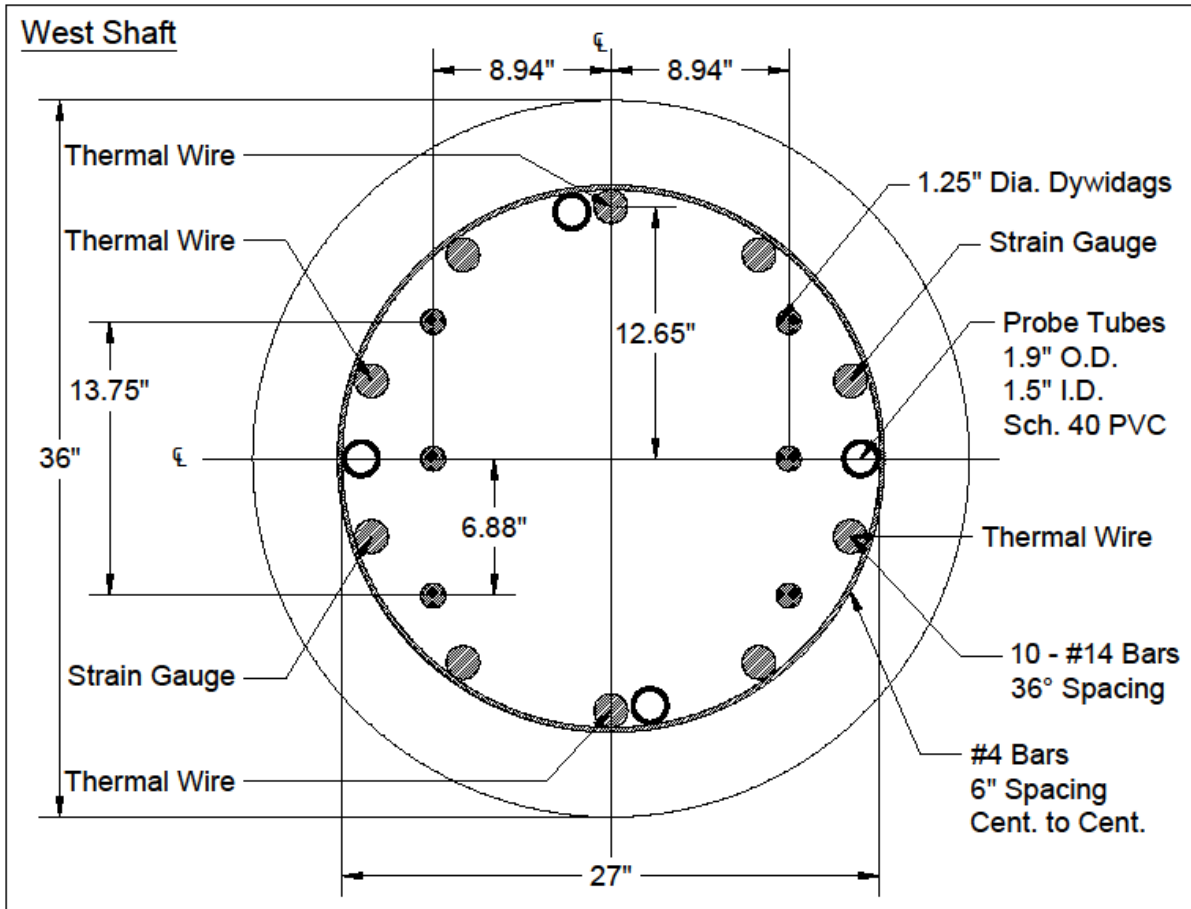


Figure 162 - West reaction shaft steel cross-section – layout 1

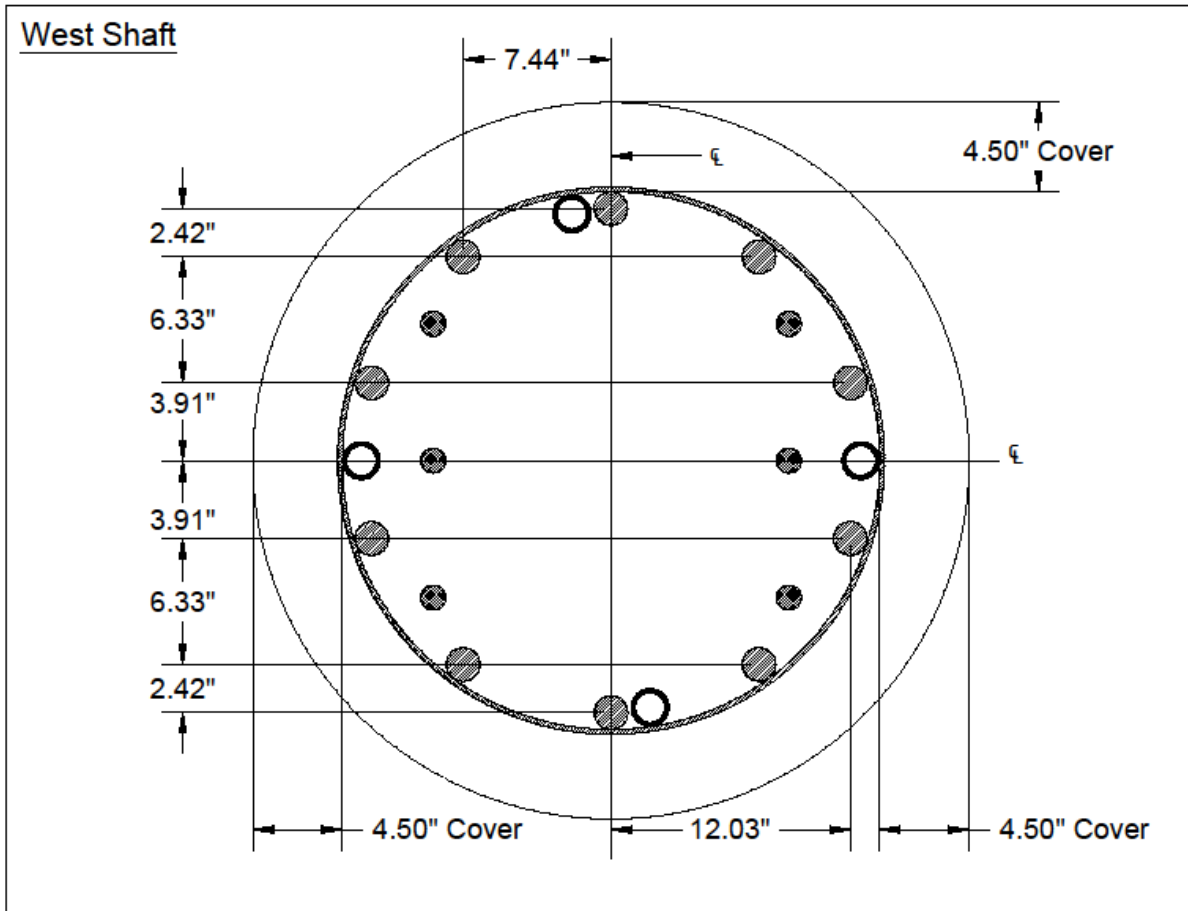


Figure 163 - West reaction shaft steel cross-section – layout 2

The reaction shaft strain gauge locations were later changed. The final design had two gauges placed 180 degrees apart at depths 40 feet and 45 feet in both shafts. A Rim-Cell was also integrated into the design at the base of each reaction shaft (Used for demonstration purposes only, analysis not included in this report). This concluded the shaft designs for the load test. Shaft spacers were used to ensure the planned rebar cage alignments were achieved. Thermal probes and thermal wire were used to analyze the alignment (Used for demonstration purposes only, analysis not included in this report). The pad at the bottom of the test shaft was tied onto the bottom of the cage in an attempt to remove end bearing and provide additional strength comparisons.

4.4 Drill Rig Investigation

Reliable Constructors, Inc. was chosen as the drilling contractor to perform the shaft installations. Reliable had several drill rigs to choose from including a Watson, Bayshore Systems Lo-drill, and a SoilMec SR30 drill rig. Out of the available rigs in their fleet, the SoilMec SR30 drill rig was chosen for the shaft installations, Figure 164.



Figure 164 - SoilMec SR30 drill rig

The SR30 was chosen because it was a crawler rig with excellent maneuverability and the drill rig was fully hydraulic which is ideal for drill monitoring with the Jean Lutz monitoring equipment. Additionally, this particular drill rig was equipped with the Drilling Mate System, DMS, which had sensors already installed throughout the rig. This provided a more simplistic hydraulic tie-in for torque and crowd using the Jean Lutz sensors. Tying into the hydraulic lines where the previously installed sensors are located provides the true hydraulic pressures used to generate torque and crowd to the bit, leading to the most accurate measurements available for these two drilling parameters. As well, pre-installed sensors are typically located in an area where they are easy to access.

The SoilMec rig also added two new challenges that monitoring efforts had not faced yet. The first being the age and condition of the drill rig. In both previous monitoring trials, the drill rigs were virtually brand new without much wear on them. This could lead to the assumption that the efficiency of these rigs may have added to the success of the

pilot project monitoring results. The SoilMec rig that was selected for the final test was a four-year-old rig that had seen quite a bit of use. Therefore, it could be assumed that the efficiency of an older rig may affect the overall outcome of the monitoring results and needed to be investigated. The second challenge was that for the first time, all drilling parameters would need to be recorded by the purchased monitoring equipment from Jean Lutz. The sensor installation will be discussed in further detail in the next section.

4.5 Monitoring Equipment Installation

For both of the previous monitoring trials, Overland and Little River, only one Jean Lutz sensor was installed. This was a crowd sensor installed on the IMT drill rig used at Little River. This was because both drill rigs used for the pilot project monitoring efforts had sensors already installed that provided compatible signals with the Jean Lutz data acquisition module, DAQ (The DIALOG). However, the SoilMec sensors produced signals that were not compatible with the Jean Lutz system. Therefore, sensors needed to be installed for rotational speed, penetration rate, torque, and crowd. As mentioned, this was a first for the research project.

4.5.1 Rotational Speed Sensor

The rotational speed proximity sensor was mounted on a stationary location on the base of the rotary table. Steel bolts were welded to the rotating collar of the rotary head where rotation occurs without wobbling. The proximity sensor detects each bolt as the collar rotates and the rotational speed can be determined directly. The steel bolts were evenly spaced around the rotary head every 60 degrees. The sensor was then calibrated by comparing rotary speeds to the DMS readout installed on the rig, and through visual inspection by counting the approximate number of rotations over a minute. The mounted sensor can be seen in Figure 165.



Figure 165 - Rotational speed sensor

4.5.2 Penetration Rate Sensor

The rotary encoder depth sensor, used to track vertical movement per unit time, was installed on the outer rim of the main cable winch. The depth sensor originally purchased from Jean Lutz was switched out for a different Jean Lutz model that is better suited for telescopic Kelly systems. Throughout the research project it was found that all of the fully hydraulic rigs used in the monitoring trials were equipped with a telescopic Kelly and the new sensor provides much better compatibility for these rig types. The depth sensor was then calibrated by comparing the tracked movement with that of the DMS readout as well as physical measurements of movement. The mounted depth sensor is displayed in Figure 166.

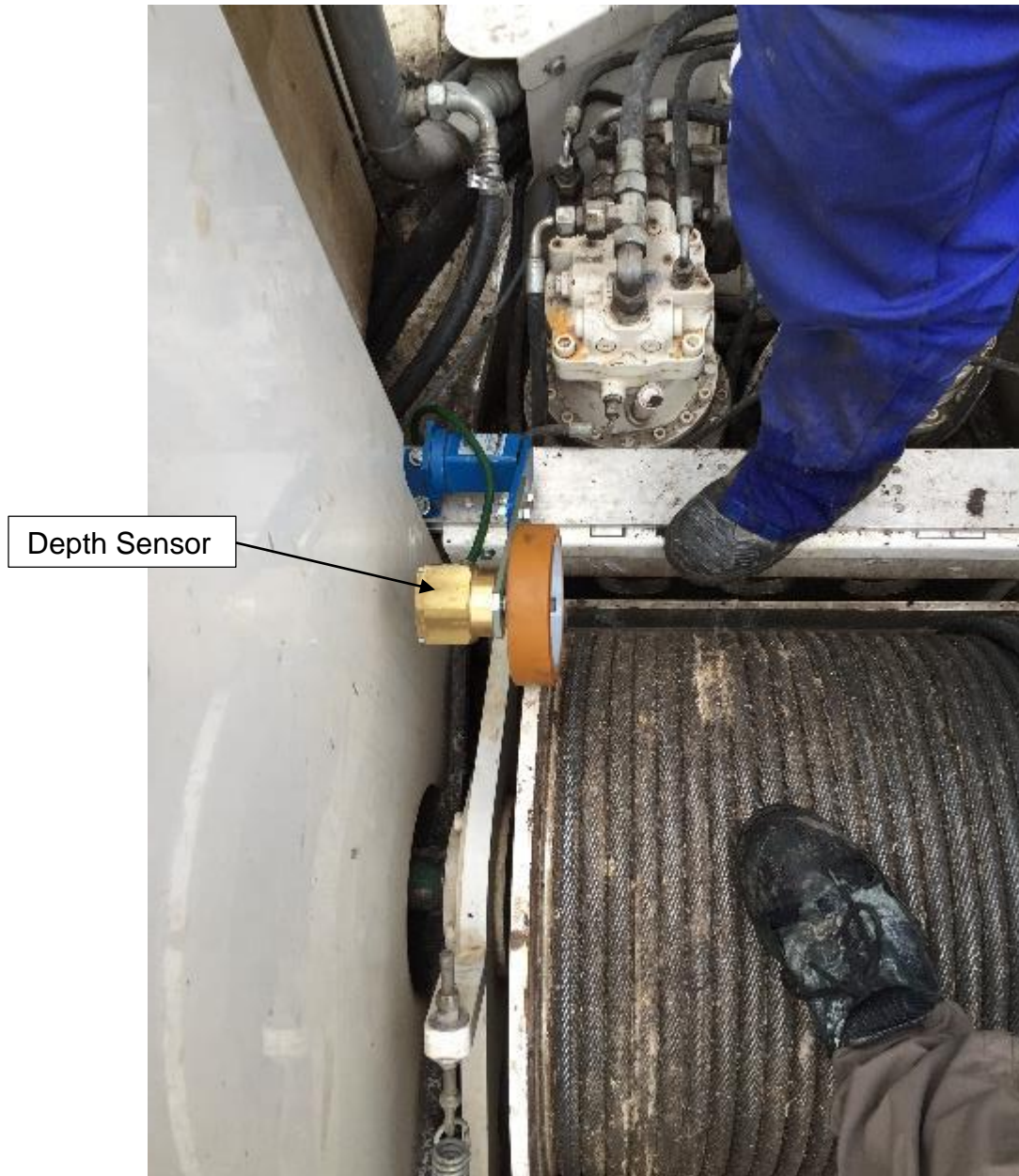


Figure 166 - Penetration rate sensor

4.5.3 Torque and Crowd Sensors

The torque and crowd sensors were tied into the hydraulic lines where the existing sensors were located. Figure 167, displays the compartment where the tie-in occurred. The junction box was also placed in this same compartment. The junction box relay was then cabled into the operators cab and the DIALOG was placed behind the rig operators seat (no pictures were available).

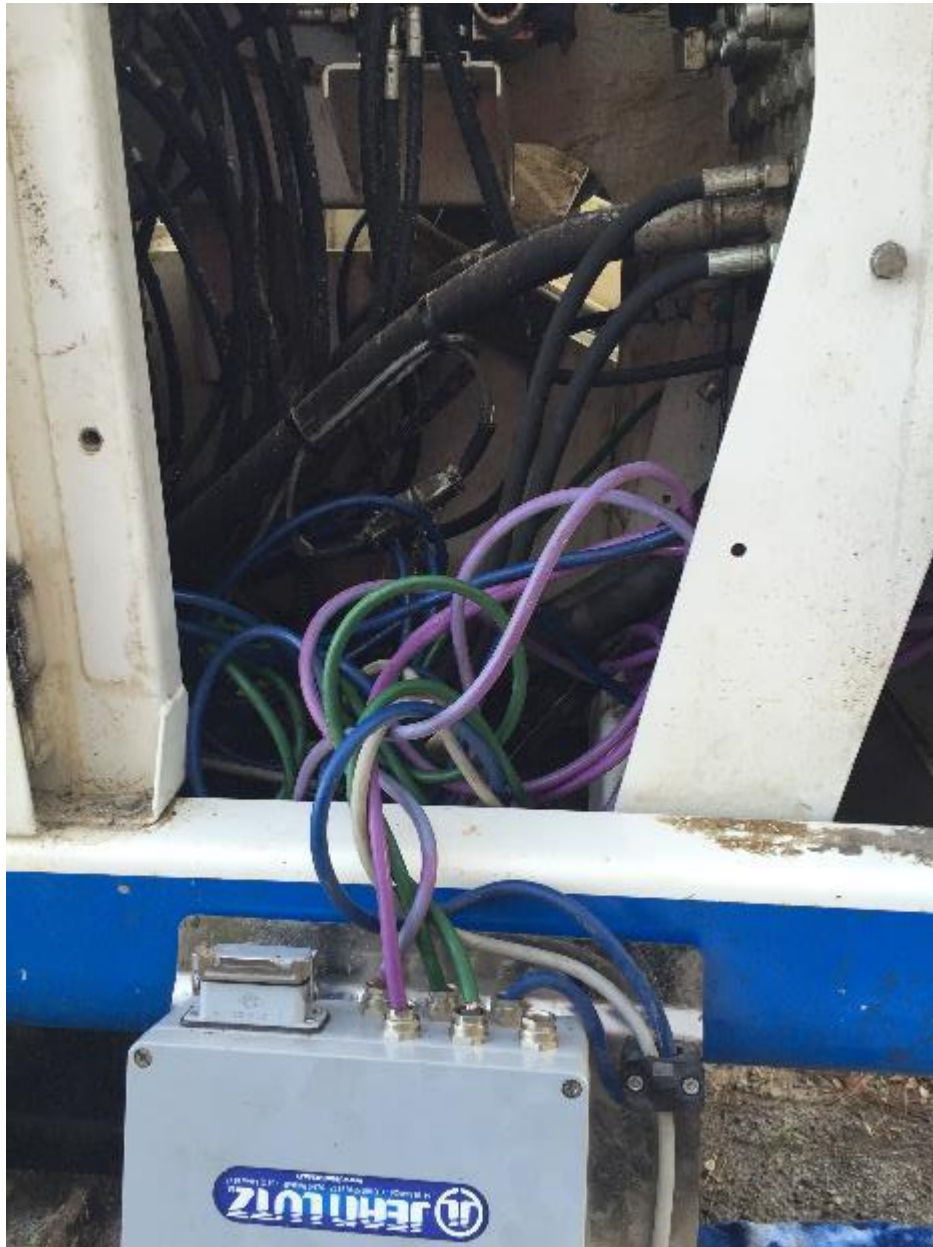


Figure 167 - Compartment where torque and crowd sensors and the junction box was placed

The following illustration gives better indication as to where the pressure transducers for torque and crowd were placed within the compartment.

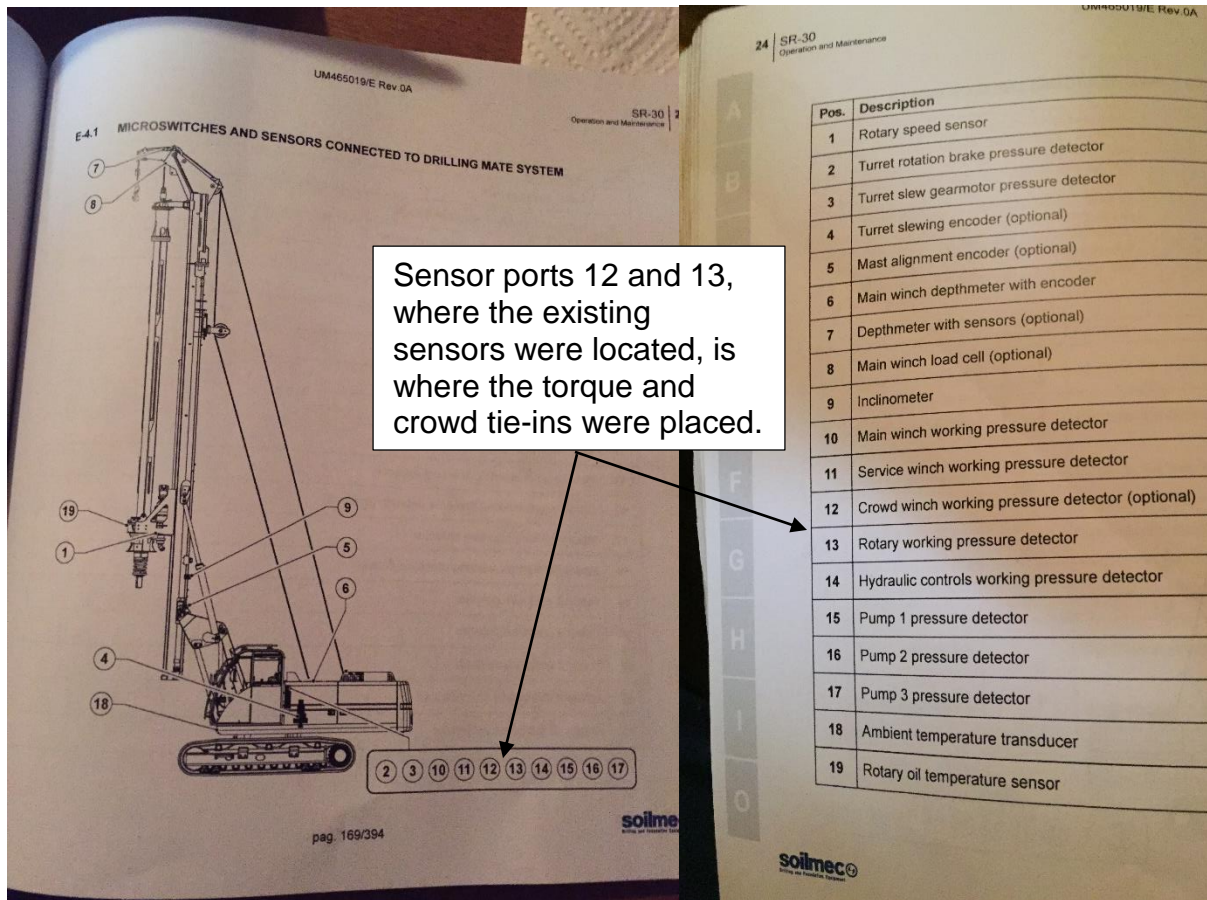


Figure 168 - Soilmec SR30 operator's manual displaying torque and crowd sensor ports

Before closing off the compartment, the pressure transducers were checked for leaks while rotating the bit. There were no leaks detected before or after the shaft installations occurred. Finally, the pressure transducers and the junction box were padded with Styrofoam to eliminate damage from vibration. This concluded the rig instrumentation and monitoring could now take place.

4.6 Rebar Cage Instrumentation

The rebar cages of all three shafts were instrumented with numerous monitoring devices. The reaction shafts were instrumented with four strain gauges, thermal integrity wire, CSL tubes (also used for thermal probe), custom shaft spacers (providing the desired cage alignment), telltale ports and a Rim-Cell at the base. The test shaft was instrumented 10 strain gauges (two gauges to determine the modulus of the concrete), thermal wire, CSL tubes (also used for thermal probe), shaft spacers and an end bearing pad to remove/reduce the end bearing. The Rim-Cell, thermal wire, and thermal probe instrumentation were only used for demonstration purposes and the

results are not included in the analysis of this report. Figure 169 through Figure 172 display all of the instrumentation that was mounted on the rebar cages.



Figure 169 - Geokon 4200 vibrating wire strain gauge attached to rebar cage

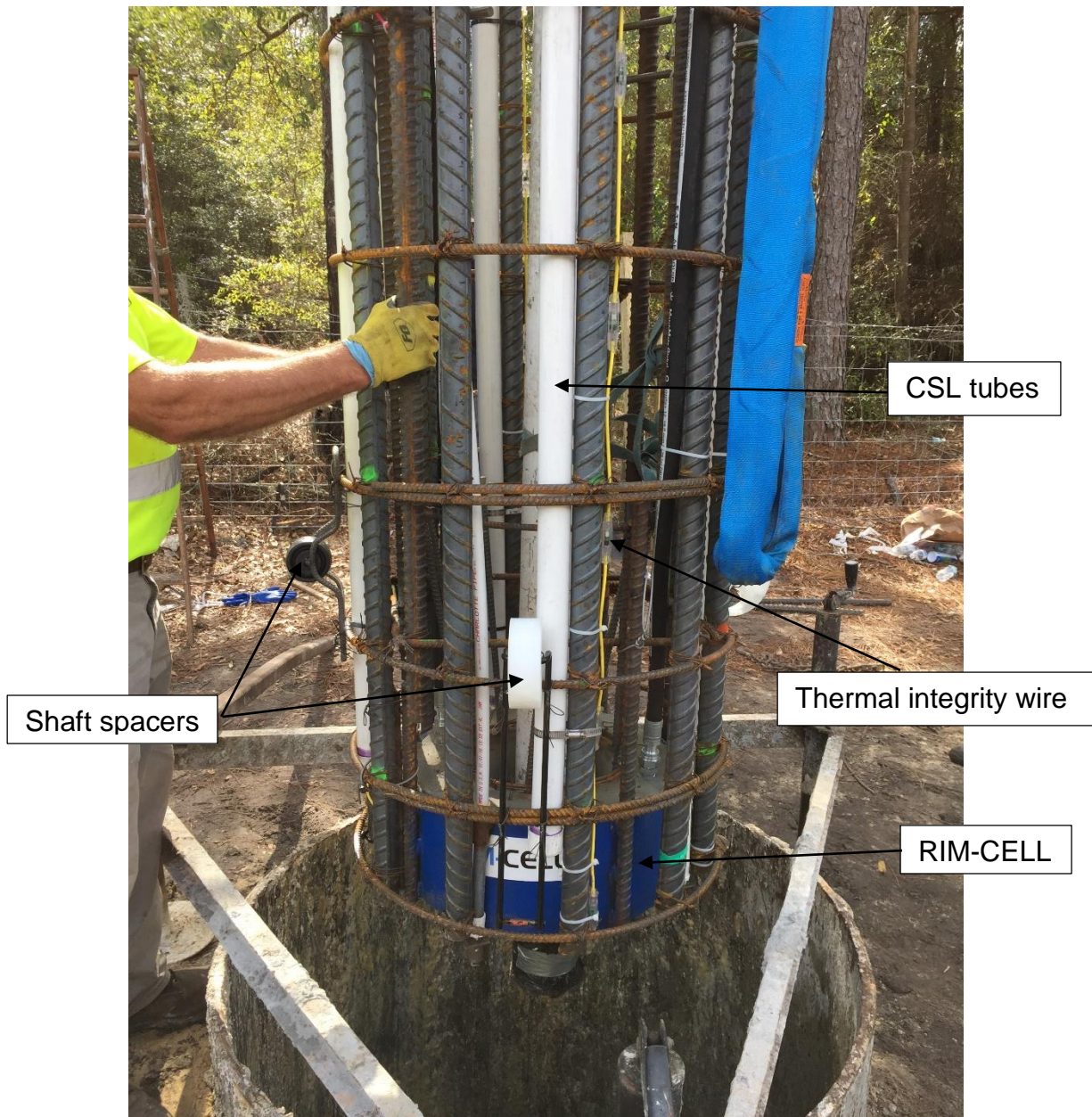


Figure 170 - East shaft rebar cage displaying instrumentation



Figure 171 - Test shaft displaying instrumentation



Figure 172 - Rebar cages displaying instrumentation

4.7 Shaft Installations

The following section provides the shaft installation procedure. The shafts were installed in the following order: east shaft, test shaft and then the west shaft.

4.7.1 East Shaft

The east shaft was first drilled to a depth of 5 feet using a 46 inch diameter earth auger and the temporary surface casing was then installed. A premixed polymer slurry was introduced to hole and the shaft was then drilled to a depth 20 feet using a 42 inch earth auger. After inspecting the shaft and excavated debris it was found that the material was a well compacted clay with traces of limestone. Therefore, the planned temporary casing was not used. The drilling continued to a depth of 50.5 feet using a 36 inch diameter rock auger. The base of the shaft was then over reamed using a clean out bucket and the hole was left open overnight. The following day the hole was over reamed again and the rebar cage was dropped in.

During drilling with the 36" auger, real time monitoring of the installation with the Jean Lutz equipment occurred. For instance, shown in Figure 173 is the rotational speed, penetration rate, crowd, and torque recorded with depth for the east shaft.



Figure 173 - East reaction shaft real-time drill monitoring



Figure 174 - Rebar cage being lifted by two cranes to reduce bending



Figure 175 - Rebar cage being placed over the hole

Once the cage was dropped in, it was then secured to chains attached to the top of the outer casing. After the cage was secured, concrete was placed in the hole.



Figure 176 - Rebar cage hung using chains and shaft being concreted

Surveying equipment was used to properly align the dywidags. Once the concrete approached the top of the shaft the chains were removed and the cage was able to settle into its final position. A 36 inch diameter beauty ring was then placed and the top of the shaft was leveled off.



Figure 177 - East shaft completed

4.7.2 Test Shaft

After experiencing the east shafts successful installation, it was decided to try and drill the test shaft using only the 36 inch rock auger bit once the temporary surface casing was placed. This was done in attempt to remove any added resistance of the test shaft during load testing from using a larger bit diameter. The decision didn't impact the shaft's construction and the entire shaft was able to be drilled using only the 36 inch bit after the surface casing was installed. Again the hole was left open overnight with

polymer slurry, and was over reamed the following day and the same procedure for cage placement and concreting was performed.

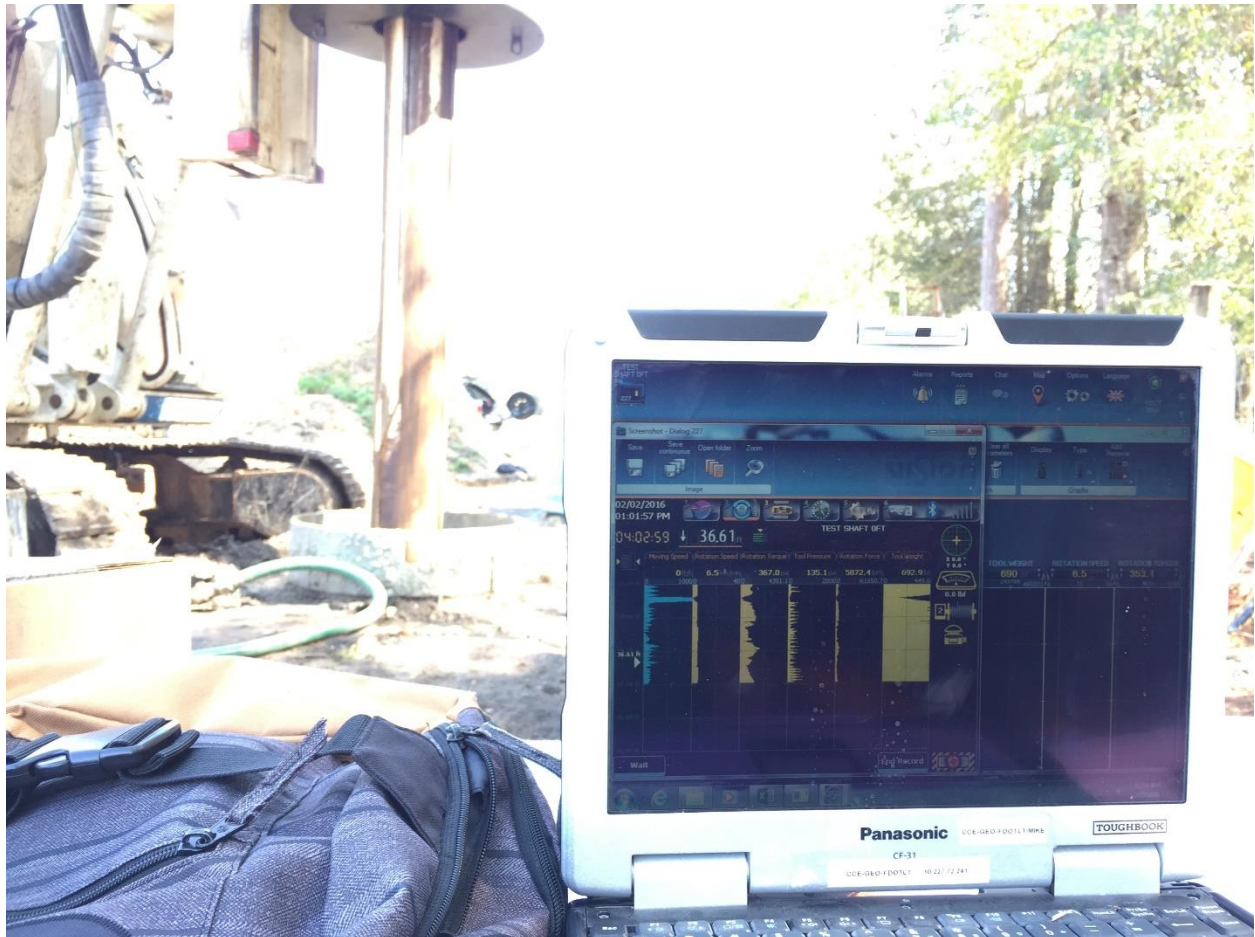


Figure 178 - Test shaft real-time drill monitoring



Figure 179 - Rebar cage being placed into the hole



Figure 180 - Rebar cage hung by chains before concreting



Figure 181 - Test shaft with beauty ring placed before final leveling

4.7.3 West Shaft

The test shaft rebar cage placement and concreting was completed in sufficient time to start drilling the west shaft the same day. The same procedure used for the east shaft was used for the west shaft and the first 20 feet of the drilling was completed the same day the test shaft was installed.



Figure 182 - West shaft real-time monitoring

Again, the temporary casing was not needed and the hole was left open overnight to be completed the next day. However, upon returning to the site the next day there was nearly a complete loss of slurry down to the base of the 20 foot excavation.



Figure 183 - West shaft displaying slurry loss

The slurry head was then raised again and monitored for loss. The slurry was somewhat declining but not at a rate that would prevent further excavation of the hole. The 36 inch rock auger was then used to start drilling in the limestone layer. However, around 24 feet of depth, the sidewalls of the shaft began to cave in and the slurry was completely lost. At this point, it was decided to backfill the hole five feet in order to fill the side wall void.



Figure 184 - West shaft cave-in and slurry loss

Once the side walls were packed with backfilled soil the slurry was reintroduced and drilling continued. However, sidewall cave-in repeatedly occurred and was believed to be a result of the fluctuating slurry head developed while advancing and removing the bit from the hole.



Figure 185 - West shaft cave-in and slurry loss down to the water table

As a result of the repeated cave-in, the desired drilling depth of 50.5 feet was not able to be completed on the second day. The slurry head was left stabilized at 27 feet of depth (at the water table) overnight. Returning to the site the next day researchers found that the sidewalls of the shaft excavation stayed relatively stable overnight. The constant slurry head method was again attempted in hopes that the sidewalls had stabilized but this was not the case. Again the sidewalls began to cave in from the fluctuating elevation head of the slurry. A decision was then made to abandon adding slurry above the cave-in location. This resolved the issue and the hole was able to be drilled to the final depth without significant cave-in of the sidewalls in the troubled zone. Once the final depth was reached, the base of the shaft was over reamed and the shaft was monitored for additional cave-in. After several runs of over reaming and monitoring, the sidewalls finally stabilized and the cage was able to be placed. The shaft was concreted using the same procedure as the first two shafts. During concreting, the hole was continuously monitored for loss of concrete. Although far more concrete was used to fill the west shaft than initially planned, the caved in portion of the shaft remained stable and concreting was able to be completed. The dywidags were adjusted to be

nearly perfectly in line with the east shaft dywidags and the center of the test shaft. The beauty ring was placed and the top of the shaft was leveled off. This completed the shaft installations for the final load test.



Figure 186 - West shaft before final leveling and elevation adjustment

4.8 Top-Down Static Load Test

The final load test was a traditional top-down static load test, following ASTM's standard quick test procedure (ASTM-D1143) for limestone socketed drilled shafts. The load test

took place at FDOT's Kanapaha site 28 days after final shaft construction. Before the load test was conducted the load frame needed to be transported to the site and constructed. The following section covers the construction procedure used at Kanapaha.

4.8.1 Load Frame Construction

The load frame construction began by placing the reaction shaft adapters on top of the reaction shafts, leveling the supports, securing the frame in place, and attaching the dywidag extensions.



Figure 187 - Reaction shaft adapter secured to the shaft

The next step was to place the girders onto the reaction shaft adapters and level the load frame.



Figure 188 - Girders being placed on the reaction shaft adapters and leveled

Once the girders were in place, straps were placed around both girders to prevent either one of them from falling off the shaft stands. Cross beams were then placed between the dywidag connector plates on top of the girders and secured using the dywidag tie-in bolts.



Figure 189 - Cross beam being secured in place on top of the girders

Once the girders were secured and leveled, the bottom loading pyramid of steel plates was lifted in place, centered above the test shaft and secured. The hydraulic jack and load cell were then set underneath the loading pyramid and centered on top of the test shaft. Finally, steel plates were added on top of the load cell to eliminate the spacing between the load cell and the loading pyramid.



Figure 190 - Completed load frame setup



Figure 191 - Steel plates being secured between the load cell and loading pyramid

4.8.2 Load Test Instrumentation

Before the load test began, instrumentation to monitor the top movement of both the reaction shaft and test shaft was installed. The reaction shafts were instrumented with two CDI dial gauges attached to a reference beam, a Leica barcode staff for real time top shaft displacement, and two tell tales that were tracked digitally in real time. The test shaft was instrumented with two CDI dial gauges attached to reference beams and two Leica barcode staffs. The loading of the hydraulic jack was tracked by a digital display on the load cell readout box.

4.8.3 Load Test Procedure

The estimated ultimate load anticipated, to completely fail the test shaft, was 1000 kips (500 tons). Therefore, the loading was implemented in 20 increments of 50 kips (25 tons) following the ASTM-D1143 procedure. After each desired load was reached, the load was then sustained for the following time increments: 0.5, 1, 2, 4 and 8 minutes. After reaching the 20th load increment (1000 kips), the shaft resistance had not been fully mobilized. At this time researchers decided to increase the load phase increments to 100 kips (50 tons) and proceed with loading until the full shaft resistance was mobilized. The final load that was applied which mobilized full resistance in the test shaft was 1800 kips (900 tons). This load was sustained for 32 minutes. Failure was noted by the continuous movement of the test shaft under the sustained loading (i.e., The shaft continuously moved for 32 minutes under the sustained 1,800 kip load). The following table lists each loading increment and the recorded load at the time of measurement:

Table 86 - Load test loading log sheet

Logged By: Mike								
Loading Phase		Time (min)						
Increment	Load (tons)	0.5	1	2	4	8	16	32
0	0	0.00	0.00	0.00	0.00	0.00		
1	25	25.00	25.05	25.05	25.02	25.05		
2	50	50.05	50.02	50.02	50.03	49.99		
3	75	74.99	75.02	75.04	75.00	75.01		
4	100	100.04	100.00	100.03	100.00	100.01		
5	125	125.00	125.03	125.01	125.01	125.00		
6	150	150.00	150.02	150.02	150.01	150.00		
7	175	175.01	175.01	175.00	175.02	175.02		
8	200	200.01	200.01	200.01	200.01	200.00		
9	225	225.02	225.01	225.00	225.01	225.01		
10	250	250.02	250.00	250.01	250.00	250.01		
11	275	275.02	275.02	275.01	275.01	275.00		
12	300	300.08	300.02	300.00	300.02	300.01		
13	325	325.01	325.05	325.05	325.01	325.01		
14	350	349.99	350.06	350.01	350.00	350.00		
15	375	375.04	375.02	375.00	375.01	375.01		
16	400	400.03	400.02	400.00	400.01	400.02		
17	425	425.04	425.02	425.00	425.01	425.01		
18	450	450.04	450.04	450.03	450.01	450.03		
19	475	475.02	475.02	475.03	475.00	475.02		
20	500	500.01	500.02	500.03	500.01	500.01		
21	550	550.02	550.04	550.01	550.01	550.03		
22	600	600.03	600.06	600.08	600.03	600.00		
23	650	648.00	649.00	650.06	649.00	650.03		
24	700	700.10	700.20	700.18	700.10	700.07		
25	750	750.15	750.10	750.15	750.25	750.07		
26	800	800.40	800.25	800.18	800.03	800.05		
27	850	849.95	850.00	850.05	850.06	850.04		
28	900	899.75	899.45	899.96	900.00	899.99	899.96	899.94

CHAPTER 5 KANAPAHA DRILLED SHAFT MONITORING AND LOAD TEST ANALYSIS

5.1 Drilling Data

The analysis began by comparing the monitored drilling rock strength data, q_u , from all shafts combined, with the measured laboratory core data at different depths. This provided comparison between the monitoring results and the core data for the site as a whole, a general comparison of measured vs. predicted strength.

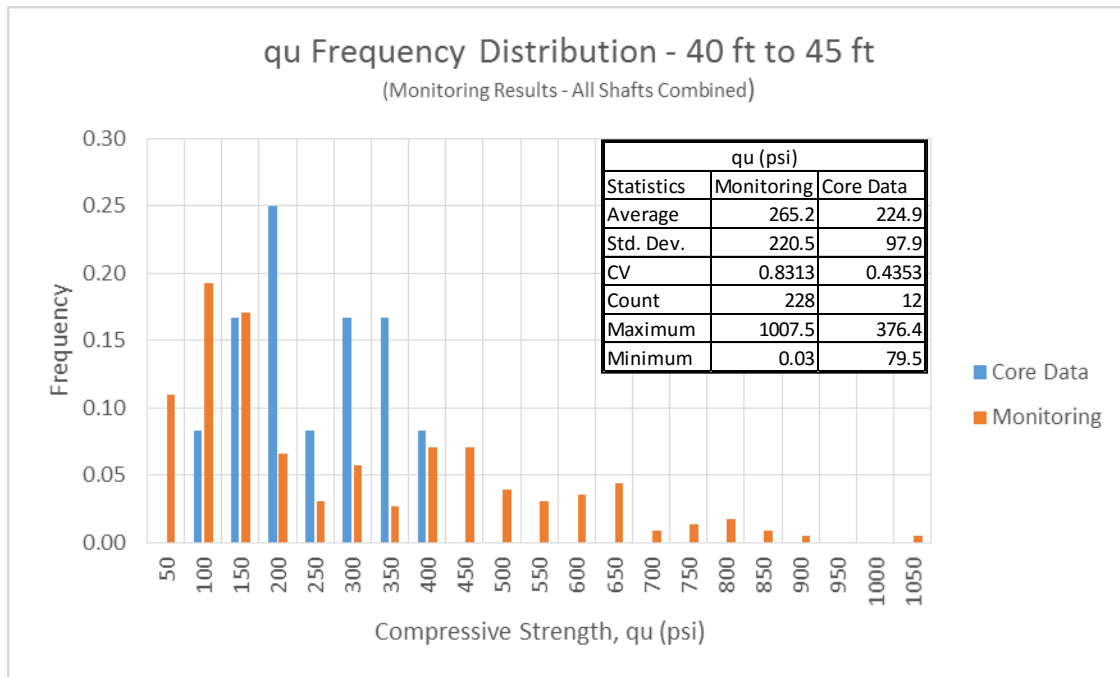


Figure 192 – q_u frequency distribution – 40 to 45 feet

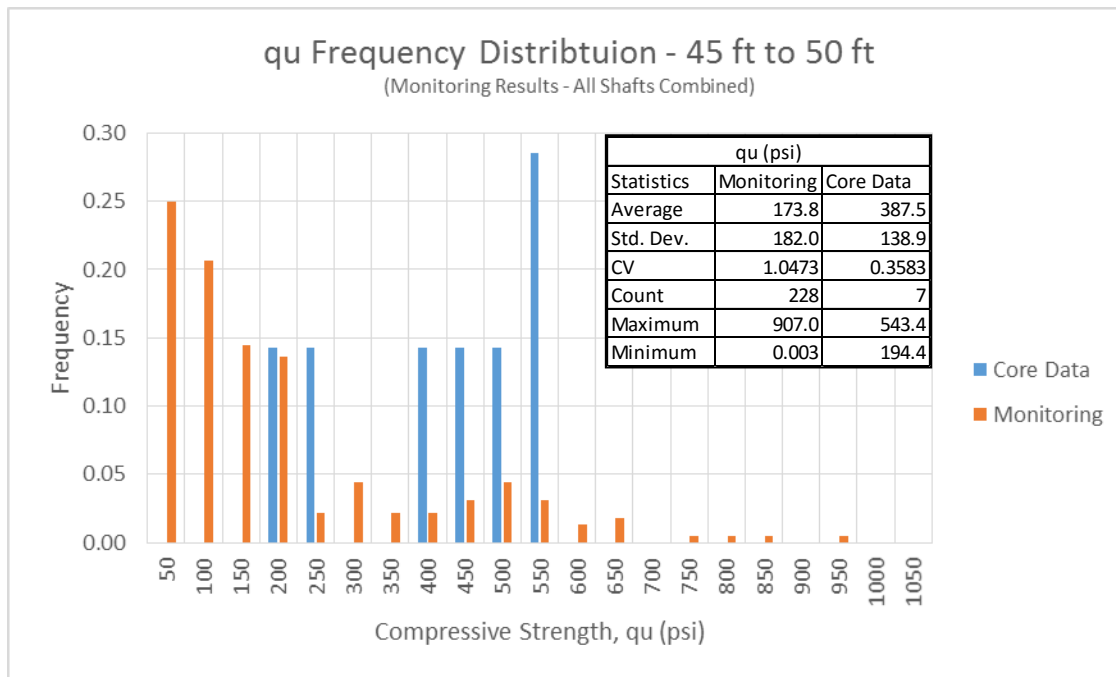


Figure 193 – q_u frequency distribution – 45 to 50 feet

From 40 to 45 feet, the strength comparison was fairly similar between the monitoring and the laboratory core data. However, from 45 to 50 feet, the monitoring indicated the strength of the rock was less than that of the lab tested core data. Also of great interest was the comparison of CV values between the core data and the monitoring results. The monitoring indicated the variability of the rock was much higher than the core data. The difference was more extreme in the bottom five feet, where monitoring indicated the CV was more than double that of the core data. This gives rise to concern for the standard practice of determining phi factors for LRFD design. As monitoring indicated the variability can be much higher than expected from typical site investigation. This will be discussed further in the next section.

5.2 Individual Shaft Analysis

The following section will cover multiple types of analysis for each individual shaft. The first analysis is similar to the previous section except the combined core data from the site is compared to each shaft individually. The results are provided here in the form of frequency distributions for each layer.

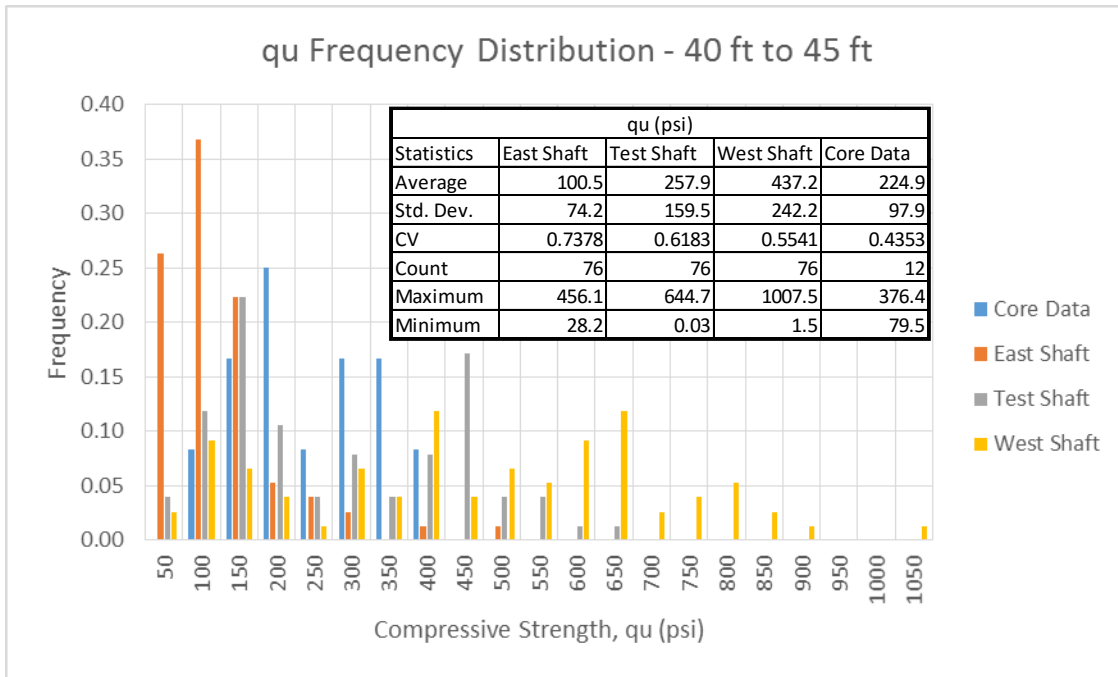


Figure 194 – q_u frequency distribution of individual shafts – 40 to 45 feet

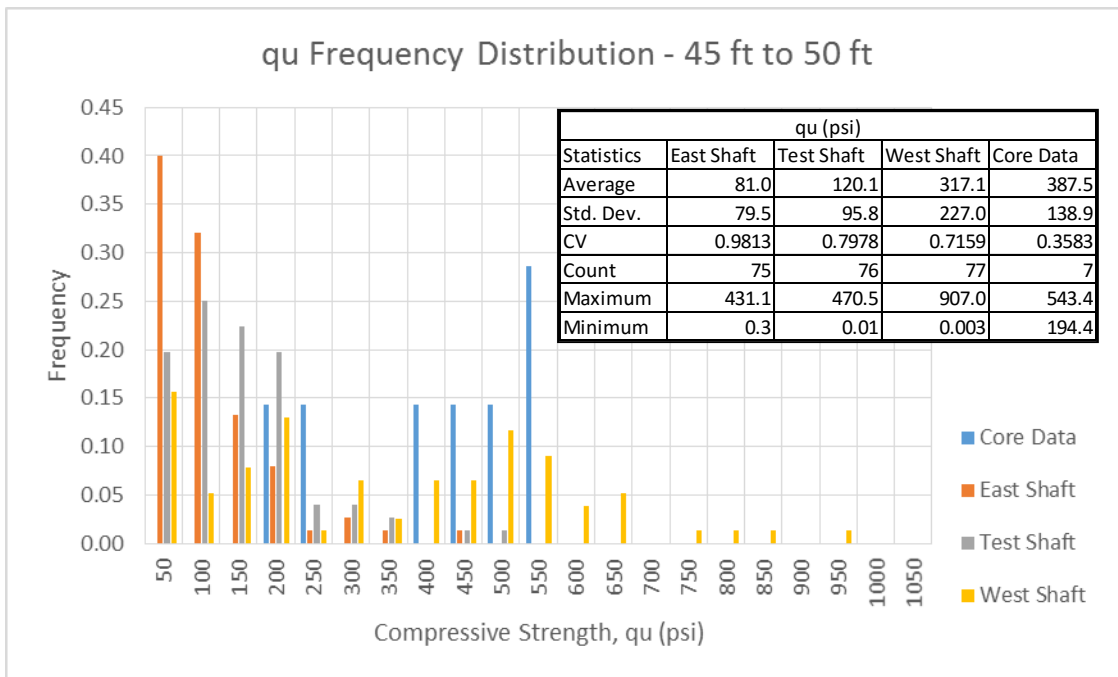


Figure 195 - q_u frequency distribution of individual shafts – 45 to 50 feet

As was predicted from the site investigation core data, the monitoring showed the strength of the rock increased moving east to west. Again, it can be seen that the monitoring indicated higher variability than the core data for all shafts in both layers. It

should also be noted that from 45 to 50 feet the core data strength estimates were much higher than that of the east and test shaft monitoring results, even though three of the seven core samples were obtained from the three borings closest to the east shaft and one of the seven core samples was obtained from the test shaft borings. This was due to poor recoveries within the depth range. Generally the recoveries for each boring location ranged from 20% to 40% (30% on average) between these depths, whereas the average recovery from 40 to 45 feet was 40%. Therefore, the only specimens recovered from 45 to 50 feet were from the most competent limestone, typically higher compressive strengths, which was not representative of the majority of the limestone found at Kanapaha. Under current FDOT practice, the outlying values (one standard deviation above and below the mean) from the core data would be eliminated and a new average would be found. Following this methodology the new average would be even higher, 439.7 psi, providing an even larger overestimate compared to monitoring results. Possible solutions using new design methods were investigated.

For the analysis, new design methods using the core data were compared to the q_u monitoring results for each shaft at different depths. The following methods were used:

Core Data:

Simply uses the q_u values obtained from lab testing. The SFH recommended elimination method was not used for comparison because in all but one location, three or fewer q_u values were obtained from lab testing.

Johnston:

Implements Johnston's criteria to generate additional q_u values using obtained q_t values from laboratory core testing. The q_u values are generated using the q_t/q_u versus q_u relationship previously discussed.

J.C. FDOT:

Follows the same approach as the Johnston method. However, once the new q_u values are generated, a new mean and standard deviation is found and anything outside of one standard deviation above and below the mean is eliminated (SFH method).

Rodgers:

Uses Johnston criteria to generate additional q_u values similar to the Johnston method. All of the q_u values, original and Johnston generated, are then multiplied by their respective recoveries, REC%. The original values, including Johnston generated, are then combined with the new reduced values obtained using REC%. This doubles the amount of q_u values that the Johnston method produces and provides far more spread

to the data by estimating lower end values that are not accounted for by core testing but are present within drilled strata.

The results of the analysis are provided here:

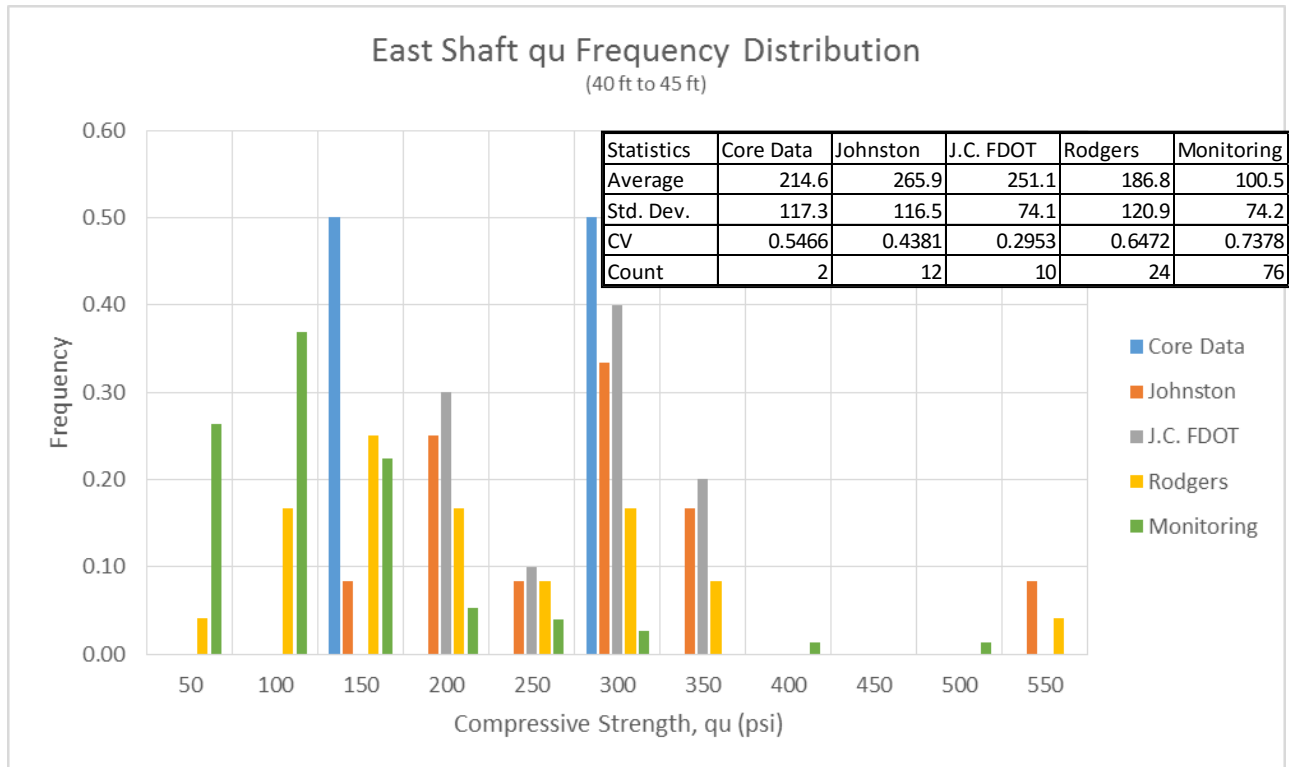


Figure 196 – East Shaft q_u Frequency Distribution, 40 ft to 45 ft.

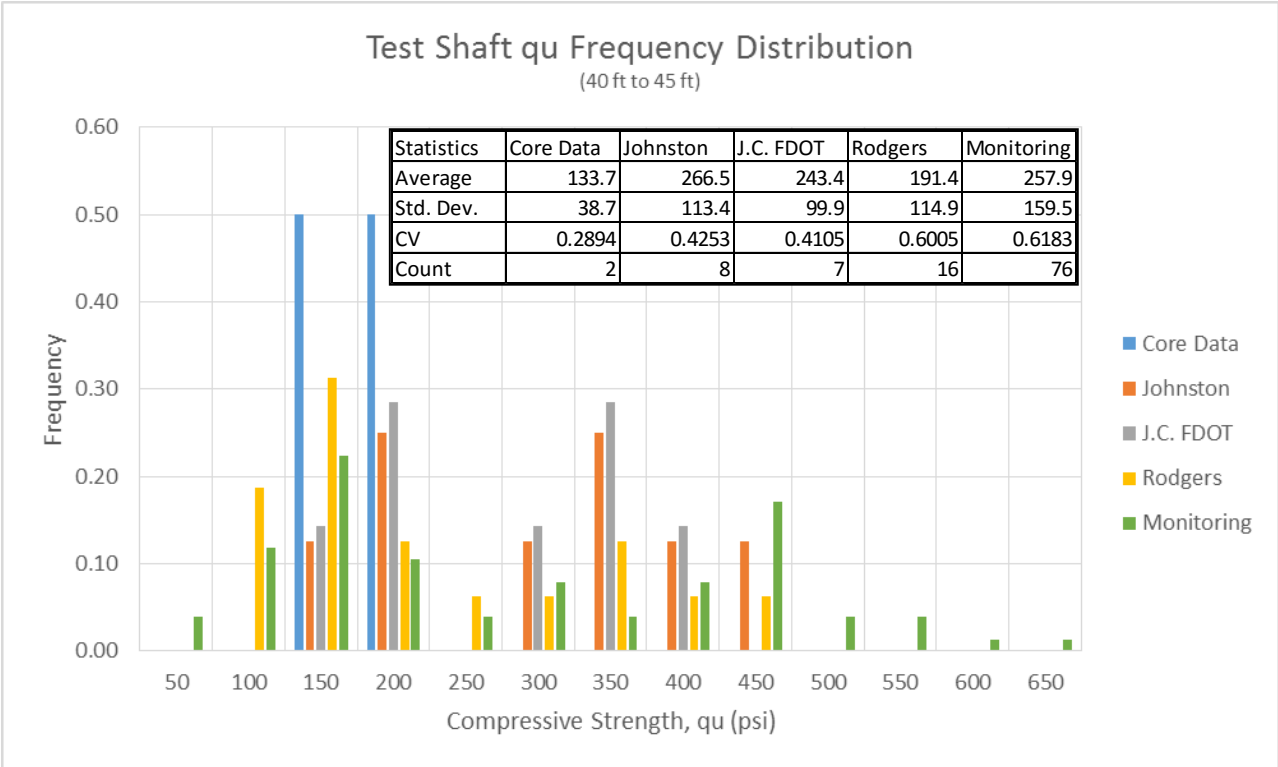


Figure 197 - Test Shaft q_u Frequency Distribution, 40 ft to 45 ft.

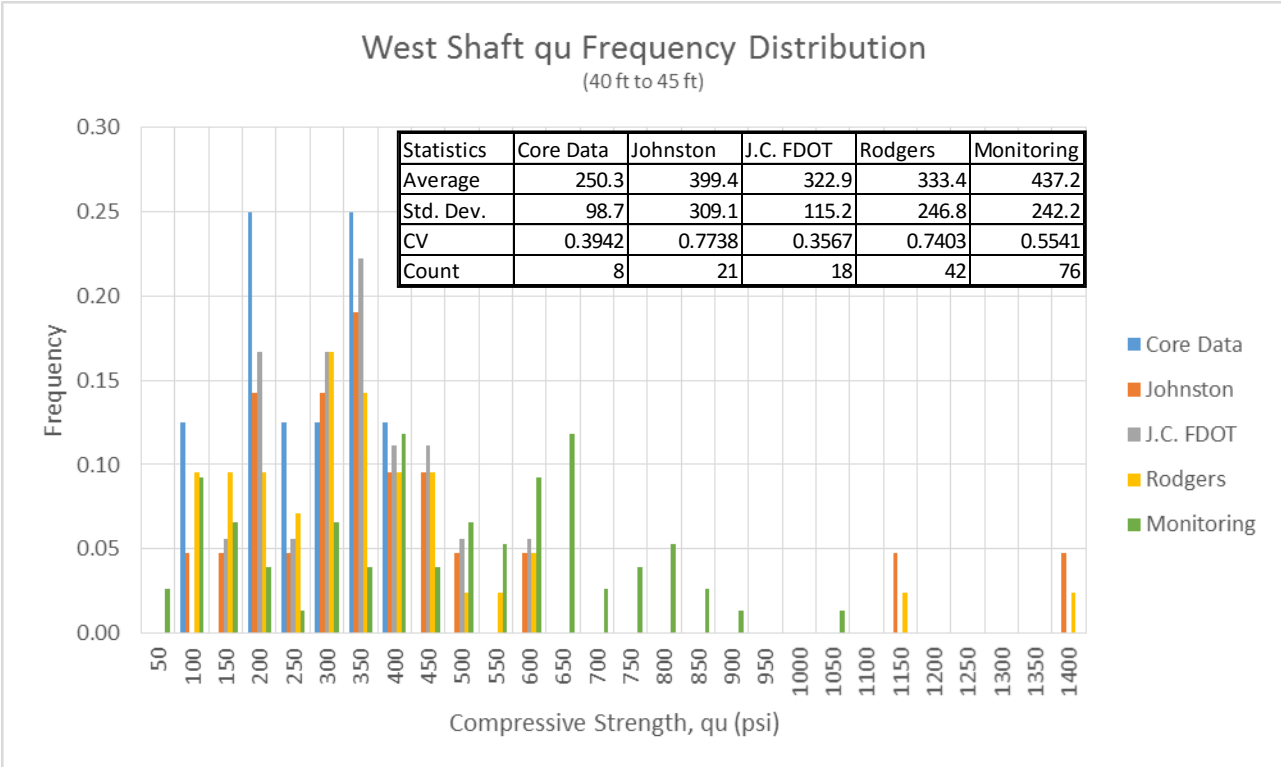


Figure 198 - West shaft q_u frequency distribution, 40 ft to 45 ft.

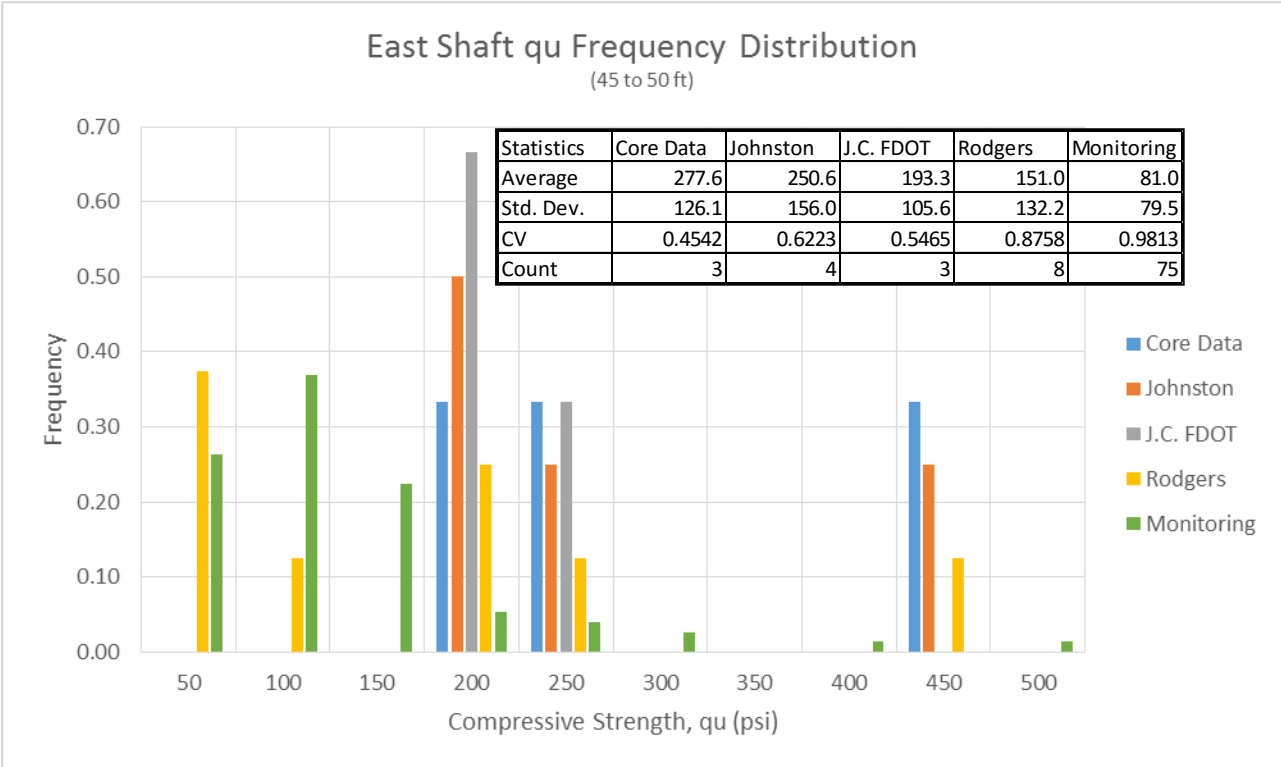


Figure 199 - East shaft q_u frequency distribution, 45 ft to 50 ft.

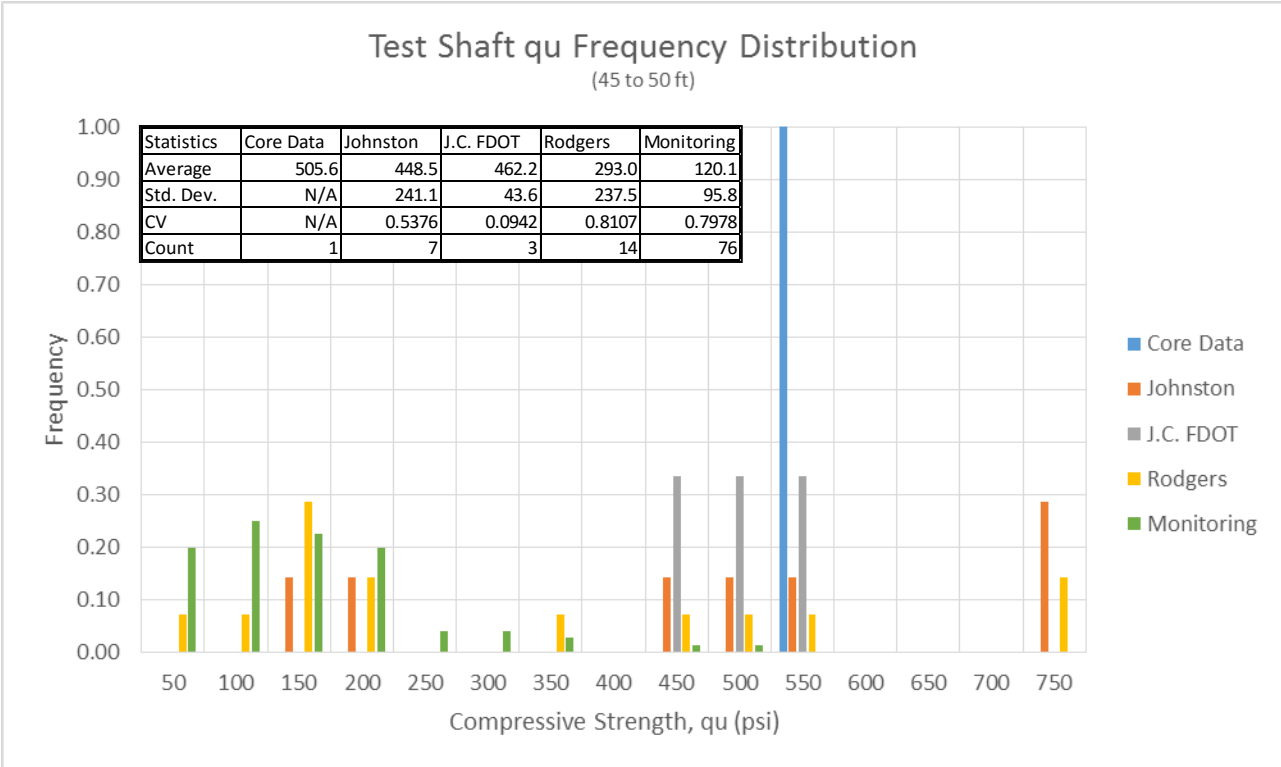


Figure 200 - Test shaft q_u frequency distribution, 45 ft to 50 ft.

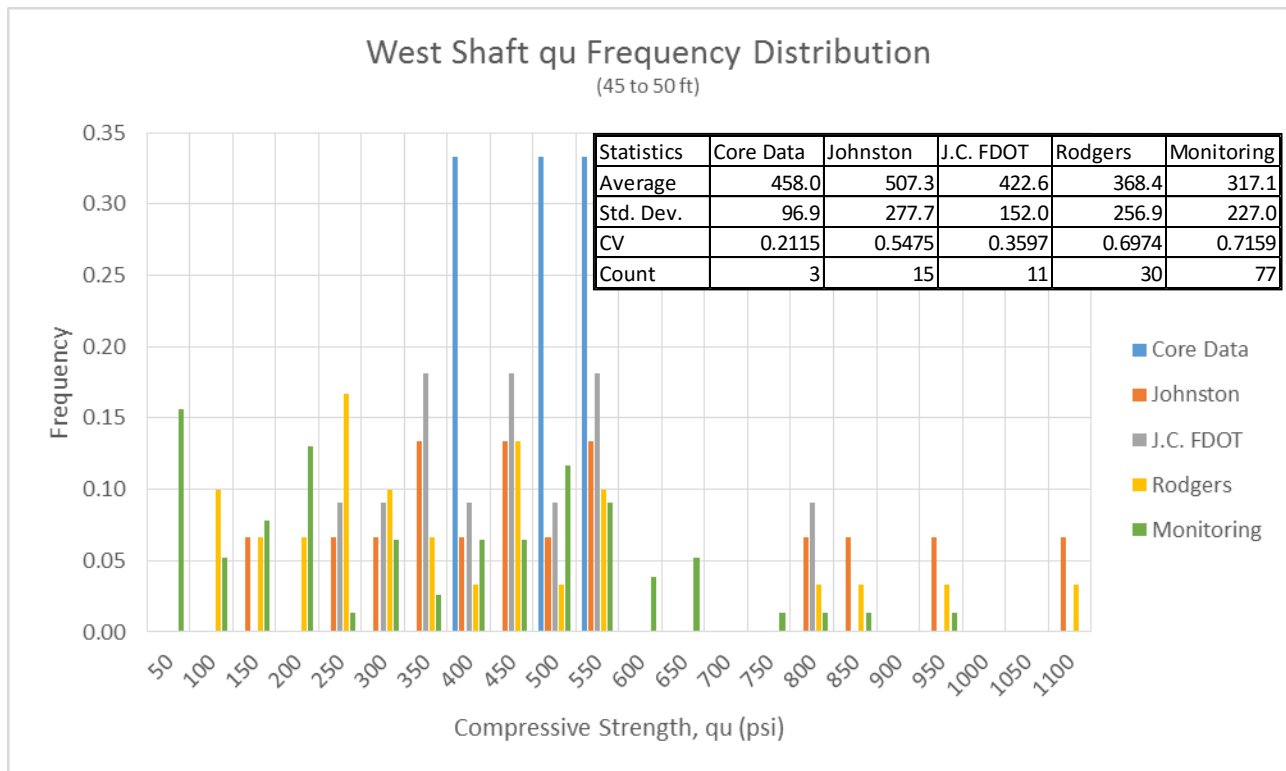


Figure 201 - East shaft q_u frequency distribution, 45 ft to 50 ft.

From the analysis it was found that Rodgers method was the closest to the average obtained from monitoring in four of the six comparisons. This can be seen in Table 87, which displays each methods' ranking based on the closest average to the monitoring average at each location (The lower the total score the better).

Table 87 - Design method rankings

Location	Core Data	Johnston	J.C. FDOT	Rodgers
ES (40-45ft)	2	4	3	1
TS (40-45ft)	4	1	2	3
WS (40-45ft)	4	1	3	2
ES (45-50ft)	4	3	2	1
TS (45-50ft)	4	2	3	1
WS (45-50ft)	3	4	2	1
Total	21	15	15	9

In the two locations where Rodgers method did not provide the closest estimate, the average recoveries were the highest for the site, (44% and 54.7%). The average recoveries for all other locations were 20%, 28.3%, 36% and 42.3%. It appears using the Johnston method is more accurate when recoveries are better. However, Rodgers method provided one of the closest averages in all locations regardless of recovery.

The method also produced similar CV values to that of the monitoring, providing a better understanding of the true site variability. Although Rodgers method produced the best result, it is recommended that each new design method be further investigated. New design methods should be developed to provide more accurate estimations of shaft capacity and site variability, especially for sites with poor recoveries, leading to a reduction in overdesign based on current practice.

The following three sections provide analysis for each shaft where rock was encountered. In these sections compressive strength and skin friction frequency distributions are provided for each shaft and broken up into layers for comparisons with load test results. The sections also provide depth vs. compressive strength, skin friction, and specific energy plots.

5.2.1 Test Shaft Analysis

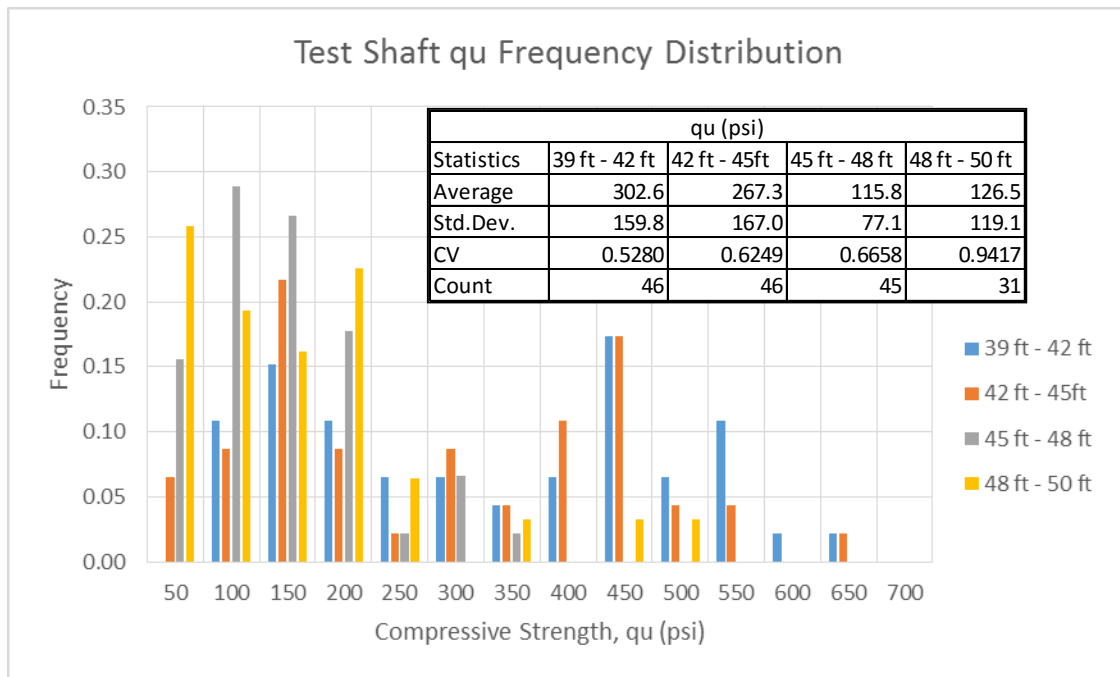


Figure 202 - Test shaft q_u frequency distribution

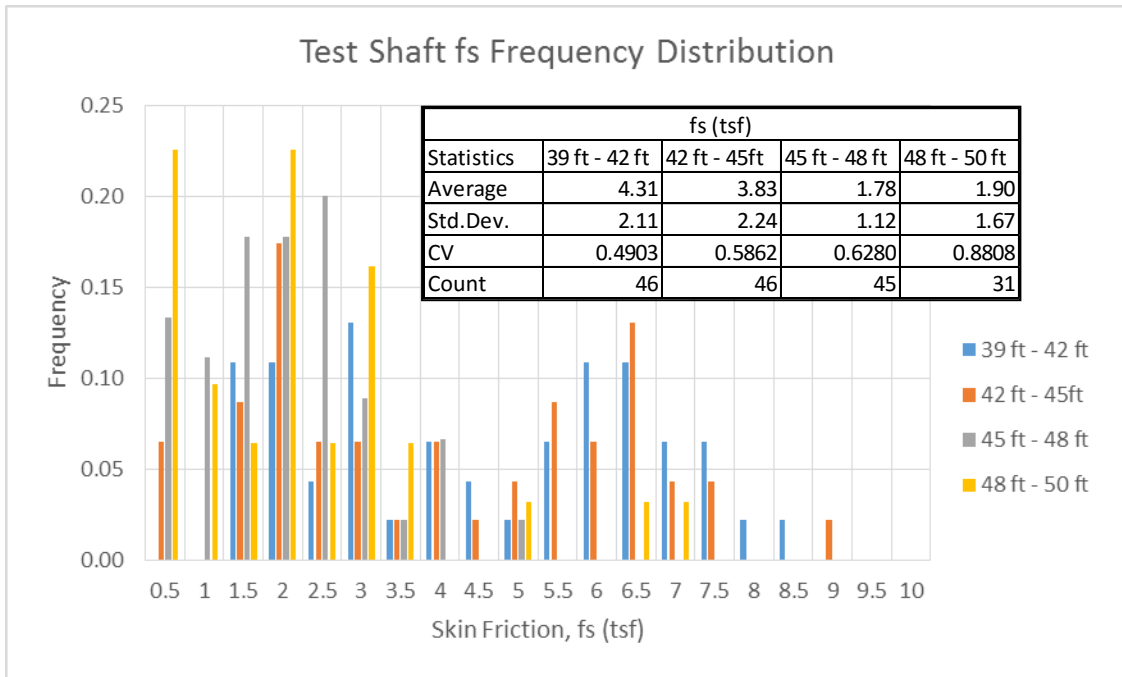


Figure 203 - Test Shaft f_s frequency distribution

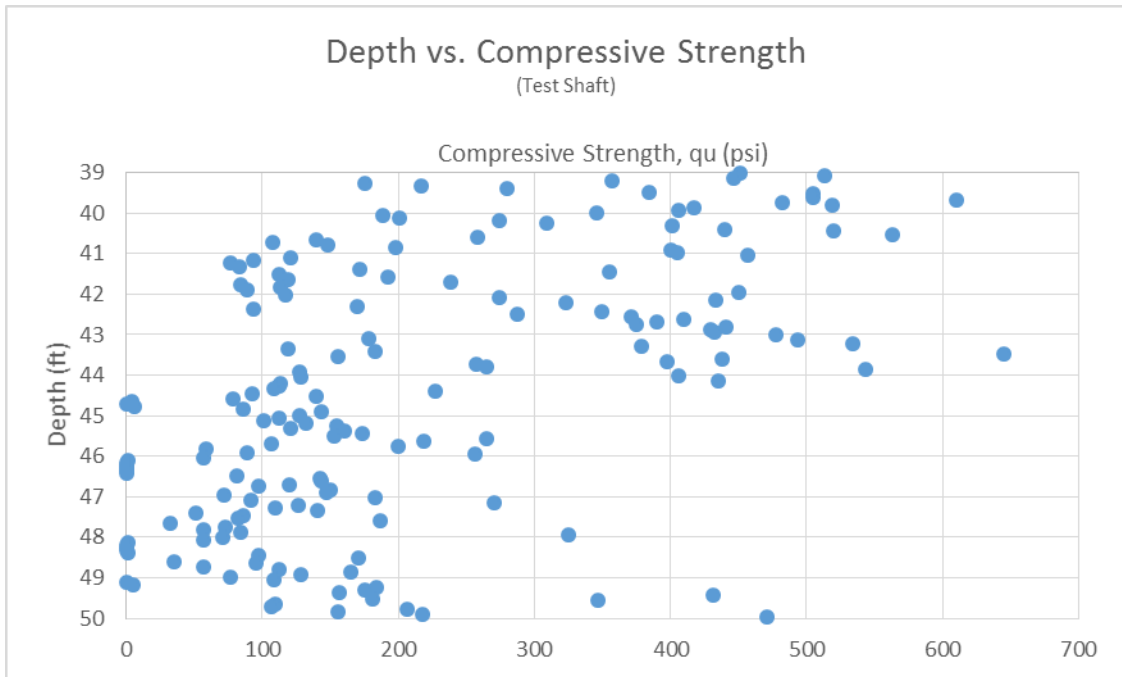


Figure 204 - Test shaft depth vs. q_u

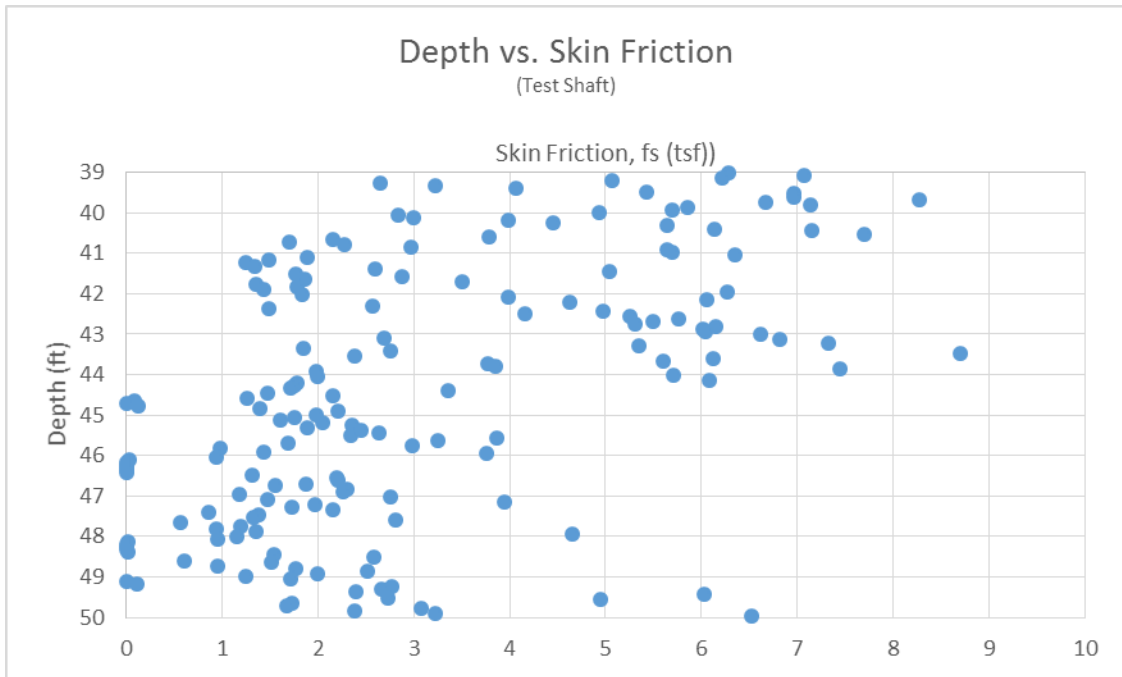


Figure 205 - Test shaft depth versus skin friction

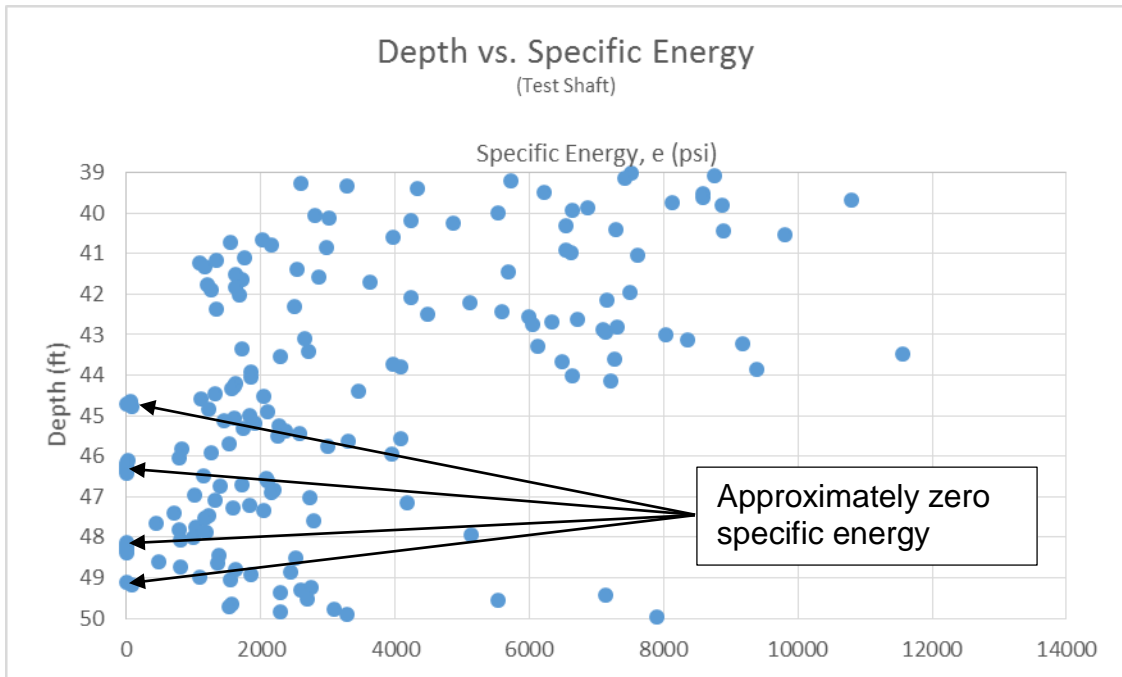


Figure 206 - Test shaft depth vs. specific energy

In Figure 206, it is shown that approximately zero specific energy was recorded in several sections near the bottom five feet of the shaft. This was due to rig malfunction where the cable on the winch was spooled incorrectly during drill bit extraction. This

was likely due to the mast not being properly aligned. The drill rig inclinometer was not functioning and the mast inclination had to be checked periodically to ensure proper alignment. As a result, when the bit was lowered after clean out, the cable would quickly release and the drill bit would drop uncontrollably. This caused the DIALOG to record vertical movement that was not yet achieved. Because there was virtually no crowd or torque applied when the bit dropped, the DIALOG recorded the data in these sections as zero specific energy. Note, if a certain depth has previously been reached (e.g., spooling too far), the DIALOG will not record over the data when advancing the bit to that depth again. Additionally, the quick release causes back pressure in the hydraulic lines which theoretically increases the threshold pressure and changes the developed k coefficients. Visualization is provided using Equation 7:

$$T = k_T \times (\text{Operating Pressure} - \text{Threshold Pressure}) \text{ Torque or Crowd} \\ = K * (\text{Operating Pressure} - \text{Threshold Pressure}) \dots \text{Eq 7}$$

After watching replays of the drillings on the DIALOG, it was noticed the hydraulic pressures eventually stabilize to normal conditions. This typically occurred when the bit was removed from the hole and back spinning was completed. However, recorded rock strengths were lower while the back pressure was locked in. Therefore, not only did the rig malfunction produce recorded readings at $q_u = 0$ psi from the quick cable release; until the back pressure was returned to normal, the additional recorded rock strengths were lowered and produced an underestimate of the material. This was a result of using an older drill rig to complete the drilling. This phenomenon appeared to have occurred in the east and west shafts as well. However, the east shaft actually experienced voids and the following will explain the difference in readings and how to interpret the results to make the determination.

In the test shaft around 46 feet, rig malfunction occurred and is highlighted in Table 88. The malfunction was witnessed in the field as the falling bit produced an extremely loud sound when it crashed.

Table 88- Monitored readings indicating rig malfunction

Depth (ft)	Pen. Rate u (in/min)	Rotation N (rpm)	Torque T (in-lbs)	Crowd F (lbf)	Sp. Energy e (psi)	qu (psi)
45.90	16.3	6.43	519716	2525	1268.59	88.9
45.96	5.4	6.53	530608	2926	3946.19	256.7
46.03	27.5	6.61	532757	693	791.67	56.3
46.10	52.0	1.97	73385	408	17.52	1.3
46.16	109.1	0.00	5385	258	0.25	0.0
46.23	114.8	0.00	5507	256	0.25	0.0
46.29	116.5	0.00	5642	257	0.25	0.0
46.36	115.0	0.00	5710	259	0.25	0.0
46.42	149.0	0.00	5365	261	0.26	0.0
46.49	15.6	7.09	410576	1873	1153.92	81.2
46.56	8.6	7.11	407152	1809	2084.81	142.6
46.62	7.9	7.26	370936	1787	2101.55	143.7

As seen in Table 88, between 46.16 to 46.42 feet, there was zero recorded bit rotation which only occurs when the bit is being lowered into the hole. This also indicates there was zero torque applied to advance the bit. The recorded values for torque come from residual pressure in the hydraulic lines, slightly above the estimated threshold pressure. Therefore, the only specific energy recorded was from the residual pressure in the hydraulic crowd lines, as Teale's equation compensates for penetration without bit rotation. This results in virtually zero specific energy required to advance the bit which should not occur. The reading at 46.10 feet was a result of the DIALOG averaging the drilling parameters for every 2 cm of penetration. Consequently, a portion of the average was recorded before the rig malfunction occurred and a portion of the average was recorded during the rig malfunction. This also leads to an underestimate for the reading which needs to be eliminated for the overall average of the drilled section.

In the east shaft, at a depth of 32.19 feet, a void was encountered.

Table 89 - Monitored readings indicating a void was encountered

Depth (ft)	Pen. Rate u (in/min)	Rotation N (rpm)	Torque T (in-lbs)	Crowd F (lbf)	Sp. Energy e (psi)	qu (psi)
31.99	3.3	5.41	168874	1281	1728.40	119.5
32.05	1.2	5.39	159893	1364	4547.36	291.4
32.12	2.0	5.43	159781	1543	2736.05	183.7
32.19	66.4	1.41	34563	271	4.81	0.4
32.25	2.2	4.53	122209	963	1533.51	106.6
32.32	2.4	5.82	170090	2351	2592.85	174.8
32.38	4.7	5.78	195211	1315	1496.66	104.2

Table 89, shows that although the specific energy reading was extremely low, every drilling parameter produced a non-zero reading. As a result, large differences in the drilling parameters can be used to distinguish between void detection and rig malfunction. The first indication is the differences in penetration rate. The rig malfunction section consistently produced a rate of penetration nearly double that of the voided section. The rig malfunction penetration rates were also increasing as penetration occurred, indicating acceleration from freefall. The second indication is the voided section recorded rotation, confirming drilling was taking place and torque was being applied. The recorded torque value from the voided section is also on a higher order of magnitude than the rig malfunction section. Additionally, the torque values in the rig malfunction section are two orders of magnitude lower than the torque values recorded before and after the malfunction occurred. Finally, the specific energy for the voided section produced a result on a higher order of magnitude than the rig malfunction section, where the specific energy value, 0.25 psi, was repeatedly recorded. It is highly unlikely the same recorded value would occur for specific energy at this degree of precision. This was verified through visual inspection by looking at the variability of specific energy readings before and after the rig malfunction and voided sections. In the test shaft at depths 46.10 and 46.42 feet, a 1.10 psi difference in q_u produced nearly a 15 psi difference in specific energy. This led to the conclusion that rig malfunction occurred in the test shaft and voids were encountered in the east shaft. As a result, it was decided to perform the analysis (test shaft q_u and f_s frequency distributions) with the zero specific energy data points removed.

Note: The previous and following frequency distributions reflect the zero specific energy data points being removed for the analysis in all shafts. This does not include Figure 202 Figure 203. The zero specific energy points were left in these figures to show the difference between including them and removing them. There were no zero specific energy points recorded in the east shaft. However, the west shaft had a few sections where zero specific energy was recorded. These can be seen in the depth vs. q_u , f_s and

e plots (Figure 216Figure 218) at depths 35.20 to 35.47 feet, 36.71 to 37.17 feet, and 46.62 to 46.69 feet.

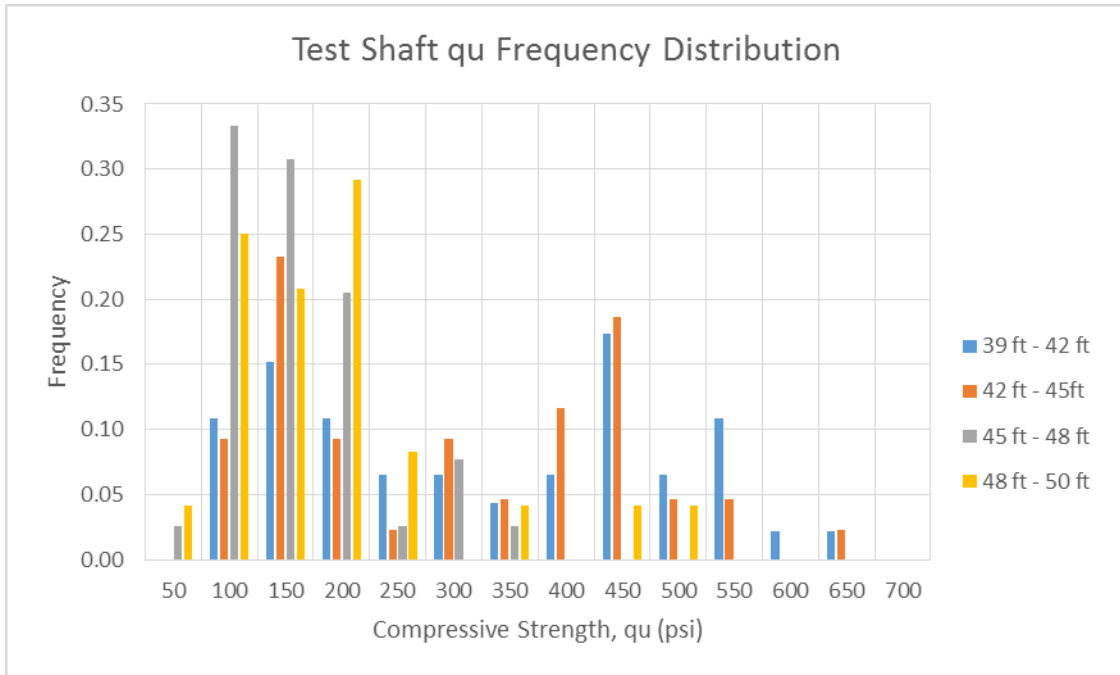


Figure 207 - Test shaft q_u frequency distribution with zero specific energy data points removed

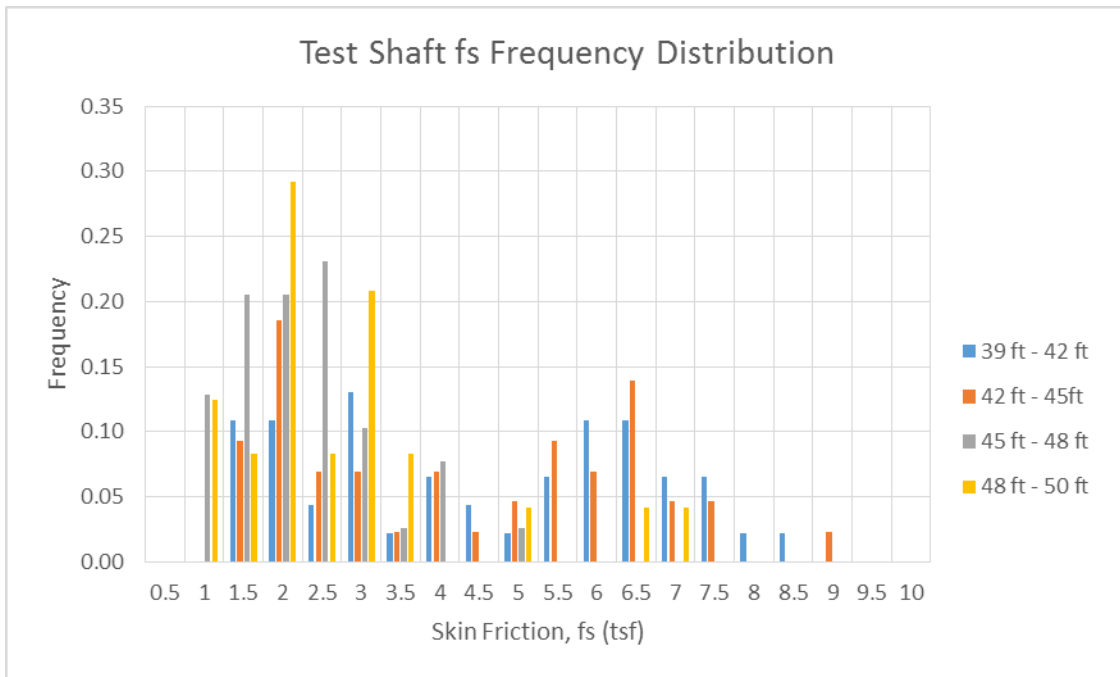


Figure 208 - Test shaft: f_s frequency distribution with zero specific energy data points removed

5.2.2 East Shaft Analysis

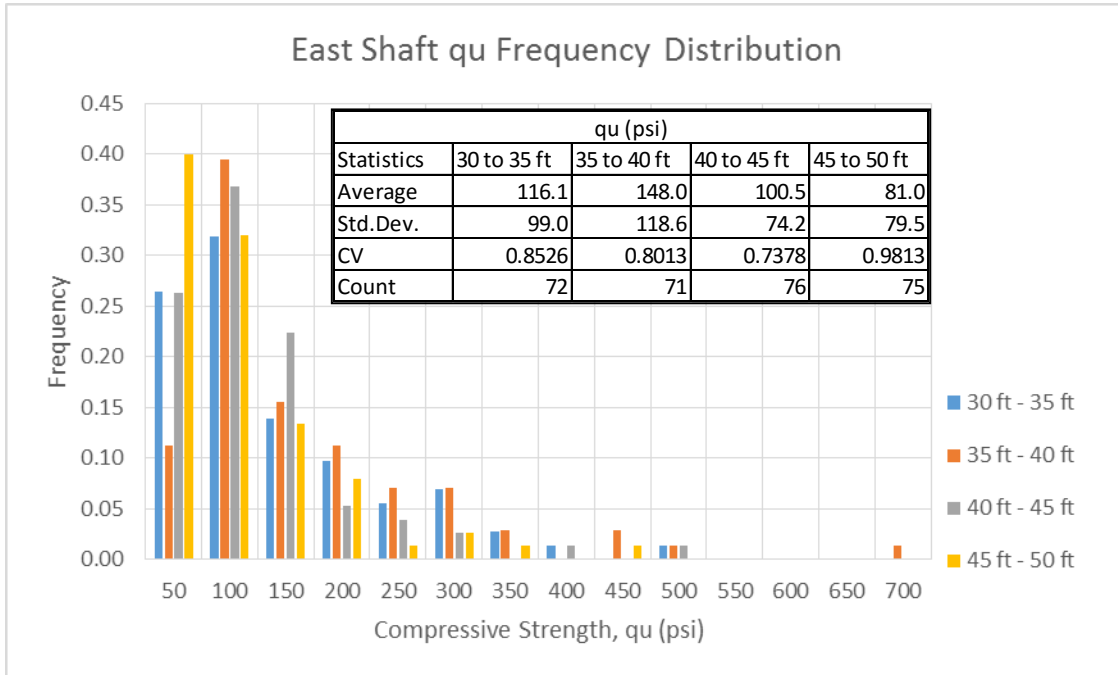


Figure 209 - East shaft q_u frequency distributions

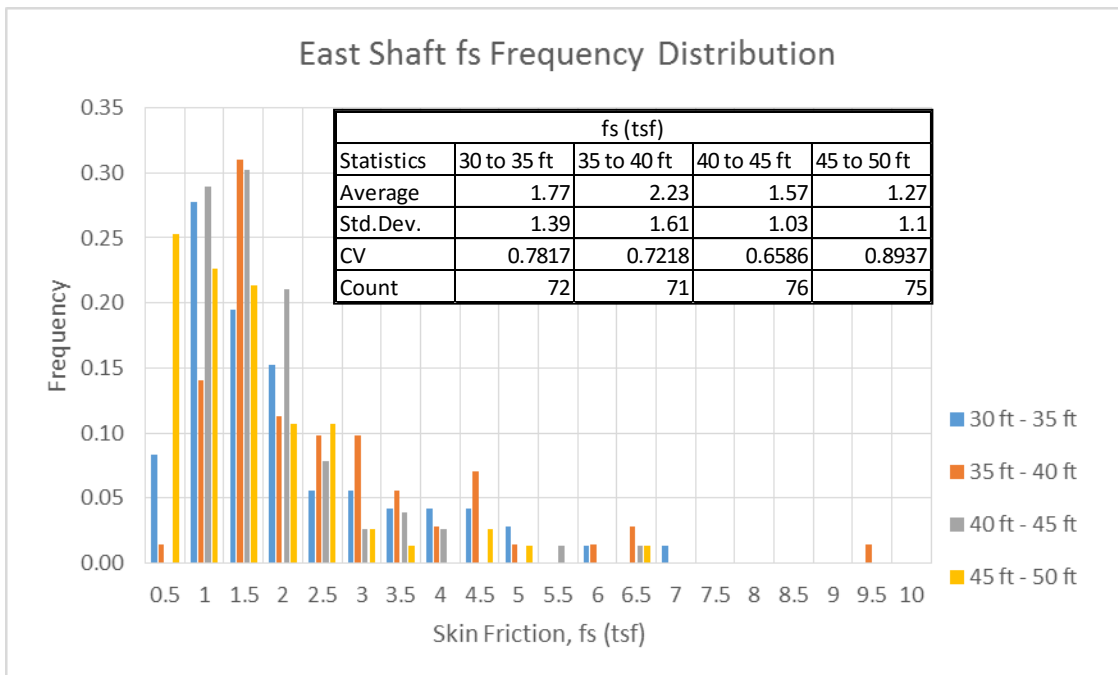


Figure 210 - East shaft f_s frequency distribution

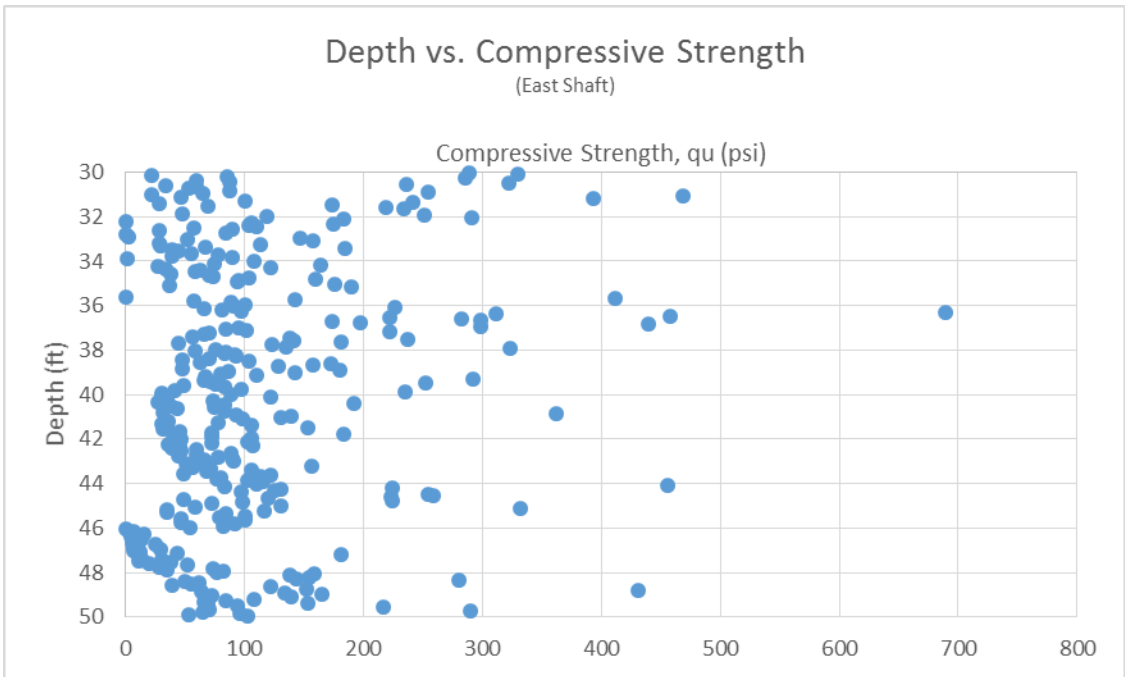


Figure 211 - East shaft depth vs. compressive strength

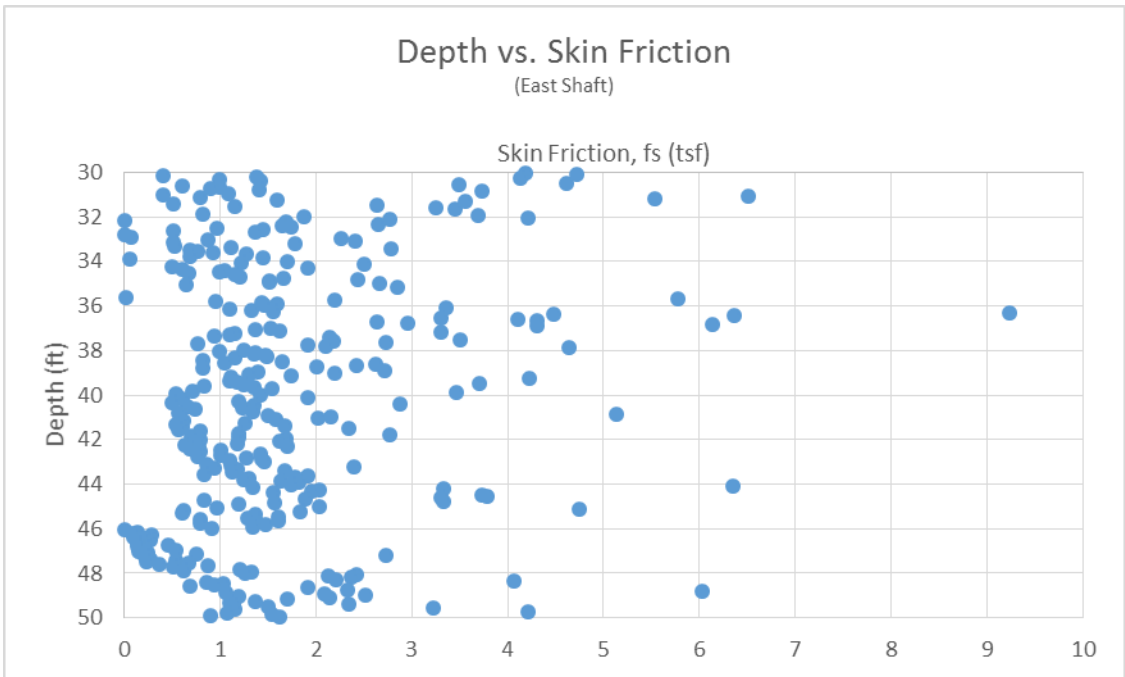


Figure 212 - East shaft depth vs. skin friction

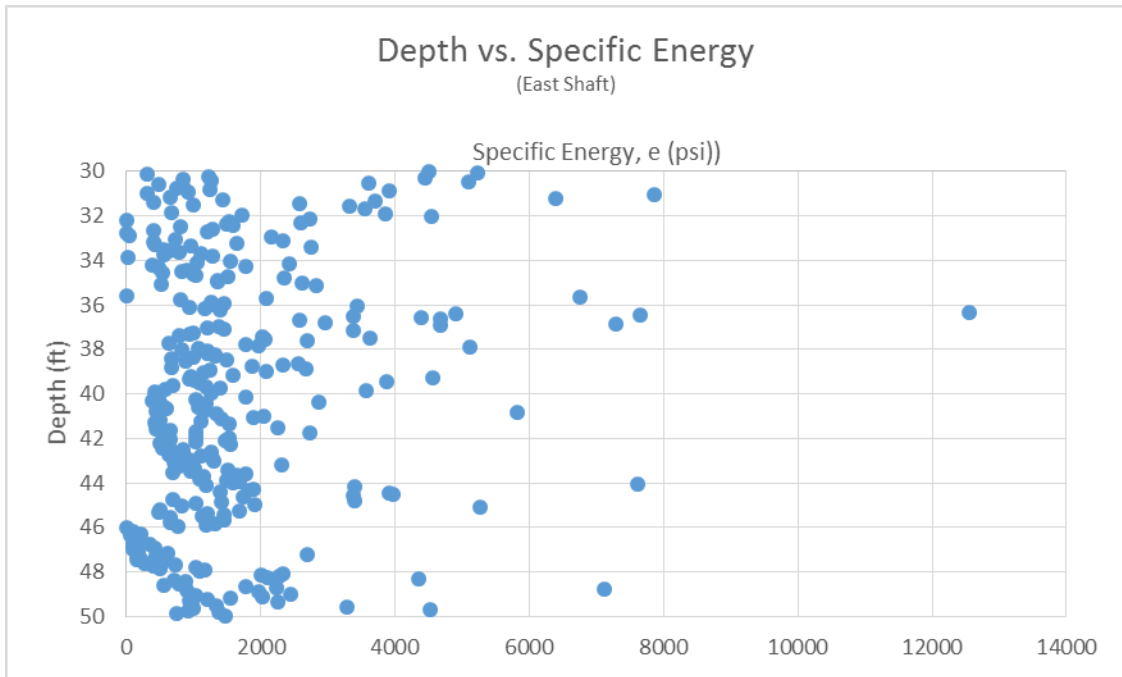


Figure 213 - East shaft depth vs. specific energy

5.2.3 West Shaft Analysis

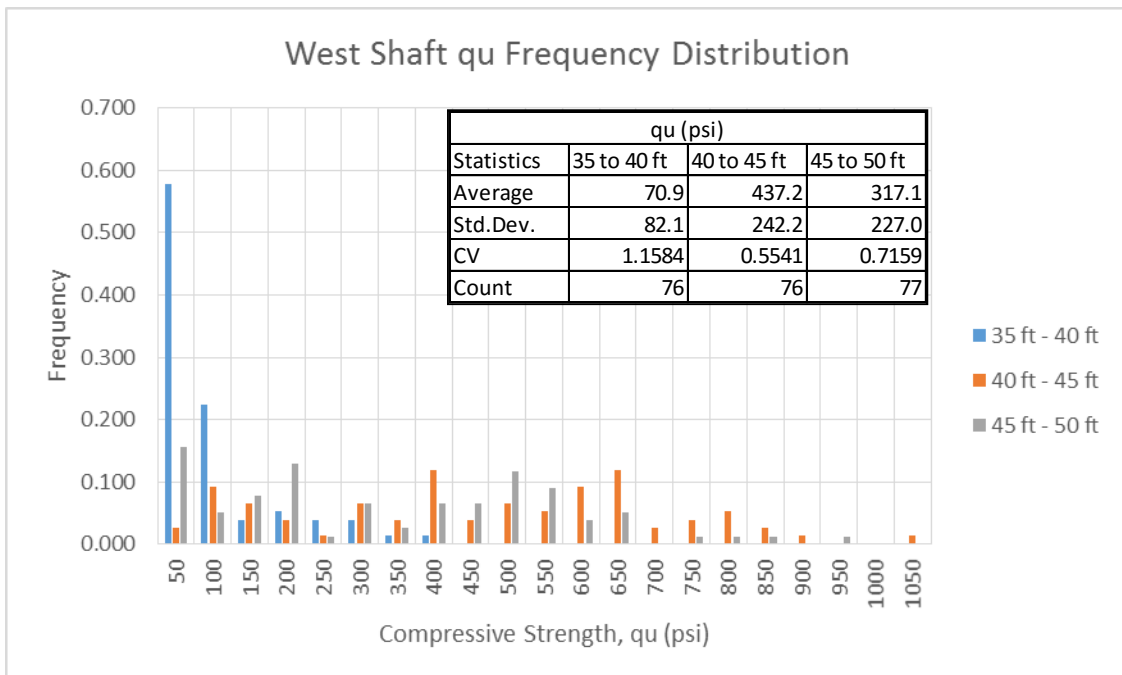


Figure 214 - West shaft q_u frequency distribution

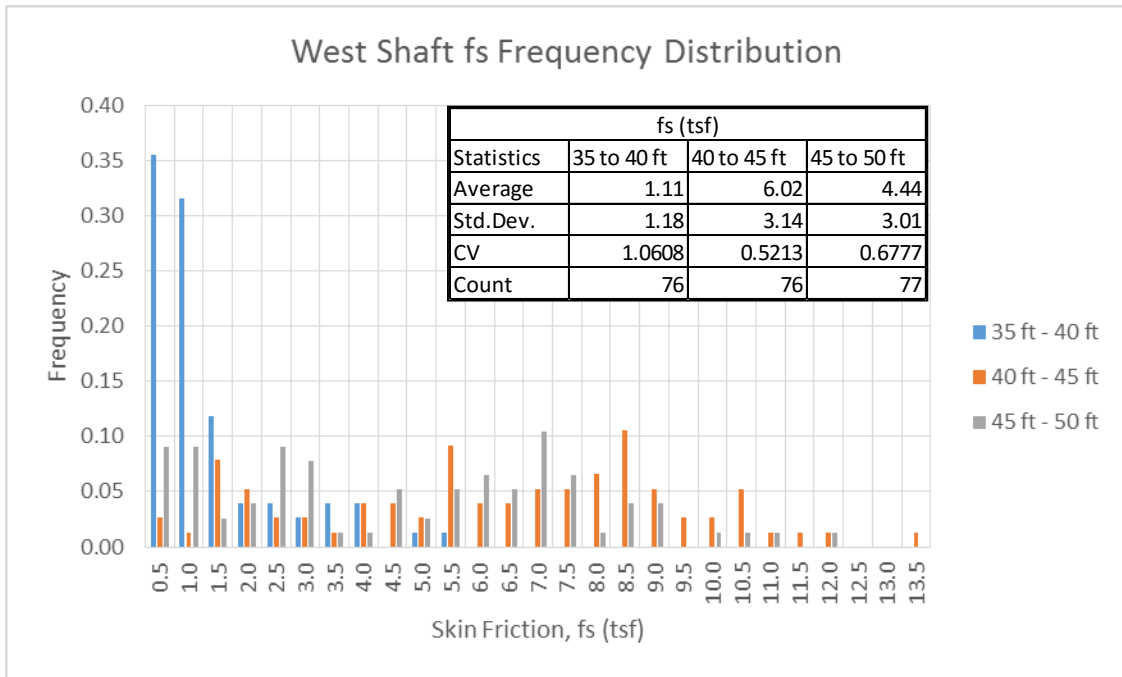


Figure 215 - West shaft f_s frequency distribution

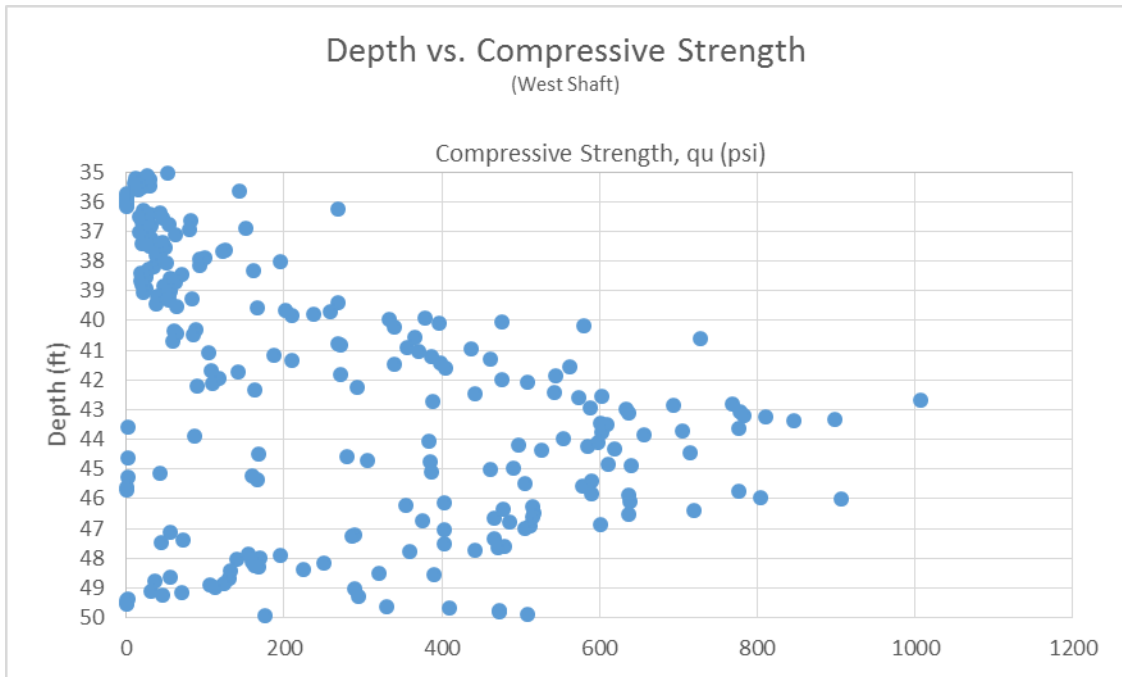


Figure 216 - West shaft depth vs. compressive strength

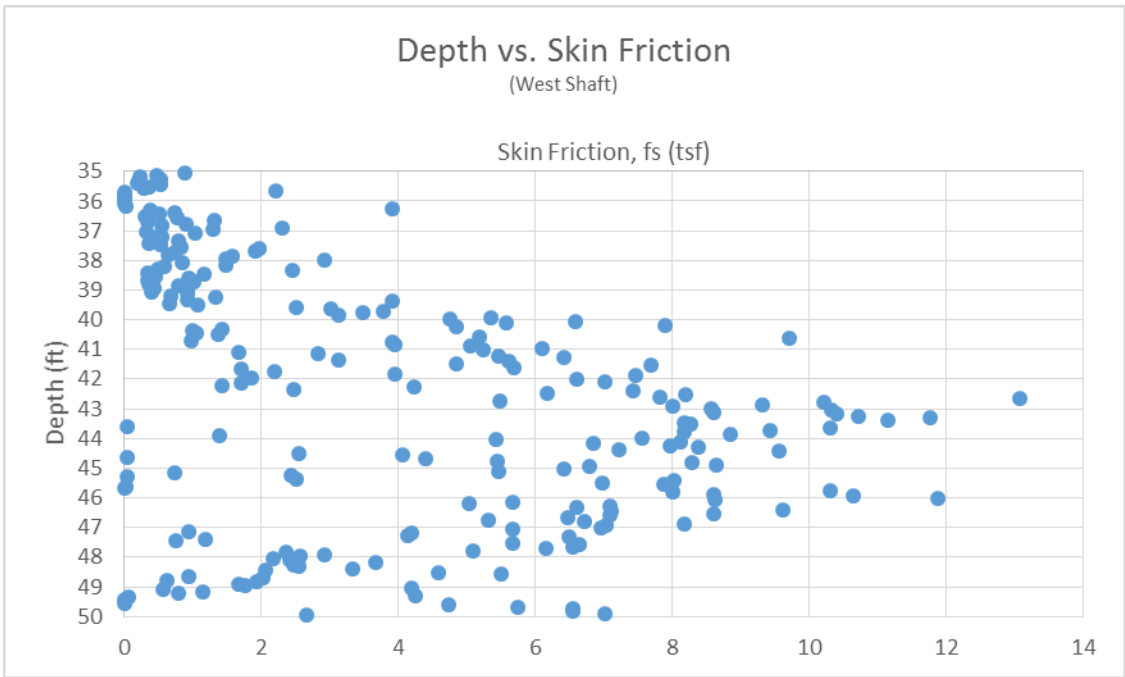


Figure 217 - West shaft depth vs. skin friction

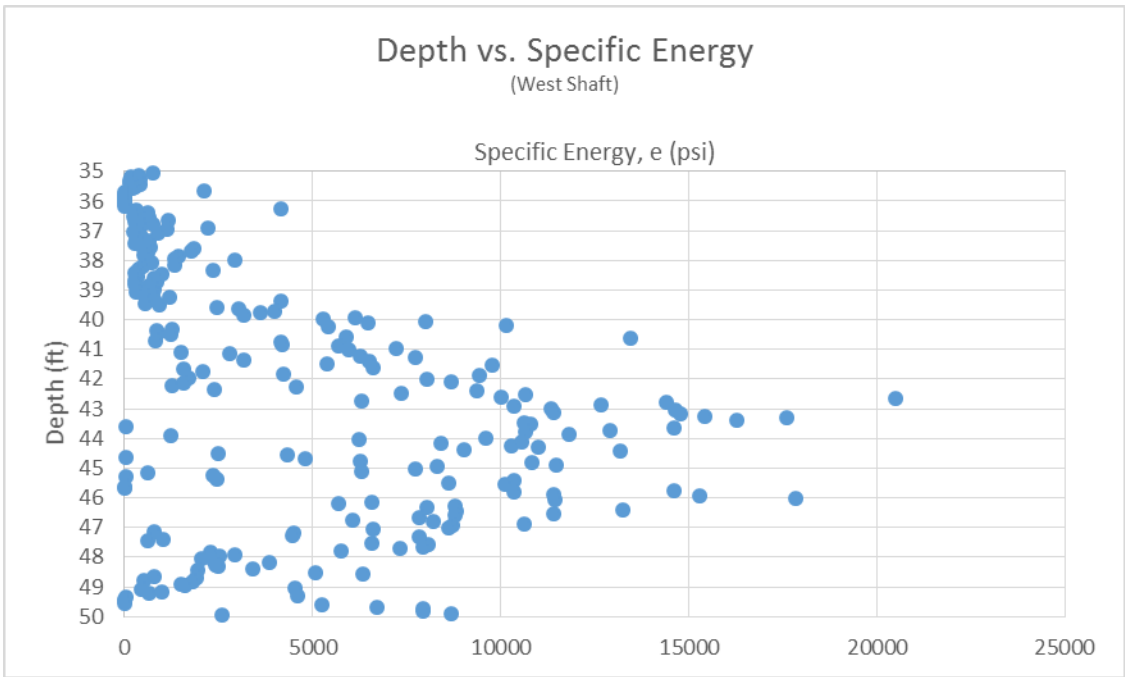


Figure 218 - West shaft depth vs. specific energy

5.3 Load Test Data

The following section covers the results and data reduction from the load test at FDOT's Kanapaha site in Gainesville, Florida.

5.3.1 Strain Gauge Load Distribution

The following provides the strain gauge load distributions for all three shafts.

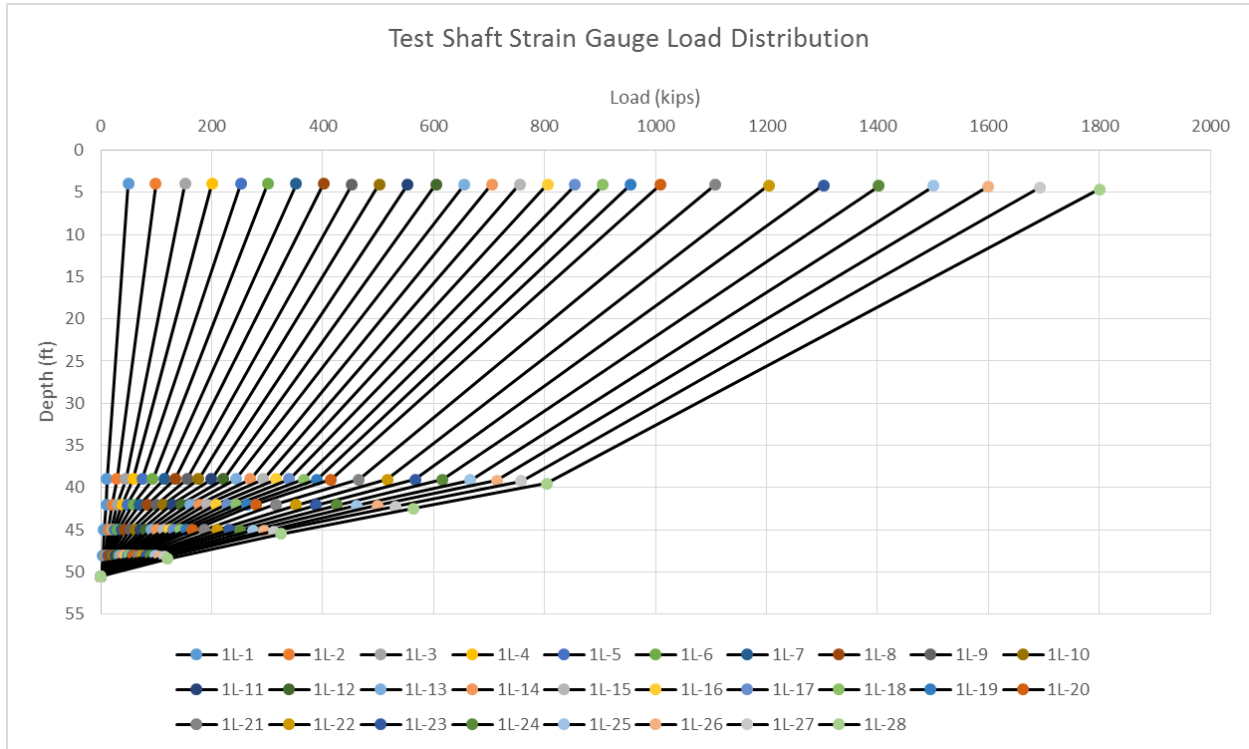


Figure 219 - Test shaft strain gauge load distribution

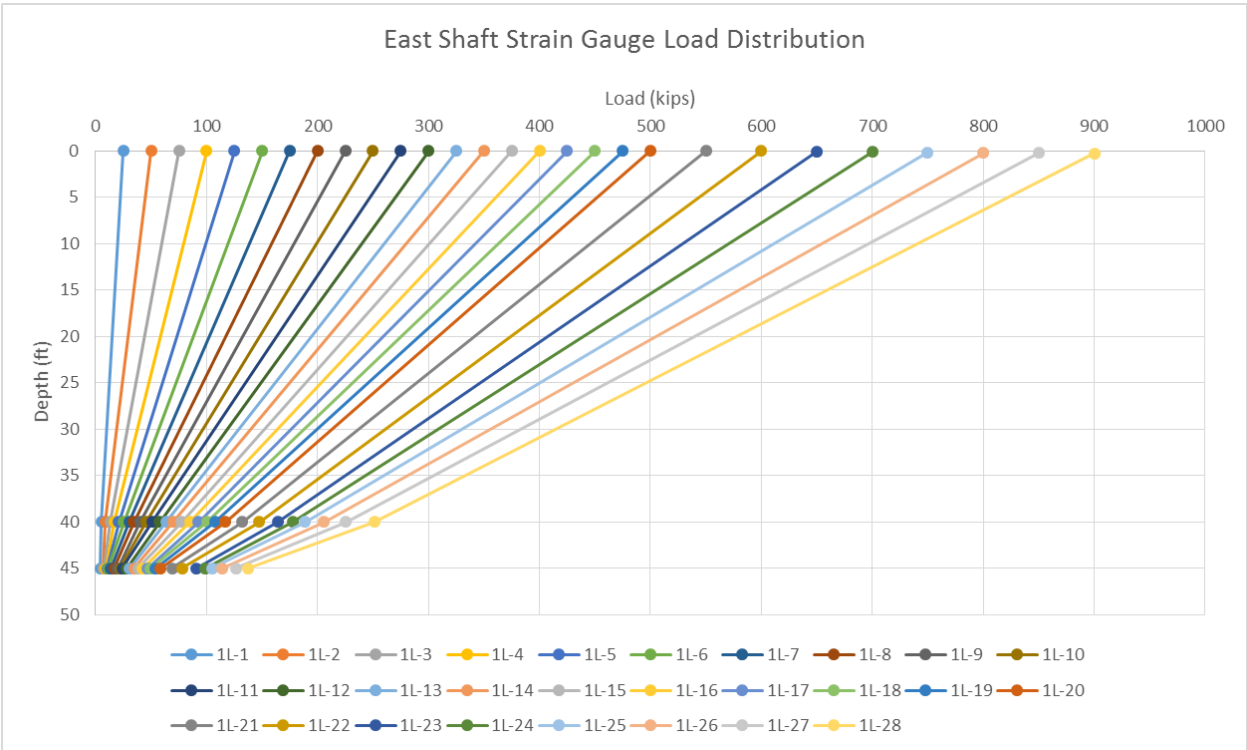


Figure 220 - East shaft strain gauge load distribution

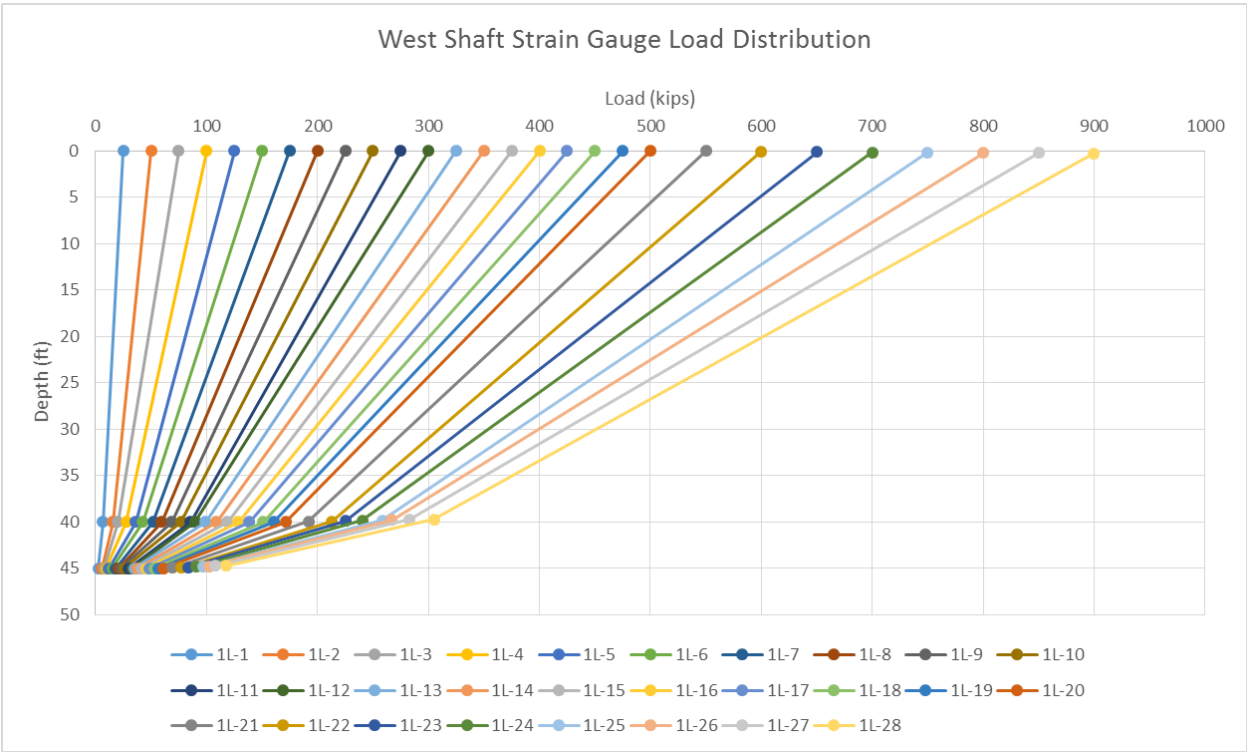


Figure 221 - West shaft strain gauge load distribution

From the distributions it appears the test shaft was nearly loaded to full mobilization in all sections during the final loading step. The test shaft T-Z curves in following section indicate the same result. The east shaft appears to have been on the verge of full mobilization but the west shaft was further away from mobilization.

It should be noted that the end bearing in the test shaft was assumed to be zero. This was considered a reasonable assumption because a 6" Styrofoam pad (Figure 179) was placed at the base of the shaft. The end bearing pad was designed to carry the weight of the reinforced cage and concrete during placement, but upon further loading, i.e., the load test, little if any bearing resistance would develop. Note, by removing end bearing from the test shaft, full side shear mobilization was possible.

5.3.2 T-Z Curves at Kanapaha Test Site

Based on the load distribution of the test shaft (Figure 219), the T-Z curves for side shear along the shaft were developed, Figure 222. Based on location of the gauges, SG1 to SG2 was from depth of 39 to 42 ft, SG2 to SG3 from 42 to 45ft, SG3 to SG4 from 45 to 48ft, and SG4 to base was from 48ft to 50ft depth. Evident from the shape of the curves, the unit skin friction was fully mobilized. Note, all the test shaft curves are for compression loading.

Presented in Figure 223 are the T-Z curves for the east and west reaction shafts embedded in limestone. The T-Z curves were developed based on the load transfer plots of Figure 220 and Figure 221, as well as collected telltale data for both shafts. Note, the east shaft (ES) for SG1 to SG2 is from a depth of 40 to 45ft, and west shaft (WS) from SG1 to SG2 was also for a depth of 40 to 45ft. Both curves in Figure 223 are for tension loading. Evident from Figure 223, the west shaft was still mobilizing side shear, whereas the east shaft was on the verge of full mobilization.

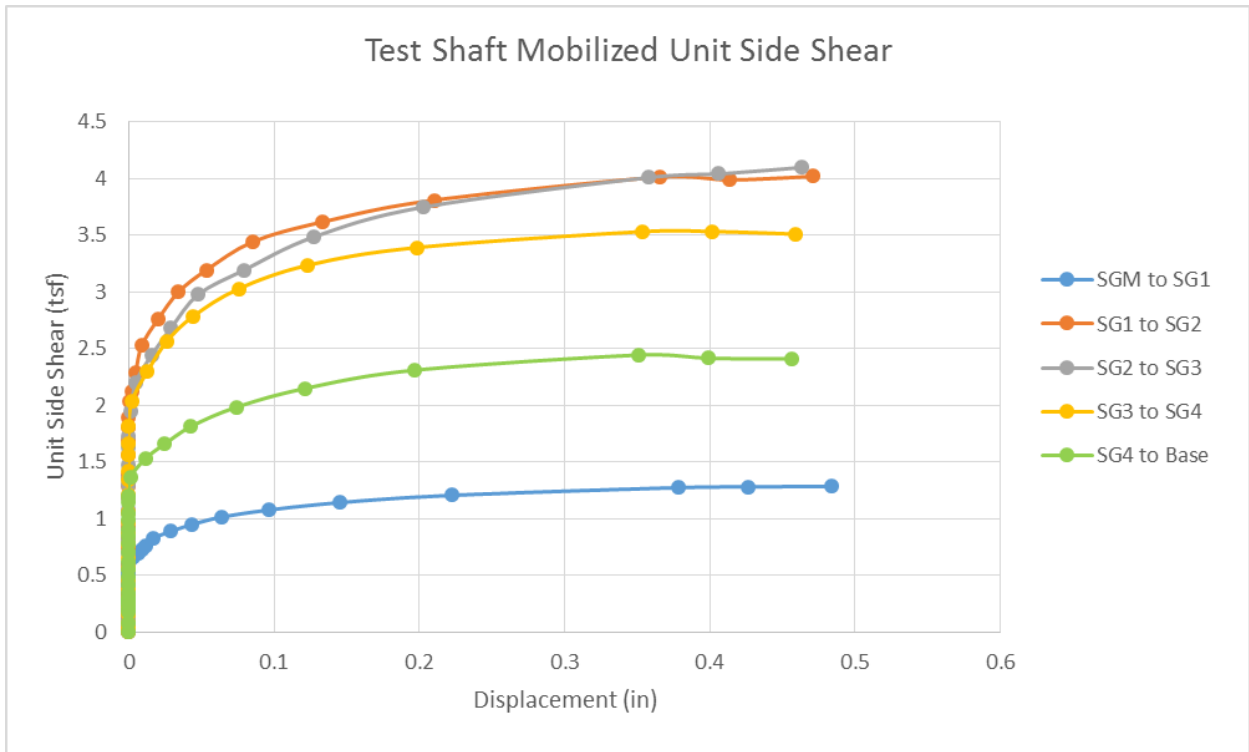


Figure 222 - Test Shaft T-Z curves

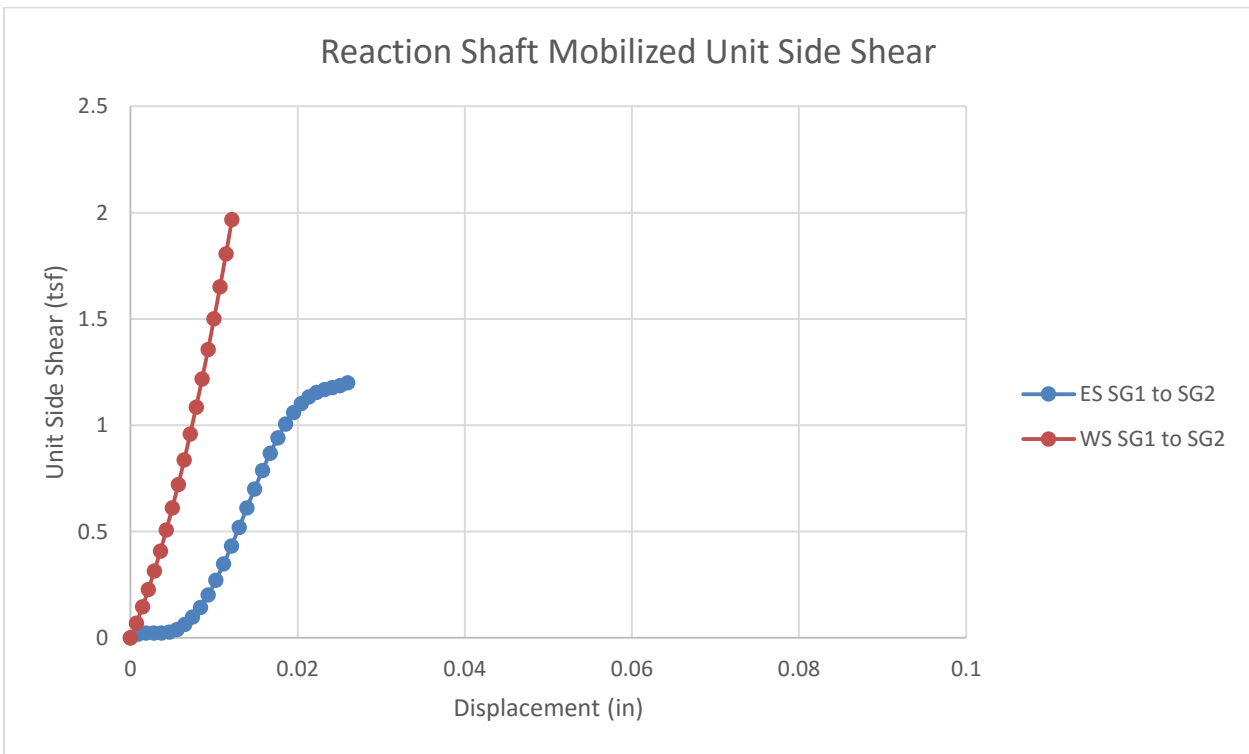


Figure 223 - East and West Shaft T-Z curves

5.4 Comparative Analysis

Before the final load test was conducted, UF researchers submitted predictions for side shear and estimated loads for each section that was monitored with strain gauges for all three shafts. The following provides the results of the load test compared to the predictions made by the researchers prior to testing. Note, the zero specific energy data points were not removed for the initial predictions.

Table 90 - Test shaft load test results (Predicted)

Test Shaft Strain Gage Level	Elevation	Skin Friction (tsf)		Percent Difference
		Predicted	Load Test	
SG Level 1 to SG Level 2	39 ft to 42 ft	4.31	4.01	7.48%
SG Level 2 to SG Level 3	42 ft to 45 ft	3.83	4.11	-6.81%
SG Level 3 to SG Level 4*	45 ft to 48 ft	1.76	3.50	-49.71%
SG Level 4 to Shaft Base	48 ft to 50 ft	1.92	2.43	-20.99%
Average Skin Friction (tsf)		3.05	3.61	-15.56%
Total Load (tons)		316.1	374.4	-15.56%
*Monitoring indicated rig malfunction in the section				

Table 91 - East shaft load test results (Predicted)

East Reaction Shaft Strain Gage Level	Elevation	Skin Friction (tsf)		Percent Difference
		Predicted	Load Test	
SG Level 1 to SG Level 2*	40 ft to 45 ft	1.57	1.18	33.05%
Total Load (tons)		74.0	55.6	33.05%
*Section closely approaching full mobilization				

Table 92 - West shaft load test results (Predicted)

West Reaction Shaft Strain Gage Level	Elevation	Skin Friction (tsf)		Percent Difference
		Predicted	Load Test	
SG Level 1 to SG Level 2*	40 ft to 45 ft	6.02	1.8	234.44%
Total Load (tons)		283.7	84.8	234.44%
*Section was not fully mobilized				

It should be noted, the reaction shaft predictions did not account for load reduction in tension. When a drilled shaft is loaded in compression, elastic compression is experienced by the shaft. This is due to Poisson's effect which causes a small increase in diameter. Conversely, when shafts are placed in the tension the opposite effect occurs and the shaft diameter is slightly reduced. As a result, the unit side shear is reduced for drilled shafts loaded in tension. For design, unit side shear values for shafts in tension can be reduced to 75% of the downward loading unless static load test data justifies the use of higher values (Coduto, 2001). The reduction was determined by O'Neill and Reese (1999). O'Neill and Reese states the reduction factor should be 1.0 if

the drilled shaft is in cohesive soil or is rigid compared to harder geomaterial (IGM or Rock). A rigid drilled shaft is one in which:

$$[E_c/E_s][B/D]^2 \geq 4 \dots\dots\dots \text{Eq 21}$$

where,

- E_c = Young's modulus of the concrete and steel
- E_s = Mass Young's modulus of the rock
- B = Shaft diameter
- D = Shaft depth of embedment

Using data collected from AASHTO (2010) to determine the lowest mass modulus for Florida limestone samples and the elastic modulus of the reaction shafts, the reported modulus ratio would be $E_c/E_s = 3979 \text{ ksi} / 10.76 \text{ ksi} = 369.8$. The B/D ratio for the Kanapaha shafts was $B/D = 3 \text{ ft} / 50 \text{ ft} = 0.06$. Using the equation developed by O'Neill and Reese provided a value of 1.33, which is less than 4 and indicated the 75% reduction should be used. The reduced predicted unit side shear and total load for the reaction shafts is provided in the following tables.

Table 93 - East shaft load test results (Predicted – reduced for tension loading)

East Reaction Shaft Strain Gage Level	Elevation	Skin Friction (tsf)		Percent Difference
		Predicted	Load Test	
SG Level 1 to SG Level 2*	40 ft to 45 ft	1.18	1.18	0.00%
Total Load (tons)		55.6	55.6	0.00%
*Section closely approaching full mobilization				

Table 94 - West shaft load test results (Predicted – reduced for tension loading)

West Reaction Shaft Strain Gage Level	Elevation	Skin Friction (tsf)		Percent Difference
		Predicted	Load Test	
SG Level 1 to SG Level 2*	40 ft to 45 ft	4.515	1.8	150.83%
Total Load (tons)		212.8	84.8	150.83%
*Section was not fully mobilized				

The east shaft reduced prediction appeared to be a good estimate based on the strain gauge load distribution and T-Z curve. Both the strain gauge load distribution and T-Z curve indicated the east reaction shaft was on the verge of reaching full mobilization. The west shaft was not approaching full mobilization and therefore comparisons between the load test results and monitoring could not be made. The test shaft predictions were also good and typically on the conservative side which is the desired outcome if the results do not perfectly align. If the section where the rig malfunction produced the greatest effect is removed, 45 to 48 feet, the overall prediction is excellent. These results can be seen here:

Table 95 - Test shaft load test results (rig malfunction section, 45 to 48ft, removed)

Test Shaft Strain Gage Level	Elevation	Skin Friction (tsf)		Percent Difference
		Predicted	Load Test	
SG Level 1 to SG Level 2	39 ft to 42 ft	4.31	4.01	7.48%
SG Level 2 to SG Level 3	42 ft to 45 ft	3.83	4.11	-6.81%
SG Level 4 to Shaft Base	48 ft to 50 ft	1.92	2.43	-20.99%
Average Skin Friction (tsf)		3.53	3.65	-3.29%
Total Load (tons)		266.3	275.4	-3.29%

Furthermore, if the data points where zero specific energy was reported are removed, the prediction in the bottom three sections is improved.

Table 96 - Test shaft load test results (zero specific energy data removed)

Test Shaft Strain Gage Level	Elevation	Skin Friction (tsf)		Percent Difference
		Predicted	Load Test	
SG Level 1 to SG Level 2	39 ft to 42 ft	4.31	4.01	7.48%
SG Level 2 to SG Level 3	42 ft to 45 ft	4.09	4.11	-0.49%
SG Level 3 to SG Level 4*	45 ft to 48 ft	2.03	3.50	-42.00%
SG Level 4 to Shaft Base	48 ft to 50 ft	2.44	2.43	0.41%
Average Skin Friction (tsf)		3.29	3.61	-8.94%
Total Load (tons)		340.9	374.4	-8.94%
*Monitoring indicated rig malfunction in the section				

Finally, if the section where the rig malfunction had the largest effect is removed, and the zero specific energy data points are removed, the estimated side shear and total load is nearly perfect.

Table 97 - Test shaft results (zero specific energy data points and rig malfunction section removed)

Test Shaft Strain Gage Level	Elevation	Skin Friction (tsf)		Percent Difference
		Predicted	Load Test	
SG Level 1 to SG Level 2	39 ft to 42 ft	4.31	4.01	7.48%
SG Level 2 to SG Level 3	42 ft to 45 ft	4.09	4.11	-0.49%
SG Level 4 to Shaft Base	48 ft to 50 ft	2.44	2.43	0.41%
Average Skin Friction (tsf)		3.76	3.65	2.94%
Total Load (tons)		283.5	275.4	2.94%

Overall, the comparison between the monitoring and load test results is quite impressive, especially due to the nature of the site. As discussed, the Kanapaha site was highly variable, the limestone was highly weathered and it was very difficult to recover core specimens for lab testing. In closing, the researchers believe the results of

Table 93Table 97 best represent the monitoring efforts at Kanapaha. Before making the load test predictions it was discussed whether or not to remove the zero specific energy data points. It was agreed that including them would only provide a more conservative estimate, which is generally a prudent decision in foundation design.

CHAPTER 6 CONCLUSIONS AND RECOMMENDATIONS

6.1 Conclusions

This project focused on developing and evaluating the relationship between rock drilling parameters (crowd, torque, penetration rate, rotational speed and drill bit diameter) and rock strength (e.g., unconfined compression, q_u). This required both a laboratory and field investigation.

In the laboratory, synthetic limestone (Gatorock) was developed at four different design strengths (10 tsf, 20 tsf, 40 tsf and 120 tsf) that were representative of Florida's various limestone formations. The Gatorock was cast into large blocks (22.5" x 22.5" x 40") that were subsequently drilled using various combinations of the five drilling parameters. The results were wirelessly transmitted in real time to an external computer and recorded for analysis. During the analysis multiple developed drilling equations were investigated. From the investigation, a unique relationship was developed using Teale's specific energy equation for rotary non-percussive drilling in rock. The developed relationship provided the strongest correlation between the five drilling parameters and compressive strength. From this, a new equation was developed that could be used to measure rock strength in real time during field drilling. In total, 81 drilling data points were used to develop the equation.

In the field, Jean Lutz monitoring equipment was acquired and used to measure the same five drilling parameters on the drill rig. The drilling parameters were recorded and transmitted wirelessly to an external computer in real time away from the drilling. The Jean Lutz equipment included pressure transducers used to tap into the hydraulic lines providing torque and crowd to the drill bit, a proximity sensor to monitor rotational speed at the rotary table, a rotary encoder mounted on the rim of the main cable winch to monitor penetration rate, a junction box to receive the signals from each sensor, and a data acquisition module to record, display and transmit the data wirelessly to an external computer in real time via Bluetooth.

During the course of the research project, field monitoring took place at three separate locations where load testing occurred. The locations were in Quincy, Florida (Little River Bridge), Jacksonville, FL (Overland Bridge) and Gainesville, Florida (Kanapaha). Monitoring in these locations provided direct comparison of the estimated shaft capacity obtained during monitored drilling to the actual capacity of installed shafts measured using conventional load testing methods. Additionally, each location used a different type of load test: O-cell testing at Little River, Statnamic testing at Overland, and a traditional top-down static load test at Kanapaha. This provided direct comparative data from three of the most conventional load testing methods used throughout the state. The field investigation also provided three variations in the following categories: location, drill rigs used to install the shafts, shaft diameters, drilling crews, drill bits, drill bit tooth configurations, and limestone formations encountered. These variable drilling

conditions provided great insight on how well the laboratory drilling equations perform when drilling conditions, rig configurations and Florida limestone formations change.

The following presents the monitoring results versus the load test results for skin friction at each monitored location. The presented results are in portions of the shafts, at each location, where the side shear was either fully mobilized or being mobilized; thereby, providing direct comparison of monitoring to conventional methods for estimating shaft capacity.

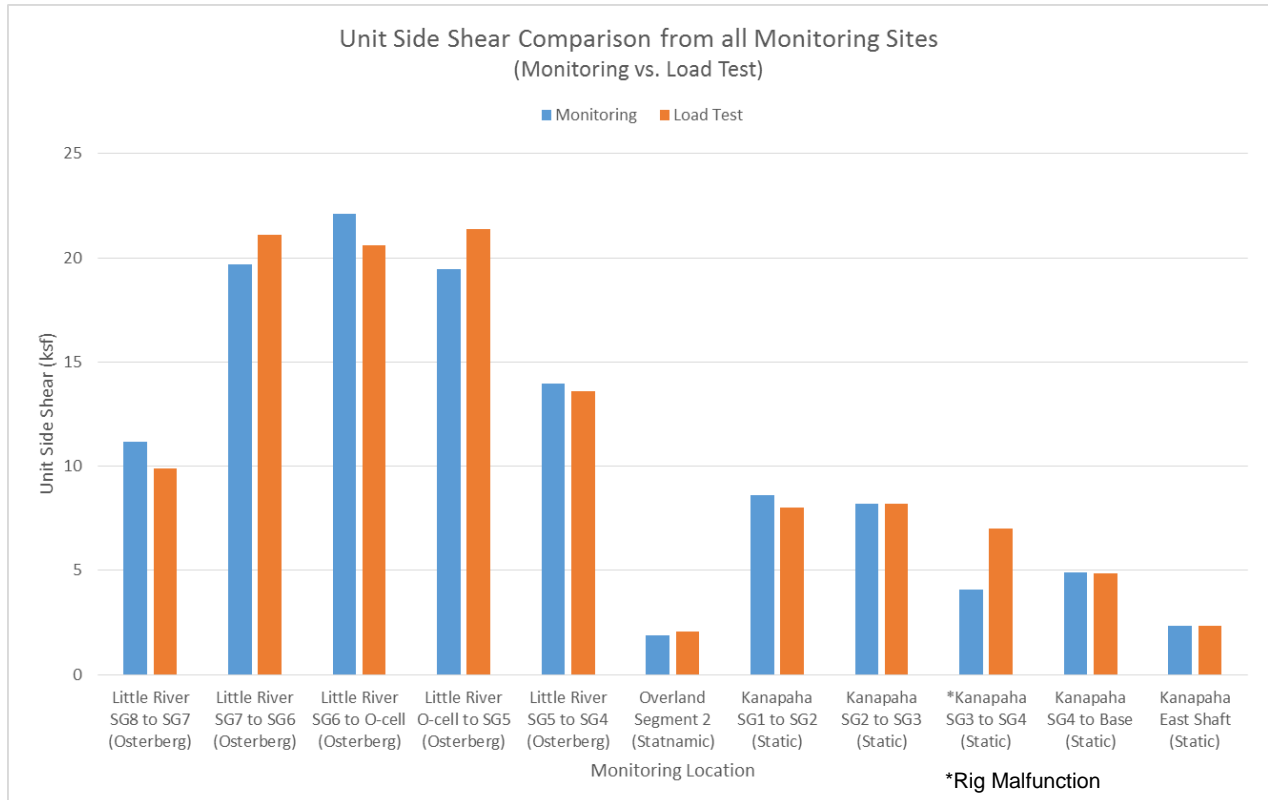


Figure 224 - Unit side shear comparison from all monitoring sites

As seen in Figure 224, the developed drilled shaft monitoring system and methods of analysis were not only successful, but highly accurate. This was confirmed by conducting a bias analysis. The following provides the bias analysis which includes the monitoring result at Kanapaha where rig malfunction occurred and a more accurate assessment where the rig malfunction result is removed.

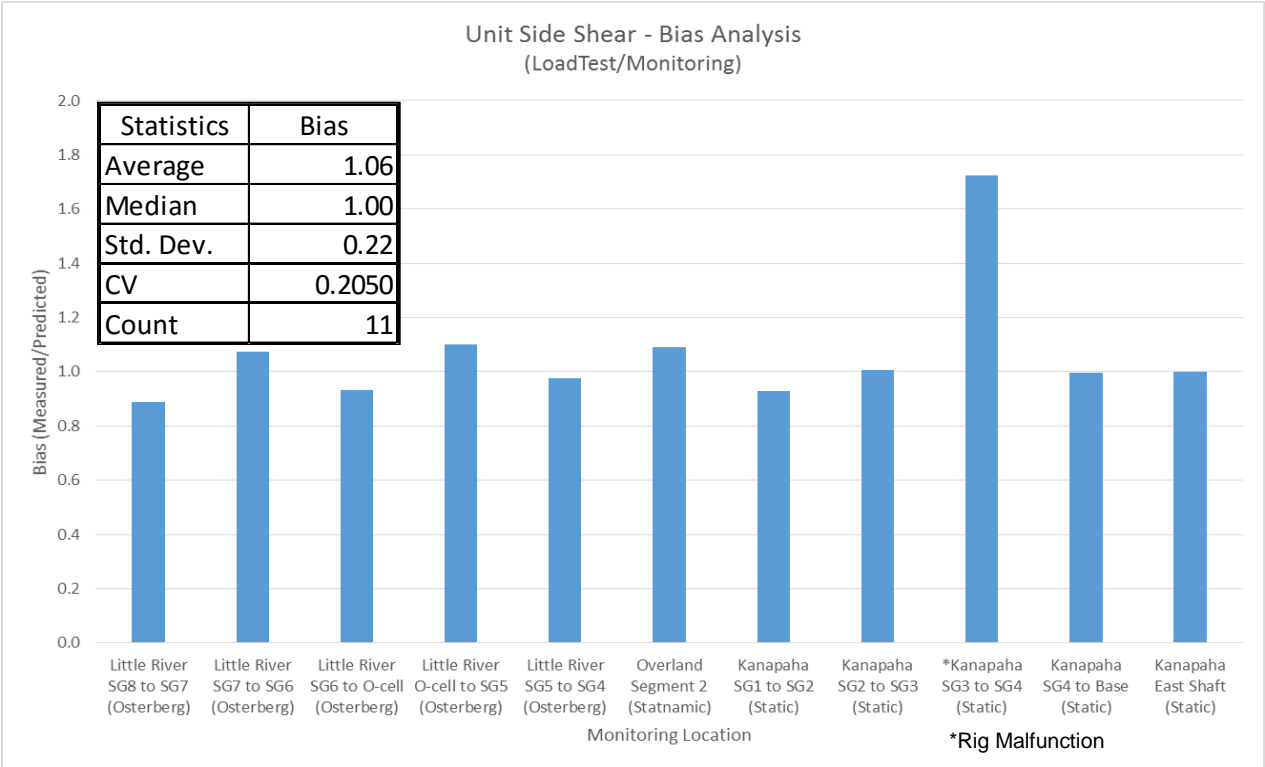


Figure 225 - Unit side shear bias analysis

As seen in Figure 225, the rig malfunction result is more than three standard deviations away from the mean and would be considered a significant outlier. However, the median bias is still 1.00 and the CV is relatively low. The following figure provides a more accurate interpretation of the results with the rig malfunction section removed from the bias analysis.

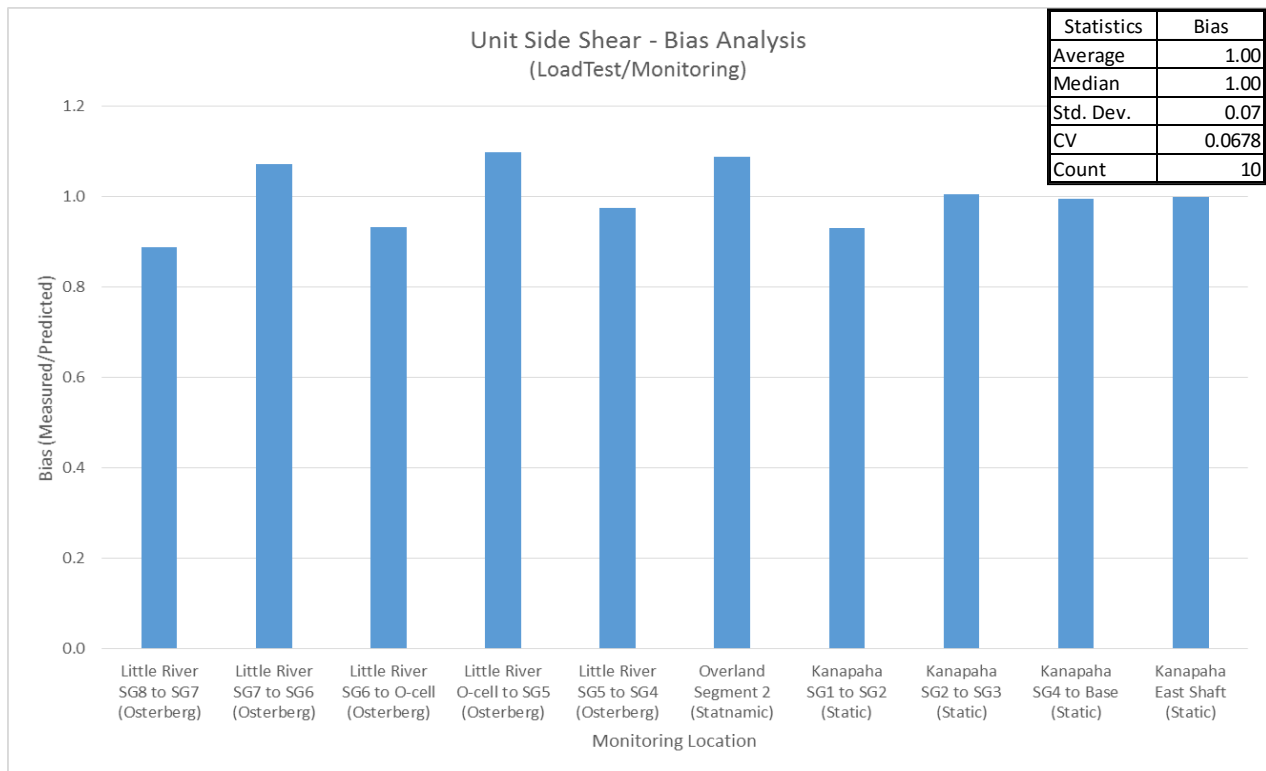


Figure 226 - Unit side shear bias analysis (rig malfunction section removed)

With the rig malfunction result removed, the mean and median bias is 1.00. The CV is less than 0.1 which indicates the monitoring has limited variability. Tabular results summarizing the entire research effort are provided in the following table.

Table 98 – Comparative analysis summary for the entire research project

Comparative Analysis Summary						
Location	Section	Test Type	Thickness (ft)	Measured (ksf)	Predicted (ksf)	% Difference
Little River	SG8 to SG7	Osterberg	10.0	9.90	11.15	12.63%
Little River	SG7 to SG6	Osterberg	5.0	21.10	19.67	-6.78%
Little River	SG6 to O-cell	Osterberg	5.5	20.60	22.09	7.23%
Little River	O-cell to SG5	Osterberg	3.5	21.40	19.46	-9.07%
Little River	SG5 to SG4	Osterberg	5.0	13.60	13.95	2.57%
Overland	Segment 2	Statnamic	5.0	2.06	1.90	-7.77%
Kanapaha	SG1 to SG2	Static	3.0	8.02	8.62	7.48%
Kanapaha	SG2 to SG3	Static	3.0	8.22	8.18	-0.49%
Kanapaha	SG4 to Base	Static	2.0	4.86	4.88	0.41%
Kanapaha	East Shaft	Static	5.0	2.36	2.36	0.00%
Average	All	All	4.70	11.21	11.23	0.12%

From the comparative analysis summary for the entire project, it is clear that drilled shaft construction monitoring is a viable solution to removing spatial uncertainties.

In addition to developing the drilling equation for real time measurement of rock strength, methods to estimate splitting tensile strength and skin friction in real time were also developed. Initially it was thought that these strength measurements would be estimated using site specific limestone q_t/q_u ratios post monitoring. However, using Johnston's criterion (1985), core data from around the state and the pilot project monitoring data, a new equation was developed that accurately estimates splitting tensile strength in real time based on compressive strength. It should be noted the results of Table 98 reflect using the Florida geomaterials equation, Eq 16, to predict q_t . The limestone equation, Eq 18, using the correction factor produced similar results with an average percent difference of 0.32%. However, the Florida geomaterials equation produced estimates closer to the measured load test results in 8 of the 10 comparisons and generally provided a more conservative approach. Therefore, Florida geomaterials equation is recommended for predicting q_t in real time. Using this equation allows the recommended SFH skin friction equation to be used in real time as well. New relationships between compressive and splitting tensile strength with void ratio, moisture content and dry unit weight were also developed. This gives rise to concept that index testing of these material properties could provide better understanding of limestone rock strengths in locations where rock cores are difficult to obtain for core testing.

6.2 Recommendations

As is evident in the conclusions, the drilled shaft monitoring methods appear to be viable, but further testing should be performed to validate the results. With this work, researchers took the first steps towards eliminating spatial variability concerns for structures supported by drilled shafts. In addition, this provides a means to quantify the quality and length of rock sockets during drilling so the as-built foundation meets/exceeds the design parameters, providing quality assurance to the drilling contractor and foundation design engineer. This would be extremely useful for projects that do not implement load testing to confirm the design of their production shafts. For all of these reasons it is recommended that more drilled shafts with planned load tests be monitored during construction in order to further verify the strength, as well as estimated side shear. Future efforts should focus on locations where different Florida limestone formations are encountered. Ideal locations would be in the Tampa area where dolomite is encountered, in Miami where oolite is encountered, along the east coast where the young Anastasia formation is found, in the panhandle where higher strength limestone is present and in larger metropolitan areas such as Jacksonville where construction is constantly growing and where both limestone and marl formations exists.

Since the developed monitoring techniques were capable of determining not only compressive strength but splitting tensile strength and skin friction in real time, the same drilling techniques could be applied in more geotechnical engineering applications such as auger cast piles, ACIP, or used as a site investigation tool, SPT. In the case of

auger cast piles, interest for the use of these foundations under bridge structures is high. Generally, ACIP piles are installed quickly (auger doesn't go in and out of hole) and they too develop large unit skin frictions in limestone. However, since the continuous flight auger does not go in and out the hole, the excavated material type is unknown; therefore, monitoring as investigated could be very useful. In the case of site investigation, drill monitoring from an SPT rig could provide the benefit of continuous data collection similar to CPT with the ability to penetrate through layers of rock that terminates a CPT test. Continuous data collection would provide great assistance for sites with poor recoveries and highly variable soil and rock. Additionally, at any time during monitoring from the SPT rig, SPT testing could be implemented or core samples could be extracted for lab testing and compared to drilling strength measurements.

Finally, covered in this report was a newly developed correlation between rock strength properties, q_u and q_t , with materials properties of rock such as void ratio, porosity, moisture content and unit weight. It is believed that developing correlation between strength and material properties of rock will lead to a better understanding of the materials being influenced by engineering design. It also gives rise to the concept of index testing where strength estimates could be made based on the material properties of the rock. Collection and testing of limestone cores from around the state could provide the basis of the investigation. From this, a stronger correlation between strength and material properties could be achieved. Additionally, Johnston's criteria for Florida geomaterials could be developed experimentally and compared to the current theoretical relationship developed for q_u and q_t . This would further improve the real time estimates of splitting tensile strength and skin friction during drill shaft monitoring as well as conventional design. In order to recreate Johnston's criteria, unconfined compression, split tension, direct tension and triaxial testing should be performed.

LIST OF REFERENCES

- “AASHTO LRFD Bridge Design Specification”, 5th Edition, Section 10 (Foundations), pp. (10-25) – (10-27), 2010
- Anoglu, N., Girgin, Z., Anoglu, E., 2006, “Evaluation of Ratio between Splitting Tensile Strength and Compressive Strength for Concrete up to 120 MPa and its Application in Strength Criterion”, ACI Materials Journal Title No. 103-M03, November-December.
- ACI 229R-99, “Controlled Low Strength Materials” (Reapproved 2005), ACI Committee 229, American Concrete Institute, Farmington Hills, MI, 1999, www.concrete.org
- ASTM D2938-95(2002),” Standard Test Method for Unconfined Compressive Strength of Intact Rock Core Specimens” (Withdrawn 2005), ASTM International, West Conshohocken, PA, 1995, www.astm.org
- Bingham, M. G., 1964, “How to Make the R/N-W/D Chart and What It Means,” Oil & Gas Journal, 62, No. 45, pp. 212–214, 216–217.
- Bingham, M. G., 1964, “How to Interpret Drilling in the Performance Region,” Oil & Gas Journal, 62, No. 46, pp. 173, 176, 179.
- Bingham, M. G., 1964, “How Rock Properties Are Related to Drilling,” Oil & Gas Journal, 62, No. 50, pp. 94, 96–98, 101.
- Bullock, P.J. (2004) *In situ Rock Modulus Apparatus*, (Florida Department of Transportation Research Report BC354-13). Gainesville, FL: University of Florida.
- Carter, J.P. and Kulhawy, F.H., 1987, "Analysis and Design of Foundations Socketed into Rock", Research Report 1493-4, Geotechnical Engineering Group, Cornell University, Ithaca, New York.
- Coduto, D. P. “Foundation Design: Principles and Practices”, 2nd Edition, Section 14.4, page 527, 2001
- FDOT 2012, “(Revised) Final Geotechnical Report SR10 (US-90) Over Little River and Hurricane Creek”, Florida Department of Transportation, Central Office, Structures Design, Geotechnical Section, FPID: 422823-1-52-01, Gadsden County, Florida, 2012
- FDOT 2015, *Soils and Foundation Handbook*, Florida Department of Transportation, State Materials Office, Gainesville, Florida, 2015, www.dot.state.fl.us

FHWA 2010, "Drilled Shafts: Construction Procedures and LRFD Design Methods", National Highway Institute and U.S. Department of Transportation Federal Highway Administration, Washington, D.C. 2010, Report No. FHWA NHI-10-016.

Hoberock, L. L., and Bratcher, G. J., 1996, "A New Approach for Determining In-Situ Rock Strength While Drilling," ASME Journal of Energy Resources and Technology, 118, pp. 249–255.

Horvath, R.G. and Kenney, T.C., 1979, "Shaft Resistance of Rock-Socketed Drilled Piers", Symposium on Deep Foundations, ASCE National Convention, Atlanta, GA, 182-214.

Johnston, I., "Strength of Intact Geomechanical Materials", ASCE Journal of Geotechnical Engineering, 1985.111:730-749.

Karasawa, H., Ohno, T., Kosugi, M., and Rowley, J.J.C., 2002a, "Methods to Estimate the Rock Strength and Tooth Wear While Drilling With Roller-Bits, Part 1: Milled-Tooth Bits", ASME Journal of Energy Resources Technology, 124, pp. 125-132.

Karasawa, H., Ohno, T., Kosugi, M., and Rowley, J.J.C., 2002b, "Methods to Estimate the Rock Strength and Tooth Wear While Drilling With Roller-Bits, Part 2: Insert Bits", ASME Journal of Energy Resources Technology, 124, pp. 133-140.

McVay, M., Townsend, F., and Williams, R., 1992, "Design of Socketed Drilled Shafts in Limestone" ASCE Journal of Geotechnical Engineering, Vol. 118, No. 10, pp. 1626-1637.

McVay, M.C., Niraula, L. (2004). *Development of P-Y Curves for Large Diameter Piles/Drilled Shafts in Limestone for FBPIER* (Florida Department of Transportation Research Report BC354-59. Gainesville, FL: University of Florida.

Mullins, G., 2007, "Drilled Shafts", [www.eng.usf.edu](http://www.eng.usf.edu/~gmullins/courses/Insitu/Drilled%20Shafts/Chapter%20Drilled%20Shafts%20071703.pdf)
<http://www.eng.usf.edu/~gmullins/courses/Insitu/Drilled%20Shafts/Chapter%20Drilled%20Shafts%20071703.pdf>

O'Neill, M.W. and Reese, L.C., "Drilled Shafts: Construction Procedures and Design Methods, Chapter 11, Page 288, Federal Highway Administration, 1999

Pessier, R. C., and Fear, M. J., 1992, "Quantifying Common Drilling Problems With Mechanical Specific Energy and a Bit-Specific Coefficient of Sliding Friction," SPE 24584, presented at the 67th Annual Technical Conference and Exhibition of the SPE, Washington, DC, October 4–7, pp. 373–388.

Scott, T.M., Campbell K.M., Rupert, F.R., Arthur, J.D., Green, R.C., Means, G.H., Missimer, T.M., Lloyd, J.M., Yon, J.W., Duncan, J.G., 2001, "Geologic Map of the State of Florida" (revised April 15, 2006 by David Anderson), http://publicfiles.dep.state.fl.us/FGS/FGS_Publications/MS/ms146_geology_of_fl.pdf

Sheppard, M.D., Bloomquist, D., Slagle, P.M., Renna, R. (2006). *Rate of Erosion Properties of Rock and Clay* (Florida Department of Transportation Research Report BD545-3). Gainesville, FL: University of Florida.

Teale, R., 1965, "The Concept of Specific Energy in Rock Drilling," *Int. J. Rock Mech. Mining Sci.* Vol., 2, pp. 57–73.

Wolcott, D. S., and Bordelon, D. R., 1993, "Lithology Determination Using Downhole Bit Mechanics Data," SPE 26492, presented at the 68th ATCE of the SPE, Houston, TX, October 3–6, pp. 769–778.